universität wien

DISSERTATION

Titel der Dissertation

Cytoplasmic functions of the tRNA ligase complex in health and disease

Verfasserin

Dipl. Biochem. Theresa Henkel

angestrebter akademischer Grad

Doctor of Philosophy (PhD)

Wien, 2015

Studienkennzahl lt. Studienblatt:	A 794 685 490
Dissertationsgebiet lt. Studienblatt:	Molekulare Biologie
Betreuerin / Betreuer:	Javier Martinez, PhD

Index

1. Abstract

tRNA ligases have been implicated in different biological processes such as unconventional mRNA splicing, RNA repair and the replication of RNA viruses. For the mammalian tRNA ligase complex enclosing RTCB as the catalytic subunit, however, no other substrates apart from tRNA exon halves had been described. Therefore, the aim of this thesis was to identify and characterize novel functions of the mammalian tRNA ligase complex. For this purpose, inducible, shRNA-mediated depletion of RTCB and/or its cofactor archease was applied, which enabled the identification of the mammalian tRNA ligase complex as the RNA ligase required for unconventional splicing of the *XBP1* mRNA in the context of the unfolded protein response (UPR). This atypical splicing reaction causes a frame shift and enables expression of the transcription factor XBP1s. In the absence of RTCB and archease *XBP1* mRNA splicing failed, which impaired XBP1s expression and thus the induction of XBP1s-specific downstream targets. This effect was not caused by changes in the RNA cleavage efficiency, as IRE1α, the endonuclease required for intron removal, remained active after loss of tRNA ligation. Similarly, depletion of RTCB and archease did not change overall UPR signaling but specifically disrupted XBP1s expression.

Furthermore, RNA sequencing and subsequent confirmation by RT-qPCR and Western Blot analysis revealed that RTCB- and archease-depleted HeLa cells showed alterations in the activation of cellular signaling pathways such as ERK MAPK or TGFβ signaling, which in principle can cause changes in cell proliferation. Indeed, tRNA ligase-depleted cells were detected to slightly accumulate in the G_0/G_1 phase of the cell cycle leading to overall reduced proliferation kinetics in comparison to control cells. This function of RTCB seemed to be independent of its role in *XBP1* mRNA splicing as overexpression of XBP1s failed to restore normal mRNA expression profiles, signaling levels, or proliferation rates. Similarly, depletion of RTCB and archease in cancer cell lines affected the competitiveness in comparison

to control cells. This effect, however, most likely was not caused by a modification of signal transduction rates, as RTCB and archease-dependent variations of the mRNA transcriptome for the most part could not be verified in these cancer cell lines. Therefore, modulations of the mRNA expression profile after loss of tRNA ligase function seem to be primarily cell type-specific and therefore might reflect a general stress reaction caused by the loss of a housekeeping function rather than a specific reaction triggered by the loss of tRNA ligation.

Overall, based on the data presented in this thesis, RTCB and archease were identified as ligation factors required for the catalysis of unconventional *XBP1* mRNA splicing as part of the unfolded protein response. Furthermore, loss of tRNA ligase activity was shown to reduce the proliferation of HeLa cells and to lower the competitiveness of cancer cell lines.

2. Zusammenfassung

tRNA Ligasen werden mit unterschiedlichen biologischen Prozessen wie etwa dem unkonventionellen *splicing* zellulärer mRNAs, der Reparatur von RNA oder der Replikation von RNA Viren in Verbindung gebracht. Für den humanen tRNA Ligase Komplex jedoch, welcher unter anderem aus der katalytisch aktiven Untereinheit RTCB aufgebaut ist, konnten neben den Exons intron-haltiger tRNAs keine weiteren Substrate identifiziert werden. Das Ziel dieser Dissertation bestand daher in der Identifikation und Charakterisierung weiterer Funktionen des humanen tRNA Ligase Komplexes. Zu diesem Zweck wurde die Expression von RTCB und/oder dessen Cofaktors Archease mithilfe induzierbarer shRNAs reduziert. Auf diese Art konnte gezeigt werden, dass der humane tRNA Ligase Komplex für das unkonventionelle *splicing* der *XBP1* mRNA als Teil der *unfolded protein response* (UPR) benötigt wird. Diese unkonventionelle *splicing* Reaktion verursacht einen *frame shift* und ermöglicht so die Expression des Transkriptionsfaktors XBP1s. Das *splicing* der *XBP1* mRNA blieb in Abwesenheit von RTCB und Archease aus, sodass die Expression von XBP1s und die Induktion XBP1s-spezifischer Zielproteine scheiterte. Dieser Effekt wurde nicht durch Veränderungen in der RNA Spaltung hervorgerufen, da die Aktivität von IRE1α, der Endonuklease, welche für das *splicing* der *XBP1* mRNA benötigt wird, auch bei inhibierter tRNA Ligase Funktion erhalten blieb. Darüber hinaus konnte nachgewiesen werden, dass ein Verlust der tRNA Ligase nicht zu einer generellen Inhibition des UPR *signalings* führt, sondern spezifisch die Expression von XBP1s unterdrückt.

Durch RNA-Sequenzierung und anschließender Verifizierung der Ergebnisse mithilfe von RT-qPCRs und Western Blot Analysen konnten außerdem Veränderungen in der Aktivität unterschiedlicher zellulärer Signalwege in HeLa-Zellen mit verringerter Expression von RTCB und Archease festgestellt werden. Diese Variationen könnten zu einem abweichenden Proliferationsverhalten der betroffenen Zellen führen. Tatsächlich zeigte die RTCB/Archease RNAi-Zelllinie eine leichte Akkumulation von

Zellen in der G_0/G_1-Phase des Zellzyklus, sowie eine Reduktion der Proliferationskinetik. Diese Funktion des tRNA Ligase Komplexes schien unabhängig von dessen Funktion im unkonventionellen *splicing* der *XBP1* mRNA zu sein, da die Veränderungen in Proliferation und *signaling*-Aktivität der Zellen auch nach einer Überexpression von XBP1s zu detektieren waren. Darüber hinaus zeigten Tet-On Krebszelllinien mit einer reduzierten Expression von RTCB und Archease eine verringerte Wettbewerbsfähigkeit im Vergleich zu Kontrollzellen. Dieser Effekt wurde jedoch aller Voraussicht nach nicht durch Veränderungen in der Signaltransduktion hervorgerufen, da RTCB- und Archease-abhängige Variationen des mRNA Transkriptoms in diesen Zellen zum Großteil nicht verifiziert werden konnten. Folglich sind Modulationen des mRNA Transkriptoms nach Verlust der tRNA Ligasefunktion hauptsächlich zelltypspezifisch und könnten daher eine allgemeine Stressantwort darstellen, welche aller Voraussicht nach durch den Verlust einer *housekeeping*-Funktion und nicht durch den spezifischen Verlust der RTCB-Expression hervorgerufen wurde.

Insgesamt konnte auf Grundlage der in dieser Dissertation präsentierten Daten nachgewiesen werden, dass RTCB und Archease das unkonventionelle *splicing* der *XBP1* mRNA als Teil der *unfolded protein response* katalysieren. Darüber hinaus wurde gezeigt, dass ein Verlust der tRNA Ligase Aktivität zu einer verringerten Proliferation von HeLa Zellen und zu einer verminderten Wettbewerbsfähigkeit von Krebszelllinien führt.

3. Introduction

3.1. Insights into tRNA splicing

In all three domains of life, transfer RNAs (tRNA) can be encoded by intron-containing pre-tRNA sequences, which need to be spliced in order to become active in translation (Popow et al., 2012). The occurrence of such discontinuous pre-tRNA genes ranges from about 70 % of all genetically encoded tRNA sequences in archaea to about 20 % in yeast, while in the human genome only 6 % of all tRNAs contain intervening sequences (Chan and Lowe, 2009). Despite this large phylogenetic distribution and their discovery back in the 1970s (Goodman et al., 1977; Valenzuela et al., 1978), the defined function of tRNA introns still remains elusive. Studies in *Saccharomyces cerevisiae* suggest that at least in the case of particular pre-tRNAs, splicing is required for the establishment of posttranslational modifications such as methylation (Strobel and Abelson, 1986) and pseudouridylation (Choffat et al., 1988; Johnson and Abelson, 1983; Szweykowska-Kulinska et al., 1994). Yet, the removal of all introns from a particular tryptophan isodecoder family did not affect growth or translation of *S. cerevisiae* under laboratory conditions (Mori et al., 2011) and *Caenorhabditis elegans* defective in pre-tRNA splicing show normal growth and lifespan after expression of pre-spliced tRNAs (Kosmaczewski et al., 2014). These results question an essential function of tRNA introns.

The mechanism of tRNA splicing

In contrast to canonical mRNA splicing, the removal of introns from tRNAs is a two step enzymatic process entailing an endonucleolytic cleavage followed by an RNA ligation reaction (Abelson et al., 1998). Both, in yeast and mammals, the introductory cleavage of exon-intron boundaries is carried out by the tetrameric Sen complex

(termed TSEN in humans) that is composed of two catalytic and two structural subunits (Paushkin et al., 2004; Trotta et al., 1997). As eukaryal tRNA introns greatly differ in their size and do not contain any conserved structural motifs despite a strictly conserved A:I base pair in the anticodon arm (Baldi et al., 1992), the Sen complex does not recognize a particular consensus sequence but rather cleaves at a defined distance from a conserved structural feature located in the mature domain (Reyes and Abelson, 1988). Consequently, tRNA introns can be mutated extensively without affecting proper recognition by the tRNA endonuclease (Johnson et al., 1980).

Cleavage by the Sen complex yields two tRNA exon halves displaying a 2', 3'-cyclic phosphate at the 3'-end of the 5'-exon and a 5'-hydroxyl at the 5'-end of the 3'-exon as well as a linear intron showing the same chemistry at the respective ends (Popow et al., 2012). The liberated exons are subsequently recognized and ligated by a tRNA ligase. Hereby, the mechanism of ligation greatly differs between the yeast tRNA ligase Trl1 and the mammalian tRNA ligase complex. Trl1 is a multifunctional protein that entails a phosphodiesterase activity to hydrolyze the 2', 3'-cyclic phosphate, a kinase activity to phosphorylate the 5'-hydroxyl group at the 3'-exon, and a nucleotidyl transferase domain to catalyze ATP-dependent adenylation of the generated 5'-phosphate and subsequent ligation of the two exon halves under the release of AMP (Apostol et al., 1991; Greer et al., 1983; Phizicky et al., 1986; Sawaya et al., 2003). This ligation mechanism is referred to as 5'-3' ligation or the "healing and sealing" pathway (Popow et al., 2012; Schwer et al., 2004) and is characterized by incorporation of an ATP- or GTP-derived phosphate into the splice junction (Greer et al., 1983; Phizicky et al., 1986). Furthermore, ligation by Trl1 leaves a 2'-phosphate at the newly generated linkage that is removed by a phosphotransferase termed Tpt1 (Culver et al., 1997; Culver et al., 1993; McCraith and Phizicky, 1990).

In contrast to yeast, tRNA exon ligation in mammals is carried out by a 3'-5' or "direct" ligation mechanism during which the phosphate at the 3'-end of the 5'-exon is directly incorporated into the new splice junction (Filipowicz et al., 1983; Filipowicz and Shatkin, 1983; Laski et al., 1983). This reaction is GTP-dependent (Chakravarty and Shuman, 2012) and consists of a sequential 2', 3'-cyclic phosphodiesterase and a 3'-phosphate/5'-hydroxyl ligation step in *Escherichia coli*. Even though biochemical assays soon revealed the presence of this alternative ligation mechanism in mammalian cells (Filipowicz et al., 1983; Filipowicz and Shatkin, 1983; Laski et al., 1983), RTCB proteins have only recently been identified as the RNA ligases required for this reaction (Englert et al., 2011; Popow et al., 2011).

The mammalian tRNA ligase complex

In mammalian cells, RTCB is part of a pentameric complex consisting of RTCB itself as the catalytic subunit, the DEAD-box helicase DDX1 and three subunits of unknown function: FAM98B, ashwin and CGI99 (Popow et al., 2011). As such, the tRNA ligase has only poor catalytic activity and requires an additional cofactor termed archease to achieve maximal turnover rates (Popow et al., 2014). Mechanistically, archease stimulates guanylation of RTCB during the reaction cycle and thereby enables the tRNA ligase to catalyze multiple rounds of turnover. This cofactor requirement is surprising, as bacterial RtcB is able to autonomously form RtcB-guanylate intermediates (Chakravarty and Shuman, 2012; Tanaka et al., 2011a). Furthermore, maximal activity of RTCB in the presence of archease depends

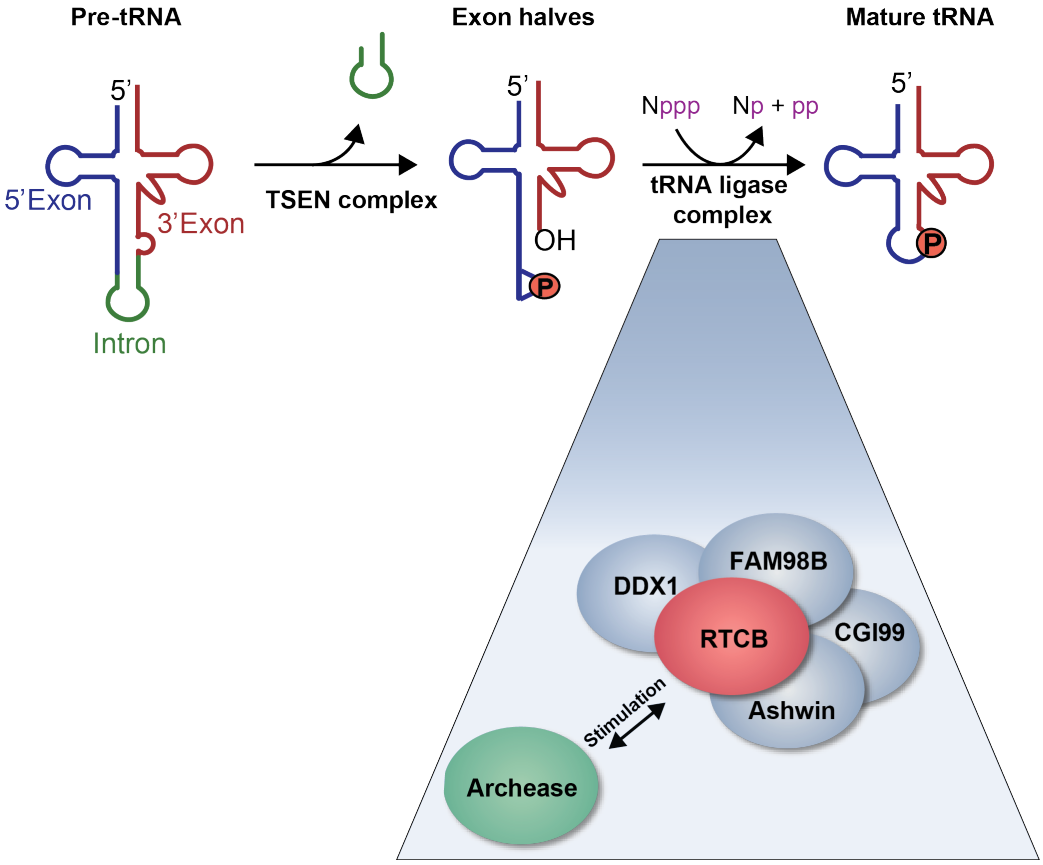

Figure 1: Splicing of intron-containing pre-tRNAs in mammals

In mammalian cells, intron-containing pre-tRNAs need to undergo a two-step enzymatic process termed tRNA splicing in order to become active in translation. This process is catalyzed by the tRNA endonuclease complex TSEN as well as the mammalian tRNA ligase complex comprising RTCB as the catalytic subunit, DDX1, FAM98B, CGI99, and ashwin. During RTCB-mediated ligation, the cleavage site-derived phosphate is incorporated into the new splice junction. This ligation mechanism is referred to as 3'-5' ligation. Furthermore, tRNA splicing depends on the action of archease, a small cofactor heavily stimulating the catalytic activity of RTCB. Image adopted from Popow et al., 2012.

on ATP hydrolysis mediated by the DEAD-box helicase DDX1 (Popow et al., 2014). This helicase exhibits 3'-5' RNA unwinding activity (Chen et al., 2002) and has been associated with many molecular functions such as mRNA processing (Bleoo et al., 2001; Chen et al., 2002), recognition of DNA double-strand breaks (Li et al., 2008) and modulation of HIV-1 replication (Robertson-Anderson et al., 2011).

The precise functions of the additional members of the mammalian tRNA ligase complex remain largely elusive. RNAi-mediated silencing of CGI99, FAM98B or ashwin does not seem to severely affect RNA ligase activity in HeLa cell extracts (Popow et al., 2011). This suggests that these complex members might perform catalysis-independent functions such as conferring a correct subcellular localization to the tRNA ligase, ensuring substrate recognition and specificity, or increasing the stability of RTCB (Popow et al., 2012). Furthermore, one or more of these accessory factors could also be involved in mediating the shuttling of the complex in and out of the nucleus (Perez-Gonzalez et al., 2014). Aside from tRNA splicing, additional functions and processes have been assigned to CGI99, FAM98B and ashwin:

CGI99 is a component of many cytoplasmic and nuclear protein complexes that are involved in different aspects of RNA metabolism: It associates with active RNA polymerase II (Perez-Gonzalez et al., 2006), viral RNAs and proteins (Emmott et al., 2013; Huarte et al., 2001; Kula et al., 2011; Lee et al., 2011c), the spliceosome (Rappsilber et al., 2002), the 7SK snRNA methylphosphate capping complex (Jeronimo et al., 2007) and with RNA maturation-related proteins (Freibaum et al., 2010). Depletion of CGI99 inhibits cellular mRNA transcription by about 50 %, which results in the downregulation of a number of important genes (Perez-Gonzalez et al., 2006). Furthermore, in dendrites CGI99 together with FAM98B and RTCB is part of cytoplasmic kinesin-associated mRNA-granules involved in local protein synthesis (Kanai et al., 2004).

The molecular function of FAM98B is only poorly studied. As part of the tRNA ligase complex, FAM98B could serve as an interaction platform recruiting accessory factors or RNA substrates (Popow et al., 2012). Accordingly, FAM98B has been shown to interact with archease after chemical crosslinking with DSP (dithiobis(succinimidyl propionate)) (Popow et al., 2014).

Ashwin expression seems to be specific for vertebrates as no homologous genes were detected in *Drosophila melanogaster* or *Caenorhabditis elegans* (Patil et al., 2006). In *Xenopus laevis* ashwin is expressed during early neuronal development and its depletion leads to severe developmental defects (Patil et al., 2006).

Localization of tRNA splicing

Similar to the mechanism of tRNA splicing also the localization of tRNA processing events is not conserved amongst all eukaryotes. In vertebrates pre-tRNA splicing is believed to occur in the nucleus, as subunits of the human tRNA endonuclease are restricted to the nuclear compartment (Paushkin et al., 2004) and efficient nuclear export of tRNAs depends on intron removal (Arts et al., 1998; Lund and Dahlberg, 1998). In contrast, the yeast tRNA endonuclease localizes to the mitochondria (Huh et al., 2003; Mori et al., 2010) while the tRNA ligase Trl1 is dispersed throughout the cytoplasm (Mori et al., 2010; Nikawa et al., 1996; Sidrauski et al., 1996). Therefore, in *S. cerevisiae* maturation of intron-containing pre-tRNAs is a cytoplasmic event requiring nucleus-to-cytoplasm transport of tRNAs.

Functions of RNA ligases unrelated to tRNA splicing

The substrate specificity of tRNA ligases does not seem to be restricted to tRNA exons but rather involves a variety of RNA species and ranges from tRNA exon halves to artificial substrates such as RNA fragments and linear introns liberated by tRNA endonucleases (Englert and Beier, 2005; Filipowicz et al., 1983; Filipowicz and Shatkin, 1983; Konarska et al., 1981). In humans and plants, genome replication of RNA viruses and viroids depends on the activity of host RNA ligases (Flores et al., 2011), which probably are required for RNA cyclization (Reid and Lazinski, 2000). Furthermore, RNA ligases are proposed to be involved in RNA repair: The viral T4 RNA ligase for example facilitates a tRNA repair mechanism required to evade a host antiviral response (Amitsur et al., 1987). Also ribotoxin-induced broken anticodon stem loops can be repaired by plant AtRNL or bacterial RtcB (Nandakumar et al., 2008; Tanaka and Shuman, 2011).

In addition, the mammalian tRNA ligase seems to exhibit specialized functions in the central nervous system of vertebrates as two recent reports point towards a role of RTCB in axon regeneration (Kosmaczewski et al., 2015; Song et al., 2015). Furthermore, RTCB has been found to interact with kinesin-associated RNA transport granules in mouse brain extracts (Kanai et al., 2004) and to associate with TDP-43-containing ribonucleoprotein particles accumulating in amyotrophic lateral sclerosis (Freibaum et al., 2010).

Last but not least, tRNA ligases have also been implicated in an unconventional mRNA splicing event, which is part of a cytoplasmic stress response pathway termed the unfolded protein response.

3.2. The unfolded protein response

The endoplasmic reticulum (ER) is a site of extensive protein translation, modification and quality control activity. In most eukaryotic cells roughly 30 % of all proteins are synthesized on ER-bound ribosomes, which leads to ER luminal protein concentrations of up to 100 mg/ml (Gardner et al., 2013; Hetz, 2012). In order to support proper protein folding and to prevent protein aggregation in this environment, numerous ER-resident chaperones and folding enzymes assist protein maturation by signal-peptide cleavage, glycosylation, and disulfide bond formation (Araki and Nagata, 2011). However, if the ER fails to satisfy this high demand of protein folding activity, the cell activates a series of signaling pathways and adaptive mechanisms to reprogram gene expression and to alleviate ER stress (Hetz, 2012; Walter and Ron, 2011). Collectively these adaptation mechanisms are called the unfolded protein response (UPR).

The unfolded protein response in Saccharomyces cerevisiae

In *S. cerevisiae*, accumulation of unfolded proteins inside the ER can be sensed by the type I transmembrane protein Ire1 (inositol-requiring enzyme 1), which consists of an ER luminal and two cytoplasmic domains entailing a kinase and an endonuclease activity (Walter and Ron, 2011). Under homeostatic conditions, the luminal domain associates with the ER chaperone Bip (immunoglobulin heavy chain-binding protein), which is a small ATPase involved in numerous functions such as protein folding, translocation of nascent polypeptides, and maintenance of calcium homeostasis (Hendershot, 2004; Otero et al., 2010). This interaction stabilizes the monomeric, inactive form of Ire1 and thereby prevents Ire1 from hyper-responding to low levels of protein folding stress (Pincus et al., 2010). In situations of increased protein folding demand, BiP is titrated away from Ire1 to allow the formation of smaller oligomers mediated by self-association of the liberated luminal domains (Walter and Ron, 2011). Besides regulated BiP release, Ire1 is also activated by directly sensing the occurrence of unfolded proteins by means of a major histocompatibility complex (MHC)-like groove in its luminal domain (Credle et al., 2005). *In vitro*, this groove enables direct binding to exposed basic and hydrophobic residues of unfolded proteins (Gardner and Walter, 2011). Further experiments also showed that *in vitro* peptide binding alone can be enough to induce Ire1 oligomerization (Gardner and Walter, 2011).

Oligomerization of activated Ire1 drives trans-autophosphorylation of its cytoplasmic domains. These phosphorylation events, however, are not directly involved in downstream signaling but the binding of nucleotides to the kinase domain itself induces a conformational change activating the RNase domain that is required to

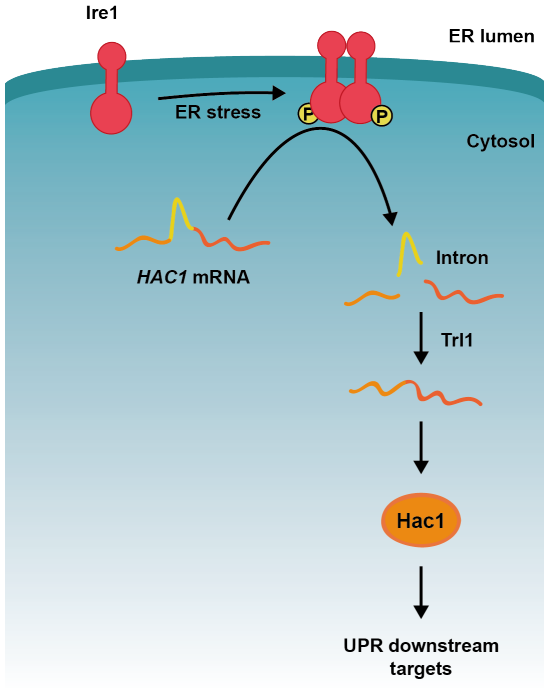

Figure 2: The unfolded protein response in yeast

In yeast, accumulation of unfolded proteins in the ER lumen drives oligomerization and trans-autophosphorylation of Ire1, an ER transmembrane kinase/endoribonuclease. The accompanying conformational changes enable activation of the cytoplasmic RNase domain of Ire1, which thereafter is able to cleave the *HAC1* mRNA releasing an unconventional intron. The resulting exon halves are joined by the tRNA ligase Trl1 to form a new mRNA isoform that is relieved from translational block. After translation, nuclear translocation of the transcription factor Hac1 leads to the activation of UPR downstream targets serving to resolve protein-folding stress.

initiate UPR-mediated gene transcription (Aragon et al., 2009; Korennykh et al., 2009; Papa et al., 2003). Accordingly, Ire1 mutants defective in nucleotide binding loose UPR-signaling activity while mutants defective in phosphotransfer do not (Chawla et al., 2011; Rubio et al., 2011). Besides Bip release, dimerization and nucleotide binding, full activation of the RNase domain also requires the formation of higher order oligomers, which is facilitated by the induced conformational change (Korennykh et al., 2009). In yeast, the formation of such foci can be visualized by microscopy (Aragon et al., 2009; Kimata et al., 2007). In contrast, the phosphotransferase activity of Ire1 plays an important role in the attenuation of UPR signaling and therefore in cell survival, which is decreased after prolonged UPR activation. Consequently, Ire1 mutants unable to trans-autophosphorylate show prolonged RNase activity and delayed disassembly of Ire1 foci (Chawla et al., 2011; Rubio et al., 2011).

ER-to-nucleus signaling mediated by the activated RNase domain of Ire1 is based on unconventional splicing of the *HAC1* mRNA. Differing from others this particular mRNA retains a 252-nucleotide intron after canonical splicing (Cox and Walter, 1996)

that blocks translation by forming a base-pairing interaction with the 5' untranslated region (UTR). At conditions of increased ER stress this intron is released by activated Ire1 cleaving at exon-intron boundaries (Ruegsegger et al., 2001; Sidrauski and Walter, 1997) and the resulting exon halves are joined by the tRNA ligase Trl1 (Sidrauski et al., 1996). To increase the efficiency of this splicing reaction, the *HAC1* mRNA is specifically recruited to the ER membrane by means of a bipartite element in its 3' UTR (Aragon et al., 2009). As liberation of the intron releases the translational block, UPR signaling enables translation of the transcription factor Hac1, which upon synthesis drives UPR-mediated gene transcription. In yeast, this transcriptional program compromises around seven to eight percent of the genome and serves to counteract ER stress (Cox and Walter, 1996; Travers et al., 2000) by increasing the transcription of genes encoding for ER-localized protein-folding catalysts and protein chaperones such as Kar2p, a member of the heat shock protein 70 family and Pdi1p, a protein disulfide isomerase (Gething and Sambrook, 1992; Kozutsumi et al., 1988; Lee, 1987). Furthermore, the UPR also activates the transcription of genes involved in membrane biosynthesis (Cox et al., 1997).

The unfolded protein response in vertebrates

Similar to yeast, also vertebrate cells express a transmembrane kinase/endoribonuclease termed IRE1α, which is involved in stress signaling during the UPR. The activation of this stress sensor is greatly conserved between lower and higher eukaryotes with the exception that the luminal MHC-like groove of IRE1α is only built upon dimerization and appears to be too narrow for peptide binding (Zhou et al., 2006). Activation of IRE1α initiates unconventional splicing of the *XBP1* mRNA—an ortholog of yeast *HAC1* (Walter and Ron, 2011)—which ultimately causes the removal of a short, 26-nucleotide intron and induces a frame shift changing parts of the open reading frame (Yoshida et al., 2001). Differing from yeast *HAC1*, the *XBP1* mRNA is translated in its spliced as well as in its unspliced form leading to the generation of two different proteins termed XBP1u (unspliced) and XBP1s (spliced). While both isoforms share the same N-terminal domain they greatly differ in their C-terminal parts, which causes differences in the protein's characteristics: while XBP1s is stable and transcriptionally active, XBP1u is short-lived (Calfon et al., 2002), lacks a transcriptional activator domain (Yoshida et al., 2001), and mainly serves as a negative feedback regulator of XBP1s mediating its proteasomal degradation (Yoshida et al., 2006). Furthermore, the expression of XBP1u is required to target the *XBP1* mRNA to the ER membrane and thus to the site of mRNA splicing. Upon translation, a hydrophobic stretch unique to the C-terminal domain of XBP1u drags the ribosome-mRNA-nascent chain complex to the ER membrane while a second carboxy-terminal region induces translational pausing (Yanagitani et al., 2009). As XBP1s auto-regulates its own promoter (Lee et

al., 2002; Yoshida et al., 2001), increased expression of XBP1u after prolonged activation of IRE1α also serves to attenuate XBP1s signaling.

Due to its high transcriptional activity, XBP1s activates a multitude of downstream targets involved in ER-associated protein degradation (ERAD), the entry of proteins into the ER, and protein folding (Acosta-Alvear et al., 2007; Lee et al., 2003). Amongst these are the ERAD component EDEM1 (ER degradation enhancer, mannosidase alpha-like 1) mediating the degradation of misfolded glycoproteins as well as the co-chaperone DNAJB9 (DnaJ Homolog, Subfamily B, Member 9). XBP1s also modulates phospholipid synthesis and therefore is required for expansion of the ER membrane under ER stress (Shaffer et al., 2004; Sriburi et al., 2007; Sriburi et al., 2004). The transcriptional activity of XBP1s is regulated by different interaction

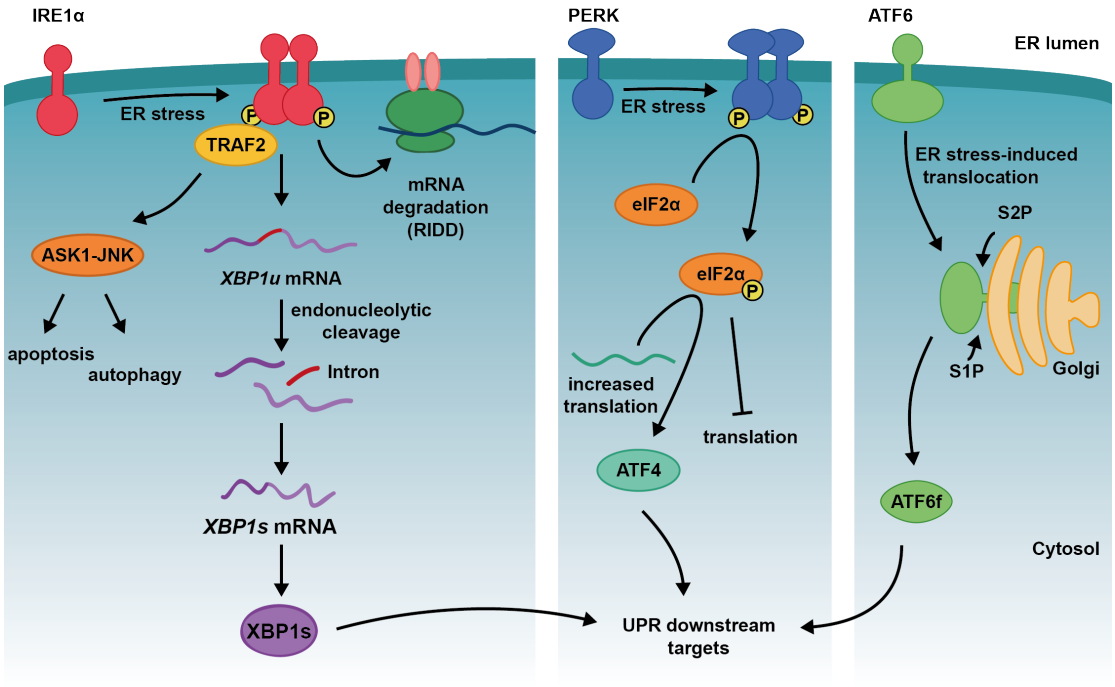

Figure 3: The unfolded protein response in vertebrates

In vertebrate cells, accumulation of unfolded proteins in the ER lumen triggers the activation of three different UPR sensors, namely IRE1α, PERK and ATF6. Activated IRE1α oligomerizes and trans-autophosphorylates to activate a cytoplasmic RNase domain that subsequently cleaves the XBP1 mRNA to release an unconventional intron. This splicing reaction enables the translation of the transcription factor XBP1s. Additionally, IRE1α is able to cleave mRNAs translated by ER-associated ribosomes and to target them for degradation by regulated IRE1-dependent decay (RIDD). Trans-autophosphorylation of IRE1α also mediates binding to the adaptor protein TRAF2, which activates apoptosis and autophagy. In contrast, oligomerization and trans-autophosphorylation of PERK induces phosphorylation of eIF2α. While protein translation in general is greatly inhibited, mRNAs containing an upstream open reading frame in their 5' UTR are preferentially translated under these conditions. One such mRNA encodes for the transcription factor ATF4. ATF6, however, translocates to the Golgi apparatus where it is cleaved by site-1 and site-2 proteases (S1P and S2P) releasing the cytoplasmic domain (ATF6f). Similar to XBP1s and ATF4, this domain acts as a transcription factor activating UPR downstream targets.

partners such as ATF6, HIF1α and the p85α regulatory subunit of phosphatidylinositol 3-kinase (Chen et al., 2014; Park et al., 2010; Yamamoto et al., 2007) as well as by posttranslational modifications including phosphorylation, acetylation or sumoylation (Chen and Qi, 2010; Lee et al., 2011b; Wang et al., 2011).

In metazoan cells IRE1α does not only mediate the splicing of the *XBP1* mRNA but also initiates the rapid degradation of mRNAs in a process termed regulated IRE1-dependent decay (RIDD) (Hollien et al., 2009; Hollien and Weissman, 2006). As RIDD substrates preferably encode for membrane and secreted proteins, this process serves to decrease the flux of newly synthesized proteins into the stressed ER. Its substrate specificity is mediated by a low stringency consensus site and the localization of the mRNA close to the ER membrane and thus to foci of high IRE1α activity (Hollien and Weissman, 2006). Prominent RIDD substrates include the insulin mRNA in pancreatic β-cells (Lee et al., 2011a; Lipson et al., 2008) or PDGF receptor (Hollien et al., 2009). Interestingly, *XBP1* mRNA splicing and RIDD seem to be two separable functions of IRE1α with distinct requirements for their activation: While *XBP1* mRNA splicing and the induction of its downstream targets can be artificially induced with 1NM-PP1, an ATP analog that can bind to IRE1α mutants with enlarged ATP binding pockets, RIDD activity can only be detected when nucleotide binding is accompanied by ER stress (Hollien et al., 2009).

Besides *XBP1* mRNA splicing and RIDD, IRE1α has additional functions in cell signaling independent of RNA processing. The cytosolic domain of activated IRE1α binds to the adaptor protein TRAF2 (TNFR-associated factor 2), which results in activation of ASK1 (apoptosis signaling kinase) and its downstream target JNK (JUN N-terminal kinase) (Urano et al., 2000). The ASK1-JUN pathway activates macroautophagy (hereafter referred to as autophagy) but also serves as an important pro-apoptotic signal after UPR stimulation (Kanda and Miura, 2004; Mauro et al., 2006; Nishitoh et al., 2002). Furthermore, IRE1α engages “alarm pathways” such as ERK (extracellular signal-regulated kinase) (Nguyen et al., 2004) and NF- κB signaling (nuclear factor-κB) (Hu et al., 2006) regulating redox metabolism and inflammatory processes. Collectively, these adaptor and signaling proteins form a dynamic platform called the UPRosome (Hetz and Glimcher, 2009). Besides the activation and modulation of downstream signaling events, the UPRosome is also involved in shaping the amplitude and duration of IRE1α signaling itself. Thereby most of the regulators—such as the pro-apoptotic proteins BAX and BAD (Hetz et al., 2006)—increase IRE1α signaling, possibly as a result of enhanced or sustained activation.

From metazoans onwards, IRE1α signaling is complemented by two additional UPR branches, which are initiated by the transmembrane sensors ATF6 (activating transcription factor 6) and PERK (protein kinase RNA-like ER kinase) (Walter and

Ron, 2011). While all three UPR pathways signal from the ER to the nucleus, they do so by very diverse mechanisms.

The luminal stress-sensing domain of PERK is functionally and structurally related to the luminal domain of IRE1α and its dissociation from BIP leads to trans-autophosphorylation and activation of a cytosolic kinase domain phosphorylating the eukaryotic translation initiation factor 2α (eIF2α). Phosphorylation of eIF2α decreases overall protein translation rates and thereby—similar to RIDD—reduces the load of newly synthesized proteins entering the ER (Harding et al., 1999). At the same time, mRNAs containing an otherwise inhibitory upstream open reading frame in their 5' UTR are preferentially translated when eIF2α is phosphorylated (Jackson et al., 2010). One such mRNA encodes for the transcription factor ATF4 (activating transcription factor 4), which is required for the activation of various UPR downstream targets such as CHOP (transcription factor C/ EBP homologous protein) or the protein phosphatase regulatory subunit GADD34 (growth arrest and DNA damage-inducible 34) (Harding et al., 2000; Scheuner et al., 2001). As part of a negative feedback loop, ATF4-mediated GADD34 expression initiates dephosphorylation of eIF2α and thereby serves to attenuate PERK signaling (Novoa et al., 2001). In contrast, CHOP is a pro-apoptotic transcription factor facilitating the induction of apoptosis under conditions of prolonged ER stress (Walter and Ron, 2011).

The small chaperone BIP also associates with ATF6 and masks a Golgi localization signal in its luminal domain (Shen et al., 2002). After accumulation of unfolded proteins and consequent BIP release, ATF6 therefore translocates to the Golgi apparatus where it is cleaved by site-1 and site-2 proteases releasing its amino-terminal cytoplasmic domain (Gardner et al., 2013). This liberated domain functions as a bZIP transcription factor and migrates to the nucleus to activate a series of downstream targets involved in ER expansion or serving as chaperones (e.g. BIP), foldases, and ERAD components (Adachi et al., 2008; Bommiasamy et al., 2009). In comparison to PERK and IRE1α, the ATF6 signaling pathway is far less studied.

The interplay and different timing of the three UPR signaling branches in metazoans leads to a complex signaling output that depends on the stimulus but also on the particular cell type affected (Hetz, 2012). As an immediate response, phosphorylation of eIF2α by activated PERK and the selective degradation of mRNAs initiated by RIDD decreases the load of newly synthesized proteins entering the ER (Hetz, 2012). At the same time, IRE1α signaling initiates macroautophagy to remove damaged ER and protein aggregates (Kroemer et al., 2010). Only in a second wave, the three transcription factors activated by the UPR initiate a massive transcriptional response. Expression of UPR downstream targets mainly serves to mediate adaptation to ER stress or, in conditions of prolonged ER stress, to induce apoptosis.

3.3. Regulation of cell proliferation

Besides the alleviation of protein folding stress, many UPR proteins are involved in additional cellular processes ranging from angiogenesis (Drogat et al., 2007; Karali et al., 2014) to cell adhesion (Dejeans et al., 2012) and cell proliferation (Bobrovnikova-Marjon et al., 2010). Thereby, possible links between cell proliferation and UPR signaling receive particular attention, as malignant cells are especially prone to protein misfolding due to nutrient deprivation and dysregulation of protein synthesis.

The proliferation of cells occurs as a consequence of continuous cell cycle progression. Hereby, four major cell cycle phases can be distinguished: two gap phases (G_1 and G_2) separated by an S phase (DNA synthesis phase) and an M phase (mitosis). During the S phase, the cell's DNA content is duplicated by means of DNA replication while the following M phase serves to equally distribute the genomic information to two daughter cells. In contrast, the two gap phases are characterized by high metabolic activity, which causes cells to grow in size and to increase the supply of proteins, lipids and organelles (Rhind and Russell, 2012). In summary, this results in recurrence of the different cell cycle phases in the following order: G_1-S-G_2-M. Furthermore, cells can exit active cell cycle progression to enter the so-called G_0 phase, in which they remain metabolically active but do not divide any more. This is especially the case for differentiated cells in multicellular organisms such as neurons or skeletal muscle cells.

Regulation of cell cycle progression

There are mainly two key classes of regulatory molecules that control cell cycle progression: cyclins and cyclin-dependent kinases (CDKs). CDKs exhibit serine-threonine kinase activity and are expressed at relatively constant levels throughout the cell cycle as well as in quiescent, aging, and terminally differentiated cells. Yet, in the absence of cyclin expression CDK activity is very low. Cyclins therefore act as regulatory subunits of CDK-cyclin complexes. In contrast to CDKs, the expression of cyclins greatly varies and oscillates in defined patterns, which directly transmit to oscillations in CDK activity driving cell cycle progression. Thereby, cyclin expression is regulated at the level of mRNA stability, translational control and subcellular localization but the two main regulatory mechanisms compromise transcriptional regulation and ubiquitin-dependent proteolysis (Duronio and Xiong, 2013).

Cyclin expression and CDK activity regulate cell cycle progression at two major transition points: the progression from G_1 to S phase and the transition from G_2 to M phase. Accordingly, cyclins can be grouped into two main classes: G_1/S phase cyclins compromising D-type, E-type and A-type cyclins as well as the G_2/M cyclins of type B. D-type cyclins associate with CDK4 and CDK6 and even though their

overall role in cell cycle progression seems to be relatively minor (Kozar et al., 2004; Malumbres et al., 2004; Meyer et al., 2000) they appear to be essential to couple extracellular mitogenic signals to the G_1/S phase transition (Sherr and Roberts, 2004). Furthermore, an important function of cyclin D is to control and induce cyclin E expression (Geng et al., 1999). While mammalian cells express a total of three different D-type cyclins (cyclin D1, D2 and D3), only two E-type cyclins are known so far (cyclin E1 and E2). These E-type cyclins associate with and activate CDK2. Cyclin E expression peaks at the G_1/S phase transition and is relatively low or absent at other times of the cell cycle. Similar to cyclin D, E-type cyclins seem to respond to growth factor stimulation as cyclin E expression is repressed in serum-deprived cells (Herrera et al., 1996). Likewise, mouse embryonic fibroblasts (MEFs) lacking cyclin E1 and cyclin E2 proliferate more slowly than normal cells and show a significantly reduced response to mitogenic stimulation (Geng et al., 2003).

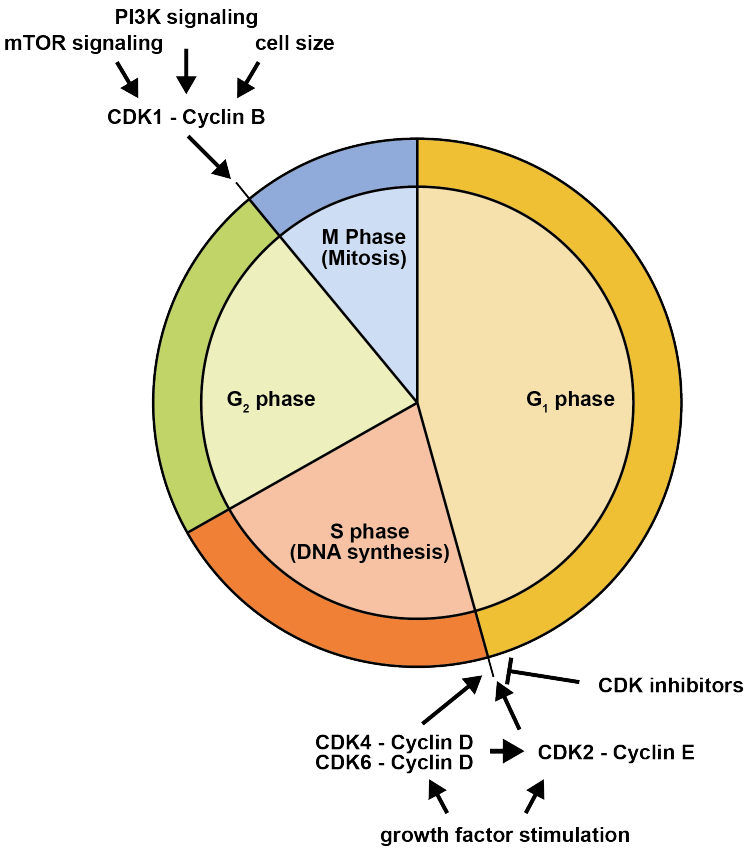

Figure 4: Cell cycle regulation

The cell cycle can be divided into four major phases: the two Gap phases 1 and 2 (G_1 and G_2), the DNA synthesis phase (S phase) as well as the M phase (mitosis) during which the cell finally divides. Cell cycle progression in mainly controlled at the G_1/S phase and G_2/M phase transition where diverse external and cell internal signals are integrated.

D-type and E-type cyclins regulate the G_1/S phase transition by initiating the phosphorylation of so-called pRB proteins, which are named after the first tumor suppressor identified, the retinoblastoma protein (Friend et al., 1986). pRB proteins are expressed as hypophosphorylated, active proteins in cell exiting from mitosis as well as in quiescent cells. In this form they associate with and inhibit numerous chromatin-associated proteins and transcription factors, particularly members of the E2F family. G_1-CDKs activated by D- or E-type cyclins phosphorylate as many as 16 different sites in pRB proteins (Akiyama et al., 1992; Kitagawa et al., 1996), which causes pRB to dissociate from E2Fs allowing the transcription of E2F target genes, many of which are required for entry into and progression through S phase (Dyson, 1998). Following S phase entry, G_1 phase cyclins are eliminated by ubiquitin-mediated proteasomal degradation. This degradation process is initiated by phosphorylation of cyclin D and cyclin E by glycogen synthase kinase 3 (GSK3) and in the case of E-type cyclins also by CDK2 (Duronio and Xiong, 2013). Under conditions of decreasing abundance of these cyclins CDK2 associates with cyclin A to promote DNA replication (Rhind and Russell, 2012).

Besides cyclins, CDK inhibitors (CKIs) play an important role in G_1/S phase transition as they lead to G_1 cell cycle arrest in response to various stimuli such as growth factor deprivation or DNA damage. The family of p21 CKIs consists of three different members: p21 itself (also known as CIP1 or WAF1), p27 (also known as KIP1) and p57 (also known as KIP2). These CKIs are short-lived and cause a transient and fast cell cycle arrest. They inhibit the activity of multiple cyclin-CDK complexes by contacting both subunits via different motifs to block kinase activity and substrate binding. A second class of CKIs, the INK4 CKIs, comprises p16 (also known as INK4A), p15 (INK4B), p18 (INK4C) and p19 (INK4D) and specifically inhibits CDK4 and CDK6 to prevent cyclin binding. As INK4 proteins have long half-lives they maintain a long-term or permanent cell cycle arrest in stem cells, senescent, and postmitotic cells (Duronio and Xiong, 2013; Sherr and Roberts, 2004).

A different cyclin-dependent kinase, CDK1, regulates a multitude of S-phase events as well as the G_2/M transition in conjunction with B-type cyclins. As a serine-threonine kinase CDK1 phosphorylates hundreds of different target proteins. According to the quantitative model, comparably low levels of CDK1-cyclin B activity trigger S phase events whereas the onset of mitosis requires increased CDK1 function (Coudreuse and Nurse, 2010; Stern and Nurse, 1996). This gradual activation of CDK1 is possible because the binding of cyclin B, which is already expressed at the onset of S phase, is not sufficient for full activation of CDK1. Instead, robust CDK1 activity requires phosphorylation of a threonine residue near the active site, which is catalyzed by CDK-activating kinase (CAK). As CAK and CDK1 levels do not greatly vary during the cell cycle but phosphorylation by CAK requires CDK1 to be cyclin-bound, the transition to M phase is mainly regulated by

the abundance of cyclin B (Duronio and Xiong, 2013; Rhind and Russell, 2012; Ward and Thompson, 2012).

Besides activation and nuclear translocation of CDK1, the G_2/M transition is also regulated by and coordinated with the cell size to ensure that a cell nearly doubles its mass before it undergoes division. This coordination is achieved by linking the activation of CDK1 to the attainment of a specific cell size (Jorgensen and Tyers, 2004). Even though different mechanisms have been proposed over the years, the precise mechanism of cell size measurement is still unknown. Furthermore, the size at which cells initiate mitosis is also linked to nutritional conditions and thus to PI3K and mTOR signaling (Rhind and Russell, 2012).

Signaling pathways involved in the regulation of cell proliferation

Control of cell proliferation generally occurs during the first gap phase (G_1) of the eukaryotic cell cycle as the decision to enter S phase represents a point of no return that commits the cell to complete a full round of the cell cycle (Duronio and Xiong, 2013). Consequently, the G_1/S phase transition is tightly controlled and integrates extracellular signals transmitted by growth factors and mitogens as well as intracellular signals reflecting the cell's metabolic state. Growth factors such as FGF or TGFβ bind to and activate specific, high-affinity surface receptors, which subsequently trigger cellular signaling pathways, for instance PI3K/AKT (Phosphatidylinositol 3-kinase/ V-Akt Murine Thymoma Viral Oncogene Homolog 1) or ERK MAP kinase (mitogen-activated protein kinase) signaling. In contrast, intracellular nutritional cues are integrated by the two mTOR protein complexes (Ward and Thompson, 2012).

The PI3K/AKT pathway is a highly conserved signal transduction pathway that can be activated by the stimulation of receptor tyrosine kinases (RTKs), G-protein-coupled receptors (GPCRs) or cytokine receptors. All of these receptors activate PI3K, which thereafter phosphorylates membrane phosphatidylinositol lipids generating phosphatidylinositol-(3,4,5)-trisphosphate (PIP_3). This lipid modification can be recognized by pleckstrin homology (PH) domains and serves to recruit PH domain-containing kinases such as AKT or PDK1 to the plasma membrane. Phosphorylation of AKT on threonine 308 by PDK1 and on serine 473 by the mTOR complex 2 (mTORC2) initiates AKT downstream signaling and increases glucose uptake, the overall glycolytic rate as well as cholesterol and fatty acid biosynthesis (Ward and Thompson, 2012). AKT signaling also increases protein translation and HIF1α-mediated transcription via activation of mTORC1. In addition, active AKT signaling promotes G_1/S phase transition by inhibiting several cell cycle inhibitors and increasing cyclin D1 activity (see Figure 33).

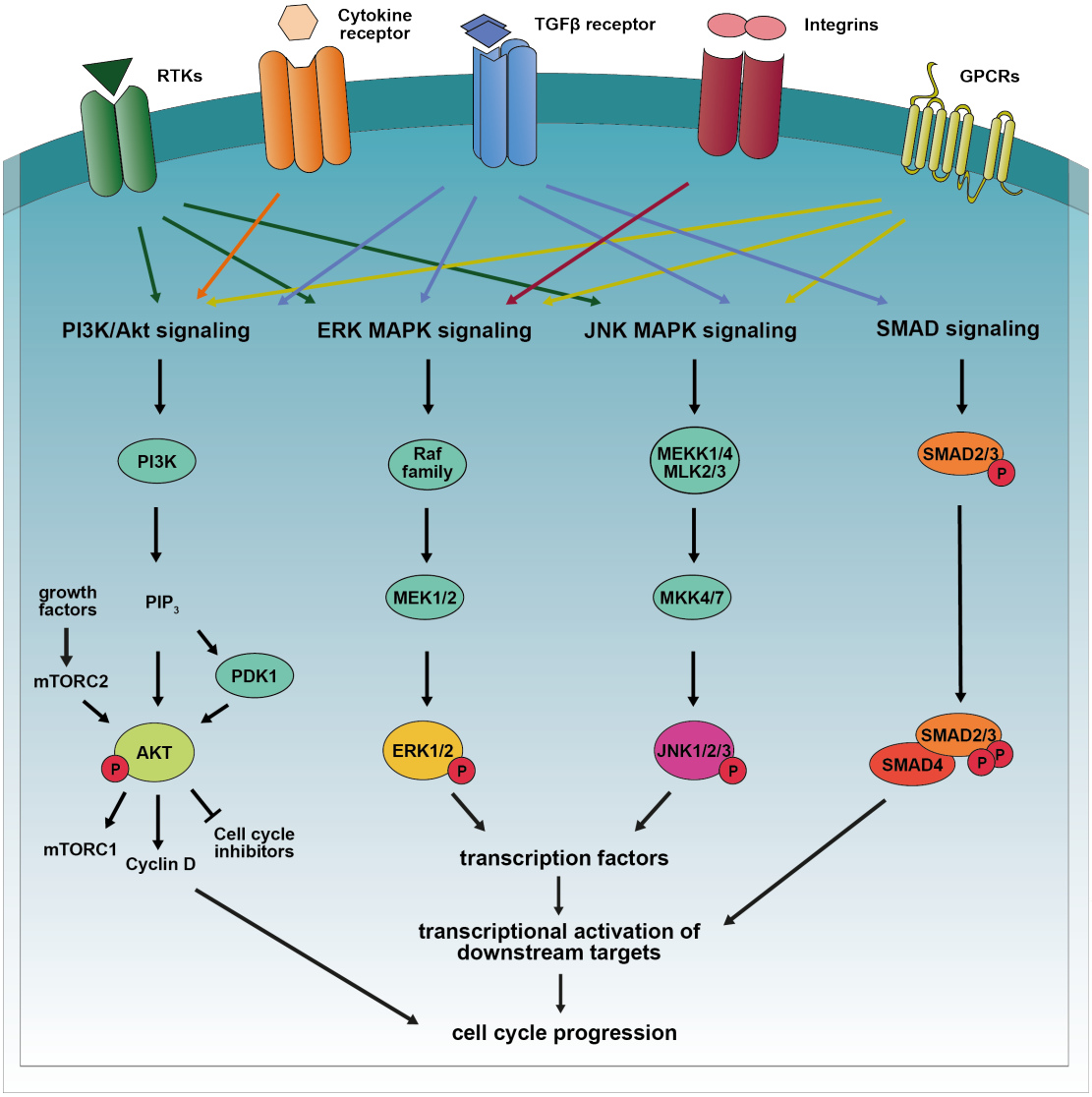

Figure 5: Regulation of cell proliferation by growth factor signaling

Growth factors regulate cell proliferation mainly by activating PI3K/AKT, ERK MAPK, JNK MAPK or, in the case of TGFβ signaling, SMAD signaling. Common to all of these signal transduction pathways is the phosphorylation of downstream signaling molecules such as ERK1/2 or AKT, which in turn regulate cyclin expression and cell cycle progression directly or via additional transcription factors such as MYC.

Stimulation of RTKs and GPCRs by growth factors or mitogens also leads to the activation of the ERK MAPK pathway (see Figure 34). Central to this signaling pathway are three sequentially activated protein kinases, namely kinases of the Raf family, MEK1/MEK2 and ERK1/ERK2. The binding of growth factors to RTKs initiates receptor trans-autophosphorylation and allows SH2 (Src homology 2) domain-containing adaptor molecules such as GRB2 to assemble signaling platforms on the cytoplasmic side of the plasma membrane. Recruitment of the guanine nucleotide exchange factor SOS by GRB2 promotes activation of members of the Ras superfamily of small GTPases by facilitating the exchange of Ras-bound GDP to GTP. Activated Ras-GTP thereafter is able to stimulate the MAPK phosphorylation

cascade activating the serine/threonine kinase ERK1/2. Activated ERK1/2 translocates to the nucleus where it stimulates various transcription factors and triggers cell cycle progression. This Ras-mediated activation of the ERK MAPK pathway is not only utilized by RTKs but also characterizes integrin signaling. In contrast, stimulated GPCRs trigger Raf activation via cAMP synthesis by the adenyly cyclase and activation of the protein kinase PKA (Morrison, 2012).

A second MAP kinase pathway stimulated by RTKs and GPCRs is the JNK MAPK pathway. Even though this pathway is mainly activated by environmental stresses such as ionizing radiation or oxidative stress, also growth factors and inflammatory cytokines trigger JNK phosphorylation. Central to JNK MAPK activation are the small GTPase Rac and other members of the Rho family such as Ras and Cdc42. While RTKs use the GRB2-SOS-Ras route described above to signal to Rac, trimeric GTPases activated by GPCRs stimulate Rac directly or via Cdc42. Rac in turn activates a MAP kinase cascade to phosphorylate and thus activate JNK1/2/3. Additionally, the JNK MAP kinase pathway can also be triggered by the action of ASK1 activated by oxidative stress, the UPR or inflammatory cytokines. Phosphorylated JNK1/2/3 migrates to the nucleus to regulate the activity of several transcription factors involved in growth, differentiation and apoptosis, amongst others (see Figure 35) (Morrison, 2012).

Similar to RTKs, also stimulated transforming growth factor beta (TGFβ) receptors can activate ERK1/2 signaling via GRB2, SOS, and Ras or JNK signaling via TRAF6 and TAK1 (see Figure 36). In general, signaling by the TGFβ superfamily is initiated by the ligand-induced formation of heterotetramers containing two type II and two type I receptors. This oligomerization allows the constitutively active type II receptors possessing serine/threonine kinase activity to phosphorylate a specialized region in the type I receptors, which enables the recruitment of downstream signaling components. Besides GRB2, these signaling components also include receptor-regulated SMAD proteins (SMAD2 and SMAD3), which can be phosphorylated by the activated type I receptor. Phosphorylation of SMAD2/3 induces dissociation from the receptor and enables association with SMAD4 and subsequent nuclear accumulation of the SMAD complexes. In corporation with corepressors, coactivators, and other DNA-binding partners, the SMAD complex regulates the transcription of a variety of downstream targets. Amongst these are SMAD6 and SMAD7 acting as negative feedback regulators to shut down TGFβ and SMAD signaling. In summary, the TGFβ-SMAD pathway regulates cell-fate determination, cell-cycle arrest, apoptosis, and actin rearrangements (Wrana, 2013).

3.4. Aims of this thesis

Given the variety of functions assigned to RNA ligases and the fact that so far RTCB is the only RNA ligase identified in mammalian cells it seems unlikely that the tRNA ligase complex only functions in splicing of intron-containing pre-tRNAs. Using shRNA-mediated protein depletion this study therefore aims to identify novel functions of the mammalian tRNA ligase complex. The *XBP1* mRNA exon halves generated under conditions of increased ER stress seem to be likely RTCB substrates as both, IREα and the tRNA endonuclease TSEN, generate cleavage products bearing 2', 3'-cyclic phosphate and 5'-OH ends (Gonzalez et al., 1999; Popow et al., 2012; Shinya et al., 2011). Furthermore, the functional equivalent yeast tRNA ligase Trl1 has been shown to mediate a similar unconventional mRNA splicing event as part of the UPR (Cox and Walter, 1996; Sidrauski et al., 1996).

Based on PAR-CLIP data, RTCB is one of the main RNA-binding proteins in mammalian cells (Baltz et al., 2012). As these data suggest that besides pre-tRNA exon halves and the *XBP1* mRNA, RTCB might regulate a variety of RNA substrates, this study intends to take a broader look on the cellular functions of RTCB and to identify additional RNA substrates. For this purpose, the mRNA transcriptomes of RTCB- and archease-depleted cell lines were analyzed by RNA sequencing. Based on a comparison of these transcriptomes and recent publications reporting the overexpression of XBP1s to be associated with disease progression in variety of cancers (Chen et al., 2014; Kharabi Masouleh et al., 2014; Tang et al., 2014), this work also aims to address the question if the targeting of RTCB and/or archease might be a new and promising strategy in the treatment of human diseases.

4. Results

4.1. Generation and characterization of RTCB- and archease-depleted Tet-On HeLa cell lines

Generation and validation of short hairpin RNAs targeting RTCB and archease

In order to reveal additional functions of the mammalian tRNA ligase complex, doxycycline (Dox)-inducible expression of short hairpin RNAs (shRNAs) was used to reduce tRNA ligation in HeLa cells (Fellmann et al., 2013; Zuber et al., 2011). As *in vitro* the catalytic activity of RTCB is greatly enhanced by the expression of its cofactor archease (Popow et al., 2014), it appeared likely that full inhibition of RNA ligation activity could only be achieved by a simultaneous depletion of both proteins. For this reason, candidate shRNAs targeting both, RTCB and archease, were designed (see Figure 6), cloned into an shRNA expression vector (see Figure 7A), and tested for their protein depletion efficiency by means of a reporter assay (Fellmann et al., 2013). A full list of all shRNA sequences tested is given in Table 3.

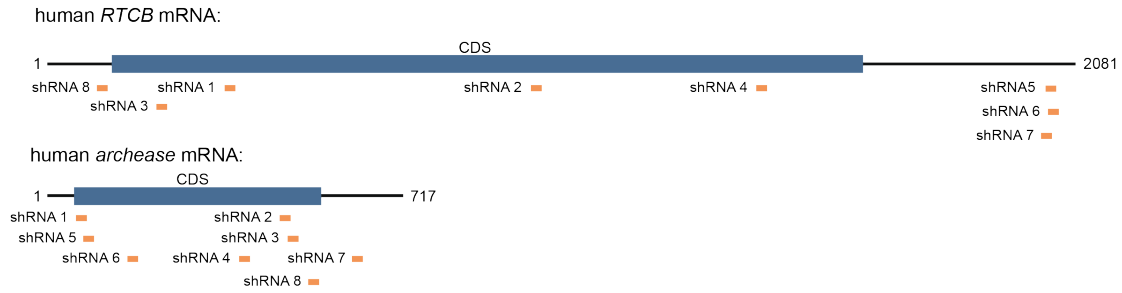

Figure 6: Design of shRNAs targeting human RTCB or archease

To deplete RTCB and archease expression, eight short hairpin RNAs (shRNAs) complementary to the mRNA of RTCB or archease were designed (CDS = coding sequence). The figure shows the position of the nucleotides targeted by the individual shRNAs.

The protein depletion efficiency of the individual shRNAs was determined by means of their depletion efficiency of a reporter construct (see Figure 7). This TtNPT construct was designed to contain the recognition sites of all shRNAs targeting the same mRNA cloned into the 3' UTR of the fluorescent reporter dTomato (Fellmann et al., 2013). Efficient recognition of a target site by its corresponding shRNA would therefore lead to a decrease in the dTomato signal, which can be used as an indicator of shRNAs depletion efficiency. To enable a comparison with shRNAs of known depletion efficiencies, two control RNAs of strong or intermediate depletion activity and their respective target sequences were included in the assay (Fellmann et al., 2013). All shRNAs were cloned into a pLMN-GFP-miR-30 construct (Zuber et al., 2011) enabling a constitutive expression of shRNAs as miR-30 mimetics as well as of GFP to mark shRNA-positive cells.

After cloning, RAg-MEF cells expressing the Tet Repressor to hypothetically enable doxycycline-inducible expression of the TtNPT-encoded Neomycin resistance gene were retrovirally infected using amphotropic packaging of the reporter construct

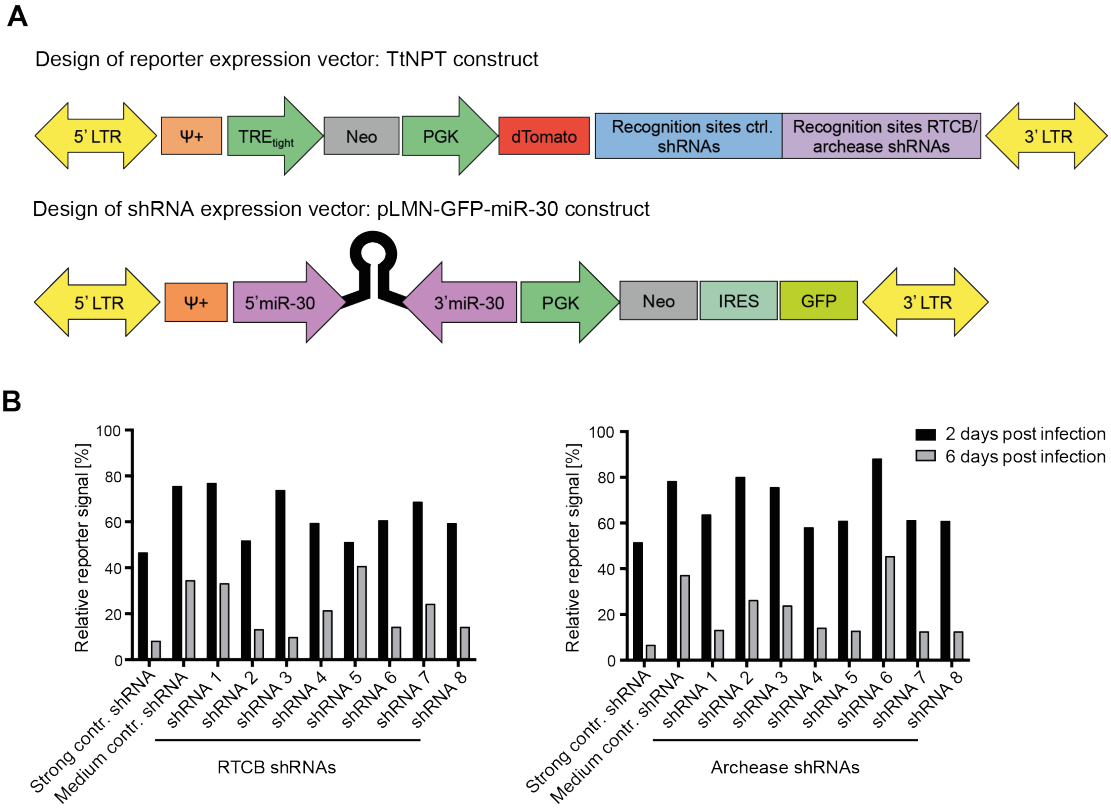

Figure 7: Reporter assay to evaluate shRNA efficiency

To assess the protein depletion efficiency of the individual shRNAs, each RNA sequence was cloned into an shRNA expression vector (**A**) and transduced to RAg-MEF cells stably expressing a fluorescent shRNA reporter construct (the design of the reporter construct is shown in panel **A**) carrying the respective shRNA recognition site in the 3' UTR of dTomato. Two and six days post infection, the evolution of the dTomato signal in relation to shRNA-negative, TtNPT-positive Rag-MEF cells was determined (**B**) and used as a readout for the depletion efficiency of the respective shRNA.

(TtNPT, Figure 7A). Infected cell were enriched by fluorescence-activated cell sorting (FACS) based on dTomato expression and subsequently transduced with one of the corresponding shRNA constructs using ecotropic retroviral packaging. During the following six days, the evolution of the dTomato signal was followed and used to calculate reporter depletion efficiencies (Fellmann et al., 2013). Overall, shRNAs 2 and 3 targeting RTCB and shRNAs 1, 4, 5, 7, and 8 targeting archease showed up to or nearly 90 % silencing efficiency (Figure 7B). Out of these, RTCB shRNA 3 and archease shRNA 5 were chosen for the subsequent generation of inducible Tet-On cell lines.

Generation of tetracycline-inducible HeLa shRNA cell lines

To analyze the effects of diminished tRNA ligase activity, tetracycline-inducible (Tet-On) HeLa cell lines expressing the chosen shRNAs targeting RTCB or archease were generated. For this purpose, RTCB shRNA 3 and archease shRNA 5 were subcloned into doxycycline-inducible shRNA expression vectors (RT3GEN and/or RT3REB, Figure 8A, doxycycline is an antibiotic of the tetracycline class) (Fellmann et al., 2013). These shRNA constructs enable the expression of shRNAs from the 3' UTR of a fluorescent reporter, therefore linking fluorescence intensity with shRNA expression (Zuber et al., 2011). Furthermore, the protein depletion efficiency was increased by exchanging the shRNA backbone to the more efficient miR-E backbone, which is an optimized miR-30 backbone characterized by increased shRNAmir processing (Fellmann et al., 2013).

To enable doxycycline-inducible expression of shRNAs, HeLa cells were infected with a VSV-G pseudotyped lentivirus carrying an rtTA3 construct (Figure 8A). Transduction with this virus did not only implement the expression of the Tet Repressor (rtTA3), but also of a Puromycin resistance gene serving to enrich for rtTA3-positive cells as well as of an ecotropic receptor (EcoR) enabling ecotropic lentiviral infection. These rtTA3-positive cells are referred to as RIEP cells. Following Puromycin selection, HeLa RIEP cells were infected with an ecotropic retrovirus carrying one of the newly generated miR-E-shRNA expression constructs (RT3GEN and/or RT3REB, Figure 8A). In this way, RTCB and archease single depletion Tet-On HeLa cells expressing only RTCB shRNA 3 or archease shRNA 5 as well as an RCTB/archease double depletion cell line expressing both shRNAs were generated (Figure 8B). In addition, control cell lines expressing one or two copies of a control shRNA targeting renilla luciferase were created (Zuber et al., 2011) (Figure 8B).

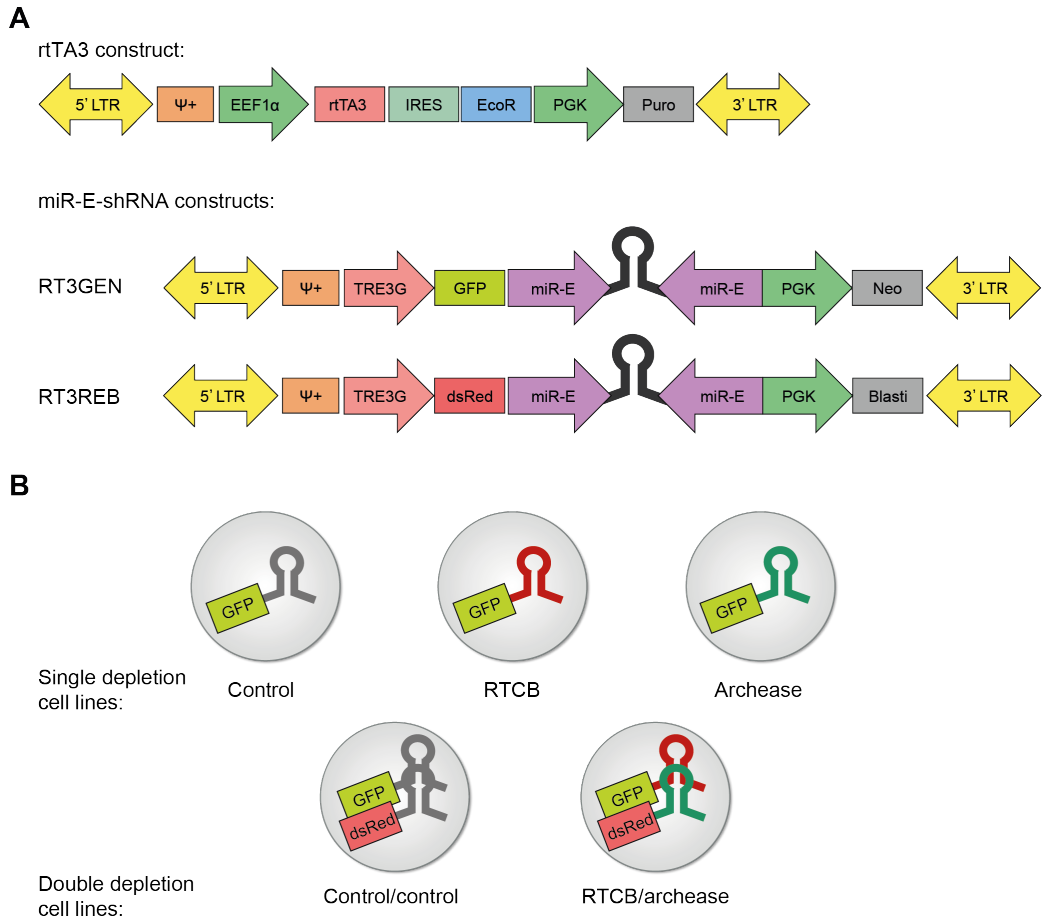

Figure 8: Generation of tetracycline-inducible HeLa shRNA cells lines

To generate RTCB- and/or archease-depleted tetracycline-inducible (Tet-On) cell lines, HeLa cells were transduced with a lentiviral construct expressing the Tet repressor (rtTA3 construct) and one or two retrovirally delivered shRNA constructs (miR-E-shRNA constructs) expressing a fluorescent marker and a short hairpin RNA under the control of a doxycycline-inducible TRE3G promoter (**A**). The thus generated Tet-On HeLa cell lines depleting RTCB and/or archease expression after doxycycline treatment and their respective control cell lines are depicted in panel **B**. An shRNA targeting renilla luciferase was used as control.

The newly generated Tet-On HeLa cell lines were subsequently analyzed for their protein depletion efficiency. After six days of doxycycline treatment, RTCB and archease expression was greatly reduced, both in the respective single depletion cells and in the double depletion cell line. This effect was evident at the protein level as evaluated by Western Blot analysis (Figure 9A) and at the mRNA level as measured by RT-qPCR (Figure 9B). Interestingly, depletion of RTCB but not of archease also decreased the expression of DDX1 and FAM98B, two additional members of the mammalian tRNA ligase complex, while the respective mRNA levels remained unchanged (Figure 9A, B). In addition, *in vitro* RNA ligation activity was evaluated by an interstrand ligation assay using the covalent joining of the two strands of a radiolabeled, double-stranded RNA (dsRNA) substrate as readout for RNA ligation activity (Popow et al., 2011). This assay confirmed that after depletion

of RTCB and/or archease RNA ligation activity was decreased in HeLa cell extracts (Figure 9C). Thereby, RTCB single depletion cells showed pronounced inhibition of RNA ligation in comparison to cells depleted of archease only. Together, these results confirm that using inducible expression of specific shRNAs, RTCB and archease expression can be decreased, which results in diminished tRNA ligation activity *in vitro*.

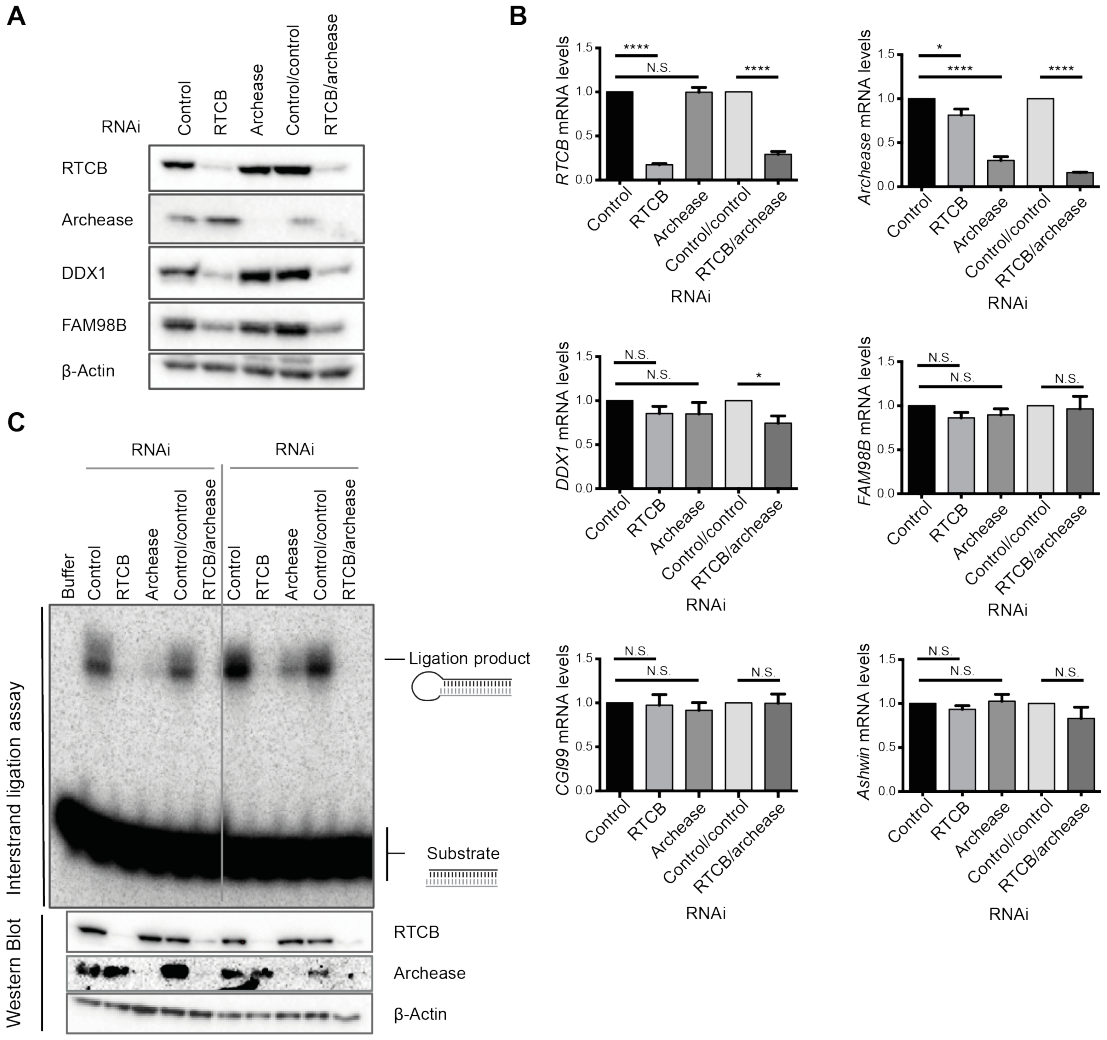

Figure 9: Efficiency of RTCB and archease depletion after doxycycline-inducible expression of short hairpin RNAs in HeLa cells

Tetracycline-inducible (Tet-On) HeLa cells were incubated with 1 µg/ml doxycycline (Dox) for six consecutive days to stimulate the expression of shRNAs targeting RTCB, archease or a non-targeting control. Subsequently, expression levels of tRNA ligase complex members were assayed by Western Blot (**A**, n = 5, representative Western Blot shown) or RT-qPCR (**B**, n = 5, mean expression levels and SEM are displayed). Expression levels were normalized to *ACTB* mRNA levels and to the respective control sample expressing one or two copies of the control shRNA. Unpaired student's t test was used to statistically analyze differences in the mRNA expression levels between control and RTCB- and/or archease-depleted cells (N.S.: not significant, *P < 0.05, **P < 0.01, ***P < 0.001, ****P < 0.0001). Additionally, whole cell lysates were assayed for interstrand ligation activity using a radiolabelled dsRNA substrate (**C**, n = 3, 30 min incubation time, two representative experiments are shown).

RTCB and archease have been linked to tRNA splicing and thus to the maturation of intron-containing pre-tRNAs in eukaryotes and in archaebacteria (Popow et al., 2011; Popow et al., 2014). Although only a subset of tRNAs is encoded by such pre-tRNA sequences, each organism possesses at least one tRNA isoacceptor family of which all or almost all members depend on intron excision in order to become active in translation. In human cells, these include Ile-TAT, Arg-TCT, Tyr-ATA and Tyr-GTA. To analyze the levels of these tRNAs under conditions of decreased tRNA ligase activity, total RNA from RTCB- and/or archease-depleted cells was isolated and examined by Northern Blot using probes specifically recognizing only splicing-dependent mature tRNAs. While RTCB depletion alone had only little effect on the levels of mature Ile-TAT and Arg-TCT transcripts, cells depleted of archease showed a decrease in the expression of splicing-dependent mature tRNAs (Figure 10A). This effect was further enhanced when archease was depleted in conjunction with RTCB (Figure 10B). In contrast, the levels of splicing-independent methionine tRNAs remained unchanged. However, this deficiency in tRNA maturation did not translate to changes in global protein translation rates or the metabolic activity of cells as measured by metabolic labeling (^{35}S-methionine and ^{35}S-cysteine incorporation) (Figure 10C, D) or by a modified MTT assay minimizing proliferation-dependent effects by plating equal amounts of cells shortly before substrate addition (Figure 10E). Taken together, these results indicate that shRNA-mediated depletion of RTCB and archease reduces the levels of splicing-dependent mature tRNAs but—at least after six days of Dox treatment—does not influence protein translation efficiency or the metabolic activity of the affected cells.

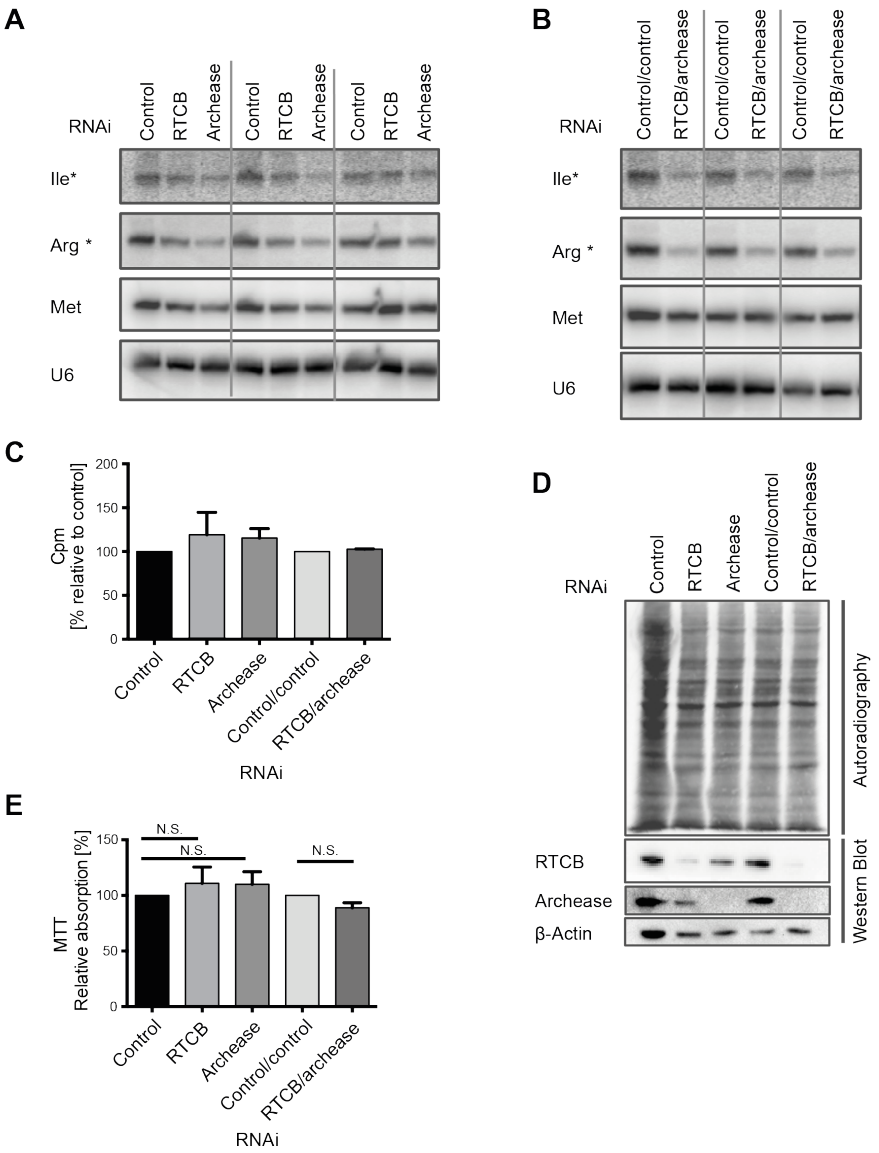

Figure 10: Depletion of RTCB and archease reduces the expression of splicing-dependent mature tRNAs

Tet-On HeLa cells expressing shRNAs targeting RTCB, archease or both and control cell lines expressing one or two copies of the control shRNA were treated with Dox for six consecutive days. Afterwards, total RNA was isolated and analyzed by Northern Blot using DNA probes complementary to the indicated mature tRNAs (**A**, **B**, Intron-containing tRNAs are marked with an asterisk, n = 3). Additionally, on day six of Dox treatment Tet-On HeLa cells were incubated with ^{35}S-labeled methionine and cysteine for one hour and subsequently lysed. Protein translation efficiency was analyzed by scintillation counting of cell lysates (cpm: counts per minute) and normalized to the respective protein concentration as evaluated by BCA assay and to the corresponding control sample (**C**, n = 2, mean and SD are displayed). Lysates were also resolved by SDS-PAGE and analyzed by autoradiography (**D**). Expression levels of RTCB and archease were visualized by Western Blot, whereby β-actin was used as a loading control (**D**). After six days of Dox treatment, Tet-On HeLa cells were also analyzed by MTT assay to measure the metabolic activity of the individual cell lines. Thereby, equal amounts of cells were plated three to four hours before substrate addition to minimize proliferation-dependent effects and to only measure NAD(P)H levels. Absorption was normalized to the respective control sample and statistical significance was analyzed using unpaired student's t test (**E**, n = 4, mean and SEM are displayed, N.S.: not significant, *P < 0.05, **P< 0.01, ***P < 0.001, ****P < 0.0001).

4.2. Depletion of RTCB and archease abrogates the expression of XBP1s after induction of the UPR

Subcellular localization of RTCB and archease

In *S. cerevisiae* the tRNA ligase Trl1 has been shown to catalyze unconventional splicing of the *HAC1* mRNA under conditions of increased protein folding-stress (Sidrauski et al., 1996). Even though this pathway is highly conserved from yeast to mammals, attempts to identify the mammalian UPR ligase have failed (Iwawaki and

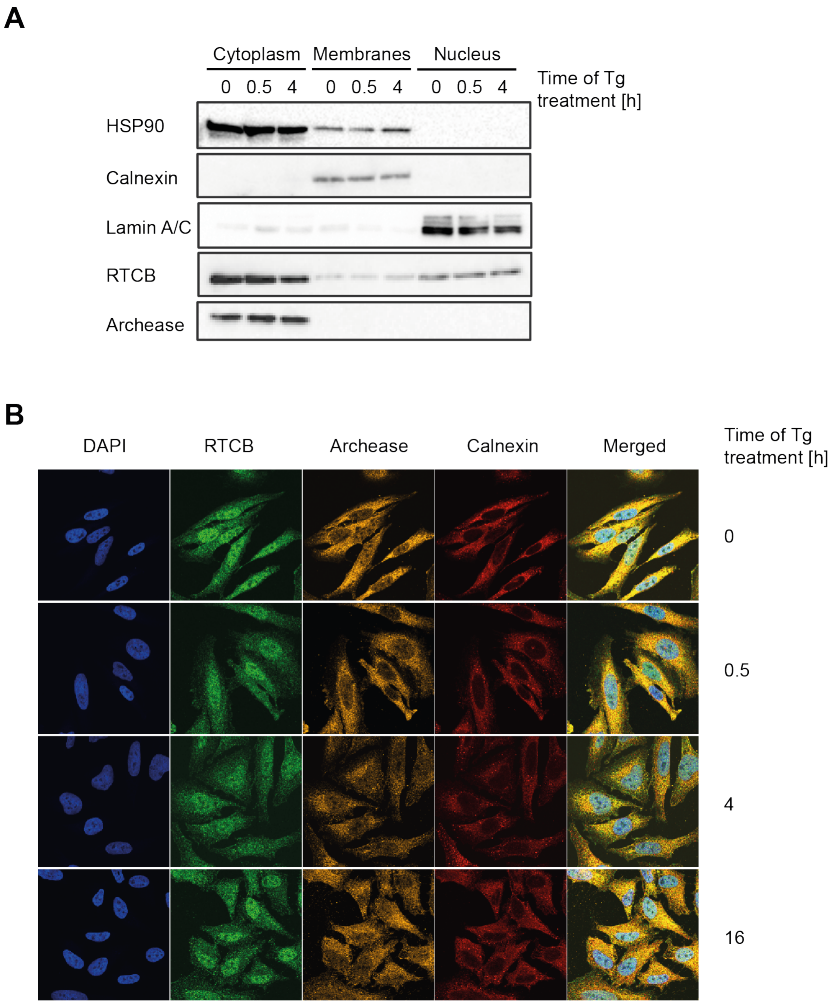

Figure 11: Subcellular localization of RTCB and archease

The subcellular localization of RTCB and archease was assessed by Western Blot analysis of fractions obtained after subcellular fractionation of HeLa cells that were treated with 300 nM thapsigargin (Tg) to induce the UPR or left untreated (**A**). HSP90 (cytoplasm), calnexin (membranes) and lamin A/C (nucleus) were used as marker proteins for the individual fractions collected (n = 5, representative Western Blot is shown). Additionally, the subcellular distribution of RTCB and archease was visualized by immunofluorescence staining of resting HeLa cells or of cells actively undergoing UPR signaling (**B**). The nucleus was visualized by DAPI staining while calnexin staining was used to mark the ER membrane (n = 4).

Tokuda, 2011). As both, the mammalian tRNA endonuclease TSEN and the mammalian UPR endonuclease IRE1α, generate RNA products bearing 2', 3'-cyclic phosphate and 5'-OH termini (Gonzalez et al., 1999; Popow et al., 2012; Shinya et al., 2011), it seemed likely that similar to the situation in yeast, RTCB might be required for the ligation of *XBP1* mRNA exon halves. To test whether the subcellular localization of RTCB and archease would be compatible with this hypothesis, subcellular fractionation (Figure 11A) and immunofluorescence staining (Figure 11B) was performed. RTCB was found to be expressed in the nucleus as well as in the cytoplasm of HeLa cells, which is in agreement with a recent report identifying the tRNA ligase as part of RNA transport complexes shuttling between these two compartments (Perez-Gonzalez et al., 2014). In contrast, archease was enriched in the cytoplasm and also localized to perinuclear regions stained by the ER membrane marker calnexin (Figure 11B). The subcellular distribution of both proteins was stable and did not change upon chemical induction of the UPR using the ER Ca^{2+}-ATPase inhibitor thapsigargin (Tg). Thus, a substantial fraction of RTCB and archease continuously localizes to the vicinity of the ER membrane, which would support an active role of both proteins in the process of unconventional *XBP1* mRNA splicing.

Simultaneous depletion of RTCB and archease abolishes XBP1s expression

To test whether RTCB or archease are required for the expression of XBP1s, depletion of both proteins was induced by doxycycline treatment of the previously generated Tet-On HeLa cells. Following UPR induction through the application of thapsigargin or the protein glycosylation inhibitor tunicamycin (Tm), reduced expression of XBP1s was mainly detected in archease-depleted cells (Figure 12A, B). In contrast, single depletion of RTCB only mildly reduced XBP1s expression. This effect was not only evident at the level of protein expression but also at the mRNA level as revealed by RT-PCR experiments using primers flanking the unconventional splice-site (Figure 12C) and, to a lesser extent, by RT-qPCR (Figure 12D, E). As XBP1s positively regulates its own promoter (Lee et al., 2002; Yoshida et al., 2001), levels of the *XBP1u* mRNA and total *XBP1* mRNA levels were likewise reduced (Figure 12D). Similarly, in comparison to control samples only depletion of archease increased the ratio of the unspliced to the total *XBP1* mRNA (Figure 12E), which is in agreement with the observations obtained by Western Blot analysis. The pronounced effect of archease depletion is surprising, as archease itself does not harbor any RNA ligation activity and is not constitutively associated with the tRNA ligase complex (Popow et al., 2014). These findings therefore indicate that differing from the results obtained by interstrand ligation assay (Figure 9C), which shows that depletion of either RTCB or archease is sufficient to decrease RNA ligation *in vitro*, *in vivo* the stimulatory effect elicited by archease seems to be sufficient to maintain ligation activity in the presence of reduced amounts of RTCB.

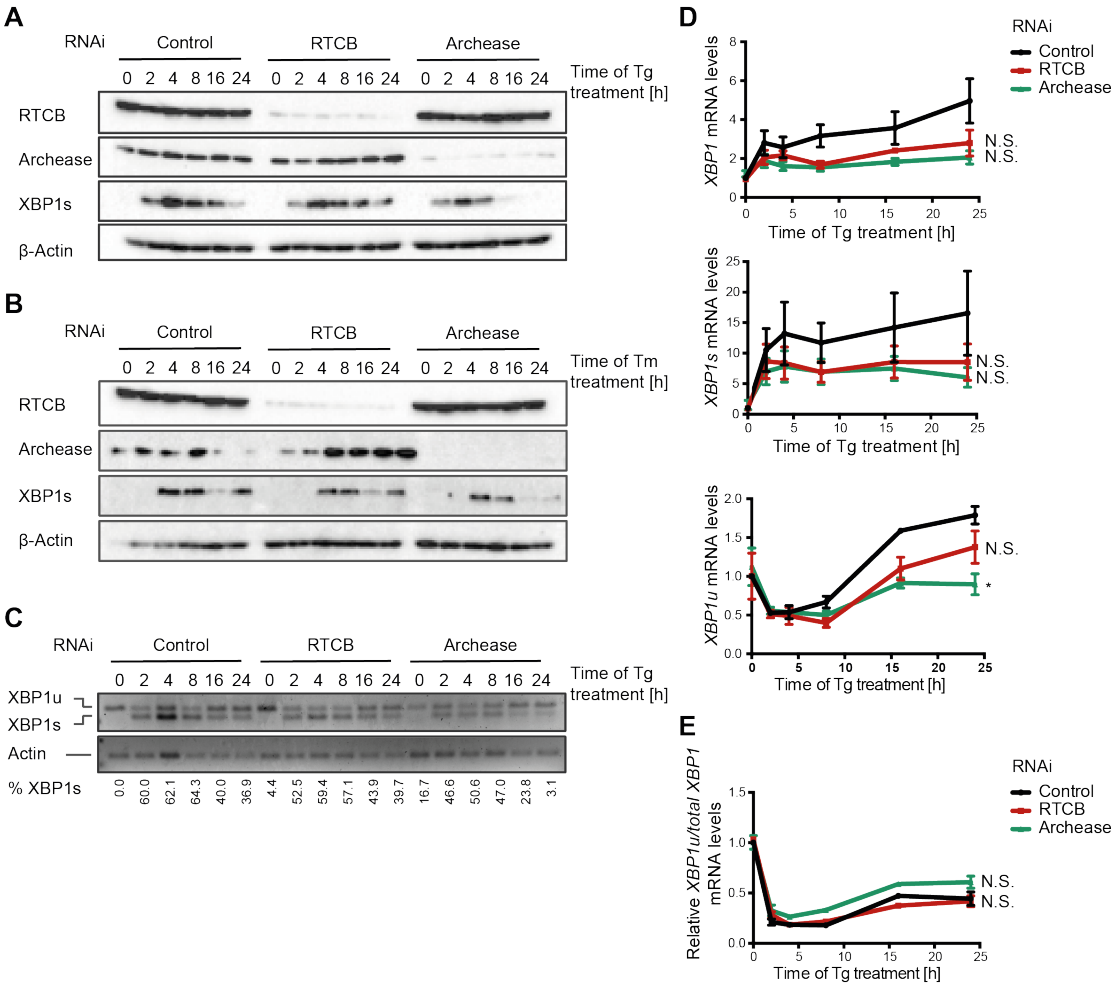

Figure 12: Single depletion of RTCB or archease does not abrogate XBP1s expression

Tet-On HeLa cells were incubated with Dox for six consecutive days to stimulate the expression of shRNAs targeting RTCB, archease or a non-targeting control followed by treatment with 300 nM Tg or 1 µg/ml Tm for the indicated time periods. Induction of XBP1s (XBP1 spliced) expression was monitored by Western Blot (**A, B**, n = 5, representative Western Blots are shown) or RT-PCR (**C**, n = 5) analysis. The relative contribution of the *XBP1s* mRNA to total *XBP1* mRNA levels was analyzed by densitometry. The expression levels of the *XBP1* mRNA and of its individual splicing forms were additionally analyzed by RT-qPCR (**D**, n = 5, mean expression levels and SEM are displayed). Expression levels were normalized to *ACTB* mRNA levels and to the untreated control sample. Likewise, the relative contribution of the *XBP1u* mRNA to the total pool of *XBP1* mRNA was determined by RT-qPCR using the total *XBP1* mRNA as a reference and the untreated control sample for normalization (**E,** n = 4, mean and SEM are displayed). Two-way ANOVA was used to statistically analyze differences in the mRNA expression between control and RTCB/archease-depleted cells (N.S.: not significant, *P < 0.05, **P< 0.01, ***P < 0.001, ****P < 0.0001).

Since depletion of neither RTCB nor archease could abrogate *XBP1* mRNA splicing, both proteins were simultaneously depleted in HeLa cells. In this double depletion Tet-On HeLa cell line XBP1s expression was no longer detectable at the protein level (Figure 13A, B) and greatly reduced at the mRNA level (Figure 13C) after induction of the UPR. Furthermore, RT-qPCR analysis of the individual *XBP1* mRNA isoforms showed that both, the spliced as well as the unspliced mRNA failed to accumulate,

leading to overall reduced *XBP1* mRNA levels, especially at later stages of UPR induction (Figure 13D). Furthermore, the relative expression of *XBP1u* was increased throughout the course of UPR signaling, which is indicative of inhibited mRNA splicing (Figure 13E). These results support the idea that *in vivo* sufficient inhibition of RTCB activity can only be achieved by simultaneous inhibition of its cofactor archease.

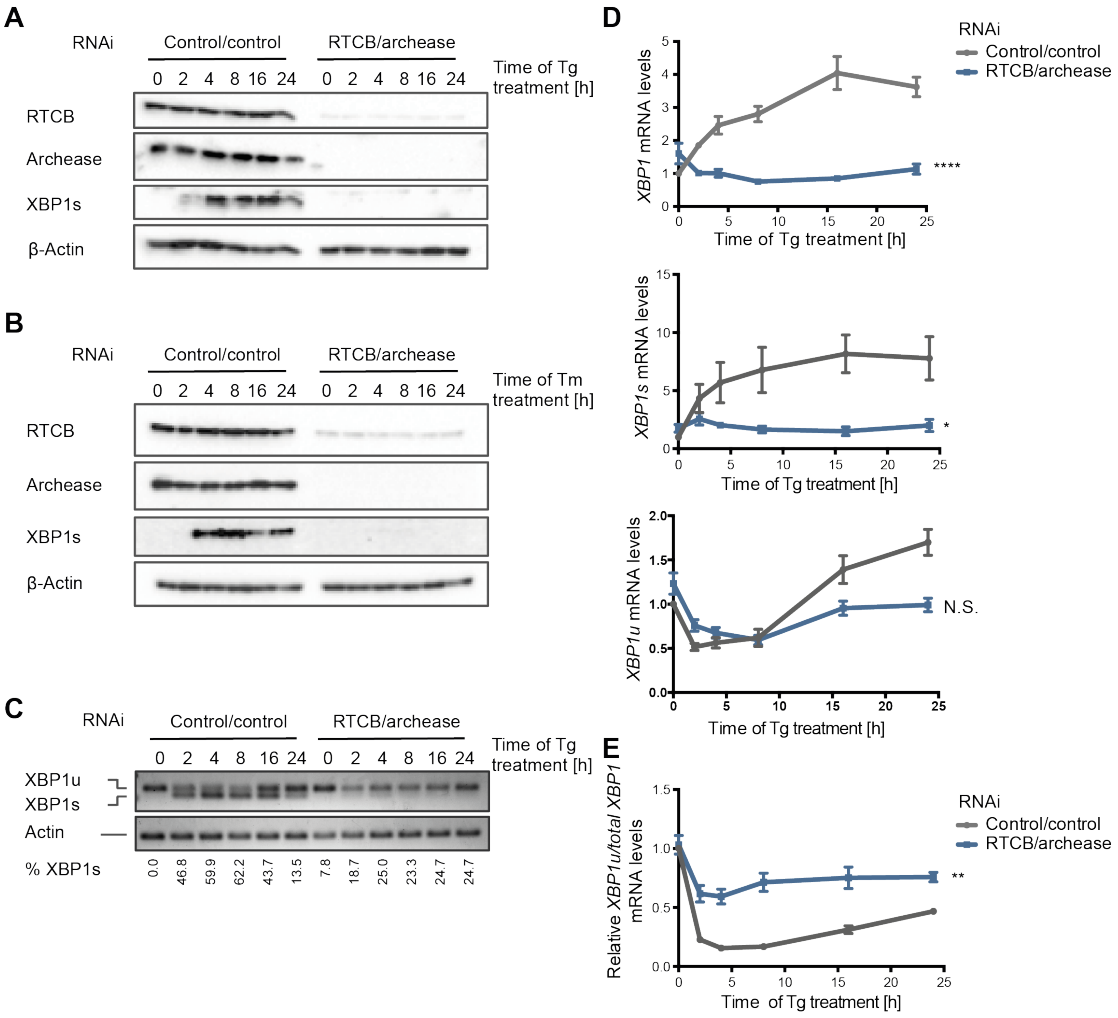

Figure 13: Simultaneous depletion of RTCB and archease abrogates XBP1s expression

Tet-On HeLa cells expressing shRNAs targeting RTCB and archease or a control cell line expressing two copies of the control shRNA were incubated with Dox for six consecutive days to stimulate shRNA expression followed by treatment with 300 nM Tg or 1 µg/ml Tm for the indicated time periods. Induction of XBP1s expression was monitored by Western Blot (**A, B**, n = 5, representative Western Blots are shown) or RT-PCR analysis (**C**, n = 5). The relative contribution of the *XBP1s* mRNA to total *XBP1* mRNA levels was analyzed by densitometry. The expression levels of the *XBP1* mRNA and of its individual splicing forms was additionally analyzed by RT-qPCR (**D**, n = 5, mean expression levels and SEM are displayed). Expression levels were normalized to *ACTB* mRNA levels and to the untreated control sample. Likewise, the relative contribution of the *XBP1u* mRNA to the total pool of *XBP1* mRNA was determined by RT-qPCR using the total *XBP1* mRNA as a reference and the untreated control sample for normalization (**E**, n = 4, mean and SEN are displayed). Two-way ANOVA was used to statistically analyze differences in mRNA levels between control/control and RTCB/archease-depleted cells (N.S.: not significant, *P < 0.05, **P< 0.01, ***P < 0.001, ****P < 0.0001).

After UPR induction, accumulation of XBP1s leads to the transcriptional activation of downstream target genes such as *EDEM1* and *DNAJB9* (Lee et al., 2003), which serve to decrease the load of unfolded proteins in the ER. While in control cells increased expression of the corresponding mRNAs could be observed after 8 to 16 hours of Tg treatment, this response was slightly decreased in single depletion cell lines (Figure 14A) and completely abolished in RTCB and archease double-depleted cells (Figure 14B). These results confirm, that loss of tRNA ligase function by simultaneous depletion of RTCB and archease efficiently abrogates XBP1s expression and thus the induction of XBP1s-specific downstream targets. The small effect exerted by RTCB or archease single depletion furthermore underlines the importance of fully inhibiting tRNA ligase activity in order to disrupt of UPR signaling.

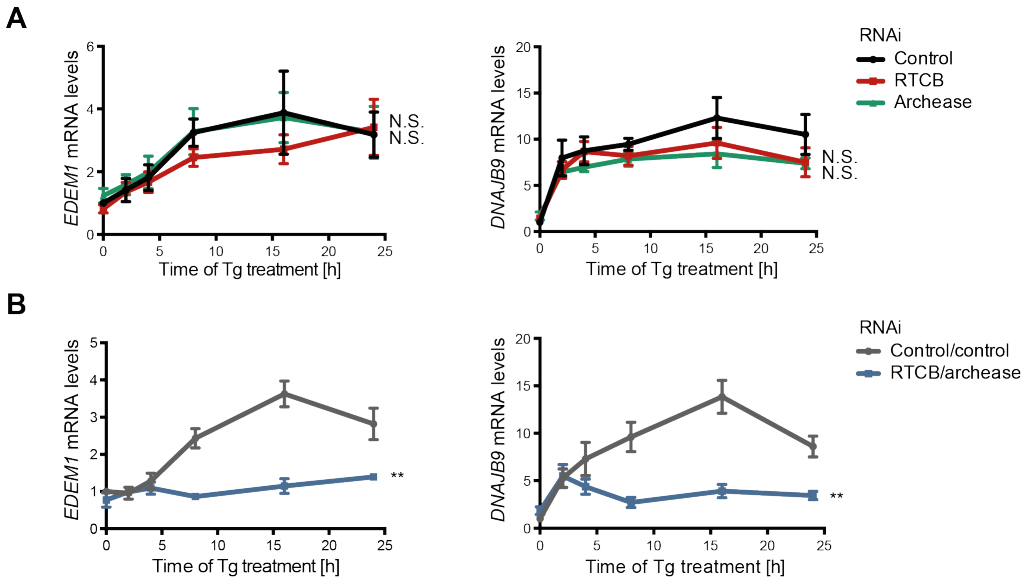

Figure 14: Simultaneous depletion of RTCB and archease abrogates the expression of XBP1s-specific downstream targets

Tet-On HeLa cells expressing shRNAs targeting RTCB or archease (**A**) or both (**B**) and control cell lines expressing one (**A**) or two (**B**) copies of the control shRNA were treated with Dox (six days) and Tg (300 nM, 24 h time course). Subsequently, relative expression levels of the *EDEM1* and *DNAJB9* mRNA were analyzed by RT-qPCR (n = 5, mean expression levels and SEM are displayed). Expression levels were normalized to *ACTB* mRNA levels and to the respective untreated control sample. Two-way ANOVA was used to statistically analyze differences in mRNA expression between control and RTCB- and/or archease-depleted cells (N.S.: not significant, *P < 0.05, **P< 0.01, ***P < 0.001, ****P < 0.0001).

Depletion of RTCB and archease does not inhibit general UPR signaling

Inhibition of unconventional *XBP1* mRNA splicing can result from alterations in RNA ligation efficiency but also from changes in RNA cleavage. To confirm, that depletion of RTCB and archease specifically disrupts mRNA ligation without influencing the endonuclease, expression levels of IREα were checked by Western Blot (Figure 15A) and RT-qPCR analysis (Figure 15B). While the loss of tRNA ligation did not change overall IREα expression, it slightly increased IREα phosphorylation. This effect was especially evident in the absence of Tg treatment (Figure 15A). Yet, in control/control cells and the RTCB- and archease-depleted cell line the RNase activity of IREα was nearly undistinguishable as examined by RT-qPCR analysis of known RIDD target mRNAs such as *BLOS1*, *SCARA3*, and *PDGFRB* (Hollien et al., 2009) (Figure 15C). Only in the absence of chemical induction of the UPR, *SCARA3* mRNA levels were reduced, again pointing towards increased IREα activation. As this effect was lost after Tg treatment, loss of tRNA ligation overall did not profoundly change the RNase activity of IREα, which in turn confirms that the decreased expression of XBP1s and of XBP1s-specific downstream targets observed resulted from inhibition of *XBP1* mRNA splicing at the step of exon ligation rather than at the step of mRNA cleavage.

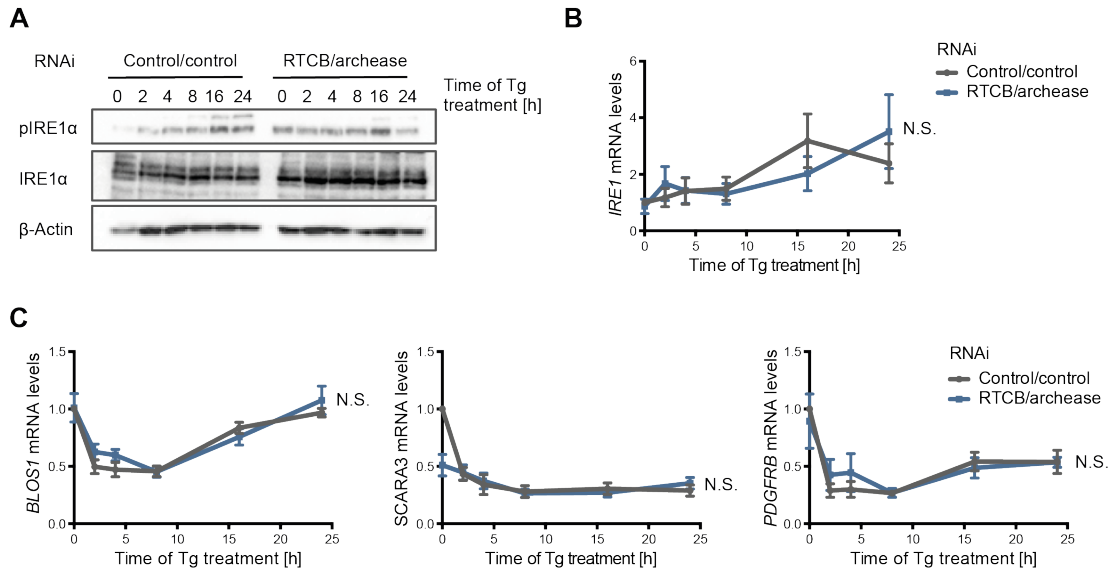

Figure 15: Simultaneous depletion of RTCB and archease increases the phosphorylation of IRE1α but does not greatly influence RIDD activity

RTCB/archease or control/control Tet-On HeLa cells were treated with Dox (six days) and Tg (300 nM, 24 h time course) and analyzed for IRE1α expression levels by Western Blot (**A**, n = 3, representative Western Blot shown) and RT-qPCR (**B**, n = 4, mean expression levels and SEM are displayed). Likewise, the phosphorylation state of IRE1α was visualized by Western Blotting (**A**). Furthermore, relative mRNA levels of the RIDD target genes *BLOS1*, *SCARA3* and *PDGFRB* were analyzed by RT-qPCR (**C**, n = 5, mean expression levels and SEM are displayed). mRNA expression levels were normalized to *ACTB* mRNA levels and to the untreated control sample. Two-way ANOVA was used to statistically analyze differences in mRNA expression between control/control and RTCB/archease-depleted cells (N.S.: not significant, *P < 0.05, **P < 0.01, ***P < 0.001, ****P < 0.0001).

In mammalian cells, accumulation of unfolded proteins in the ER does not only activate the IREα-XBP1 axis of the UPR but also induces PERK and ATF6 signaling. While some UPR downstream targets such as *EDEM1* and *DNAJB9* can be assigned to one of these branches specifically, other mRNAs are regulated by more than just one UPR sensor. The general stress responders BIP and the pro-apoptotic transcription factor CHOP are examples of such general UPR downstream targets (Acosta-Alvear et al., 2007; Chen et al., 2014; Lee et al., 2003; Yamamoto et al., 2004; Yoshida et al., 2001). Consequently, their expression should be less sensitive to changes in XBP1s levels as long as PERK and ATF6 signaling remain intact. This correlation was used to confirm that inhibition of tRNA ligation activity specifically disrupts IRE1α signaling. Using RT-qPCR analysis, the expression of the *BIP* and the *CHOP* mRNA was found to be slightly lowered in RTCB- and archease-depleted HeLa cells (Figure 16A), which is in agreement with loss of XBP1s-driven transcription. These changes in mRNA expression were only mild in comparison to the effects detected on XBP1s-specific downstream targets (Figure 14B) and did not translate to changes in the expression of BIP and CHOP on the protein level (Figure 16B). Accordingly, depletion of the tRNA ligase does not impair general UPR signaling.

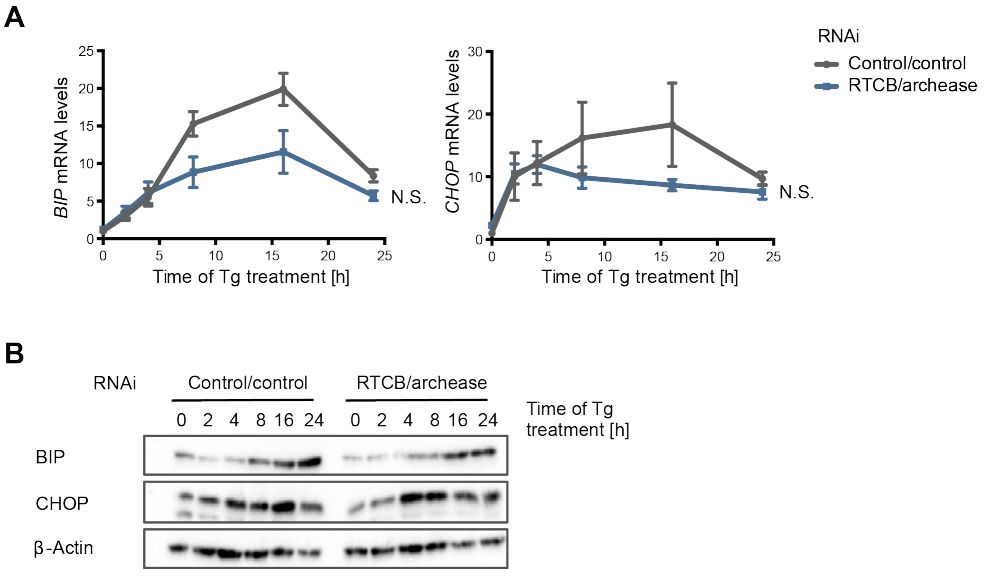

Figure 16: Simultaneous depletion of RTCB and archease only slightly influences the activation of general UPR downstream targets

Tet-On HeLa cells expressing shRNAs targeting RTCB and archease or a control cell line expressing two copies of the control shRNA were treated with Dox (six days) and Tg (300 nM, 24 h time course). Subsequently, cells were analyzed by RT-qPCR for the expression of *BIP* and *CHOP* (**A**, n = 5, normalized to *ACTB* mRNA levels and the untreated control sample, mean expression levels and SEM are displayed) and Western Blot analysis (**B**, n = 3, representative Western Blot shown). Differences in the mRNA expression were analyzed using two-way ANOVA (N.S.: not significant, *P < 0.05, **P< 0.01, ***P < 0.001, ****P < 0.0001).

The unaffected expression of CHOP upon depletion of RTCB and archease suggests that inhibition of tRNA ligation does not hinder the induction of apoptosis under conditions of prolonged ER stress (Hetz, 2012). In order to validate this hypothesis, caspase activation was measured by means of PARP cleavage in untreated cells as well as in Tet-On HeLa cells treated with thapsigargin for 24 hours (Figure 17). Under all conditions examined, inhibition of the tRNA ligase did not restrict PARP cleavage in comparison to single depletion cells and only mildly decreased caspase activation relative to the control/control cell line showing increased toxicity in response to UPR activation. Therefore, loss of RTCB and archease expression did not considerably block the induction of apoptosis. As the UPR-mediated induction of apoptosis amongst others is a consequence of pro-apoptotic PERK signaling (Hetz, 2012; Tabas and Ron, 2011) this result furthermore indicates that the depletion of RTCB and archease did not inhibit PERK activation.

To further confirm the integrity of PERK signaling, PERK expression was analyzed by Western Blot and RT-qPCR analysis (Figure 18). Even though no greater changes could be detected at the mRNA level (Figure 18A), PERK protein levels were found to be slightly elevated after RTCB and archease depletion (Figure 18B). These changes in protein expression were accompanied by an increased activation of PERK signaling as indicated by elevated phosphorylation levels of eIF2α (Figure 18B), which is a direct target of the kinase activity of PERK. Furthermore, mRNA expression levels of the PERK-specific UPR downstream target *ASNS* (Barbosa-Tessmann et al., 1999a; Barbosa-Tessmann et al., 2000; Barbosa-Tessmann et al., 1999b) were increased, especially at early time points of UPR induction and in

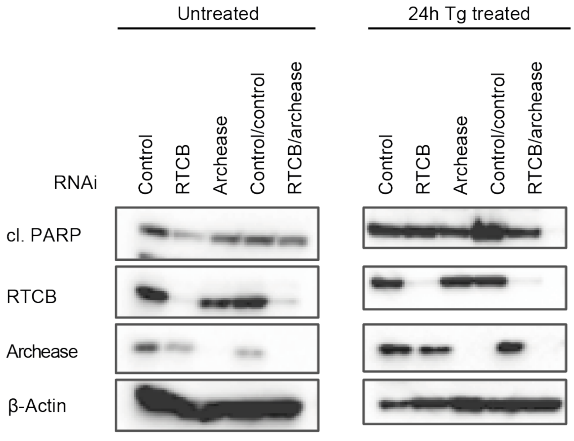

Figure 17: Depletion of RTCB and archease does not inhibit the induction of apoptosis

Tet-On HeLa cells expressing shRNAs targeting RTCB and/or archease and the respective control cell lines were treated with Dox for six consecutive days. Subsequently, the induction of apoptosis in untreated cells or in cells treated with 300 nM Tg for 24 hours was determined by Western Blot based on PARP cleavage (n = 3, respective Western Blots shown).

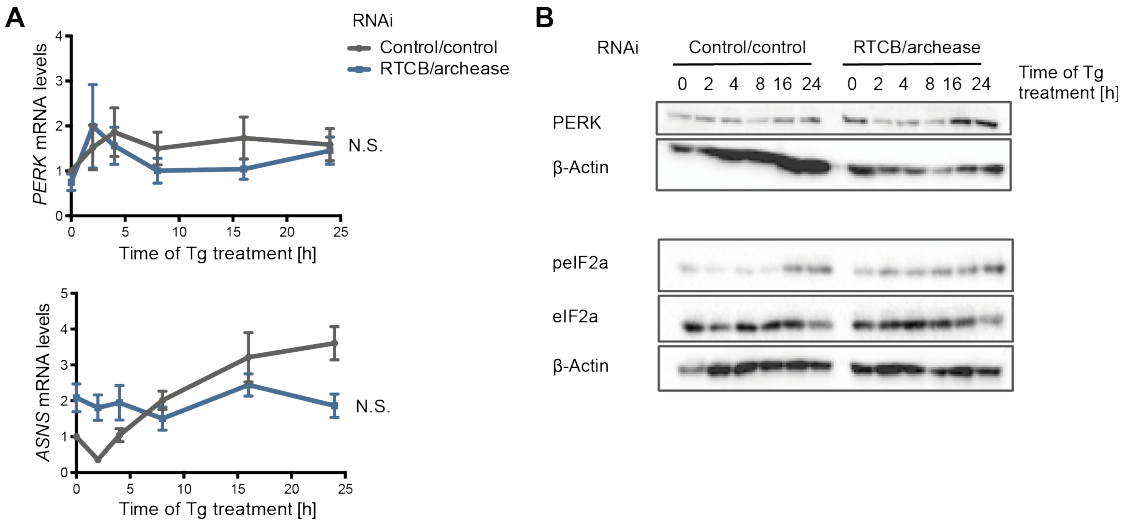

Figure 18: Simultaneous depletion of RTCB and archease does not impair the activation of PERK signaling

Tet-On HeLa cells expressing shRNAs targeting RTCB and archease or a control cell line expressing two copies of the control shRNA were treated with Dox (six days) and Tg (300 nM, 24 h time course). Subsequently, mRNA levels of *PERK* and *ASNS* (**A**) were determined by RT-qPCR (n = 5, normalized to *ACTB* mRNA levels and the untreated control sample, mean expression levels and SEM are displayed). Differences in mRNA expression were analyzed using two-way ANOVA (N.S.: not significant, *P < 0.05, **P< 0.01, ***P < 0.001, ****P < 0.0001). Furthermore, Western Blot analysis was used to monitor the expression levels of PERK and the expression and phosphorylation of eIF2α, a direct downstream target of PERK signaling (**B**, n = 3, respective Western Blot shown).

untreated cells (Figure 18A). Overall, these results confirm, that a loss of tRNA ligation does not generally impair the activation of UPR signaling. Furthermore, these data together with increased phosphorylation levels of IRE1α (Figure 15A) and decreased expression of the *SCARA3* mRNA (Figure 15C) indicate that HeLa cells depleted of RTCB and archease are characterized by a slight increase in protein folding stress in the absence of chemical induction of the UPR.

Overall, this study shows, that the tRNA ligase RTCB and its cofactor archease are required for UPR-induced, unconventional splicing of the *XBP1* mRNA, which therefore constitutes a new function of the mammalian tRNA ligase complex. While *in vitro* depletion of RTCB was enough to inhibit RNA ligation, *in vivo* efficient impairment of tRNA ligase activity could only be achieved by simultaneous depletion of its cofactor archease. Using doxycycline-inducible protein depletion in HeLa cells, RTCB and archease depletion was shown to impair the expression of XBP1s-specific downstream targets while it did not block the activation of IRE1α itself or signaling events mediated by other branches of the UPR. Therefore, the mammalian tRNA ligase complex is a new and central factor of mammalian UPR signaling.

4.3. Depletion of RTCB and archease influences cellular signaling pathways and cell proliferation in HeLa cells

Simultaneous depletion of RTCB and archease influences signal transduction in HeLa cells

Besides the splicing of intron-containing pre-tRNA sequences (Popow et al., 2011) and the unconventional splicing of the *XBP1* mRNA as part of UPR signaling (Jurkin et al., 2014; Kosmaczewski et al., 2014; Lu et al., 2014) no further substrates could yet be assigned to the mammalian tRNA ligase complex. Given that RNA ligases in general fulfill a multitude of differing functions (see section 3.1) and that in mammalian cells up to now no other RNA ligase activity could be identified, it seemed plausible that RTCB might be required for the regulation of additional cellular processes.

To characterize and identify new functions of the mammalian tRNA ligase complex, RNA sequencing was performed in control/control as well as in RTCB- and archease-depleted HeLa cells. Using this method, 104 mRNAs were found to be significantly upregulated while the expression of 129 mRNAs, including the mRNAs encoding for RTCB and archease itself, was decreased after loss of tRNA ligation (see Table 6 and Figure 19). When cells were treated with thapsigargin to induce protein-folding stress, the number of mRNAs with increased abundance remained largely constant (114 mRNAs) while the number of mRNAs with decreased expression levels rose to 267 mRNAs (see Table 8 and Figure 19). This reinforcing effect of thapsigargin treatment is probably caused by loss of XBP1s-dependent transcription as some of the main XBP1s-specific downstream targets (e.g. *EDEM1* and *DNAJB9*) as well as the *XBP1* mRNA itself failed to accumulate in Tg-treated RTCB/archease Tet-On HeLa cells.

Even though the mRNA transcriptomes of Tet-On HeLa cells were more strongly impacted by Tg treatment and thus UPR induction than by the loss of tRNA ligation activity (see Table 6 and Table 8), a subset of mRNAs was found to be solely regulated in a RTCB- and archease-dependent way. This effect exerted by the tRNA ligase complex seemed to be separate from its role in UPR signaling as these transcriptome changes were evident independently of thapsigargin treatment. To more thoroughly characterize the set of mRNAs influenced by RTCB and archease expression, gene ontology (GO) term analysis was applied (Table 7). This analysis as well as a subsequent confirmation by RT-qPCR analysis revealed that the simultaneous depletion of RTCB and archease mainly changed the abundance of mRNAs involved in signal transduction (Figure 20).

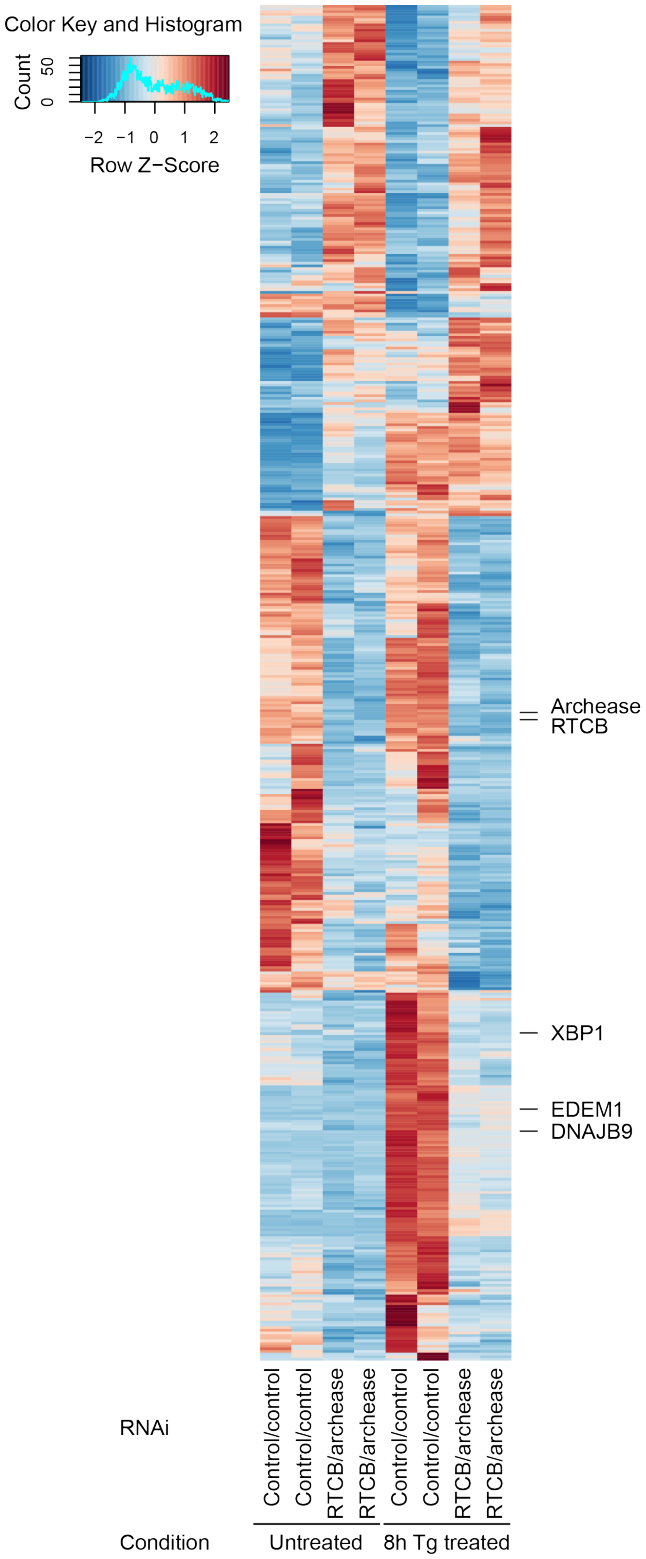

Figure 19: Depletion of RTCB and archease changes the mRNA transcriptome of HeLa cells

To identify RTCB- and archease-dependent mRNA transcriptome changes, total RNA from untreated or Tg-treated (300 nM, 8 h) Tet-On HeLa cells expressing shRNAs targeting RTCB and archease or two copies of the control shRNA was isolated and analyzed by next generation sequencing (Illumina, n = 2). The heat map displays the expression profile of all mRNAs differentially expressed after six days of Dox treatment (adjusted p-value ≤ 0,05).

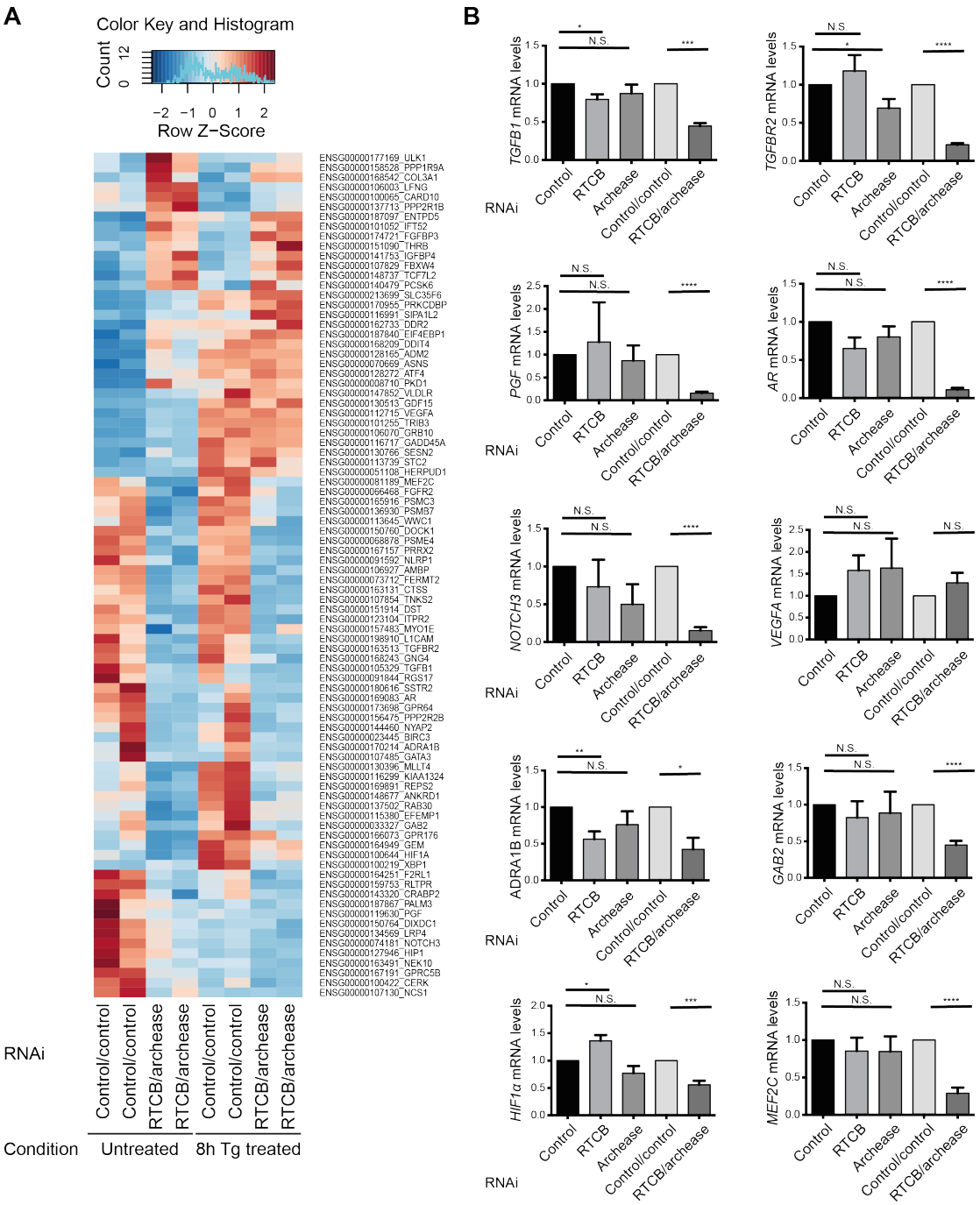

Figure 20: In HeLa cells, depletion of RTCB and archease affects the abundance of mRNAs involved in signal transduction

Total RNA from control/control and RTCB/archease-depleted cells treated with Tg (300 nM, 8 h) or left untreated was analyzed by next-generation sequencing (Illumina, n = 2). The heat map (**A**) shows the expression profile of mRNAs encoding for signal transduction components (GO:0007165) whose expression was significantly altered after loss of tRNA ligation (adjusted p-value ≤ 0,05). Some of these RTCB- and archease-dependent expression changes were subsequently verified by RT-qPCR (**B**, n = 4, mean and SEM are displayed). Expression levels were normalized to *ACTB* mRNA levels and to the respective untreated control sample. Differences in the mRNA levels were analyzed using unpaired student's t test (N.S.: not significant, *P < 0.05, **P< 0.01, ***P < 0.001, ****P < 0.0001).

The mRNA profile changes related to signal transduction suggest that in HeLa cells a depletion of RTCB and archease might cause alterations in the activation of signaling cascades. To test this hypothesis, Western Blot analysis was performed in single- as well as in double-depleted Tet-On HeLa cells. While TGFβ signaling (measured by SMAD2 phosphorylation) and the expression of the androgen receptor (AR) were greatly reduced after depletion of RTCB and archease, no differences in the activation of mTOR complexes or the protein kinase AKT could be detected under these conditions (Figure 21A). In contrast, phosphorylation and thus activation of ERK1/2 was enhanced after loss of tRNA ligase activity. When cells were additionally treated with Tg to induce stress signaling, the phosphorylation levels of the MAPK JNK were likewise reduced (Figure 21B). Interestingly, some of these alterations such as increased phosphorylation and activation of ERK1/2 or decreased phosphorylation of JNK could already be detected under single depletion conditions, even though these effects were not as reproducible as the changes observed in double-depleted cells. Therefore, the loss of tRNA ligation was found to influence the activation of diverse signaling cascades in HeLa cells.

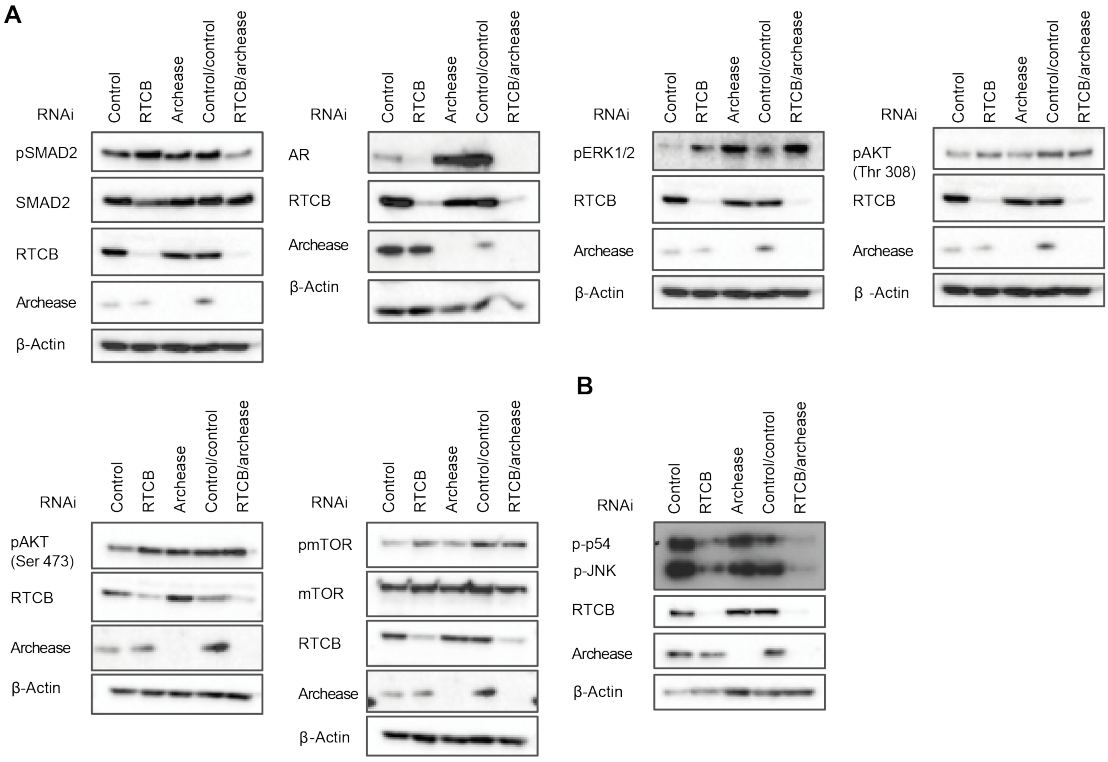

Figure 21: Depletion of RTCB and archease influences the activity of signaling pathways

Tet-On HeLa cells expressing shRNAs targeting RTCB and/or archease and the respective control cell lines were treated with Dox for six consecutive days and phosphorylation levels of SMAD2, ERK1/2, AKT as well as mTOR and the expression level of the androgen receptor (AR) were analyzed Western Blot analysis of resting cells (**A**, n = 3, respective Western Blot shown). After 24 hours of Tg treatment (300 nM), phosphorylation levels of JNK were likewise visualized by Western Blotting (**B**, n = 3, respective Western Blot shown).

Depletion of RTCB and archease decreases the proliferation of HeLa cells

The phosphorylation of the MAP kinase ERK1/2 as well as of AKT and SMAD2 are signaling events activated by growth factors and mitogens that are signaling via receptor tyrosine kinases or G protein-coupled receptors to regulate and activate cell growth and proliferation (Figure 33, Figure 34, and Figure 36). Similarly, JNK phosphorylation can be induced by growth factor signaling (Figure 35). Since the RNA sequencing dataset implied that several growth factors or mitogens themselves (such as TGFβ1, PGF and VEGFA), their receptors (AR, FGFR2, DDR2, ADRA1B, SSTR2, TGFBR2), and different components involved in signal transduction (such as GAB2 and MEF2C) were altered in abundance upon depletion of RTCB and archease, it appeared possible that inhibition of tRNA ligation might lead to changes in the proliferation of the affected cells. This hypothesis was further supported by changes in the activation of various signaling cascades (Figure 21) and by GO term analysis showing that in HeLa cells depletion of RTCB and archease affects the abundance of mRNAs involved in a positive regulation of cell proliferation (Figure 22, Table 7).

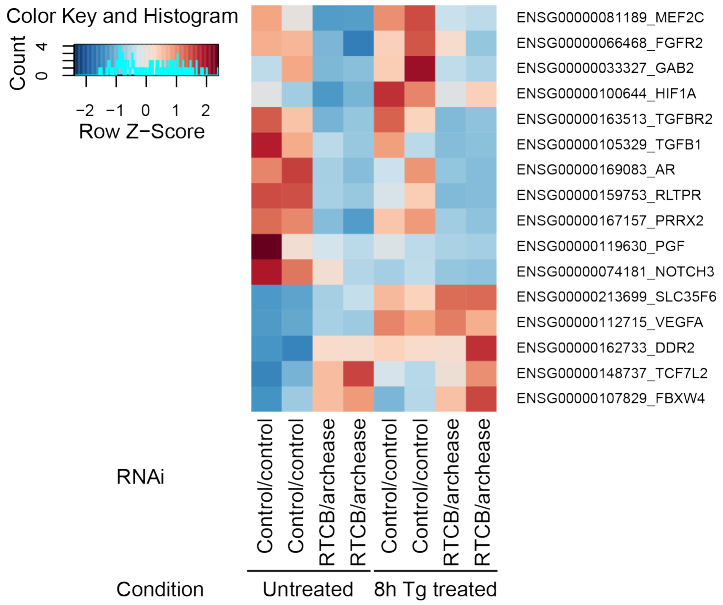

Figure 22: Depletion of RTCB and archease affects the abundance of mRNAs involved in a positive regulation of cell proliferation

Total RNA from control/control and RTCB/archease-depleted HeLa cells treated with Tg (300 nM, 8 h) or left untreated was isolated after six days of Dox treatment and subsequently analyzed by RNA sequencing (Illumina, n = 2). The heat map shows the expression profile of mRNAs involved in a positive regulation of cell proliferation (GO:0008284) whose expression was significantly influenced by a loss of RTCB and archease activity (adjusted p-value ≤ 0,05).

In order to study a possible function of the tRNA ligase complex in the regulation of cell growth and proliferation, RTCB- and/or archease-depleted Tet-On HeLa cells were analyzed for their proliferation kinetics using the cell-tracking agent CellTrace Violet (Figure 23). Nine days after induction of shRNA expression and four days after cell-labeling, the CellTrace signal was nearly completely diluted in both control and in RTCB or archease single depletion cells (Figure 23A, B). In comparison, fading of the CellTrace signal was delayed in RTCB and archease double depletion cells, which is indicative of decreased proliferation kinetics. Additionally, loss of tRNA ligation activity resulted in a progressive decline of the cell volume (Figure 23C). Even though the observed effect overall is relatively weak, it confirms that the tRNA ligase complex is involved in the regulation of the cellular growth potential of HeLa cells.

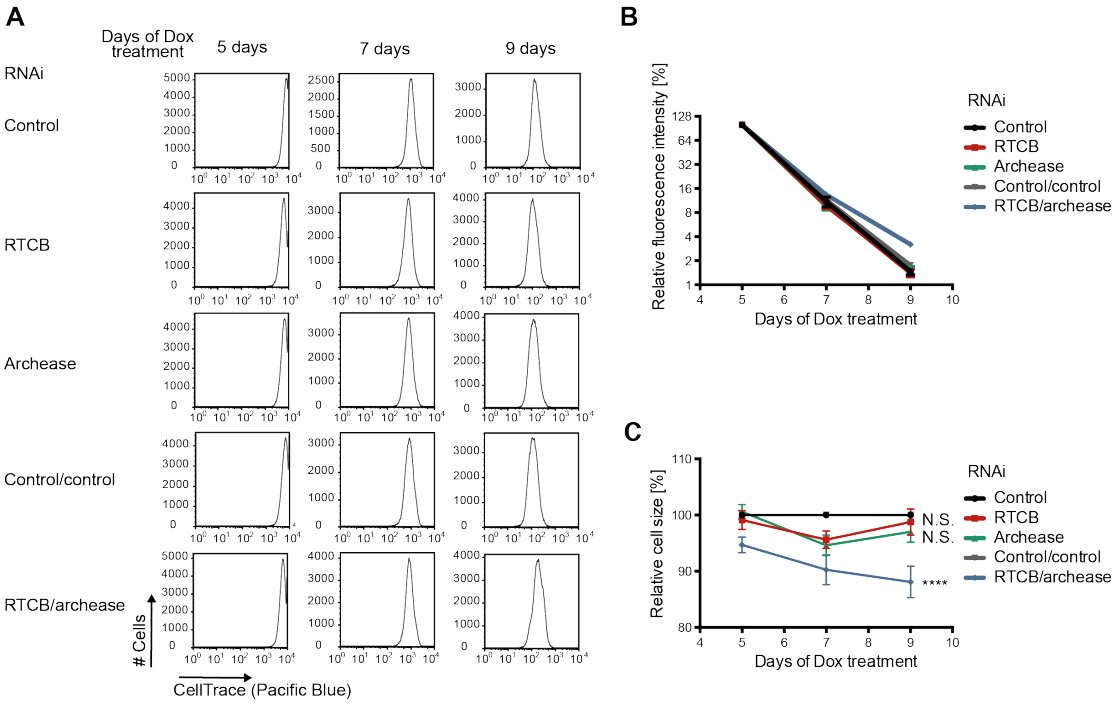

Figure 23: Depletion of RTCB and archease decreased the proliferation rate and the size of Tet-On HeLa cells

Tet-On HeLa cells were incubated with 1 µg/ml Dox for five consecutive days to stimulate the expression of shRNAs targeting RTCB, archease or a non-targeting control. On day five cells were labeled with the cell-tracking agent CellTrace Violet. Subsequently, the CellTrace signal was analyzed by flow cytometry to determine relative proliferation rates. Representative histograms of the individual cell lines are shown in panel **A**. The evolution of the CellTrace signal relative to the initial staining signal is summarized in panel **B** (n = 5, mean and SEM are displayed). The relative size of the cell lines as determined by their respective FCS signals are summarized in panel **C** (n = 5, mean and SEM are displayed). Two-way ANOVA was used to analyze differences in cell size (N.S.: not significant, *P < 0.05, **P< 0.01, ***P < 0.001, ****P < 0.0001).

The detected drop in cell proliferation could be caused by increased cell death, an overall slowdown of cell cycle progression or by accumulation of cells in a specific phase of the cell cycle. To analyze, which of these possibilities is responsible for reduced proliferation kinetics after loss of tRNA ligase activity, Tet-On HeLa cells were analyzed for PARP cleavage by Western Blot (Figure 24). Furthermore, cell cycle profiling was conducted using Hoechst 33342 staining (Figure 25A, B). Even after prolonged depletion of RTCB and archease, no increase in PARP cleavage and thus caspase activation could be observed (Figure 24, see also Figure 17), arguing against the occurrence of increased apoptosis. In contrast, loss of tRNA ligase activity influenced the cell cycle profile of Tet-On HeLa cells by significantly increasing the relative amount of cells in the G_0/G_1 phase of the cell cycle (Figure 25B, Table 1). Consequently, less cells actively undergoing DNA replication (S phase) or cell division (G_2/M phase) could be detected after depletion of RTCB and archease. Again, this effect was only evident after simultaneous depletion of archease and thus under conditions of diminished RNA ligation activity.

To confirm that a simultaneous depletion of RTCB and archease influences the cell cycle profile of HeLa cells, bromodeoxyuridine (BrdU) pulse labeling was used to visualize cells actively undergoing DNA replication. For this purpose, shRNA expression and thus protein depletion was induced by doxycycline treatment of Tet-On HeLa cell lines, which subsequently were incubated with BrdU-containing culture medium. After this pulse phase, incorporation of BrdU into newly synthesized DNA was detected using an APC-conjugated anti-BrdU antibody and flow cytometry analysis (Figure 25C, D). Similar to what could have been observed with Hoechst

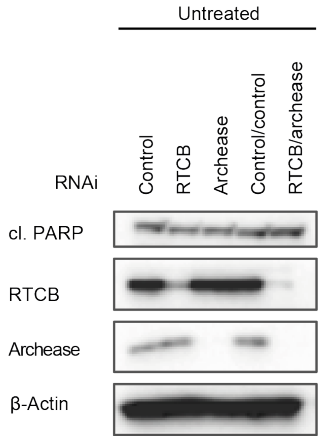

Figure 24: Prolonged RTCB and archease depletion does not increase the induction of apoptosis

Tet-On HeLa cells expressing shRNAs targeting RTCB and/or archease and the respective control cell lines were treated with Dox for nine consecutive days and the induction of apoptosis was assayed by means of PARP cleavage and Western Blot analysis (n = 3, respective Western Blot shown).

33342 staining, depletion of RTCB and archease significantly decreased the fraction of replicating cells. This effect was already evident after RTCB single depletion while archease-depleted HeLa cells were indistinguishable from control cell lines. Overall, these results confirm, that loss of tRNA ligase function influences cell cycle progression and thus cell proliferation by a yet unknown mechanism in HeLa cells.

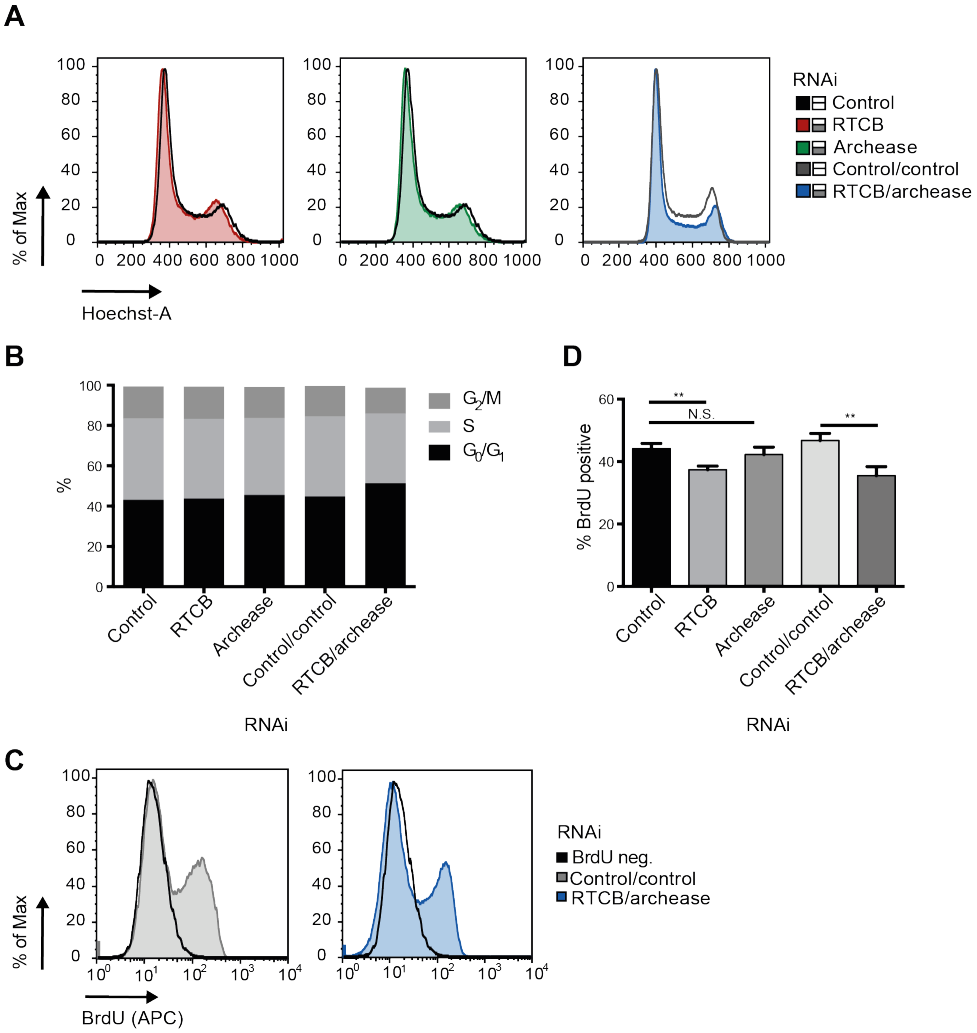

Figure 25: Cell cycle profile of HeLa cells depleted of RTCB and/or archease

Tet-On HeLa cells were incubated with 1 µg/ml Dox for six consecutive days to stimulate the expression of shRNAs targeting RTCB, archease or a non-targeting control. On day six, the DNA content of these cells was labeled with Hoechst 33342 and analyzed by flow cytometry. Representative histograms of all cell lines analyzed are shown in panel **A**. For analysis, histograms were fitted using the "pragmatic approach" of Watson (Ormerod et al., 1987; Watson et al., 1987). Mean percentages of cells in the individual cell cycle phases are displayed in panel **B** (n = 6). Furthermore, the relative fraction of cells actively undergoing DNA replication was determined by BrdU pulse labeling. For this purpose, cells were incubated with BrdU for one hour, fixed, stained with an APC-conjugated anti-BrdU antibody and analyzed by flow cytometry. Panel **C** shows two representative histograms of control/control and RTCB/archease-depleted cells. Mean percentages and the SEM are shown in panel **D** (n = 8)**.** Unpaired student's t test was used to statistically analyze differences between the individual cell lines (N.S.: not significant, *P < 0.05, **P< 0.01, ***P < 0.001, ****P < 0.0001).

Table 1: Cell Cycle profile of Tet-On HeLa cells as evaluated by Hoechst 33342 staining

RNAi	G_0/G_1			S			G_2/M		
	Mean [%]	SEM [%]	N	Mean [%]	SEM [%]	N	Mean [%]	SEM [%]	N
Control	43,017	1,140	6	40,467	0,674	6	15,867	1,334	6
RTCB	43,733	0,838	6	39,583	1,067	6	16,000	0,904	6
Archease	45,417	0,957	6	38,217	1,073	6	15,533	0,897	6
Control/control	44,700	1,287	6	39,733	1,392	6	15,167	1,284	6
RTCB/archease	51,267	1,319	6	34,633	1,133	6	12,855	0,836	6

The table lists the data displayed in Figure 25B. The relative distribution of cell cycle phases was obtained using Hoechst 33342 staining and flow cytometry analysis. The raw data was analyzed using FlowJo software (Treestar) and the "pragmatic approach" of Watson (Ormerod et al., 1987; Watson et al., 1987). SEM: standard error of the mean, N: number of experiments.

From yeast to mammals, cell cycle progression requires the expression of cyclins regulating the activity of so-called cyclin-dependent kinases (CDKs). As the name already suggests, the expression of cyclins oscillates as the cell cycle proceeds. Thereby, cyclin expression is regulated at the level of mRNA stability, translational control and subcellular localization but the two main regulatory mechanisms compromise transcriptional regulation and ubiquitin-dependent proteolysis (Duronio and Xiong, 2013). Many cyclin mRNAs are bound by RTCB based on PAR-CLIP data (Baltz et al., 2012) indicating that the tRNA ligase might be involved in the regulation of cyclin expression by potentially affecting mRNA stability, which in turn might influence the proliferation phenotype observed after depletion of RTCB and archease. To test this hypothesis the expression levels of different cyclins were analyzed by Western Blot (Figure 26A) and RT-qPCR analysis (Figure 26B). Even though slight changes in the expression levels of A-type, B-type and D-type cyclins could be observed, these variations were small and mainly reflected the alterations in cell cycle progression detected using cell cycle profiling and BrdU labeling (Figure 25). However, if one or more cyclin mRNAs would depend on RTCB for expression or stabilization, the corresponding mRNA and protein levels should be drastically reduced after loss of tRNA ligase expression, similar to what has been observed for *XBP1s* mRNA levels. As this was not the case, the tRNA ligase complex does not seem to be involved in the regulation of cyclin expression and thus appears to influence cell cycle progression by means of a different mechanism.

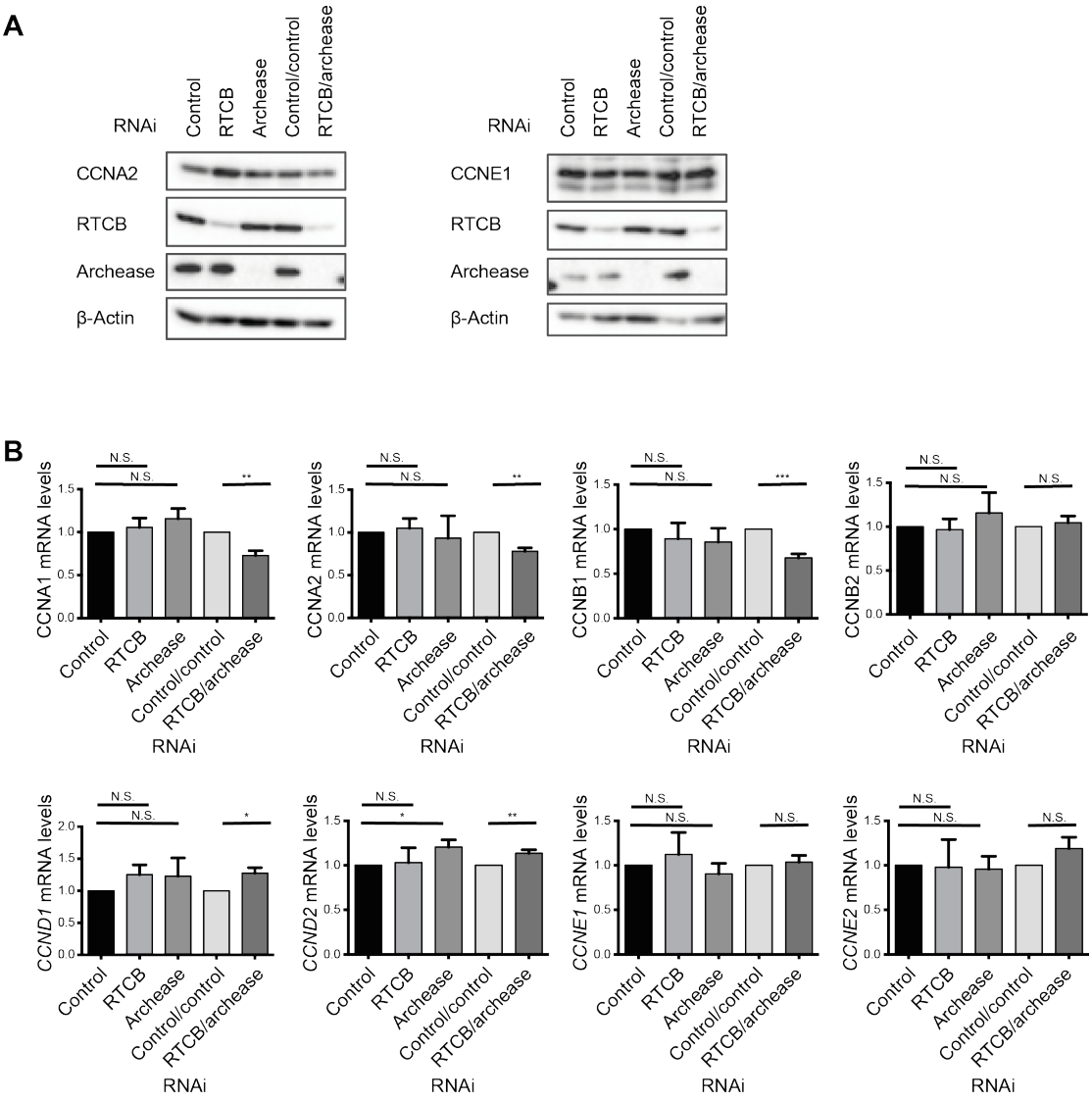

Figure 26: Depletion of RTCB and archease does not greatly affect the expression levels of cyclins

Tet-On HeLa cells expressing shRNAs targeting RTCB and/or archease and the respective control cell lines were treated with Dox for six consecutive days, whereafter the expression levels of cyclin A2 and E1 were analyzed by Western Blot analysis (**A**, n = 3, representative Western Blots shown). Furthermore, RT-qPCR was used to determine mRNA expression levels of *CCNA1*, *CCNA2*, *CCNB1*, *CCNB2*, *CCND1, CCND2*, *CCNE1* and *CCNE2* (**B**, n = 4, mean and SEM are displayed). Expression levels were normalized to *ACTB* mRNA levels and to the respective control sample. Differences in the mRNA levels were analyzed using unpaired student's t test (N.S.: not significant, *P < 0.05, **P< 0.01, ***P < 0.001, ****P < 0.0001).

In Tet-On HeLa cells, variations of the mRNA transcriptome, proliferation rate or signal transduction activity after loss of tRNA ligase function are independent from XBP1s expression

The abundance of mRNAs is regulated by the equilibrium between transcription and RNA degradation. The pronounced downregulation of mRNAs observed after depletion of RTCB and archease could thus result from decreased transcriptional activation or reduced mRNA stability. As to the current knowledge the tRNA ligase complex does not function as transcriptional activator, RTCB might influence the abundance of mRNAs by increasing their stability. However, most of the possible RTCB mRNA targets identified by RNA sequencing such as the mRNAs encoding for androgen receptor (AR), NOTCH3, and ADRA1B, do no directly interact with RTCB based on PAR-CLIP data (Baltz et al., 2012). It therefore seems likely, that the tRNA ligase complex impacts on the expression of these RNAs by means of an indirect mechanism, which might involve transcriptional regulation.

The only RTCB-dependent transcription factor identified so far is XBP1s (Jurkin et al., 2014; Kosmaczewski et al., 2014; Lu et al., 2014). Even though this protein is characterized by increased expression upon UPR induction, lower levels of XBP1s are expressed ER stress-independently and serve to mediate the transcription of a subset of target genes in the absence of acute protein folding stress (Acosta-Alvear et al., 2007; Shen et al., 2005; Wang et al., 2015). In contrast to UPR-induced upregulation, this constitutive XBP1s expression mainly drives developmental programs (Bettigole et al., 2015; Hasegawa et al., 2015; Reimold et al., 2000; Tohmonda et al., 2011; Zeng et al., 2013). Accordingly, loss of XBP1s activity might cause the proliferative and transcriptional defects observed after depletion of the tRNA ligase.

To test this hypothesis, XBP1s was overexpressed in RTCB/archease or control/control Tet-On HeLa cells (Figure 27). Increased expression of XBP1s on the protein (Figure 27A) as well as on the mRNA level (Figure 27B) resulted in rescued expression of XBP1s-specific downstream targets after induction of the UPR (Figure 27C) confirming that the overexpression construct used is transcriptionally active. However, overexpression of XBP1s failed to rescue proliferation kinetics (Figure 28A) or the decrease in cell volume observed after inhibition of tRNA ligase function (Figure 28B). Similarly, XBP1s rescue cells were indistinguishable from mock-infected RTCB- and archease-depleted HeLa cells in terms of activation of signaling pathways and the expression of mRNAs involved in signal transduction (Figure 28C, D, E). The function of the tRNA ligase complex in the regulation of cell proliferation, cell volume and the activation of cellular signaling pathways thus is XBP1s-independent.

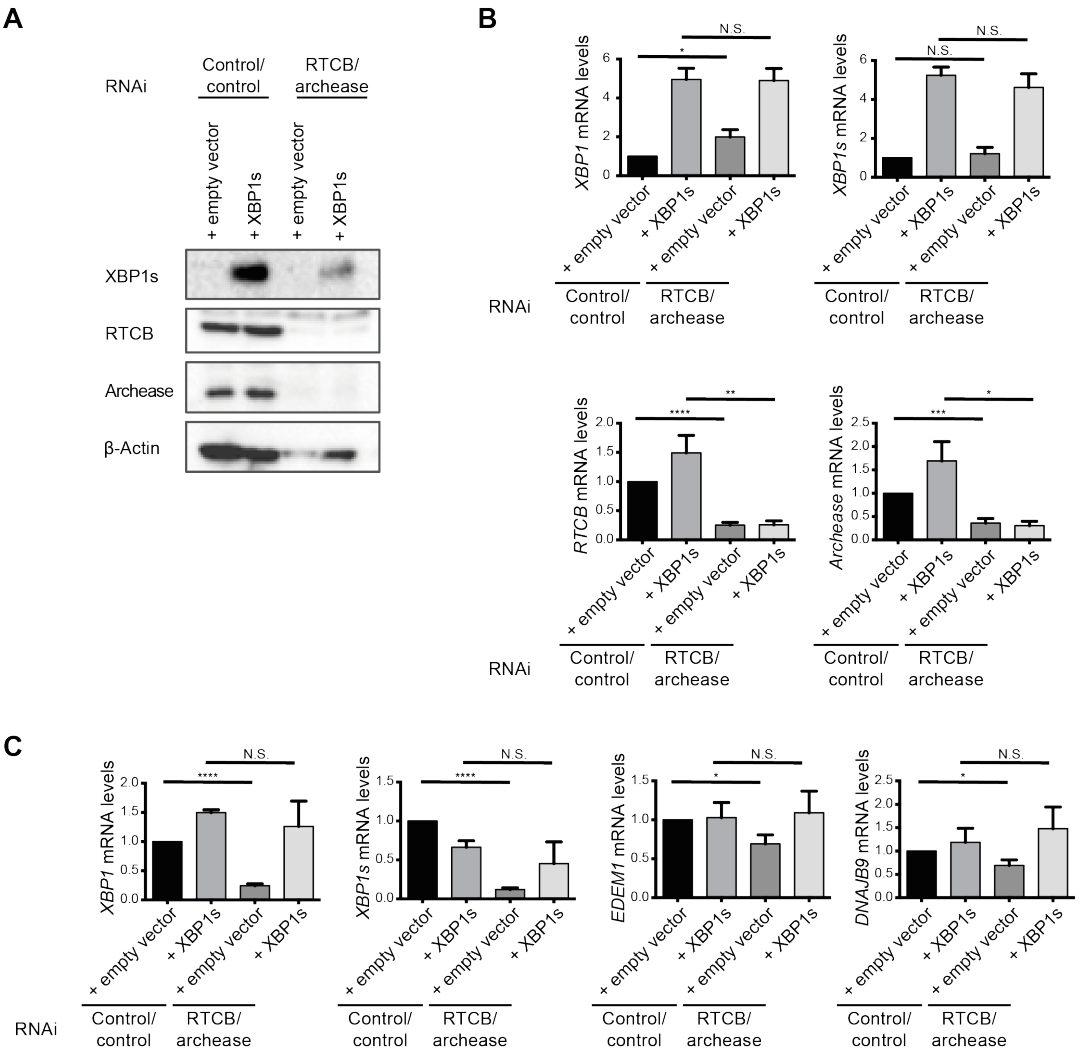

Figure 27: Overexpression of XBP1s increases the expression of XBP1s-specific downstream targets despite depletion of RTCB and archease

The transcription factor XBP1s was overexpressed in Tet-On HeLa cells expressing two copies of the control shRNA or two shRNAs targeting RTCB and archease. Infection with an empty vector served as control. After six days of Dox treatment and induction of RTCB and archease depletion, XBP1s overexpression in the absence of UPR stress was confirmed by Western Blot (**A**, n = 3, representative Western Blot shown) and RT-qPCR analysis (**B**, n = 5, mean and SEM are displayed). Furthermore, after treatment with 300 nM Tg for 8 hours expression levels of XBP1s-specific UPR downstream targets were analyzed by RT-qPCR (**C**, n = 5, mean and SEM are displayed). Expression levels were normalized to *ACTB* mRNA levels and to the control/control + empty vector sample. Differences in mRNA expression were analyzed using unpaired student's t test (N.S.: not significant, *P < 0.05, **P < 0.01, ***P < 0.001, ****P < 0.0001).

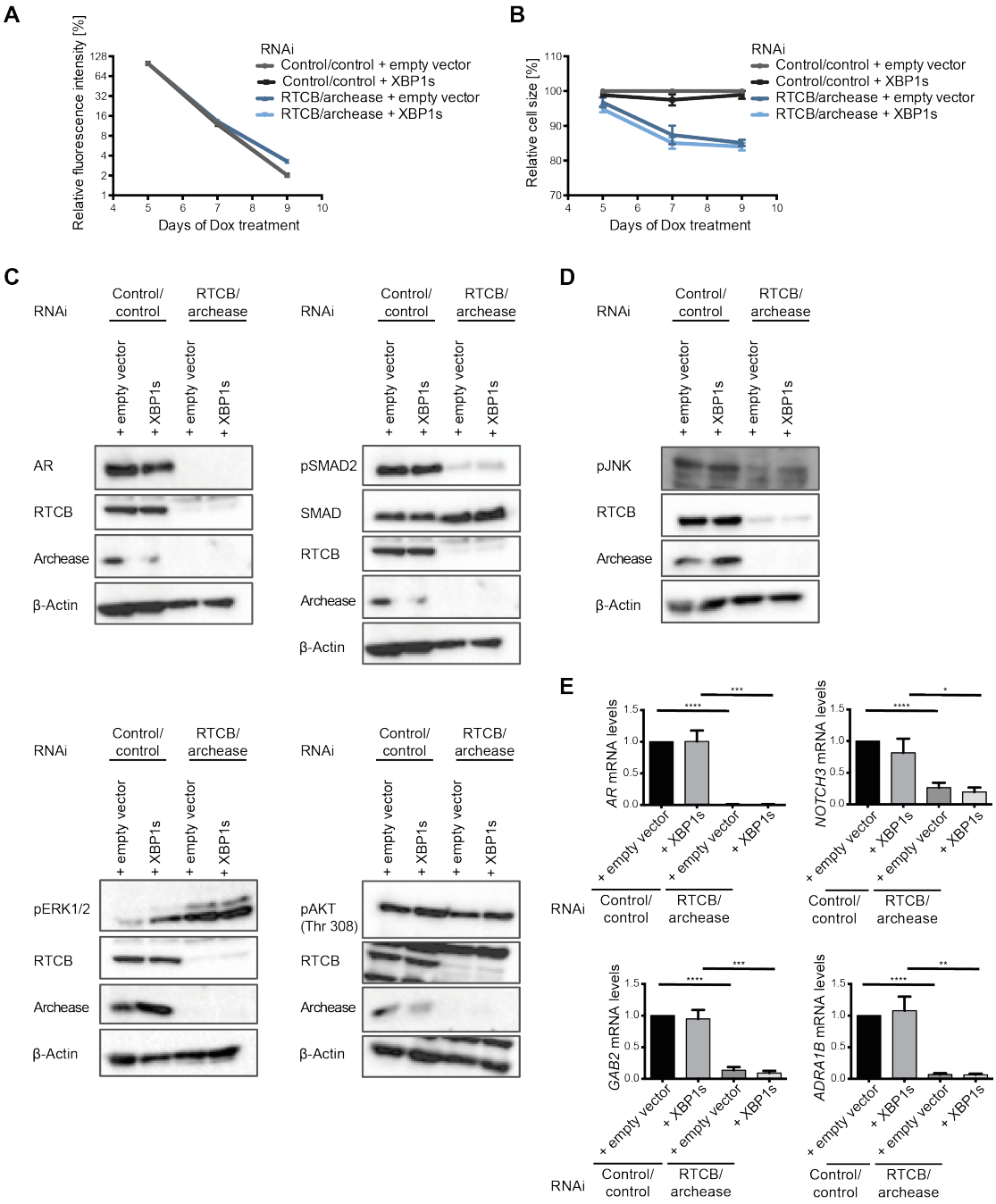

Figure 28: Overexpression of XBP1s does not rescue proliferation defects or changes in signal transduction activity and mRNA abundance after depletion of RTCB and archease

The transcription factor XBP1s was overexpressed in control/control and RTCB/archease Tet-On HeLa cells. Infection with an empty vector served as control. After five days of Dox treatment, cells were labeled with the cell-tracking agent CellTrace Violet. During the following four days, the relative intensity of the CellTrace signal was measured by flow cytometry (**A**, n = 4) and the cell volume was determined using the mean FCS signal (**B**, n = 4). To determine the activation status of different signaling pathways, Western Blot analysis of untreated (**C**, n = 3) or Tg treated cells (300 nM, 24 hours, **D**, n = 3) was used. RT-qPCR analysis was applied to determine the expression levels of the *AR, NOTCH3, GAB2*, and *ADRA1B* mRNAs (**E**, n = 5, mean and SEM are displayed). Expression levels were normalized to *ACTB* mRNA levels and to the control/control + empty vector sample. Differences in mRNA expression were analyzed using unpaired student's t test (*P < 0.05, **P< 0.01, ***P < 0.001, ****P < 0.0001).

RTCB and archease were not found to catalyze additional unconventional mRNA splicing events

Besides XBP1s, the mammalian tRNA ligase complex might also regulate other transcription factors in a similar, splicing-dependent way. In order to test this hypothesis, RNA from control/control and RTCB/archease-depleted HeLa cells was analyzed by paired-end sequencing to detect RTCB-dependent alternative splicing events (see Table 2). Non-canonical splice junctions were included in the analysis. Splicing events occurring at the canonical GT donor and AG acceptor splice sites as well as at less abundant GC-AG and AT-AC splice junctions and at the reverse complementary motifs (CT-AC, CT-GC and GT-AT) were considered as canonical splicing (Burset et al., 2000; Parada et al., 2014). In contrast, splicing events occurring at other splice junctions were defined as non-canonical and therefore as possible unconventional splicing events, which might be catalyzed by proteins other than the spliceosome. Besides unconventional splicing of the *XBP1* mRNA this analysis identified only one additional tRNA ligase-dependent unconventional splicing event, which occurs in the *SPECC1* mRNA. However, since unconventional splicing of *SPECC1* occurs with higher frequency under conditions of depleted tRNA ligase function, this splicing reaction most likely is not catalyzed by RTCB. Therefore, additional unconventional mRNA splicing events catalyzed by RTCB do not seem to account for the transcriptome changes observed.

Table 2: Alternative splicing events significantly influenced by the depletion of RTCB and archease in HeLa cells

Name	Adj. p-value	RTCB/archease		Control/control		Intron length [nt]	Motif	Position
		Sample 1 [Counts]	Sample 2 [Counts]	Sample 1 [Counts]	Sample 2 [Counts]			
NCOA7	0,0000	50,00	36,00	212,00	194,00	1511	canonical	chr6:126240578–126242088
KRT7	0,0000	20,00	14,00	45,00	37,00	2363	canonical	chr12:52626576–52628938
SHMT2	0,0000	24,00	18,00	–	1,00	142	canonical	chr12:57624444–57624585
USP40	0,0004	3,00	7,00	34,00	39,00	178	canonical	chr2:234398130–234398307
STX8	0,0009	–	–	15,00	16,00	241183	canonical	chr17:9153963–9395145
TTC39C	0,0014	9,00	9,00	–	–	2262	canonical	chr18:21593006–21595267
TNPO3	0,0025	33,00	24,00	8,00	5,00	23399	canonical	chr7:128658212–128681610
PDE4D	0,0038	31,00	38,00	8,00	4,00	1183	canonical	chr5:58334799–58335981
NCOA7	0,0055	30,00	21,00	7,00	7,00	384	canonical	chr6:126107360–126107743
RPL27A	0,0136	64,00	63,00	10,00	19,00	88	canonical	chr11:8705465–8705552
EPB41L2	0,0148	1,00	–	15,00	23,00	21377	canonical	chr6:131184859–131206235
MYOF	0,0177	–	–	11,00	8,00	1910	canonical	chr10:95117680–95119589
USH1C	0,0246	36,00	17,00	5,00	5,00	1132	canonical	chr11:17526245–17527376
CPSF3L	0,0248	2,00	2,00	19,00	11,00	750	canonical	chr1:1255086–1255835
FXYD5	0,0272	4,00	4,00	29,00	12,00	2294	canonical	chr19:35657075–35660468
SPG11	0,0282	–	–	9,00	6,00	147	canonical	chr15:44891035–44891181
RB1CC1	0,0309	12,00	17,00	5,00	3,00	416	canonical	chr8:53598081–53598496
SPECC1	**0,0316**	**14,00**	**5,00**	**–**	**–**	**35**	**non-canonical, possible uncon-ventional**	**chr17:20135559–20135593**
METTL15	0,0316	–	–	8,00	8,00	3178	canonical	chr11:28307797–28310974
RTN4	0,0336	5,00	3,00	27,00	15,00	37387	canonical	chr2:55214835–55252221
XBP1	**0,0352**	**4,00**	**–**	**25,00**	**9,00**	**26**	**non-canonical, possible uncon-ventional**	**chr22:29192112–29192137**
FYN	0,0354	3,00	1,00	17,00	23,00	324	canonical	chr6:112101839–112102162
SNRPG	0,0369	16,00	11,00	2,00	3,00	3302	canonical	chr2:70516505–70519806
SEPW1	0,0389	5,00	2,00	26,00	16,00	2049	canonical	chr19:48282072–48284120
SNRNP70	0,0398	50,00	37,00	7,00	15,00	642	canonical	chr19:49604729–49605370
METTL15	0,0458	–	–	10,00	5,00	566	canonical	chr11:28311185–28311750

RTCB/archease-dependent alternative splicing events were detected by the analysis of paired-end sequencing data (Illumina, n = 2) using STAR (v2.4.2a). All splicing events at GT-AG, GC-AG, AT-AC, CT-AC, GT-AT, CT-GC splice junctions were considered as canonical splicing events, the rest as possible unconventional splicing events. Adj. p-value: Adjusted p-value, nt: nucleotides, chr: chromosome.

4.4. Depletion of RTCB and archease in cancer cell lines

If the transcriptome changes observed after depletion of RTCB and archease in HeLa cells were specifically caused by changes in tRNA ligase activity, it should be possible to recapitulate this phenotype in other human cell lines. For this purpose, RTCB/archease-depleted Tet-On cancer cell lines as well as the respective control/control cells were generated by retroviral transduction of shRNA-expression constructs. Two pancreatic cancer cell lines (PANC-1 and MIA PaCa-2), one triple-negative breast cancer cell line (EFM-192A) and one acute lymphocytic leukemia cell line (Reh cells) were chosen based on decreased expression levels of the androgen receptor in RTCB/archease Tet-On HeLa cells (Figure 20, Figure 21 and Table 6) and the involvement of XBP1s in the pathogenesis of triple-negative breast cancer (Chen et al., 2014) and lymphocytic leukemia (Tang et al., 2014). Following six days of Dox treatment, protein depletion efficiencies were analyzed by Western Blot (Figure 29), which showed that all RTCB/archease RNAi cell lines exhibited a markedly reduced expression of both proteins. Furthermore, since XBP1s expression levels can be used as an indicator of tRNA ligase activity, cells were treated with thapsigargin before harvesting. Probing for XBP1s expression confirmed that in PANC-1, MIA PaCa-2, and EFM-192A cells the decreased expression of RTCB and archease translated into decreased tRNA ligase activity, whereby the MIA PaCa-2 cell line showed the most pronounced effect (Figure 29). In Reh cells, however, XBP1s expression could not be detected by Western Blot analysis. Overall, these results confirmed, that Dox-inducible expression of shRNAs can also be used to deplete RTCB and archease expression in cancer cell lines, even though the overall effect on tRNA ligase activity detected was diminished in comparison to Dox-treated Tet-On RTCB/archease HeLa cells (compare Figure 9A).

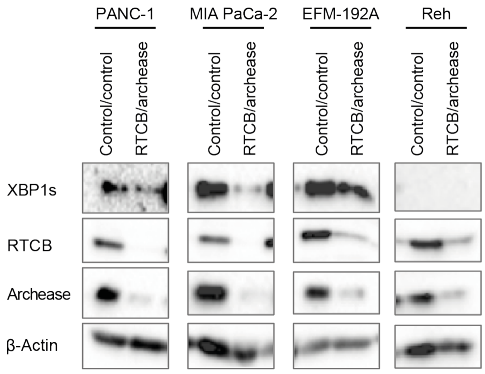

Figure 29: Depletion efficiency of RTCB and archease in Tet-On cancer cell lines

RTCB/archease Tet-On cancer cell lines were treated with Dox for six consecutive days to induce shRNA expression and subsequently treated with 100 nM Tg for 4 h to induce UPR signaling. Depletion of RTCB and archease and XBP1s expression levels indicative of tRNA ligase function were assayed by Western Blot analysis (n = 3, representative Western Blots shown).

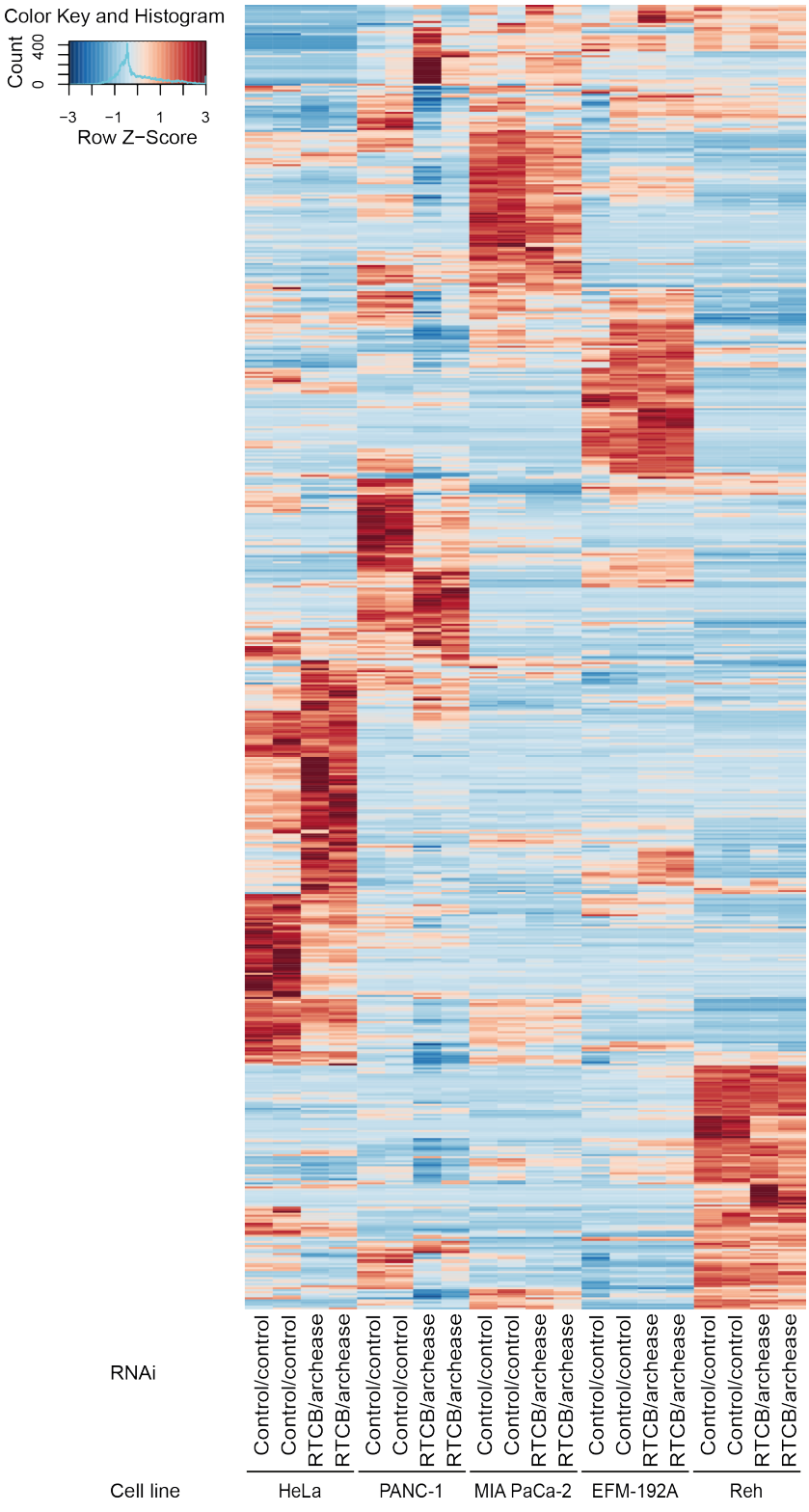

Figure 30: Transcriptome changes after depletion of RTCB and archease in Tet-On cell lines

Tet-On cells expressing shRNAs targeting RTCB and archease and the respective control cell lines were treated with Dox for six consecutive days to induce shRNA expression. Following protein depletion, total RNA was isolated and analyzed by next generation sequencing (Illumina, n = 2). The heat map displays the expression profile of all mRNAs differentially expressed after depletion of RTCB and archease in any Tet-On cell line (adjusted p-value ≤ 0,05).

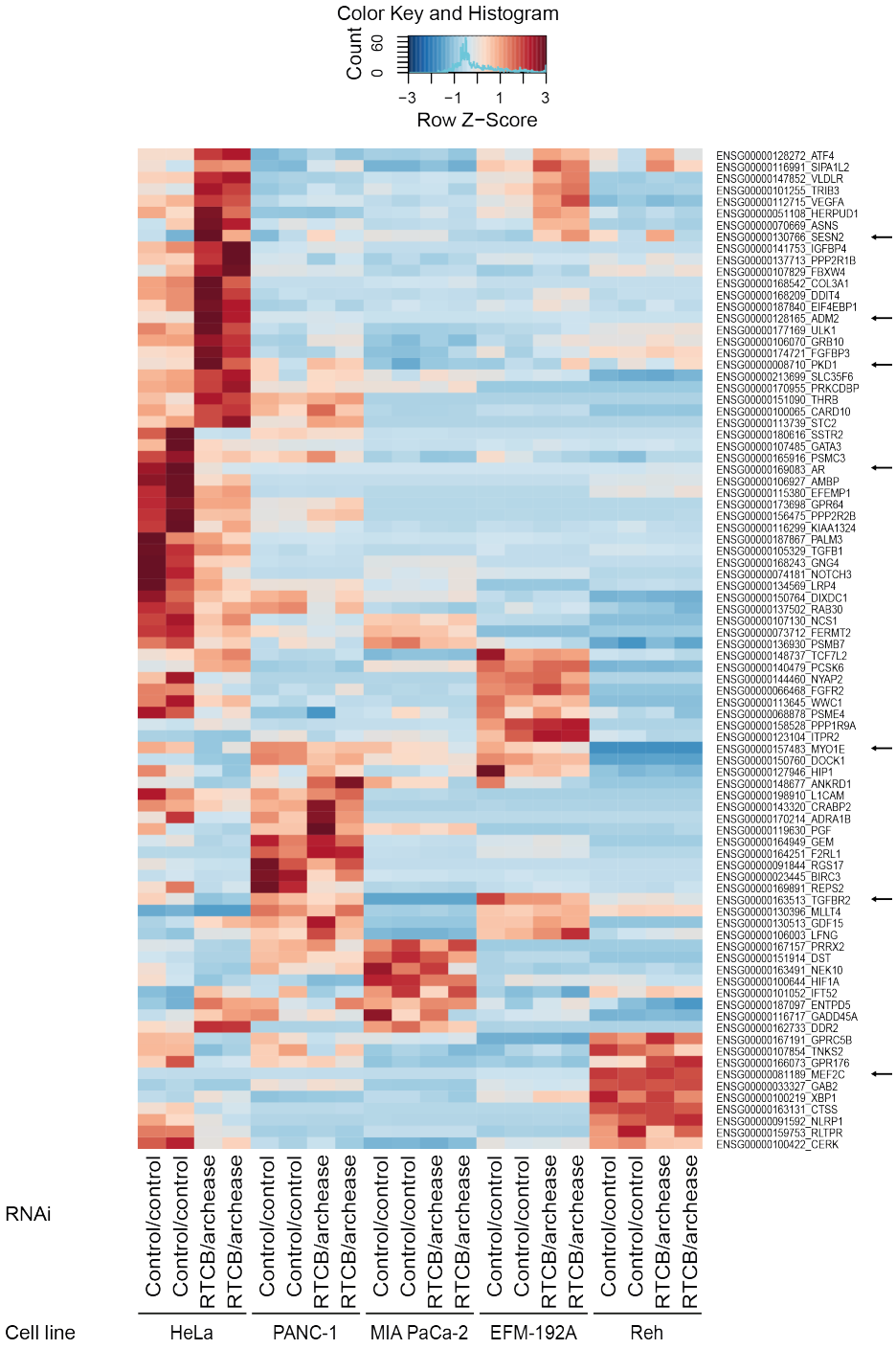

Figure 31: Expression profile of signal transduction components in RTCB/archease Tet-On cell lines

Tet-On cells expressing shRNAs targeting RTCB and archease and the respective control cell lines were treated with Dox for six consecutive days to induce shRNA expression. Following protein depletion, total RNA was isolated and analyzed by next generation sequencing (Illumina, n = 2). The heat map displays the expression profile of mRNAs assigned to signal transduction (GO:0007165) that were found to be differentially expressed in RTCB/archease Tet-On HeLa cells (adjusted p-value ≤ 0,05). mRNAs showing a similar regulation pattern in all cell lines analyzed and mentioned in the text are marked with an arrow.

In order to assess the mRNA transcriptomes of these RTCB- and archease-depleted Tet-On cancer cell lines, total RNA was isolated and analyzed by next-generation sequencing (Illumina) six days after Dox treatment. Expression changes were defined relative to the respective control/control cells. In total, less mRNA targets significantly affected by RTCB/archease depletion were found (Table 9 to Table 12, Figure 30), which is in agreement with the decreased inhibition of tRNA ligase function (Figure 29). Furthermore, looking at the mRNA targets assigned to signal transduction that were found to be altered in abundance after depletion of tRNA ligase activity in HeLa cells (Figure 20) no expression pattern common to all cell lines analyzed could be identified. In contrast, only few mRNA targets such as *TGFBR2*, *MEF2C*, *AR*, *MYOE1*, *ADM2*, *SESN2* and *PDK1* (see Figure 31, Table 6, Table 9 to Table 12) showed similar expression changes in all cell lines analyzed. These results suggest, that depletion of RTCB and archease mainly causes cell type-specific changes of the mRNA transcriptome.

Tet-On cancer cell lines were also assayed for their competitiveness in comparison to the respective control/control cells. For this purpose, cells were mixed with the corresponding RIEP cells only expressing the Tet Repressor but no shRNA construct. Five days later, shRNA expression was induced by Dox treatment and the evolution of the relative percentage of RTCB/archease or control/control cells was followed by flow cytometry based on GFP and dsRed expression. Depletion of tRNA ligase activity reduced the competitiveness of all cancer cell lines analyzed, which was characterized by gradually decreasing percentages of shRNA-positive cells (Figure 32). Thereby, the individual cell lines showed clear differences in their sensibility towards loss of tRNA ligase function with PANC-1 cells displaying the most pronounced effect and Reh cells only mildly decreasing in abundance in comparison to control/control cells. Furthermore, in EFM-192A and Reh cells, increased expression of shRNAs per se already seemed to exhibit disadvantageous effects, as marked by decreasing percentages of control/control cells especially at later time points after shRNA induction. Since not all cell lines analyzed showed pronounced inhibition of XBP1s expression (Figure 29) and thus a clear restriction of tRNA ligase activity, these experiments indicate that even an incomplete inhibition of tRNA ligase activity can result in reduced competitiveness.

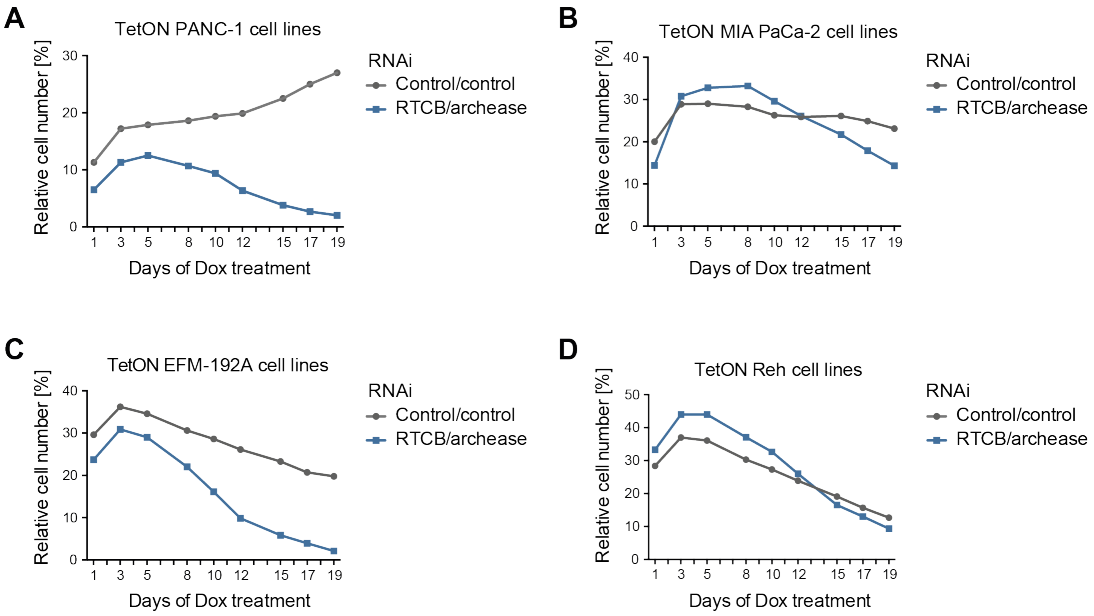

Figure 32: Reduced competitiveness after depletion of RTCB and archease in Tet-On cancer cell lines

In order to assess the competitiveness of tRNA ligase-depleted cancer cell lines, cells expressing shRNAs targeting RTCB and archease or the corresponding control cell lines expressing two copies of the control shRNA were mixed with the respective RIEP cells expressing only the Tet Repressor but no shRNA construct. Following five days of subculturing, shRNA expression was induced by Dox treatment (1 µg/ml). Subsequently, the relative percentage of shRNA-expressing cells was repeatedly determined by flow cytometry based on GFP and dsRed expression. Using this assay, RTCB- and archease-depleted PANC-1 (**A**), MIA PaCa-2 (**B**), EFM-192A cells (**C**), and, to a lesser extent, the RTCB/archease Reh cell line (**D**) were found to show reduced competitiveness in comparison to control/control cells (n = 3, one representative experiment is shown).

5. Discussion

In this study, Tet-inducible expression of shRNAs targeting RTCB, the catalytic subunit of the mammalian tRNA ligase complex (Popow et al., 2011), and/or its guanylation cofactor archease (Popow et al., 2014) enabled the investigation of novel functions of the mammalian tRNA ligase complex. Cells depleted of RTCB and archease did not only show defects in the maturation of intron-containing pre-tRNAs (Figure 10B) but also failed to induce unconventional splicing of the *XBP1* mRNA (Figure 13) and thus transcriptional activation of XBP1s-specific downstream targets (Figure 14) after chemical induction of the unfolded protein response. Furthermore, RTCB- and archease-depleted HeLa cells displayed decreased proliferation kinetics and pronounced changes of the mRNA transcriptome leading to modifications in the activation of cellular signaling cascades. Yet, the mRNA expression profiles of varying cancer cell lines depleted of RTCB and archease clearly varied from the mRNA profile of RTCB/archease Tet-On HeLa cells, which implies that the loss of tRNA ligation mainly causes cell type-specific transcriptome modifications.

5.1. Establishing a system to dissect novel functions of RTCB and archease

In contrast to conventional knockout cell lines, the RNAi-based system applied in this study did not completely abrogate protein expression (see Figure 9A) and therefore enabled only insufficient inhibition of tRNA ligation activity under conditions of decreased RTCB expression (Figure 10A and Figure 12). Consequently, in order to fully abrogate tRNA ligation *in vivo*, RTCB had to be depleted in conjunction with its cofactor archease, which required increased shRNA expression raising the likelihood of undesirable or toxic side effects: Elevated expression of small RNAs has been

shown to hold the inherent risk of competing for critical RNAi components and therefore of causing alterations in the regulatory functions of some cellular microRNAs (Castanotto et al., 2007; McBride et al., 2008). Indeed, some cancer cell lines expressing increased levels of the control shRNA showed decreased competitiveness in comparison to the respective RIEP cell lines (Figure 32), which implies that for these cells the elevated expression of shRNAs itself bears disadvantageous side effects.

Nevertheless, RNAi-mediated protein depletion is especially suited to study the function of essential proteins involved in housekeeping activities such as tRNA maturation, which is why inducible, shRNA-mediated protein depletion was chosen for this study. shRNAs offer the possibility to titrate protein depletion rates and therefore to optimize for conditions under which processes depending on the protein of interest are affected while at the same time toxic side effects are reduced. Additionally, inducible shRNA expression systems can be employed to minimize adaptation effects and to maximize protein depletion for short periods of time. In the context of the tRNA ligase complex, inducible, shRNA-mediated depletion of RTCB and archease enabled the identification and characterization of the *XBP1* mRNA as a substrate of RTCB-mediated RNA ligation under conditions of decreased levels of splicing-dependent mature tRNAs but yet unaffected global protein translation rates. Furthermore, shRNA-mediated protein depletion can be applied to a wide range of different cell lines originating not only from different organs but also from varying species.

As reported before (Popow et al., 2011), depletion of RTCB by RNAi led to a simultaneous loss of DDX1 and FAM98B expression, already under single depletion conditions (see Figure 9A). While this finding indicates, that RTCB expression is required to maintain complex integrity, it might also suggest that the concurrent decrease in DDX1/FAM98B expression could account for some of the phenotypes observed in RTCB/archease Tet-On HeLa cells. However, as the expression of tRNA ligase complex members is similarly reduced in RTCB single as well as in double depletion cells, whereby only the double depletion cell line shows profound alterations in *XBP1* mRNA splicing (see Figure 12 and Figure 13) and cell proliferation (Figure 23, Figure 25), this hypothesis seems unlikely. Furthermore, the absence of pronounced alterations in RTCB or archease single depletion Tet-On HeLa cells also argues against the presence of unspecific off-target effects causing observable phenotypes. This is further supported by the prevalence of cell type-specific transcriptome changes after shRNAs expression in various cell lines (Figure 30).

The circumstance that a full inhibition of tRNA ligation could only be achieved by simultaneous, RNAi-mediated depletion of RTCB and archease opened the

possibility to investigate, if the catalytic activity of RTCB is required for the phenotype observed: Catalysis-dependent functions were undisturbed under conditions of decreased RTCB expression but already affected by archease depletion and completely abrogated in the double depletion cell line (e.g. splicing of intron-containing tRNAs). In contrast, functions not depending on the catalytic activity but on other properties of RTCB were archease-independent and evident already after RTCB single depletion as exemplified by the loss of complex integrity. Alternatively, rescue experiments using wild type or ligase-dead RTCB expression constructs (C122A) (Popow et al., 2011) could have been used to answer these questions.

In summary, using shRNA-mediated protein depletion, a robust system to study functions of the mammalian tRNA ligase has been established. In future, this system might not only be used to identify novel functions of RTCB but it might also allow the identification of additional targets of archease activity, independent of the tRNA ligase complex. Similar to catalysis-independent functions of RTCB, these functions should already be disturbed under archease single depletion conditions and not be further influenced by an additional loss of RTCB expression.

5.2. The distinct function of archease in regulating tRNA ligase activity

In order to identify and study new functions of the mammalian tRNA ligase complex, the simultaneous depletion of RTCB and archease was crucial as unaffected levels of splicing-dependent mature tRNAs (see Figure 10A) or the unchanged expression of XBP1s after UPR induction (see Figure 12) indicated that *in vivo* RNAi-mediated depletion of RTCB alone did not profoundly inhibit tRNA ligase activity. This result is in contrast to what could have been observed *in vitro*: Whole cell extracts derived from Tet-On HeLa cell lines and analyzed by interstrand ligation assay (see Figure 9C) showed markedly decreased RNA ligation activity already under single depletion conditions. Therefore, the question arises as to why depletion of RTCB alone is not enough to abrogate tRNA ligase activity in HeLa cells even though it is sufficient to block interstrand ligation in *in vitro* assays?

A possible answer to this question arises from the molecular function of the cofactor archease, which is not directly needed for RTCB to catalyze ligation but to subsequently guanylate and thus “recharge” the tRNA ligase complex enabling additional rounds of catalysis (Popow et al., 2014). This function of archease is not only important under cellular conditions but also required to prepare RTCB for the catalysis of single or low turnover-reactions as assayed by interstrand ligation assays. Moreover, under such single turnover-conditions, decreased availability of

RTCB complexes directly causes a drop in tRNA ligation activity, which is why RTCB depletion translated to clear defects in interstrand ligation. In a cellular environment, however, multiple turnover-conditions are prevalent. As indicated by the data presented in this work, in this setting, low RTCB expression seems to be sufficient to maintain RNA ligation as long as archease is present to stimulate catalysis. Based on XBP1s and tRNA expression levels, however, *in vivo* loss of archease more potently inhibited RNA ligation than depletion of RTCB itself did (Figure 10A, Figure 12). These data indicate that archease exerts an important function in regulating RTCB activity, which might be needed to avoid re-ligation of aberrant cleavage products or to restrict tRNA ligase activity to specific substrates. Furthermore, the activity-boosting function of archease also explains why earlier attempts to inhibit XBP1s expression using RNAi-mediated RTCB depletion failed (Iwawaki and Tokuda, 2011).

The function of archease in the regulation of tRNA ligase activity is further supported by the subcellular distribution of this protein. Even though tRNA splicing is thought to be a predominantly nuclear process (De Robertis et al., 1981; Lund and Dahlberg, 1998; Nishikura and De Robertis, 1981), subcellular fractionation and immunofluorescence staining revealed that archease and the majority of RTCB localize to the cytoplasmic compartment. The cytoplasmic localization of the tRNA ligase complex and its function in *XBP1* mRNA splicing coincide with reports showing that isolated cytoplasmic fractions comprise an activity capable of ligating *XBP1* mRNA exon halves *in vitro* (Shinya et al., 2011; Uemura et al., 2009). In contrast, nuclear expression of RTCB serves to catalyze pre-tRNA splicing and potentially ER stress-independent nuclear splicing of the *XBP1* mRNA as recently described (Wang et al., 2015). As the tRNA ligase complex has also been identified as part of RNA granules shuttling between the nucleus and the cytoplasm (Perez-Gonzalez et al., 2014), the flexible localization of RTCB and the strictly cytoplasmic location of archease therefore imply, that shuttling of the tRNA ligase might not only function in RNA transport but also in enabling the archease-catalyzed formation of RTCB-guanylate intermediates. This scenario would open the possibility to adjust tRNA splicing activity and eventually constitutive XBP1s expression through the regulation of RTCB shuttling.

5.3. Protein translation after depletion of RTCB and archease

The simultaneous depletion of RTCB and archease in Tet-On HeLa cells led to a clear drop in tRNA ligase function as indicated by reduced levels of splicing-dependent mature tRNAs (see Figure 10B) and abolished expression of XBP1s after UPR induction (see Figure 13). Yet, under the conditions examined the levels of

splicing-dependent mature tRNAs were not completely eradicated and no changes in overall translation rates could be detected using metabolic labeling (see Figure 10C, D), which is in contrast to a recent report observing decreased protein synthesis in RtcB-depleted mouse ES cells (Lu et al., 2014). These results indicate that different cell systems react differently to changes in tRNA abundance and that even under conditions of greatly reduced levels of certain tRNAs normal translation can be maintained. Furthermore, the fact that following six days of shRNA expression the pool of splicing-dependent mature tRNAs was not completely eradicated implies that this time frame might have been too short to fully deplete splicing-dependent mature tRNAs, which have been reported to be extremely stable with half-lives up to weeks (Phizicky and Hopper, 2010). Alternatively, the remaining expression of RTCB and archease might have been enough to maintain low levels of tRNA maturation, or the cell might have been able to compensate for the loss of RTCB function. Possible compensation mechanisms could involve ligation of tRNA exon halves by means of a different RNA ligase as a 5'-3' RNA ligation activity has been identified in HeLa cell extracts (Zillmann et al., 1991). Alternatively, other tRNAs charged with the same amino acid could eventually compensate for the loss of splicing-dependent mature tRNAs based on wobble base pairing.

As metabolic labeling only serves to assess global protein translation rates, it cannot be excluded that also in HeLa cells the loss of tRNA ligation causes changes in the translation of certain groups of transcripts. In this respect, mRNAs enriched in AUA and TGT are especially interesting as these are the two codons exclusively decoded by splicing-dependent tRNAs in human cells. The group of AUA/TGT-enriched transcripts includes the mRNAs encoding for TTN (titin), DST (dystonin), ANK3 (ankyrin3) and MACF1 (microtubule-actin crosslinking factor 1), amongst others. Therefore, it would be interesting to more closely study the expression and translation of these proteins under conditions of impaired tRNA ligase function for example by ribosome footprinting (Ingolia et al., 2009). Furthermore, as many mRNAs enriched in AUA and TGT are involved in shaping the cellular cytoskeleton and in establishing cell adhesion (data not shown) the cell shape might considerably change after depletion of RTCB and archease. The reduced volume of RTCB/archease-depleted HeLa cells (Figure 23C) points in this direction.

In *S. cerevisiae* tRNA splicing as well as unconventional splicing of the *HAC1* mRNA are catalyzed by the RNA ligase Trl1 utilizing a 5'-3' ligation-mechanism to join 2', 3'-cyclic phosphates and 5'-OH ends (Apostol et al., 1991; Greer et al., 1983; Phizicky et al., 1992; Sawaya et al., 2003). A similar RNA ligase activity has been detected in HeLa cell extracts, yet the identity of this ligase remains to be explored (Zillmann et al., 1991). Therefore, it might appear possible that an additional 5'-3' RNA ligation activity could counterbalance RTCB-deficiency in mammalian cells. This hypothesis, however, seems unlikely as neither TRPT1, the functional orthologue of

the yeast 2'-phosphotransferase (Harding et al., 2008; Spinelli et al., 1998), nor CNP1, the only mammalian 2',3'-cyclic nucleotide phosphodiesterase generating 2'-phosphate ends identified so far (Lappe-Siefke et al., 2003), are essential for mouse viability. Northern Blot analysis of mature tRNA levels after prolonged RTCB and archease depletion or in RTCB knockout cells might shed light on the possible existence of such an additional RNA ligase function as in the absence of compensatory mechanisms and under conditions of continuous protein synthesis the levels of splicing-dependent mature tRNAs should further decrease. Nevertheless, the data presented in this work demonstrate that RTCB and the mammalian tRNA ligase complex predominantly mediate tRNA and *XBP1* mRNA splicing, at least in HeLa cells.

5.4. RTCB, archease and UPR signaling

The work presented in this thesis demonstrates that RTCB and its regulatory cofactor archease mediate the ligation of *XBP1* mRNA exon halves upon induction of the UPR. Earlier studies already pointed towards a possible function of the mammalian tRNA ligase complex in unconventional *XBP1* mRNA splicing: In complementation studies bacterial RtcB was shown to be competent and sufficient to catalyze cytoplasmic splicing of the *HAC1* mRNA in a TRL1Δ *S. cerevisiae* strain (Tanaka et al., 2011b). Furthermore, investigation of the mRNA-bound proteome by PAR-CLIP analysis revealed that RTCB is associated with the *XBP1* mRNA by binding two sites flanking the unconventional intron (Baltz et al., 2012). As the *XBP1u* mRNA localizes to the ER (Yanagitani et al., 2009) due to an encoded hydrophobic helix recruiting the mRNA-ribosome-nascent chain complex to the ER membrane (Yanagitani et al., 2011), association of this mRNA with RTCB would enable recruitment of the tRNA ligase complex to the site of *XBP1* mRNA splicing. Indeed, a recent report proved a direct association of tagged and exogenously expressed RTCB with endogenous IRE1α (Lu et al., 2014), which supports ER membrane recruitment of the tRNA ligase and enables ligation of cleaved *XBP1* mRNA exon halves shortly after cleavage. Given its importance for full enzymatic activity of IRE1α, also archease might localize to foci of increased *XBP1* mRNA splicing activity by—directly or indirectly—associating with IRE1α.

Translation of XBP1u not only serves to recruit the *XBP1* mRNA to the ER membrane but also to regulate XBP1s expression, especially after attenuation of UPR signaling. Even though XBP1u is generally short-lived (Calfon et al., 2002), XBP1u protein levels accumulate during the recovery phase of the UPR and mediate rapid degradation of XBP1s (Yoshida et al., 2006) as well as of ATF6 (Yoshida et al., 2009) by complex formation. Therefore, depletion of RTCB and archease might not

only lead to inhibition of XBP1s expression but also influence ATF6 signaling based on increased *XBP1u* mRNA expression, especially at early time points after UPR induction (Figure 13). Unfortunately, to date no ATF6-specific downstream targets have been identified and attempts to detect ATF6 activation based on ATF6 cleavage in HeLa cells failed in this study (data not shown).

Under conditions of efficient *XBP1* mRNA splicing, XBP1s expression leads to the transcriptional activation of a variation of downstream targets (Acosta-Alvear et al., 2007; Lee et al., 2003). Furthermore, XBP1s has also been implicated in the regulation of autophagy through the regulation of FOXO1 expression (Vidal et al., 2012; Zhou et al., 2011) whereby increased XBP1s levels promote proteasomal degradation of FOXO1 and therefore inhibit autophagy induction. This function of XBP1s differs from IRE1α-mediated regulation of autophagy, as IRE1α has been shown to activate autophagy and apoptosis by signaling through ASK1 and JNK (Urano et al., 2000). Since depletion of RTCB and archease efficiently inhibits XBP1s signaling without disrupting IRE1α activation (Figure 15) it would be interesting to study autophagy levels after RNAi-mediated inhibition of tRNA ligation.

5.5. Regulation of cell signaling and cell proliferation by RTCB and archease

The data presented in this work demonstrate that loss of tRNA ligation activity leads to loss of XBP1s expression (Figure 13) and consequently to loss of XBP1s-dependent transcription (Figure 14). According to its function in UPR signaling, the group of XBP1s-dependent downstream targets includes many genes involved in increasing the protein folding-capacity of the ER (Lee et al., 2003) or in modulating phospholipid synthesis (Shaffer et al., 2004; Sriburi et al., 2007; Sriburi et al., 2004). However, XBP1s is also involved in the regulation of a multitude of additional genes linked to such diverse functions as DNA damage and repair pathways, redox homeostasis and signal transduction (Acosta-Alvear et al., 2007). This suggests that XBP1s governs a wide variety of biological functions independent of ER stress. Furthermore, XBP1 overexpression enhances cell proliferation independently of growth factor signaling and confers resistance to growth factor deprivation (Fujimoto et al., 2003; Gomez et al., 2007). It is therefore possible that the alterations in cellular signaling (see Figure 20 and Figure 21) and cell proliferation (see Figure 23) observed after depletion of RTCB and archease in HeLa cells might have been caused by simultaneous loss of constitutive XBP1s expression (Acosta-Alvear et al., 2007; Shen et al., 2005; Wang et al., 2015). Yet, XBP1s rescue cell lines failed to attain normal proliferation rates or growth factor signaling levels (see Figure 27) even

though they supported UPR signaling up to wild type levels confirming that the exogenously expressed protein is transcriptionally active. Therefore, functions of the tRNA ligase complex related to cell proliferation and signal transduction are independent from its function in *XBP1* mRNA splicing. This finding is supported by XBP1s-specific ChIP assays (Acosta-Alvear et al., 2007) showing no significant overlap with genes influenced by the loss of RTCB and archease expression (see Figure 31).

By PAR-CLIP analysis, RTCB has been identified as one of the main mRNA-binding proteins of the cell (Baltz et al., 2012), which implies a possible function of the tRNA ligase complex in the regulation of localization, transport, stability, silencing, or modification of these mRNA targets (Re et al., 2014). However, only few of the RTCB-bound RNAs were differentially expressed after depletion of RTCB and archease arguing against a role of RTCB in RNA stability or silencing. This correlation is exemplified by the group of cyclin mRNAs, which are bound to RTCB in HEK293 cells (Baltz et al., 2012) (e.g. *CCNA2*, *CCNB1*, *CCNB2*, *CCND2*) but which show only modest alterations in abundance after inhibition of tRNA ligation (see Figure 26). Similarly, besides the *XBP1* mRNA, RTCB does not seem to act on other mRNAs by catalyzing unconventional splicing reactions (see Table 2). However, as the tRNA ligase complex is part of RNA transport complexes shuttling between the cytoplasm and the nucleus (Perez-Gonzalez et al., 2014) and of cytoplasmic kinesin-associated RNA-transporting granules in dendrites (Kanai et al., 2004), a function of RTCB in the regulation of nuclear RNA export or RNA localization seems feasible. Further studies will be required to shed light on the functional relation of these RTCB-mRNA interactions.

Analysis of the mRNA transcriptome by RNA sequencing revealed a variety of changes after depletion of RTCB and archease in HeLa cells (see Table 6). However, attempts to validate RTCB-dependent regulation of these transcripts in cancer cell lines mostly failed as only few mRNAs showed similar expression changes in response to loss of tRNA ligation across all cell types analyzed (see Table 6 to Table 12 and Figure 31). Variations between the individual cell lines might to some extent be explained by differences in RTCB and archease depletion efficiencies that translated to alterations in residual tRNA ligase activity as examined by XBP1s expression (see Figure 29). Especially in the EFM-192A cell line, XBP1s expression was only mildly affected while the MIA PaCa-2 cell line showed the strongest response. Nevertheless, these differences in tRNA ligation activity cannot explain all of the variation in the mRNA expression profiles. It therefore appears that loss of RTCB-dependent RNA ligation causes cell type-specific modifications of the mRNA transcriptome and does not generally translate to changes in the expression of signal transduction components as observed in HeLa cells.

Despite differences in tRNA ligation activity and mRNA expression, in all cell lines examined depletion of RTCB and archease reduced the competitiveness in comparison to control/control cells (Figure 32) even though to a greatly varying extent. Therefore, the tRNA ligase seems to influence competitiveness by a yet unknown mechanism, which however seems to be independent from the expression of signal transduction components. A recent study in *C. elegans* demonstrated that the decreased life span and the reduced growth of RtcB mutant worms can be rescued by the overexpression of pre-spliced tRNAs (Kosmaczewski et al., 2014) suggesting that disruption of pre-tRNA splicing is the main cause of the phenotypes observed. A similar approach might reveal if, according to what has been proposed before (Lu et al., 2014), alterations in the proliferation of RTCB/archease Tet-On HeLa cells and the reduced competitiveness of cancer cell lines depleted of RTCB and archease likewise are based on a decreased expression of splicing-dependent mature tRNAs. Furthermore, it would be interesting to study if the reduced competitiveness of Tet-On cancer cell lines is based on increased cell death or on decreased cell proliferation, similar to what has been observed in HeLa cells.

The high degree of variation between the transcriptomes of the individual cell lines implies that most of the modifications in mRNA abundance observed are not specifically caused by reduced RTCB activity but seem to result from a general stress response triggered by the loss of a housekeeping function. This hypothesis is strengthened by diverse signs of cellular stress detected in RTCB/archease-depleted Tet-On HeLa cells. Depletion of RTCB and archease increased ER protein folding stress in the absence of chemical UPR induction as indicated by increased expression of the total *XBP1* mRNA (Figure 13D), increased phosphorylation of IRE1α (Figure 15A), decreased expression of the RIDD-target mRNA *SCARA3* (Figure 15C), and slightly increased phosphorylation of eIF2α (Figure 18B). Likewise, RNA sequencing revealed that UPR downstream targets such as *XBP1*, *ATF4*, *ASNS*, and *VEGFA* were upregulated in untreated RTCB- and archease-depleted HeLa cells (Figure 20, Table 6). In addition, loss of tRNA ligation resulted in increased phosphorylation of ERK1/2, which has been linked to oxidative (Garg and Chang, 2003; Wang et al., 1998) and hypo-osmotic stress (Sadoshima et al., 1996; Schliess et al., 1996; Sinning et al., 1997; van der Wijk et al., 1998). It therefore appears likely, that loss of tRNA ligation leads to the activation of cellular stress signaling pathways causing some of the phenotypes observed. Yet, further experiments will be required to more closely study and characterize the nature of this stress reaction.

5.6. Targeting RTCB and archease for the treatment of human diseases

Autophagy plays an important role in the pathology of neurodegenerative diseases caused by aggregation of misfolded proteins such as Huntington's, Alzheimer's and Parkinson's disease, amyotrophic lateral sclerosis (ALS) and prion-related disorders (Matus et al., 2011). Given its function in the regulation of autophagy and apoptosis, the UPR has been extensively studied in the context of these disorders (Hetz and Mollereau, 2014). For example, CNS-specific depletion of XBP1 decreased SOD1 accumulation in the spinal cord of SOD1 transgenic mice (Hetz et al., 2009) and improved neuronal survival and motor performance in full-length mutant Huntingtin transgenic animals (Vidal et al., 2012). Furthermore, overexpression of XBP1s has been implicated in a growing number of different cancers such as multiple myeloma (Carrasco et al., 2007), triple-negative breast cancer (Chen et al., 2014), pre-B-cell acute lymphoblastic leukemia (Kharabi Masouleh et al., 2014) and B-cell-chronic lymphocytic leukemia (Tang et al., 2014). In addition, the constitutive activation of XBP1 blunts the anti-tumor activity of dendritic cells and therefore drives ovarian cancer progression (Cubillos-Ruiz et al., 2015).

To limit XBP1s expression in the context of this wide range of diseases, several compounds have been designed targeting the RNase domain of IRE1α (Cross et al., 2012; Mimura et al., 2012; Ri et al., 2012; Volkmann et al., 2011; Wang et al., 2012). However, since both, the kinase and the RNase domain of IRE1α are involved in the activation of autophagy and apoptosis under conditions of increased protein folding stress, inhibition of IRE1α might cause unfavorable side effects. Activation of apoptosis by IRE1α is not only achieved by signaling through ASK1 and JNK recruited to autophosphorylation sites of IRE1α but also involves IRE1α's RIDD activity inducing cell death by the degradation of mRNAs encoding for essential ER chaperones (Hollien et al., 2009; Hollien and Weissman, 2006) and by downregulating microRNAs that negatively regulate the expression of pro-apoptotic caspases (Upton et al., 2012). Targeting the tRNA ligase instead could therefore enhance the specificity in disrupting XBP1 signaling and might open new avenues in the treatment of diseases associated with elevated expression levels of XBP1s. First results from competition assays with RTCB/archease-depleted Tet-On cancer cell lines (see Figure 32) point towards a possible application of tRNA ligase inhibitors for cancer therapy. Furthermore, the analysis of caspase activity in Tet-On HeLa cells revealed that the depletion of RTCB and archease does not inhibit the induction of apoptosis neither under conditions of increased protein folding stress (Figure 17) nor after prolonged depletion of RTCB and archease (Figure 24). However, loss of XBP1s expression surprisingly also did not increase caspase activation, which might have been expected as a consequence of unresolved ER stress and increased

PERK signaling (Figure 18). The precise potential of RTCB and/or archease inhibitors for the treatment of cancer or neurodegenerative diseases therefore has to be determined carefully.

The IRE1-XBP1 branch of the UPR is of special importance to cells of high secretory activity such as pancreatic β cells (Harding et al., 2001) and plasma cells (Iwakoshi et al., 2003). While chronic activation of this stress response saves healthy cells from undergoing apoptosis, it also renders malignant cells more resistant to chemotherapy. A prominent example is multiple myeloma, a plasma cell malignancy that despite conventional high-dose chemotherapy and bone marrow transplantation remains incurable with a median survival of only six years (Carrasco et al., 2007; Raab et al., 2009). Persistent and elevated expression of XBP1s seemed to be a special characteristic of multiple myeloma cells because overexpression of XBP1s in plasma cells alone was enough to induce a phenotype resembling monoclonal gammopathy of undetermined significance (MGUS) in mice (Carrasco et al., 2007), a premalignant condition preceding multiple myeloma. Furthermore, elevated expression of XBP1s has been shown to ensure the growth of multiple myeloma cells in the hypoxic environment of the bone marrow (Iwakoshi et al., 2003; Romero-Ramirez et al., 2004). On the basis of these reports, multiple studies have already tried to target XBP1s signaling at the step of mRNA cleavage (Michallet et al., 2011; Mimura et al., 2012; Papandreou et al., 2011; Ri et al., 2012; Suh et al., 2012). However, increased cytotoxicity was mainly observed in combination with conventional chemotherapeutic agents, probably because inhibition of IRE1α also impaired other functions of IRE1α signaling. Therefore, targeting XBP1s expression at the step of mRNA ligation appeared to be a new and promising strategy in the treatment of multiple myeloma.

In the context of this study, this hypothesis was addressed by the generation of two RTCB- and archease-depleted Tet-On multiple myeloma cell lines (NCI-H929 and MM1.S, data not shown). Unfortunately, in these cells RTCB and archease depletion was inefficient in comparison to all other cell lines studied, which resulted in poor inhibition of XBP1s expression. Furthermore, NCI-H929 and MM1.S cells frequently lost shRNA expression, eventually due to transcriptional silencing or negative selection which overall prevented a thorough characterization of RTCB- and archease-depleted multiple myeloma cells. As newer studies question a prior function of elevated XBP1s expression for the pathogenesis of multiple myeloma (Hong and Hagen, 2013; Leung-Hagesteijn et al., 2013) the therapeutic potential of tRNA ligase inhibition for the treatment of this disease remains to be explored. Nevertheless, besides the controversial benefit of decreasing XBP1s expression, therapeutic inhibition of the tRNA ligase still might retard the progression of multiple myeloma. Even though the precise mechanism is unclear yet, all cell lines analyzed showed decreased proliferation or reduced competitiveness as a consequence of

diminished RTCB activity. Even if this effect is simply based on declining expression levels of splicing-dependent mature tRNAs as experiments in *C. elegans* suggest (Kosmaczewski et al., 2014) tRNA ligase inhibitors could potentially be used to decrease the proliferation and/or competitiveness of rapidly proliferating cancer cells.

5.7. Summary and outlook

In summary, the data presented in this work show that RTCB and its cofactor archease are not only required for the maturation of intron-containing pre-tRNAs but also mediate unconventional splicing of the *XBP1* mRNA as part of the unfolded protein response. This dual function of RTCB is facilitated by a broad subcellular distribution of the tRNA ligase complex. Upon simultaneous depletion of RTCB and archease by means of doxycycline-inducible expression of shRNAs, Tet-On HeLa cells subjected to increased protein folding stress failed to induce *XBP1* mRNA splicing and the subsequent expression of the transcription factor XBP1s. Consequently, also the induction of XBP1s-specific downstream targets was inhibited. This defect in UPR signaling was not caused by inhibition of IRE1α activity or by overall restriction of UPR induction as IRE1α activation as well as PERK and ATF6 signaling remained mostly unchanged. Therefore, the tRNA ligase complex has been identified as the long-sought RNA ligase required for unconventional splicing of the *XBP1* mRNA.

Additionally, RNA sequencing and subsequent confirmation by RT-qPCR and Western Blot analysis revealed that RTCB and archease are also involved in the regulation of cellular signaling pathways in HeLa cells. tRNA ligase-depleted cells slightly accumulated in the G_0/G_1 phase of the cell cycle leading to reduced proliferation kinetics in comparison to control cells. This function of RTCB seemed to be independent from its role in *XBP1* mRNA splicing as overexpression of XBP1s failed to rescue proliferation rates or mRNA expression levels. Similarly, RTCB- and archease-depleted Tet-On cancer cell lines showed reduced competitiveness in comparison to control cells, which however was not caused by changes of the mRNA transcriptome related to signal transduction. Therefore, modulations of the mRNA expression profile after loss of tRNA ligase function primarily are cell type-dependent and seem to reflect a general stress reaction caused by the loss of a housekeeping function rather than a specific reaction triggered by the loss of RTCB expression. Yet, the precise nature of this stress reaction still has to be explored.

Collectively, the data presented in this work demonstrate that RTCB and archease are essential for unconventional splicing of the *XBP1* mRNA. This new function of the mammalian tRNA ligase complex and the decreased competitiveness of cancer cell

lines depleted of RTCB and archease form a potential basis for the treatment of a growing number of diseases associated with elevated XBP1s expression levels such as multiple myeloma, triple-negative breast cancer, pre-B-cell acute lymphoblastic leukemia, and B-cell chronic lymphocytic leukemia.

Even though, based on the work presented in this thesis, no further function of the mammalian tRNA ligase complex could be identified it appears likely that RTCB and archease are involved in the regulation of additional cellular processes. This prediction is not only based on the multitude of mRNA targets bound to the tRNA ligase based on PAR-CLIP analysis (Baltz et al., 2012) or the diversity of functions that have been assigned to other RNA ligases (see Section 3.1): Human cell extracts have been shown to be capable of ligating RNA substrates carrying 3'-phosphate termini (Filipowicz et al., 1983; Martinez et al., 2002), which implies a relaxed substrate specificity of the RNA ligase. In addition, biochemical assays revealed that by expressing RTCD1, human cells are able to convert RNA 3'-phosphates into 2',3'-cyclic phosphates and therefore of transforming a variety of RNA termini into possible RTCB substrates (Filipowicz et al., 1985; Genschik et al., 1997). This broad range of potential RTCB substrates and the variety of cellular stress signals detected after loss of RTCB and archease expression indicate that RTCB also acts in other pathways. This hypothesis is further supported by two recent publications reporting a function of RTCB and archease in the process of axon regeneration (Kosmaczewski et al., 2015; Song et al., 2015). Further work will be required to identify and shed light on such additional functions of the mammalian tRNA ligase complex.

6. Material and methods

6.1. Design, cloning and evaluation of short hairpin RNAs

Cloning of shRNA constructs for reporter assay. For RNAi-mediated depletion of RTCB and/or archease, shRNAs were designed as described earlier (Dow et al., 2012). The respective 97-mer oligonucleotides (IDT, guide sequences see Table 3, examples of full 97mer sequences see below) were amplified by PCR using the following conditions: 0.5 ng of template DNA, 0.5 µl of Phusion polymerase (Finnzymes), 1 x buffer GC, 3 % of DMSO, 0.3 µM of each primer (miR-30_fwd: 5'-CAG AAG GCT CGA GAA GGT ATA TTG CTG TTG ACA GTG AGC G-3' and miR-30_rev: 5'-CTA AAG TAG CCC CTT GAA TTC CGA GGC AGT AGG CA-3'); cycling: 95 °C for 2 min; 33 cycles of 95 °C for 15 s, 58 °C for 30 s and 72 °C for 25 s; 72 °C for 5 min. PCR products were purified using the QIAquick® PCR Purification Kit (QIAGEN) according to manufacturer's instructions and cloned into pLMN-GFP-miR-30 (Zuber et al., 2011) (see Figure Figure 7) using the XhoI/EcoRI restriction sites (details see below).

Control shRNA, 97mer: 5'-TGC TGT TGA CAG TGA GCG CAG GAA TTA TAA TGC TTA TCT ATA GTG AAG CCA CAG ATG TAT AGA TAA GCA TTA TAA TTC CTA TGC CTA CTG CCT CGG A-3'

RTCB shRNA 3, 97mer: 5'-TGC TGT TGA CAG TGA GCG ACA GGT TGA AGG TGT TTT CTA TTA GTG AAG CCA CAG ATG TAA TAG AAA ACA CCT TCA ACC TGC TGC CTA CTG CCT CGG A-3'

Archease shRNA 5, 97mer: 5'-TGC TGT TGA CAG TGA GCG AAA GAT GTT AGA GAT TAC AAT TTA GTG AAG CCA CAG ATG TAA ATT GTA ATC TCT AAC ATC TTC TGC CTA CTG CCT CGG A-3'

Table 3: Sequences of shRNAs targeting RTCB or archease

		22 bp guide sequence	Nucleotides targeted
	Control	TAG ATA AGC ATT ATA ATT CCT A	
RTCB shRNAs	shRNA 1	TAG ATC GAT GAA CAA TTC CAG G	359–380
	shRNA 2	TTG ACT ATA ATC TTG TCT CTC T	978–999
	shRNA 3	ATA GAA AAC ACC TTC AAC CTG C	223–244
	shRNA 4	TAC GTC GAG ATT TTG CTC GGG A	1436–1457
	shRNA 5	TTG AAC AGA ACT TTC TTC ATG A	2023–2044
	shRNA 6	TTA TTG AAC AGA ACT TTC TTC A	2026–2047
	shRNA 7	TTT CTT CAT GAC ACC TCT CGG A	2012–2033
	shRNA 8	AAC TGT AGC AAA AAC TCC CGG C	103–224
Archease shRNAs	shRNA 1	TCTAACATCTTCCTCTTCCTGC	63–84
	shRNA 2	TTGCTTTGACTTCTGTTCCCTG	472–493
	shRNA 3	TTGCTGAATATGTTATTGCTTT	487–508
	shRNA 4	TTGATCAATGCTAAGTACTTTC	390–411
	shRNA 5	AATTGTAATCTCTAACATCTTC	73–94
	shRNA 6	TGTAACTGGACATCTGCTGTAT	164–185
	shRNA 7	TTAATTCATAGTGTCTTCTCAA	617–638
	shRNA 8	ATGATCACAAAAACTTCCGGGT	530–551

Bp: base pair

Cloning of reporter construct. The linker region of the reporter construct was designed as previously described (Fellmann et al., 2013). For this purpose the recognition sites of all shRNAs targeting RTCB or archease plus three additional bases 5' and two additional bases 3' of each recognition site (in total 27 base pairs) were stringed together in sequential order. In case of overlapping target sequences, the full overlapping region was treated as one enlarged target sequence. Finally, an XhoI recognition site was added to the 5' end of the linker while the 3' end was completed by an EcoRI recognition site. The full sequence was ordered from IDT and cloned into the TtNPT construct (Fellmann et al., 2013) (see Figure 7) using the XhoI/EcoRI restriction sites.

Archease reporter: 5'-GGG GGG GCT CGA GAT GGC GCA GGA AGA GGA AGA TGT TAG AGA TTA CAA TTT GAC TGG ATC ATA CAG CAG ATG TCC AGT TAC ACG CAT GAA GTG AAA GTA CTT AGC ATT GAT CAA AGA AAA CCC TCA GGG AAC AGA AGT CAA AGC AAT AAC ATA TTC AGC AAT GCA GAG AGA ACC CGG AAG TTT TTG TGA TCA TTG ACA TCC TTT TGA GAA GAC ACT ATG AAT TAA ATT CTG AAT TCC CCC CCC C-3'

RTCB reporter: 5'-GGG GGG GCT CGA GCC CTG CCT GGA ATT GTT CAT CGA TCT ATT GGG CAT GAA GAG AGA CAA GAT TAT AGT CAA TGA TCA ACA TGC AGG TTG AAG GTG TTT TCT ATG TGA ACA TTG TCC CGA GCA AAA TCT CGA CGT AAT TTA TAC ATT CCG AGA GGT GTC ATG AAG AAA GTT CTG TTC AAT AAG GTT TGC GGA GCC GGG AGT TTT TGC TAC AGT TTT CGC GAA TTC CCC CCC CC-3'

Restriction enzyme digestion. For restriction enzyme digestion, up to 1 µg of DNA was incubated with 1 µl (10–20 U) of each restriction enzyme (obtained from New England Biolabs) in 40 µl reactions for 3 h at the conditions recommended by the manufacturer. Subsequently, the restriction digest was stopped by heat inactivation (65 °C, 20 min). For plasmid DNA digestion, 1 µl (1 U) of FastAP® (Fermentas) was subsequently added followed by further incubation for 15 min at 37 °C. Afterwards, DNA was purified by agarose-gel electrophoresis and the desired bands were eluted using the gel QIAquick® Gel Extraction Kit (QIAGEN) according to manufacturer's instructions. Both, digested plasmid DNA and PCR products were eluted in 25 µl of DNase-free water.

Ligation. For ligation 2 µl of reaction buffer, 7 µl of digested and purified shRNA or reporter sequence, 1 µl of digested vector and 1 µl (1 U) of T4 DNA ligase (Roche) were mixed in a total volume of 20 µl and incubated at 16 °C overnight. After heat inactivation of the ligation reaction at 65 °C for 10 min, 1 µl of the reaction mixture was transformed into chemically competent DH5α bacteria.

Transformation of chemically competent bacteria. For transformation, 100 µl of competent DH5α bacteria were mixed with 1 µl of the ligation mixture. After an incubation period of approximately 10 min on ice, the bacteria were heat shocked at 42 °C for 45 to 90 s. Cells were immediately returned on ice and incubated for additional 2 min. Around 500 µl of antibiotic-free LB medium was added to the obtained suspension, which was subsequently incubated for one hour at 37 °C with shaking at 750 rpm. After this, bacteria were plated onto agar plates supplemented with the appropriate antibiotic and incubated at 37 °C overnight.

Isolation of plasmid DNA. For isolation of plasmid DNA, competent DH5α bacteria transformed with the desired vector were grown in 5 ml or 250 ml of LB medium supplemented with the appropriate antibiotic at 37 °C overnight while shaking. Cells were harvested by centrifugation and the plasmid was purified using the QIAprep® Miniprep or Maxiprep Kit according to the manufacturer's instructions. The purified DNA was finally eluted in 20 to 100 µl of DNase-free water.

Reporter assay. Within the framework of the reporter assay (Fellmann et al., 2013), immortal Rosa26-rtTA-M2 MEFs (RAg-MEFs) expressing the Tet Repressor were retrovirally infected with one of the reporter constructs using amphotropic packaging (TtNPT construct, detailed description of retroviral packaging and target cell infection see section "Retro- and lentiviral packaging") and subsequently enriched by

fluorescence-activated cell sorting (LSR Aria II system, BD Biosciences) based on dTomato expression. Afterwards, the thus generated reporter cell lines were transduced with an ecotropic retrovirus delivering one of the RTCB- or archease-specific shRNAs cloned into the pLMN-GFP-miR-30 construct (Zuber et al., 2011). Additionally, two control shRNAs with known silencing activity were included in the assay: one shRNA targeting Renilla luciferase and showing 90 to 95 % of silencing efficiency as well as the Pten1524 shRNA exhibiting medium strong activity (Fellmann et al., 2013). Hereby, infection efficiencies of 5 to 20 %, which predominantly result in a single viral integration per cell, were pursued (Fellmann et al., 2011). Two days after infection the transduction efficiency was determined on an LSR Fortessa (BD Biosciences) flow cytometer based on GFP expression. Furthermore, two and six days post infection the mean dTomato signal of GFP-positive and thus shRNA-expressing cells relative to the dTomato signal of GFP-negative cells was determined by flow cytometry and used as a measure for shRNA silencing activity (Fellmann et al., 2013). For this analysis, at every time point at least 5000 GFP-positive cells were recorded and analyzed.

Renilla shRNA (control), 97mer: 5'-TGC TGT TGA CAG TGA GCG CAG GAA TTA TAA TGC TTA TCT ATA GTG AAG CCA CAG ATG TAT AGA TAA GCA TTA TAA TTC CTA TGC CTA CTG CCT CGG A-3'

Pten1524 shRNA, 97mer: 5'-TGC TGT TGA CAG TGA GCG ACA GCT AAA GGT GAA GAT ATA TTA GTG AAG CCA CAG ATG TAA TAT ATC TTC ACC TTT AGC TGG TGC CTA CTG CCT CGG A-3'

Subcloning of shRNA constructs for the generation of Tet-On stable cell lines. For the generation of Dox-inducible RTCB and/or archease depletion cell lines, the two shRNAs showing the best depletion efficiency based on the reporter assay (RTCB shRNA 3 and archease shRNA 5) and the control shRNA targeting renilla luciferase were subcloned into the optimized miR-E backbone of RT3GEN (pSIN-TRE3G-turboGFP-miR-E-PGK-NeoR, see Figure 8, (Fellmann et al., 2013)) or into a derived construct expressing dsRed instead of GFP and a blasticidin resistance cassette instead of Neo (RT3REB, see Figure 8, pSIN-TRE3G-dsRed-miR-E-PGK-BlastiR). For cloning, the protocol described above ("Cloning of shRNA constructs for reporter assay") was followed using the 97mer sequences obtained from IDT as template and the following primers (Fellmann et al., 2013): miR-E_fwd: 5'-TAC AAT ACT CGA GAA GGT ATA TTG CTG TTG ACA GTG AGC G-3' and miR-E_rev: 5'-TTA GAT GAA TTC TAG CCC CTT GAA GTC CGA GGC AGT AGG CA-3'.

6.2. Tissue culture and generation of stable cell lines

Cell culture. HeLa cells were cultured at 37 ºC, with 5 % CO_2 in 1 x Dulbecco's Modified Eagle's Medium (DMEM, Invitrogen) supplemented with 10 % fetal bovine serum (Sigma), 3 mM glutamine (Sigma), 100 U/ml penicillin, 100 µg/ml streptomycin sulfate (Sigma), and 20 mM HEPES pH 7.0. For lenti- or retroviral packaging, LentiX (Clontech), Platinum-A or Platinum-E cells (CellBiolabs) were cultured in the same way. PANC-1 and MIA PaCa-2 cells were likewise cultured at 37 ºC, with 5 % CO_2 in 1 x DMEM (Invitrogen) supplemented with 10 % fetal bovine serum (Sigma), 3 mM glutamine (Sigma), 100 U/ml penicillin, 100 µg/ml streptomycin sulfate (Sigma), 1 x MEM Non-Essential Amino Acids (ThermoFisher) and 20 mM HEPES pH 7.0. In contrast, EFM-192A and Reh cells were cultured at 37 ºC, with 5 % CO_2 in 1 x Advanced RPMI Medium 1640 (ThermoFisher) with 10 % fetal bovine serum (Sigma), 3 mM glutamine (Sigma), 100 U/ml penicillin, 100 µg/ml streptomycin sulfate (Sigma), and 20 mM HEPES pH 7.0. All cell lines were regularly tested for mycoplasma infection.

Retro- or lentiviral packaging. Lenti- or retroviral packaging was performed using LentiX (Clontech), Platinum-A or Platinum-E cells (Cell Biolabs) according to established protocols (Fellmann et al., 2011). For lentiviral packaging, LentiX cells were transfected with 20 µg of plasmid DNA (pWXLd-RIEP or pRRL-RIEP), 7 µg of pcDNA3.GP.4xCTE, 1 µg of pMD.G VSVG and 5 µg of pRSV.Rev using calcium phosphate transfection: In a total volume of 500 µl, the DNA was supplemented with 250 µM $CaCl_2$, mixed with 500 µl of 2x HBS solution (280 mM NaCl, 50 mM HEPES, 1.5 mM Na_2HPO_4, 12 mM Dextrose or Glucose, 10 mM KCl) and incubated at room temperature for 15 min. Thereafter, the transfection mix was dropwise added to LentiX cells plated in DMEM supplemented with 10 % fetal bovine serum, 3 mM glutamine and 20 mM HEPES pH 7.0. After incubating the cells for up to 16 hours, the transfection media was exchanged to full DMEM containing 10 % fetal bovine serum (Sigma), 3 mM glutamine (Sigma), 100 U/ml penicillin, 100 µg/ml streptomycin sulfate (Sigma), and 20 mM HEPES pH 7.0. Retroviral packaging was performed by transfecting Platinum-A or Platinum-E cells with 20 µg of plasmid DNA (pLMN-GFP-miR-30, TtNPT, RT3GEN, RT3REB GFP-RV-XBP1s or pBMN-iGFP-Flag) and 10 µg of helper plasmid (pCMV-Gag-Pol, Cell Biolabs) using calcium phosphate transfection. Virus-containing supernatants were harvested 36, 48, and 60 h after transfection, filtered through 0,45 µm membranes, supplemented with 5 µg/ml polybrene (Merck Millipore) and directly used for the transduction of target cells.

Generation of Tet-On cell lines and Tet-RNAi studies. To generate ecotropically infectable Tet-On cells, lentiviral constructs coexpressing the ecotropic receptor (EcoR), the Tet Repressor (rtTA3) and a puromycin resistance (Puro) were generated by shuttling the according expression cassette from pRIEP (Zuber et al., 2011) into the pWPXLd (pWPXLd-EEF1A-rtTA3-IRES-EcoR-PGK-Puro) or pRRL backbone (pRRL-SFFV-rtTA3-IRES-EcoR-PGK-Puro). HeLa, PANC-1, MIA PaCa-2 and EFM-192A cells were lentivirally transduced with pWXLd-EEF1A-rtTA3-IRES-EcoR-PGK-Puro (pWPXLd-RIEP) while Reh cells were lentivirally infected with pRRL-SFFV-rtTA3-IRES-EcoR-PGK-Puro (pRRL-RIEP). Subsequently, all cell lines were selected with Puromycin (VWR) for one week and transduced with an ecotropic retrovirus delivering RT3GEN or RT3REB as described earlier (Zuber et al., 2011). For single knockdown conditions, HeLa cells were transduced with a single shRNA expression vector (RT3GEN) and selected with 1 mg/ml G418 (Gibco). Double knockdown HeLa cells were obtained by sequential retroviral infection with two shRNA expression vectors (RTCB or control shRNA in RT3GEN and archease or control shRNA in RT3REB) and subsequent selection using 1 mg/ml G418 and 10 µg/ml Blasticidin (VWR). In contrast, double depletion PANC-1, MIA PaCa-2, EFM-192A and Reh cells were generated by sequential retroviral infection with ecotropically packaged shRNA expression vectors and subsequently sorted for GFP and dsRed-positive cells using an FACS Aria II (BD Biosciences) flow cytometer. In all cell lines, Tet-regulated shRNA expression was induced by treatment with 1 µg/ml doxycycline (Dox, Sigma), which was added to the cell culture media. Cell culture media supplemented with selection antibiotics and/or Dox was replaced every second day.

Generation of XBP1s rescue cell lines. To rescue XBP1s expression in an RTCB/archease-deficient background, control/control and RTCB/archease Tet-On HeLa cells were transduced with ecotropically packaged retrovirus carrying GFP-RV-XBP1s (mus musculus) (Iwakoshi et al., 2003) or empty pBMN-iGFP-Flag as mock control (details see “Retro- or lentiviral packaging”). GFP-positive cells were enriched by flow cytometry cell sorting using an FACS Aria II (BD Biosciences) flow cytometer not earlier than 48 h after transduction.

6.3. Preparation and analysis of RNA

Interstrand ligation assay. The interstrand ligation assay was essentially performed as described before (Popow et al., 2011). The dsRNA substrate was generated by ligating 1.11 MBq [5'-^{32}P]cytidine-3',5'-bisphosphate (111 TBq/mmol, Perkin Elmer) to 50 pmol RNA oligonucleotide (5'-UCG AAG UAU UCC GCG UAC GU- 3', obtained from IBA) with 20 units T4 RNA ligase 1 (NEB) at 16 °C in 15 % (v/v) DMSO, 50 mM Tris-HCl pH 7.6, 10 mM $MgCl_2$, 10 mM β-mercaptoethanol, 200 µM ATP, 0.1 mg/ml BSA for 1 h in a total reaction volume of 10 µl. Labeling was stopped by the addition of 10 µl of 8 M urea, 50 mM Tris-HCl pH 8.0. Subsequently the labeled substrate was resolved by denaturing gel electrophoresis with 15 % polyacrylamide gels (SequaGel®, National Diagnostics), visualized by autoradiography and eluted from gel slices in 300 mM NaCl at 4 °C for 12 h. RNA was precipitated by the addition of 3 volumes of ethanol, recovered by centrifugation and annealed to non-labeled complementary RNA oligonucleotides (5'-CGU ACG CGG AAU ACU UCG A-3', obtained from IBA) by heating 50 nM labeled and non-labeled RNA oligonucleotides in 30 mM HEPES KOH pH 7.5, 2 mM $MgCl_2$ and 100 mM KCl to 95 °C for 2 min and subsequent incubation at 37 °C for one hour.

For interstrand ligation, 1 µl of the thus labeled substrate was mixed with 2 µl of ligation cocktail (250 µM EDTA pH 8.0, 100 mM KCl, 3 mM $MgCl_2$, 12.5 mM DTT, 7.5 mM ATP, 0.5 mM GTP, 10 U/ml RNasin® (Promega), 65 % [w/v] glycerol) and 2 µl protein extract containing at least 1 mg/ml protein in 30 mM HEPES-KOH pH 7.4, 5 mM $MgCl_2$, 100 mM KCl, 10 % [w/v] glycerol, 0.1 mM AEBSF, 1 mM DTT. This reaction mixture was incubated for 30 min at 30 °C. Reactions were stopped by the addition of 5 µl of 2 x FA buffer (0.1 % [w/v] bromophenol blue, 5 µM EDTA pH 8.0, 95 % [v/v] deionized formamide) and by boiling at 95 °C for 5 min. Subsequently, the occurrence of RNA ligation was analyzed by 15 % denaturing polyacrylamide gel electrophoresis and by phosphorimaging.

Isolation of RNA. For isolation of total RNA, cells were lysed in TRIzol® reagent (Invitrogen). Subsequently, RNA was purified according to the manufacturer's instructions. In brief, samples were collected in 1 ml of TRIzol® reagent, homogenized at room temperature for 5 min and supplemented with 0.2 ml of chloroform. After phase separation and centrifugation at 12.000 x g and 4 °C for 15 min, the upper aqueous phase was collected. Total RNA was precipitated at room temperature using 1 ml of isopropanol, pelleted by centrifugation at 12.000 x g and 4 °C for 10 min and washed with 1 ml of 75 % ethanol. Finally, RNA was pelleted by centrifugation at 7.500 x g and 4 °C for 5 min and dissolved in 20 µl of RNase-free water.

cDNA synthesis. RNA was isolated from Tet-On cell lines treated with 1 µg/ml Dox for six consecutive days to induce shRNA expression and protein depletion. For UPR-related studies, on day six of Dox treatment cells were additionally treated with 300 nM Tg. Subsequently, total cellular RNA was isolated using TRIzol® reagent (Invitrogen, details see "Isolation of RNA") and subjected to DNase treatment and cDNA synthesis using the Maxima First Strand cDNA synthesis Kit for RT-qPCR with dsDNase (Thermo Scientific). DNase treatment as well as cDNA synthesis was carried out according to the manufacturer's instructions. In brief, up to 5 µg of total RNA were incubated with 1 x dsDNase in a total reaction volume of 10 µl at 37 °C for 2 min. Subsequently, DNase-treated RNA was supplemented with 1 x Maxima Enzyme Mix and 1 x Reaction Mix to a total volume of 20 µl and incubated for 10 min at 25 °C followed by 15 min at 50 °C. Finally, the reaction was terminated by heating to 85 °C for 5 min and the thus obtained cDNA was diluted to a total volume of 200 µl using nuclease-free water.

Quantitative reverse transcriptase PCR. RT-qPCR analysis was performed using the GoTaq® qPCR Master Mix (Promega). The PCR reaction was performed in 20 µl reactions containing 3 µl of diluted cDNA (see "cDNA synthesis"), 0.5 µM of the respective forward and reverse primers and 10 µl of GoTaq® qPCR Master Mix. Reactions were pipetted using a Bravo LT96 Liquid Handling system (Agilent). All RT-qPCR primers used for this study (see Table 4) are exon-exon spanning and were designed using Primer3 software (version 0.4.0). The forward primer used to detect human *XBP1s* mRNA has been reported before (Majumder et al., 2012). The quality of PCR primers was evaluated by melting curve analysis, DNA gel electrophoresis of the PCR products and by determination of amplification efficiency. The reaction was performed using the following parameters: 50 °C for 10 min, 95 °C for 5 min, followed by 60 cycles in total at 95 °C for 10 sec and 60 °C for 30 sec. The obtained data were analyzed according to the ΔΔCt method normalizing to human *ACTB*. Additionally, expression levels were normalized to the untreated control sample.

Table 4: Sequences of RT-qPCR primers

Gene	Forward primer	Reverse primer
ACTB	TTG CCG ACA GGA TGC AGA AGG A	AGG TGG ACA GCG AGG CCA GGA T
RTCB	CAT CGA CCA TAA GGG ACA GG	GAT TCG AGC ACA AGC CAA CT
Archease	GCA TGG GGA GAT ACT CTG GA	CTT CCC GGG GTA TGA AGA AT
DDX1	GGA AGA CTA GAT GAC TTG GTG TCA	TCA GAA TAA CCT TGA GAA AGA AGC
FAM98B	TGG TAT ACC CAA GTC AAC AAC TTC	CCA CAT GAT TTT TCT GGA CCT
CGI99	GGT TTA GCT GTT AGA CTT GAA TAT GG	TGA TCA ATG GTT CTG CAT TTT T
Ashwin	GTC CCA GGA GTT CCT TCT CC	ACG ATG AGG GGT CTT TTC CT
XBP1s	GAG TCC GCA GCA GGT G	GGA AGG GCA TTT GAA GAA CA
Total *XBP1*	GCG CTG AGG AGG AAA CTG AAA AAC	CCA AGC GCT GTC TTA ACT CC
XBP1u	ACT ACG TGC ACC TCT GCA G	GGA AGG GCA TTT GAA GAA CA
EDEM1	GAT TCC ATA TCC TCG GGT GA	ATC CCA AAT TCC ACC AGG AG
DNAJB9	TGC TGA AGC AAA ATT CAG AGA	CCA CTA GTA AAA GCA CTG TGT CCA
IRE1α	GAG ACC CTG CGC TAT CTG AC	CCA TTG AGG GAG AGG CAT AG
BLOS1	GAG GCG AGA GGC TAT CAC TG	GCC TGG TTG AAG TTC TCC AC
SCARA3	TGC CTT GTG CGT TAC AGA AG	GAA AAC CAG AGA GGC CAA CA
PDGFRB	GCT CAC ACT GAC CAA CCT CA	TCT TCT CGT GCA GTG TCA CC
BIP	GTG GAA TGA CCC GTC TGT G	GTG GAA TGA CCC GTC TGT G
CHOP	CAT TGC CTT TCT CCT TCG GG	CCA GAG AAG CAG GGT CAA GA
PERK	CCT GTC TTG GTA GGA TCT GAT G	ATG TGG GTT GTC GAG GAA TC
ASNS	TCC GTA TTT GTG GCT CTG TT	TTG CTC AAT TCC TCC TTT GTC
CCNA1	GAG GGA AAC TGC AGC TCG TA	CTT TCA GAA GCA AGT GTT CCA
CCNA2	GGT ACT GAA GTC CGG GAA CC	ATC CAC ATG AAT GGT GAA CG
CCNB1	ATC CTA ATT GAC TGG CTA GTA CAG G	AAA CAT GGC AGT GAC ACC AA
CCNB2	TGT ACA TGT GCG TTG GCA TT	GAA GCC AAG AGC AGA GCA GT
CCND1	GGA GAC CAT CCC CCT GAC	CCA CTT GAG CTT GTT CAC CA
CCND2	AGA GAC CAG CCC GCT GAC	CGC AAG ATG TGC TCA ATG AA
CCNE1	CAG CTT ATT GGG ATT TCA TCT TT	CTC CTG AAC AAG CTC CAT CTG
CCNE2	GAT GGT GCT TGC AGT GAA GA	GGA GAA AGA GAT TTA GCC AGG A
TGFB1	GTA CCT GAA CCC GTG TTG CT	GTA TCG CCA GGA ATT GTT GC
TGFBR2	CAG GAA GTC TGT GTG GCT GT	GGA GAA GCA GCA TCT TCC AG
PGF	GCG ATG AGA ATC TGC ACT GT	AAC GTG CTG AGA GAA CGT CA
AR	TGA AGC AGG GAT GAC TCT GG	TCT GGT TGT CTC CTC AGT GG
NOTCH3	GTG TCA ATG GCT GGA CAG G	TCA TCC AGG TGA CAC AGG AG
VEGFA	AAG GAG GAG GGC AGA ATC AT	GGG TAC TCC TGG AAG ATG TCC
ADRA1B	AAG AAA GCA GCT AAG ACG TTG G	TCA GGG TGG AGA ACA AGG AG
GAB2	GCT TCA ATC AGG CTG AGG AG	GCT GGC TAG AGC TGC TGA
HIF1α	TCA GCT ATT TGC GTG TGA GG	TCA GAA ATG TAA ATC ATG TCA CCA
MEF2C	AAT TCC TGC TGT TCC ACC TC	GTG AGC CAG TGG CAA TAG GT

RT-PCR. *XBP1s* and *XBP1u* mRNA levels were monitored by semi-quantitative real time PCR using cDNA synthesized from dsDNase-treated total RNA as described above ("cDNA synthesis") and the following reaction conditions: in a 25 µl reaction volume 2 µl of cDNA were mixed with 12.5 µl of RedTaq® ReadyMix™ PCR Reaction Mix (Sigma) and 0.2 µM of the amplification primers (XBP1u/s_fwd: 5'- TAA TAC GAC TCA CTA TAG GGG AAT GAA GTG AGG CCA GT-3' and XBP1u/s_rev: 5'-AAT CCA TGG GGA GAT GTT CTG GAG-3'). Amplification of DNA was performed using the following cycling parameters: 98 °C for 3 min; 27 cycles of 98 °C for 30 s, 55 °C for 45 s and 72 °C for 1 min; 72 °C for 10 min. For *ACTB* mRNA levels, cDNA was amplified by 22 cycles and the following primers were used: 5'-TTG CCG ACA GGA TGC AGA AGG A-3' (fwd) and 5'-AGG TGG ACA GCG AGG CCA GGA T-3' (rev). PCR products were resolved by 2.5 % agarose gel electrophoresis. Densitometric analysis was performed using Fiji software (version 1.47i) and corrected by subtraction of the appropriate background values.

Northern Blotting. Northern Blot analysis was done as previously described (Karaca et al., 2014). In brief, 5 µg of total RNA were resolved by denaturing urea gel electrophoresis in 10 % polyacrylamide gels (Sequagel, National Diagnostics). Subsequently, RNA was blotted on Hybond® N+ membranes (GE Lifesciences) and fixed by ultraviolet crosslinking. Subsequently, the membranes were pre-hybridized in 5 x SSC, 20 mM Na_2HPO_4 pH 7.2, 7 % SDS, and 0.1 mg/ml sonicated salmon sperm DNA (Stratagene) at 50 °C for 1 h. Hybridization was carried out in the same buffer at 50 °C overnight using 100 pmol of the following [5'-^{32}P] labeled DNA probes: Arginine tRNA 5' exon probe: 5'-TAG AAG TCC AAT GCG CTA TCC-3', Isoleucine tRNA 5' exon probe: 5'-TAT AAG TAC CGC GCG CTA ACC-3', Methionine tRNA 5' exon probe: 5'-GGG CCC AGC ACG CTT CCG CTG CGC CAC TCT GC-3'. Equal loading was confirmed by hybridization of the membranes with a [5'-^{32}P] labeled DNA probe detecting U6 snRNA (5'-GCA GGG GCC ATG CTA ATC TTC TCT GTA TCG-3'). Blots were washed twice for 1 min with 5 x SSC, 5 % SDS and once with 1 X SSC, 1 % SDS at 50 °C and RNA was visualized by phosphorimaging. For stripping, membranes were boiled for 5 min in 0.1 % SDS and 0.1 X SSC.

Library preparation and RNA sequencing. For RNA sequencing, total RNA was isolated from Tet-On cell lines treated with Dox for six consecutive days as described above ("Isolation of RNA"). mRNAs were subsequently enriched by polyA enrichment (Dynabeads® mRNA purification Kit, Ambion, HeLa cells) or by depletion of ribosomal RNA using the Ribo-Zero™ rRNA Removal Kit (epicenter, PANC-1, MIA PaCa-2, EFM-192A, or Reh cells). For all samples, the cDNA library preparation was performed using the NEBNext® Ultra™ Directional RNA Library Prep Kit for

Illumina® (New England Biolabs). Sequencing was performed on Illumina HiSeq 2500 instruments in single read 50 bp or paired end 125 bp modus.

Analysis of 50 bp single read RNA sequencing data. Adapters from single end-fragments were removed using cutadapt (v1.5) and reads with a length of less than 18 base pairs in any sample of the duplicates were discarded. The adaptor-free reads were aligned against human rRNA and the ERCC sequences (bowtie2 v2.1.0). The rRNA-cleaned reads were aligned against the human genome (GRCh38/hg20) using STAR (v2.4.2a) with the help of the ENSEMBL gene annotation (ENSEMBL 78). The uniquely aligning reads were used for counting per gene with htseq-count (v0.6.1p1). The resulting counts per gene of all samples were merged and differential gene expression was calculated with DESeq2 (v1.6.3). GO term analysis was carried out using goseq (v1.18.0) and only considering RNA transcripts whose expression was significantly altered after depletion of RTCB and archease (adjusted p-value ≤ 0.05). Heat maps were generated with the heatmap.2 function of the gplots package (v2.17.0).

Analysis of 125 bp paired-end RNA sequencing data. RNA-sequencing reads were aligned to the human genome (GRCh37/hg19) using STAR 2.4.2a in a two-pass mode, where splice-junction discovery is performed before final alignment (see also (Engstrom et al., 2013)). Paired-end sequencing adaptors were trimmed off using Trim Galore (v0.3.7) and reads mapping to ribosomal RNA were filtered out using Bowtie (v.0.12.9) (Krueger F Trim Galore, see also (Langmead et al., 2009). The splice junction database was created in a first STAR run using reads from all samples. Splice junction read coverage per sample was obtained in a second STAR run with a genome index using the splice junction database. Splice junctions with coverage of at least 10 reads over all samples were retained, aggregated by gene and tested for differential usage using DEXSeq (v1.6.2, R v3.1.2) (see also (Anders et al., 2012; DeBoever et al., 2015)).

6.4. Molecular biology

Immunofluorescence. Wild type HeLa cells were seeded on coverslips and eventually treated with 300 nM Thapsigargin (Tg) for 30 min, 4 h or 16 h, respectively. Subsequently, cells were fixed with 2 % (w/v) paraformaldehyde for 20 min at room temperature (RT). Permeabilization was carried out by incubation in 0.2 % (v/v) Triton-X100/PBS for 5 min at RT where after cells were kept in blocking solution (5 % (w/v) BSA, 0.1 % (v/v) Tween20 in PBS, sterile filtered) for 30 min.

After this blocking step, coverslips were incubated for one hour at RT with the following primary antibodies dissolved in blocking solution: RTCB (Santa Cruz, 1:500), archease (monoclonal, 1:2), calnexin (Santa Cruz, 1:100). The archease monoclonal antibody was generated by immunizing mice with wild type histidine-tagged archease purified as described previously (Popow et al., 2014), fusion of splenocytes and the generation of hybridoma (Monoclonal Antibody Facility, Max F. Perutz Laboratories, Vienna). Cells were washed three times in 0.1 % PBST for 3 min each and incubated for one hour at RT with fluorescent secondary antibodies diluted in blocking solution: Alexa Fluor® 488 Donkey Anti-Rabbit IgG (Invitrogen, 1:500), Alexa Fluor® 568 Donkey Anti-Mouse IgG (Invitrogen, 1:500), Alexa Fluor® 647 Donkey Anti-Goat IgG (Invitrogen, 1:500). Subsequently, coverslips were washed four times with 0.1 % PBST for 5 min each and finally mounted in ProLong® Gold Antifade Mountant with DAPI (Invitrogen). Images were taken using a laser scanning confocal microscope (LSM780, Zeiss).

Subcellular fractionation. Wild type HeLa cells were seeded at equal cell densities and eventually treated with 300 nM Tg for 30 min or 4 h. Subcellular fractionation analysis was performed using the Subcellular Protein Fractionation Kit for Cultured Cells (Thermo Scientific). In brief, cells were harvested by trypsinization, washed with ice-cold PBS and lysed in 10 volumes of ice-cold CEB buffer containing protease inhibitors by incubation at 4 °C for 10 min while gentle mixing. After centrifugation at 500 x g for 5 min at 4 °C, the supernatant was collected (cytoplasmic extract). The pellet was further lysed by incubation in 10 volumes of ice-cold MEB containing protease inhibitors at 4 °C for 10 min while gentle mixing and the membrane extract was collected by centrifugation at 3.000 x g for 5 min at 4 °C. The remaining pellet containing the soluble as well as insoluble nuclear fraction was lysed by boiling at 98 °C for 5 min in 10 volumes of 2 x SDS loading buffer. Equal amounts of the fractions obtained were subsequently used for Western Blot analysis as described below.

Preparation of whole cell extracts. For the preparation of whole cell extracts, cells were seeded at equal cell numbers, eventually subjected to Tg treatment and harvested by scraping. The obtained cell pellet was incubated on ice for 15 min in high salt buffer (20 mM Tris pH 7.5, 400 mM NaCl, 0.5 % NP40, 0.3 % [w/v] Triton® X-100) freshly supplemented with 1 mM of PMSF and cOmplete™ Protease Inhibitor Cocktail (Roche). After lysis, samples were centrifuged at 13.000 rpm and 4 °C for 20 min in a tabletop centrifuge and the supernatant obtained was used for further analysis.

Determination of protein concentration by Bradford assay. The protein concentration of whole cell extracts was determined using Bradford assay. For this purpose, one volume of Bradford reagent (BioRad) was diluted with 4 volumes of water. Subsequently, 1 ml of diluted Bradford reagent was mixed with 1 µl of whole cell extract, incubated at RT for 5 min and used for absorption measurement at 595 nm. Diluted Bradford reagent mixed with 1 µl of high salt buffer was used as blank reference. Additionally, a standard curve based on a dilution series of BSA (NEB) in high salt buffer ranging from 5 µg/ml to 0,313 µg/ml was generated and used to calculate protein concentrations.

Western blotting. For Western Blot analysis cells were treated with Dox for six days. At day five of Dox treatment, cells seeded at equal cell densities. 24 h later, cells were stressed with 300 nM Tg over a 24-h time course and lysed in high salt buffer. Protein concentrations were determined using Bradford assay (details see "Determination of protein concentration by Bradford assay"). Subsequently, 30 µg of each sample were diluted with appropriate amounts of 5 x SDS loading buffer (62,5 mM Tris pH 6.8, 25 mM EDTA pH 8.0, 5 % [w/v] SDS, 5 % [v/v] β-mercaptoethanol, 0,025 % [w/v] bromophenol blue, 50 % [v/v] glycerol), boiled at 98 °C for 5 min and separated by SDS-PAGE. SDS denaturing protein gels were cast using appropriate amounts of 4 x separation gel buffer (1.44 M Tris-HCl pH 8.8, 0.4 % [w/v] SDS) or 8 x stacking gel buffer (0.92 M Tris-HCl pH 6.8, 0.8 % [w/v] SDS), 30 % ProtoGel® (National Diagnostics) and water in the presence of Ammonium persulphate and TEMED. Electrophoresis was performed in 1 x Tris-glycin-SDS PAGE buffer (National Diagnostics) at 80 to 120 V. Afterwards, proteins were transferred to activated Immobilon-P membranes (Millipore) using semidry transfer (1 mA/cm^2) in 1 x semidry blotting buffer (192 mM glycin, 25 mM Tris, 0.02 % [w/v] SDS, 10 % [v/v] methanol). Membranes were incubated in 3 % BSA/PBST (0.5 % [v/v] Tween®-20 in PBS) for 1 h at RT. Primary antibodies (for details refer to Table 5) were diluted in 5 % skimmed milk/PBST or in 3 % BSA/PBST and used to incubate the membranes at RT for 1 h or at 4 °C overnight. Subsequently, membranes were washed three times in PBST for 5 to 10 min, incubated with secondary antibody in 5 % milk/PBST for 1 h at RT, and again washed in PBST. Western Blots were developed using Clarity™ Western ECL Blotting Substrate (BioRad) and a ChemiDoc™ MP System (BioRad).

Table 5: Antibodies

Target protein		Dilution	Dilution buffer
β-Actin	Sigma, A2066	5000	5 % milk/PBST
Androgen Receptor	Cell signaling, 5153	1000	5 % milk/PBST
Archease	(Jurkin et al., 2014)	500	3 % BSA/PBST
BIP	Cell signaling, 3177	1000	5 % milk/PBST
Calnexin	Santa Cruz, sc-6465	1000	5 % milk/PBST
CHOP	Cell signaling, 2895	1000	5 % milk/PBST
Cleaved PARP	Cell signaling, 9541	1000	5 % milk/PBST
Cyclin A2	Cell signaling, 4656	2000	5 % milk/PBST
Cyclin E1	Cell signaling, 4129	1000	5 % milk/PBST
DDX1	Bethyl, A300-521A	1000	5 % milk/PBST
eIF2α	Cell signaling, 2103	1000	5 % milk/PBST
FAM98B	Sigma, HPA008320	500	5 % milk/PBST
HSP90	Abcam, 13495	10000	5 % milk/PBST
IRE1	Thermo, PA5-20189	1000	5 % milk/PBST
Lamin A/C	Sigma, SAB4200236	10000	5 % milk/PBST
LC3B	Cell signaling, 2775	1000	5 % milk/PBST
mTOR	Cell signaling, 2983	1000	5 % milk/PBST
PERK	Santa Cruz, sc-9481	1000	5 % milk/PBST
Phospho-4E-BP1 (Thr37/46)	Cell signaling, 2855	1000	3 % BSA/PBST
Phospho-AKT (Ser473)	Cell signaling, 4060	2000	3 % BSA/PBST
Phospho-AKT (Thr308)	Cell signaling, 2965	1000	3 % BSA/PBST
Phospho-eIF2α	Cell signaling, 3398S	1000	3 % BSA/PBST
Phospho-IRE1 (Ser724)	GeneTex, GTX63722	10000	3 % BSA/PBST
Phospho-mTOR (Ser2448)	Cell signaling, 5536	1000	3 % BSA/PBST
Phospho-ERK1/2	Cell signaling, 4370	2000	3 % BSA/PBST
Phospho-p70 S6 Kinase (Ser371)	Cell signaling, 9208	1000	3 % BSA/PBST
Phospho-p70 S6 Kinase (Thr389)	Cell signaling, 2983	1000	3 % BSA/PBST
Phospho-JNK (Thr183/Tyr1850)	Cell signaling, 4668	1000	3 % BSA/PBST
Phospho-SMAD2	Cell signaling, 3101S	1000	3 % BSA/PBST
RTCB	(Popow et al., 2011)	5000	5 % milk/PBST
SMAD2	Cell signaling, 5339S	1000	5 % milk/PBST
XBP1s	Bioledgend, 619502	500	5 % milk/PBST

Metabolic labeling. Tet-On HeLa cell lines were treated with 1 µg/ml Dox to induce shRNA expression. On day six of Dox treatment, cells first were starved in DMEM without L-methionine and L-cysteine (Gibco) for 2 h at 37 °C and then cultured for one hour at 37 °C in Met and Cys-free DMEM supplemented with 16 MBq/ml [^{35}S]-labeled methionine and cysteine (Perkin Elmer, EasyTag™ EXPRESS^{35}S Protein Labeling Mix). After this labeling period, cells were lysed in 2 % (w/v) SDS, 20 mM HEPES pH 7.4 and proteins were pelleted by acetone precipitation at -20 °C overnight. After spinning at 13.000 rpm and 4 °C for 20 min in a tabletop centrifuge, the obtained protein pellet was resuspended in 50 µl lysis buffer and protein concentration was determined by BCA assay (Thermo Scientific). Furthermore, scintillation counts of the obtained cell lysates were measured and normalized to the respective protein concentrations. For autoradiography, cells were directly lysed in 1 x SDS Loading buffer at 95 °C for 5 min. Proteins were separated by SDS-PAGE, transferred to Immobilon-P membranes (Millipore) and radioactively labeled proteins were visualized by autoradiography. Furthermore, membranes were analyzed by Western Blot analysis using the indicated primary antibodies.

MTT assay. Tet-On HeLa cells were treated with 1 µg/ml Dox for six consecutive days to induce shRNA expression. On day six of Dox treatment, cells were plated in 96well plates at a cell density of 50.000 cells/well. Cells were plated in triplicates and in phenol red-free DMEM (Gibco) supplemented with 10 % fetal bovine serum (Sigma), 3 mM glutamine (Sigma), 100 U/ml penicillin, 100 µg/ml streptomycin sulfate (Sigma), and 20 mM HEPES pH 7.0. Three to four hours after seeding, the MTT assay was performed using the Vybrant® MTT Cell Proliferation Assay Kit (Life Technologies). For this purpose, the cell culture medium was replaced with 100 µl of fresh phenol red-free DMEM supplemented with 1 µM of MTT stock solution. Additionally, a negative control containing 1 μM of MTT stock solution in 100 μL of cell culture medium without cells was used for background measurements. Cells were incubated for 3 h at 37 °C and subsequently lysed by the addition of 100 μl of 0.1 % [w/v] SDS in 0.01 M HCl. Lysates were incubated at 37 °C overnight and analyzed by absorbance measurement at 570 nm. For analysis, the mean absorbance of the individual triplicates was calculated, subtracted by the background absorbance and normalized to the absorbance of the respective control cell line expressing one or two copies of the control shRNA.

Proliferation assay. Cell proliferation was assayed using the CellTrace™ Violet Cell Proliferation Kit (life technologies) according to manufacturer's instructions. In brief, Tet-On HeLa cells were treated with Dox to induce shRNA expression. On day five of Dox treatment, cells were harvested by trypsinization and counted. 1 x 10^6 cells were

washed with PBS and resuspended in 1 ml of PBS supplemented with CellTrace Violet Stock solution to a final concentration of 5 µM. Cells were incubated in the dark at 37 °C for 20 min, mixed with five volumes of full DMEM containing 10 % of FBS (Sigma) and incubated for 5 min at RT. Subsequently, cells were washed with PBS and roughly 50 % of cells were resuspended in 0.5 ml of FACS buffer (0.5 % BSA in PBS). These samples were analyzed using an LSR Fortessa (BD Biosciences) flow cytometer, whereby at least 100.000 GFP-positive or GFP/dsRed-positive cells were recorded. The remaining 50 % of cells were supplemented with full DMEM containing fresh Dox and cultured for two additional days at 37 °C with 5 % CO_2. On day seven of Dox treatment, cells were subcultured whereby 50 % of cells were used for flow cytometry analysis while the remaining 50 % were again supplemented with full DMEM containing fresh Dox and cultured for two additional days. These cells were harvested for flow cytometry analysis on day nine of Dox treatment. Analysis was performed using FlowJo software (Treestar).

Cell cycle profiling. Tet-On HeLa cells were treated with Dox for six consecutive days to induce the expression of shRNAs and plated at equal cell numbers at day five of Dox treatment. For Hoechst staining, cells were trypsinized, resuspended in full cell culture medium to obtain a single cell suspension and incubated with 20 µM Hoechst 33342 (Sigma) for 30 min at 37 °C with occasional mixing. Subsequently, cells were pelleted by centrifugation and resuspended in 0.5 ml of FACS buffer (0.5 % BSA in PBS). Cells were analyzed using an LSR Fortessa (BD Biosciences) flow cytometer. For every cell line at least 100.000 GFP-positive or GFP/dsRed-positive cells were recorded and analyzed. Cell cycle profiles were calculated using the “Watson Pragmatic approach” (Ormerod et al., 1987; Watson et al., 1987) and the FlowJo software (Treestar). Cell duplicates were excluded from the analysis based on the FSC-A versus FSC-W signal.

BrdU labeling. The relative percentage of cells undergoing DNA replication was analyzed by BrdU labeling using the BrdU Staining Kit for Flow Cytometry (eBioscience) according to manufacturer’s instructions. For this purpose, Tet-On HeLa cells were treated with Dox for six consecutive days to induce shRNA expression and 1 x 10^6 cells were plated on 6 cm-plate at day five of Dox treatment. On day six of Dox treatment, 10 µM BrdU was added to the culture medium in the presence of Dox and cells were incubated for 1 h at 37 °C. After incubation, cells were harvested by trypsinization, washed with and resuspended in 100 µl of Flow Cytometry Staining buffer (0.5 % BSA in PBS, sterile filtered). After fixation of cells with 1 ml of 1 x BrdU Staining Buffer for 15 min at RT, all samples were washed again and treated with DNase I for 1 h at 37 °C in the dark. Cells were stained with

5 µl of APC-coupled Anti-BrdU antibody and incubated for 30 min at RT in the dark. Finally, cells were washed and resuspended in Flow Cytometry Staining buffer and analyzed using an LSR Fortessa (BD Biosciences) flow cytometer. For every cell line at least 100.000 GFP-positive or GFP/dsRed-positive cells were recorded and analyzed.

Competition assay. To assess the relative competitiveness of RTCB- and archease-depleted Tet-On cancer cell lines, RTCB/archease or control/control cells were mixed at random ratios with the respective RIEP cell line expressing only the Tet Repressor but no shRNA construct. After subculturing of these cell mixtures for five days, shRNA expression was induced by doxycycline treatment (1 µg/ml) and the evolution of shRNA-positive cells was followed based on GFP and dsRed expression. For this purpose, an LSR Fortessa (BD Biosciences) flow cytometer was used and at least 100.000 cells were recorded at each of the time points analyzed. During the duration of the experiment, cells were kept subconfluent and under Dox treatment, whereby Dox-containing cell culture medium was replaced every second day.

7. Appendix

7.1. Supplementary data and figures

Results of RNA sequencing analysis

Table 6: RNA sequencing targets Tet-On HeLa cells, untreated

Gene ID	Gene name	Fold change [log2]	Adjusted p-value
ENSG00000147041	synaptotagmin-like 5	-2,36	0,0000
ENSG00000132205	elastin microfibril interfacer 2	-2,28	0,0000
ENSG00000180616	somatostatin receptor 2	-2,09	0,0000
ENSG00000169083	androgen receptor	-2,04	0,0000
ENSG00000280237	NA	-2,02	0,0000
ENSG00000176261	zinc finger and BTB domain containing 8 opposite strand	-1,99	0,0000
ENSG00000080573	collagen, type V, alpha 3	-1,93	0,0000
ENSG00000081189	myocyte enhancer factor 2C	-1,86	0,0000
ENSG00000221955	solute carrier family 12, member 8	-1,78	0,0001
ENSG00000100220	RNA 2',3'-cyclic phosphate and 5'-OH ligase	-1,77	0,0000
ENSG00000159251	actin, alpha, cardiac muscle 1	-1,77	0,0000
ENSG00000179046	tripartite motif family-like 2	-1,73	0,0001
ENSG00000182836	phosphatidylinositol-specific phospholipase C, X domain containing 3	-1,65	0,0008
ENSG00000163131	cathepsin S	-1,54	0,0004
ENSG00000165181	chromosome 9 open reading frame 84	-1,52	0,0023
ENSG00000080854	immunoglobulin superfamily, member 9B	-1,52	0,0034
ENSG00000163513	transforming growth factor, beta receptor II (70/80kDa)	-1,51	0,0000
ENSG00000198915	RasGEF domain family, member 1A	-1,50	0,0002
ENSG00000127324	tetraspanin 8	-1,49	0,0055
ENSG00000133943	chromosome 14 open reading frame 159	-1,48	0,0042
ENSG00000135346	glycoprotein hormones, alpha polypeptide	-1,46	0,0068
ENSG00000103534	transmembrane channel-like 5	-1,46	0,0040
ENSG00000144460	neuronal tyrosine-phosphorylated phosphoinositide-3-kinase adaptor 2	-1,43	0,0075
ENSG00000170214	adrenoceptor alpha 1B	-1,42	0,0103
ENSG00000159753	RGD motif, leucine rich repeats, tropomodulin domain and proline-rich containing	-1,40	0,0000
ENSG00000128564	VGF nerve growth factor inducible	-1,40	0,0020
ENSG00000074181	notch 3	-1,40	0,0009
ENSG00000147872	perilipin 2	-1,38	0,0144
ENSG00000065325	glucagon-like peptide 2 receptor	-1,36	0,0010
ENSG00000173210	actin binding LIM protein family, member 3	-1,36	0,0096
ENSG00000168243	guanine nucleotide binding protein (G protein), gamma 4	-1,35	0,0020
ENSG00000106780	multiple EGF-like-domains 9	-1,35	0,0053
ENSG00000169891	RALBP1 associated Eps domain containing 2	-1,35	0,0077
ENSG00000106927	alpha-1-microglobulin/bikunin precursor	-1,34	0,0042
ENSG00000178150	zinc finger protein 114	-1,31	0,0033
ENSG00000139793	muscleblind-like splicing regulator 2	-1,30	0,0000
ENSG00000205302	sorting nexin 2	-1,29	0,0000
ENSG00000138646	HECT and RLD domain containing E3 ubiquitin protein ligase 5	-1,29	0,0110
ENSG00000023445	baculoviral IAP repeat containing 3	-1,25	0,0344
ENSG00000164949	GTP binding protein overexpressed in skeletal muscle	-1,25	0,0010

ENSG00000167157	paired related homeobox 2	-1,25	0,0364
ENSG00000150551	LY6/PLAUR domain containing 1	-1,23	0,0450
ENSG00000066468	fibroblast growth factor receptor 2	-1,22	0,0055
ENSG00000135678	carboxypeptidase M	-1,22	0,0005
ENSG00000273301	NA	-1,22	0,0477
ENSG00000170500	LON peptidase N-terminal domain and ring finger 2	-1,21	0,0363
ENSG00000157470	family with sequence similarity 81, member A	-1,19	0,0000
ENSG00000104833	tubulin, beta 4A class IVa	-1,18	0,0443
ENSG00000167191	G protein-coupled receptor, class C, group 5, member B	-1,18	0,0258
ENSG00000091592	NLR family, pyrin domain containing 1	-1,17	0,0279
ENSG00000166073	G protein-coupled receptor 176	-1,16	0,0040
ENSG00000113083	lysyl oxidase	-1,15	0,0000
ENSG00000139370	solute carrier family 15 (oligopeptide transporter), member 4	-1,14	0,0004
ENSG00000248323	lung cancer associated transcript 1 (non-protein coding)	-1,14	0,0198
ENSG00000198910	L1 cell adhesion molecule	-1,14	0,0002
ENSG00000033327	GRB2-associated binding protein 2	-1,12	0,0423
ENSG00000163491	NIMA-related kinase 10	-1,12	0,0326
ENSG00000171303	potassium channel, subfamily K, member 3	-1,12	0,0152
ENSG00000116299	KIAA1324	-1,11	0,0223
ENSG00000105971	caveolin 2	-1,11	0,0003
ENSG00000151914	dystonin	-1,10	0,0000
ENSG00000135083	cyclin J-like	-1,06	0,0138
ENSG00000074410	carbonic anhydrase XII	-1,05	0,0203
ENSG00000165272	aquaporin 3 (Gill blood group)	-1,04	0,0012
ENSG00000101000	protein C receptor, endothelial	-1,04	0,0364
ENSG00000182326	complement component 1, s subcomponent	-1,02	0,0402
ENSG00000109586	polypeptide N-acetylgalactosaminyltransferase 7	-1,00	0,0010
ENSG00000145569	family with sequence similarity 105, member A	-0,98	0,0159
ENSG00000113657	dihydropyrimidinase-like 3	-0,98	0,0103
ENSG00000133216	EPH receptor B2	-0,97	0,0274
ENSG00000085276	MDS1 and EVI1 complex locus	-0,96	0,0136
ENSG00000196843	AT rich interactive domain 5A (MRF1-like)	-0,94	0,0171
ENSG00000151151	inositol polyphosphate multikinase	-0,94	0,0034
ENSG00000108448	tripartite motif containing 16-like	-0,94	0,0019
ENSG00000050555	laminin, gamma 3	-0,93	0,0090
ENSG00000165240	ATPase, Cu++ transporting, alpha polypeptide	-0,93	0,0197
ENSG00000150760	dedicator of cytokinesis 1	-0,93	0,0001
ENSG00000163710	procollagen C-endopeptidase enhancer 2	-0,92	0,0412
ENSG00000138829	fibrillin 2	-0,92	0,0271
ENSG00000173706	heart development protein with EGF-like domains 1	-0,92	0,0093
ENSG00000115380	EGF containing fibulin-like extracellular matrix protein 1	-0,91	0,0010
ENSG00000117519	calponin 3, acidic	-0,90	0,0093
ENSG00000134569	low density lipoprotein receptor-related protein 4	-0,89	0,0370
ENSG00000275216	NA	-0,89	0,0004
ENSG00000172954	lysocardiolipin acyltransferase 1	-0,89	0,0040
ENSG00000160408	ST6 (alpha-N-acetyl-neuraminyl-2,3-beta-galactosyl-1,3)-N-acetylgalactosaminide alpha-2,6-sialyltransferase 6	-0,88	0,0171
ENSG00000153956	calcium channel, voltage-dependent, alpha 2/delta subunit 1	-0,87	0,0046
ENSG00000120708	transforming growth factor, beta-induced, 68kDa	-0,87	0,0023
ENSG00000073712	fermitin family member 2	-0,86	0,0002
ENSG00000122545	septin 7	-0,85	0,0001
ENSG00000173821	ring finger protein 213	-0,85	0,0360
ENSG00000131725	WD repeat domain 44	-0,82	0,0187
ENSG00000226742	heat shock factor binding protein 1-like 1	-0,81	0,0480
ENSG00000109686	SH3 domain containing 19	-0,81	0,0080
ENSG00000209082	NA	-0,79	0,0059
ENSG00000253729	protein kinase, DNA-activated, catalytic polypeptide	-0,79	0,0002
ENSG00000115355	coiled-coil domain containing 88A	-0,78	0,0006
ENSG00000113615	SEC24 family member A	-0,77	0,0008
ENSG00000196739	collagen, type XXVII, alpha 1	-0,76	0,0041
ENSG00000221926	tripartite motif containing 16	-0,76	0,0069
ENSG00000105329	transforming growth factor, beta 1	-0,75	0,0341
ENSG00000107854	tankyrase, TRF1-interacting ankyrin-related ADP-ribose polymerase 2	-0,75	0,0046
ENSG00000143320	cellular retinoic acid binding protein 2	-0,75	0,0440
ENSG00000132589	flotillin 2	-0,74	0,0263
ENSG00000123104	inositol 1,4,5-trisphosphate receptor, type 2	-0,74	0,0128
ENSG00000140262	transcription factor 12	-0,74	0,0390
ENSG00000103642	lactamase, beta	-0,74	0,0385
ENSG00000274627	NA	-0,74	0,0214
ENSG00000197579	topoisomerase I binding, arginine/serine-rich, E3 ubiquitin protein ligase	-0,72	0,0062
ENSG00000213281	neuroblastoma RAS viral (v-ras) oncogene homolog	-0,70	0,0483
ENSG00000006118	transmembrane protein 132A	-0,70	0,0500
ENSG00000083312	transportin 1	-0,69	0,0111
ENSG00000134970	transmembrane emp24 protein transport domain containing 7	-0,68	0,0430
ENSG00000136026	cytoskeleton-associated protein 4	-0,68	0,0066
ENSG00000163249	cyclin Y-like 1	-0,67	0,0404
ENSG00000119414	protein phosphatase 6, catalytic subunit	-0,67	0,0245
ENSG00000183283	DAZ associated protein 2	-0,67	0,0021
ENSG00000107130	neuronal calcium sensor 1	-0,65	0,0483
ENSG00000068878	proteasome (prosome, macropain) activator subunit 4	-0,64	0,0092
ENSG00000119912	insulin-degrading enzyme	-0,64	0,0077
ENSG00000114416	fragile X mental retardation, autosomal homolog 1	-0,64	0,0187

ENSG00000188070	chromosome 11 open reading frame 95	-0,63	0,0299
ENSG00000204388	heat shock 70kDa protein 1B	-0,63	0,0236
ENSG00000074695	lectin, mannose-binding, 1	-0,60	0,0142
ENSG00000101350	kinesin family member 3B	-0,60	0,0141
ENSG00000168275	cytochrome c oxidase assembly factor 6 homolog (S. cerevisiae)	-0,59	0,0359
ENSG00000136819	chromosome 9 open reading frame 78	-0,58	0,0202
ENSG00000163527	STT3B, subunit of the oligosaccharyltransferase complex (catalytic)	-0,57	0,0198
ENSG00000165219	GTPase activating protein and VPS9 domains 1	-0,54	0,0311
ENSG00000181852	ring finger protein 41, E3 ubiquitin protein ligase	0,55	0,0386
ENSG00000065060	UHRF1 binding protein 1	0,60	0,0202
ENSG00000147123	NADH dehydrogenase (ubiquinone) 1 beta subcomplex, 11, 17.3kDa	0,61	0,0385
ENSG00000112715	vascular endothelial growth factor A	0,61	0,0247
ENSG00000125534	pancreatic progenitor cell differentiation and proliferation factor	0,64	0,0274
ENSG00000242498	actin-related protein 2/3 complex inhibitor	0,64	0,0486
ENSG00000204387	chromosome 6 open reading frame 48	0,65	0,0459
ENSG00000179912	R3H domain containing 2	0,66	0,0370
ENSG00000126822	pleckstrin homology domain containing, family G (with RhoGef domain) member 3	0,68	0,0236
ENSG00000170955	protein kinase C, delta binding protein	0,69	0,0293
ENSG00000151876	F-box protein 4	0,69	0,0167
ENSG00000065911	methylenetetrahydrofolate dehydrogenase (NADP+ dependent) 2, methenyltetrahydrofolate cyclohydrolase	0,69	0,0191
ENSG00000187097	ectonucleoside triphosphate diphosphohydrolase 5	0,71	0,0359
ENSG00000006757	patatin-like phospholipase domain containing 4	0,71	0,0164
ENSG00000213995	carbohydrate kinase domain containing	0,71	0,0369
ENSG00000168209	DNA-damage-inducible transcript 4	0,72	0,0164
ENSG00000130724	charged multivesicular body protein 2A	0,73	0,0370
ENSG00000137133	histidine triad nucleotide binding protein 2	0,74	0,0141
ENSG00000196998	WD repeat domain 45	0,74	0,0248
ENSG00000153879	CCAAT/enhancer binding protein (C/EBP), gamma	0,76	0,0144
ENSG00000137713	protein phosphatase 2, regulatory subunit A, beta	0,77	0,0066
ENSG00000164318	EGF-like, fibronectin type III and laminin G domains	0,77	0,0164
ENSG00000214941	zinc finger, SWIM-type containing 7	0,78	0,0477
ENSG00000196547	mannosidase, alpha, class 2A, member 2	0,78	0,0031
ENSG00000161677	Josephin domain containing 2	0,79	0,0393
ENSG00000185989	RAS p21 protein activator 3	0,79	0,0239
ENSG00000185453	chromosome 19 open reading frame 68	0,80	0,0203
ENSG00000059804	solute carrier family 2 (facilitated glucose transporter), member 3	0,82	0,0111
ENSG00000146733	phosphoserine phosphatase	0,82	0,0107
ENSG00000116991	signal-induced proliferation-associated 1 like 2	0,83	0,0110
ENSG00000128272	activating transcription factor 4	0,84	0,0000
ENSG00000090861	alanyl-tRNA synthetase	0,84	0,0002
ENSG00000140044	Jun dimerization protein 2	0,85	0,0107
ENSG00000135069	phosphoserine aminotransferase 1	0,86	0,0023
ENSG00000049239	hexose-6-phosphate dehydrogenase (glucose 1-dehydrogenase)	0,86	0,0310
ENSG00000268205	NA	0,86	0,0227
ENSG00000074935	tubulin, epsilon 1	0,86	0,0001
ENSG00000187840	eukaryotic translation initiation factor 4E binding protein 1	0,87	0,0038
ENSG00000158528	protein phosphatase 1, regulatory subunit 9A	0,88	0,0197
ENSG00000135480	keratin 7	0,89	0,0094
ENSG00000008710	polycystic kidney disease 1 (autosomal dominant)	0,89	0,0009
ENSG00000139410	serine dehydratase-like	0,90	0,0476
ENSG00000164695	charged multivesicular body protein 4C	0,91	0,0106
ENSG00000198208	ribosomal protein S6 kinase-like 1	0,91	0,0437
ENSG00000115902	solute carrier family 1 (glutamate/neutral amino acid transporter), member 4	0,92	0,0031
ENSG00000105136	zinc finger protein 419	0,92	0,0351
ENSG00000232677	long intergenic non-protein coding RNA 665	0,94	0,0498
ENSG00000141753	insulin-like growth factor binding protein 4	0,95	0,0060
ENSG00000106003	LFNG O-fucosylpeptide 3-beta-N-acetylglucosaminyltransferase	0,96	0,0459
ENSG00000169715	metallothionein 1E	0,96	0,0020
ENSG00000133678	transmembrane protein 254	0,98	0,0025
ENSG00000265972	thioredoxin interacting protein	0,98	0,0437
ENSG00000140105	tryptophanyl-tRNA synthetase	0,99	0,0006
ENSG00000147852	very low density lipoprotein receptor	0,99	0,0171
ENSG00000116761	cystathionine gamma-lyase	0,99	0,0018
ENSG00000092621	phosphoglycerate dehydrogenase	0,99	0,0006
ENSG00000153823	phosphotyrosine interaction domain containing 1	1,00	0,0245
ENSG00000174721	fibroblast growth factor binding protein 3	1,01	0,0283
ENSG00000166123	glutamic pyruvate transaminase (alanine aminotransferase) 2	1,02	0,0000
ENSG00000119938	protein phosphatase 1, regulatory subunit 3C	1,03	0,0062
ENSG00000204291	collagen, type XV, alpha 1	1,04	0,0449
ENSG00000272398	CD24 molecule	1,04	0,0001
ENSG00000107829	F-box and WD repeat domain containing 4	1,04	0,0030
ENSG00000106948	AT-hook transcription factor	1,05	0,0073
ENSG00000225177	uncharacterized LOC441172	1,06	0,0252
ENSG00000187735	transcription elongation factor A (SII), 1	1,06	0,0000
ENSG00000151090	thyroid hormone receptor, beta	1,08	0,0170
ENSG00000106479	zinc finger protein 862	1,09	0,0470
ENSG00000178172	serine peptidase inhibitor, Kazal type 6	1,09	0,0363
ENSG00000102452	sodium leak channel, non-selective	1,09	0,0124
ENSG00000239887	chromosome 1 open reading frame 226	1,10	0,0203

ENSG00000005059	coiled-coil domain containing 109B	1,11	0,0033
ENSG00000136010	aldehyde dehydrogenase 1 family, member L2	1,12	0,0016
ENSG00000135540	NHS-like 1	1,13	0,0018
ENSG00000157514	TSC22 domain family, member 3	1,15	0,0068
ENSG00000111432	frizzled class receptor 10	1,21	0,0040
ENSG00000205309	5',3'-nucleotidase, mitochondrial	1,23	0,0187
ENSG00000175197	DNA-damage-inducible transcript 3	1,23	0,0000
ENSG00000266208	NA	1,25	0,0002
ENSG00000198929	nitric oxide synthase 1 (neuronal) adaptor protein	1,25	0,0068
ENSG00000169031	collagen, type IV, alpha 3 (Goodpasture antigen)	1,26	0,0042
ENSG00000005379	benzodiazepine receptor (peripheral) associated protein 1	1,26	0,0040
ENSG00000130766	sestrin 2	1,27	0,0004
ENSG00000163053	solute carrier family 16, member 14	1,27	0,0001
ENSG00000196517	solute carrier family 6 (neurotransmitter transporter, glycine), member 9	1,28	0,0000
ENSG00000278970	NA	1,28	0,0001
ENSG00000150051	mohawk homeobox	1,32	0,0068
ENSG00000101255	tribbles pseudokinase 3	1,34	0,0000
ENSG00000253741	uncharacterized LOC100288181	1,35	0,0043
ENSG00000162733	discoidin domain receptor tyrosine kinase 2	1,41	0,0000
ENSG00000160094	zinc finger protein 362	1,42	0,0014
ENSG00000070669	asparagine synthetase (glutamine-hydrolyzing)	1,43	0,0001
ENSG00000130513	growth differentiation factor 15	1,49	0,0000
ENSG00000250208	FZD10 antisense RNA 1 (head to head)	1,56	0,0003
ENSG00000174951	fucosyltransferase 1 (galactoside 2-alpha-L-fucosyltransferase, H blood group)	1,61	0,0005
ENSG00000007314	sodium channel, voltage-gated, type IV, alpha subunit	1,64	0,0008
ENSG00000207827	microRNA 30a	1,78	0,0000
ENSG00000111981	UL16 binding protein 1	1,79	0,0000
ENSG00000100889	phosphoenolpyruvate carboxykinase 2 (mitochondrial)	1,88	0,0000
ENSG00000163331	death associated protein-like 1	2,05	0,0000
ENSG00000135842	family with sequence similarity 129, member A	2,10	0,0000
ENSG00000139269	inhibin, beta E	2,12	0,0000
ENSG00000128165	adrenomedullin 2	2,24	0,0000
ENSG00000128965	ChaC, cation transport regulator homolog 1 (E. coli)	2,32	0,0000

Table 7: Gene ontology analysis of RNA sequencing targets, untreated Tet-On HeLa cells

	Category	Term	Adj. p-value, overrepresentation
Molecular function	GO:0005539	glycosaminoglycan binding	0.04484461
Biochemical process	GO:0023052	signaling	0.002211320
	GO:0044700	single organism signaling	0.002211320
	GO:0007165	signal transduction	0.002211320
	GO:0048513	organ development	0.002211320
	GO:0007154	cell communication	0.002689433
	GO:0006520	cellular amino acid metabolic process	0.002692593
	GO:0007166	cell surface receptor signaling pathway	0.002697834
	GO:0044763	single-organism cellular process	0.003011363
	GO:0009725	response to hormone	0.007666867
	GO:0050896	response to stimulus	0.007666867
	GO:0048518	positive regulation of biological process	0.007666867
	GO:0048522	positive regulation of cellular process	0.008694078
	GO:1901700	response to oxygen-containing compound	0.008694078
	GO:0048731	system development	0.015381109
	GO:0044699	single-organism process	0.018855215
	GO:0010033	response to organic substance	0.020925508
	GO:0043436	oxoacid metabolic process	0.021113529
	GO:0030198	extracellular matrix organization	0.022532698
	GO:0043062	extracellular structure organization	0.022532698
	GO:0006082	organic acid metabolic process	0.022532698
	GO:0048856	anatomical structure development	0.023730631
	GO:0044767	single-organism developmental process	0.023730631
	GO:0019752	carboxylic acid metabolic process	0.025614555
	GO:0032502	developmental process	0.025970393
	GO:0009719	response to endogenous stimulus	0.025993552
	GO:0044707	single-multicellular organism process	0.030229252
	GO:0051716	cellular response to stimulus	0.034359623
	GO:0032501	multicellular organismal process	0.036827185
	GO:0008284	positive regulation of cell proliferation	0.036827185
	GO:0042325	regulation of phosphorylation	0.037998053
	GO:0007275	multicellular organismal development	0.041007033
	GO:0006564	L-serine biosynthetic process	0.043874511
	GO:0051099	positive regulation of binding	0.046387389
	GO:2000379	positive regulation of reactive oxygen species metabolic process	0.048646919
Cellular localization	GO:0005576	extracellular region	0.002211320
	GO:0044421	extracellular region part	0.002668848
	GO:0009986	cell surface	0.041683757

Table 8: RNA sequencing targets Tet-On HeLa cells, 8h Tg-treated

Gene ID	Gene name	Fold change [log2]	Adjusted p-value
ENSG00000180535	basic helix-loop-helix family, member a15	-3,05	0,0000
ENSG00000176261	zinc finger and BTB domain containing 8 opposite strand	-2,16	0,0000
ENSG00000163131	cathepsin S	-2,16	0,0000
ENSG00000179046	tripartite motif family-like 2	-2,05	0,0000
ENSG00000165181	chromosome 9 open reading frame 84	-2,04	0,0000
ENSG00000100220	RNA 2',3'-cyclic phosphate and 5'-OH ligase	-1,99	0,0000
ENSG00000248323	lung cancer associated transcript 1 (non-protein coding)	-1,91	0,0000
ENSG00000132205	elastin microfibril interfacer 2	-1,89	0,0000
ENSG00000280237	NA	-1,87	0,0001
ENSG00000113083	lysyl oxidase	-1,83	0,0000
ENSG00000163814	CUB domain containing protein 1	-1,80	0,0001
ENSG00000169083	androgen receptor	-1,80	0,0002
ENSG00000065325	glucagon-like peptide 2 receptor	-1,75	0,0000
ENSG00000080573	collagen, type V, alpha 3	-1,73	0,0000
ENSG00000182836	phosphatidylinositol-specific phospholipase C, X domain containing 3	-1,72	0,0003
ENSG00000138646	HECT and RLD domain containing E3 ubiquitin protein ligase 5	-1,70	0,0001
ENSG00000139793	muscleblind-like splicing regulator 2	-1,68	0,0000
ENSG00000103534	transmembrane channel-like 5	-1,67	0,0004
ENSG00000273301	NA	-1,62	0,0013
ENSG00000169891	RALBP1 associated Eps domain containing 2	-1,62	0,0003
ENSG00000120519	solute carrier family 10, member 7	-1,60	0,0000
ENSG00000086619	ERO1-like beta (S. cerevisiae)	-1,56	0,0000
ENSG00000103888	cell migration inducing protein, hyaluronan binding	-1,56	0,0015
ENSG00000130487	kelch domain containing 7B	-1,52	0,0000
ENSG00000129910	cadherin 15, type 1, M-cadherin (myotubule)	-1,50	0,0038
ENSG00000169429	chemokine (C-X-C motif) ligand 8	-1,50	0,0039
ENSG00000143850	pleckstrin homology domain containing, family A member 6	-1,49	0,0009
ENSG00000128590	DnaJ (Hsp40) homolog, subfamily B, member 9	-1,48	0,0000
ENSG00000144460	neuronal tyrosine-phosphorylated phosphoinositide-3-kinase adaptor 2	-1,48	0,0036
ENSG00000258927	NA	-1,47	0,0031
ENSG00000184500	protein S (alpha)	-1,47	0,0007
ENSG00000080854	immunoglobulin superfamily, member 9B	-1,46	0,0045
ENSG00000164342	toll-like receptor 3	-1,45	0,0031
ENSG00000235531	uncharacterized LOC100132891	-1,44	0,0040
ENSG00000163513	transforming growth factor, beta receptor II (70/80kDa)	-1,44	0,0000
ENSG00000205302	sorting nexin 2	-1,43	0,0000
ENSG00000184867	armadillo repeat containing, X-linked 2	-1,42	0,0021
ENSG00000170500	LON peptidase N-terminal domain and ring finger 2	-1,41	0,0060
ENSG00000144821	myosin, heavy chain 15	-1,40	0,0050
ENSG00000137959	interferon-induced protein 44-like	-1,39	0,0071
ENSG00000109452	inositol polyphosphate-4-phosphatase, type II, 105kDa	-1,37	0,0096
ENSG00000196954	caspase 4, apoptosis-related cysteine peptidase	-1,36	0,0023
ENSG00000178150	zinc finger protein 114	-1,35	0,0016
ENSG00000101605	myomesin 1	-1,35	0,0108
ENSG00000171658	NmrA-like family domain containing 1 pseudogene	-1,35	0,0022
ENSG00000150551	LY6/PLAUR domain containing 1	-1,32	0,0164
ENSG00000198855	FIC domain containing	-1,31	0,0001
ENSG00000164220	coagulation factor II (thrombin) receptor-like 2	-1,31	0,0178
ENSG00000111801	butyrophilin, subfamily 3, member A3	-1,30	0,0036
ENSG00000100219	X-box binding protein 1	-1,30	0,0000
ENSG00000133943	chromosome 14 open reading frame 159	-1,29	0,0164
ENSG00000198915	RasGEF domain family, member 1A	-1,29	0,0034
ENSG00000019549	snail family zinc finger 2	-1,29	0,0001
ENSG00000203761	NA	-1,29	0,0012
ENSG00000114279	fibroblast growth factor 12	-1,28	0,0075
ENSG00000078177	NEDD4 binding protein 2	-1,27	0,0000
ENSG00000163565	interferon, gamma-inducible protein 16	-1,26	0,0179
ENSG00000147041	synaptotagmin-like 5	-1,25	0,0056
ENSG00000113441	leucyl/cystinyl aminopeptidase	-1,25	0,0000
ENSG00000202538	RNA, U4 small nuclear 2	-1,24	0,0106
ENSG00000150961	SEC24 family member D	-1,23	0,0000
ENSG00000168016	tetratricopeptide repeat and ankyrin repeat containing 1	-1,22	0,0345
ENSG00000253775	NA	-1,22	0,0086
ENSG00000172037	laminin, beta 2 (laminin S)	-1,20	0,0242
ENSG00000173221	glutaredoxin (thioltransferase)	-1,19	0,0007
ENSG00000173210	actin binding LIM protein family, member 3	-1,19	0,0263
ENSG00000135052	golgi membrane protein 1	-1,18	0,0000
ENSG00000168685	interleukin 7 receptor	-1,18	0,0451
ENSG00000172061	leucine rich repeat containing 15	-1,17	0,0320
ENSG00000162804	sushi, nidogen and EGF-like domains 1	-1,17	0,0298
ENSG00000106927	alpha-1-microglobulin/bikunin precursor	-1,16	0,0164
ENSG00000180616	somatostatin receptor 2	-1,16	0,0451
ENSG00000166741	nicotinamide N-methyltransferase	-1,15	0,0092
ENSG00000026950	butyrophilin, subfamily 3, member A1	-1,15	0,0100
ENSG00000134516	dedicator of cytokinesis 2	-1,15	0,0367
ENSG00000134363	follistatin	-1,14	0,0229

ENSG00000122545	septin 7	-1,13	0,0000
ENSG00000128564	VGF nerve growth factor inducible	-1,13	0,0194
ENSG00000033327	GRB2-associated binding protein 2	-1,13	0,0264
ENSG00000125730	complement component 3	-1,12	0,0247
ENSG00000253802	NA	-1,12	0,0225
ENSG00000172954	lysocardiolipin acyltransferase 1	-1,11	0,0000
ENSG00000151883	poly (ADP-ribose) polymerase family, member 8	-1,10	0,0071
ENSG00000095752	interleukin 11	-1,10	0,0404
ENSG00000134970	transmembrane emp24 protein transport domain containing 7	-1,10	0,0000
ENSG00000144824	pleckstrin homology-like domain, family B, member 2	-1,10	0,0008
ENSG00000213949	integrin, alpha 1	-1,10	0,0310
ENSG00000182326	complement component 1, s subcomponent	-1,09	0,0143
ENSG00000059915	pleckstrin and Sec7 domain containing	-1,09	0,0323
ENSG00000107854	tankyrase, TRF1-interacting ankyrin-related ADP-ribose polymerase 2	-1,08	0,0000
ENSG00000049192	ADAM metallopeptidase with thrombospondin type 1 motif, 6	-1,08	0,0082
ENSG00000175426	proprotein convertase subtilisin/kexin type 1	-1,07	0,0074
ENSG00000255414	NA	-1,07	0,0242
ENSG00000091592	NLR family, pyrin domain containing 1	-1,07	0,0451
ENSG00000135678	carboxypeptidase M	-1,06	0,0044
ENSG00000090339	intercellular adhesion molecule 1	-1,04	0,0489
ENSG00000132256	tripartite motif containing 5	-1,04	0,0060
ENSG00000176018	LysM, putative peptidoglycan-binding, domain containing 3	-1,04	0,0001
ENSG00000115414	fibronectin 1	-1,04	0,0034
ENSG00000130477	unc-13 homolog A (C. elegans)	-1,03	0,0100
ENSG00000139370	solute carrier family 15 (oligopeptide transporter), member 4	-1,03	0,0021
ENSG00000168243	guanine nucleotide binding protein (G protein), gamma 4	-1,02	0,0364
ENSG00000108679	lectin, galactoside-binding, soluble, 3 binding protein	-1,02	0,0319
ENSG00000165240	ATPase, Cu++ transporting, alpha polypeptide	-1,02	0,0053
ENSG00000134109	ER degradation enhancer, mannosidase alpha-like 1	-1,02	0,0001
ENSG00000070081	nucleobindin 2	-1,01	0,0000
ENSG00000109686	SH3 domain containing 19	-1,01	0,0001
ENSG00000124783	signal sequence receptor, alpha	-1,00	0,0000
ENSG00000074181	notch 3	-1,00	0,0451
ENSG00000081189	myocyte enhancer factor 2C	-1,00	0,0329
ENSG00000159753	RGD motif, leucine rich repeats, tropomodulin domain and proline-rich containing	-1,00	0,0039
ENSG00000150760	dedicator of cytokinesis 1	-1,00	0,0000
ENSG00000171951	secretogranin II	-0,99	0,0192
ENSG00000102158	magnesium transporter 1	-0,99	0,0000
ENSG00000116299	KIAA1324	-0,99	0,0402
ENSG00000155850	solute carrier family 26 (anion exchanger), member 2	-0,99	0,0005
ENSG00000156463	SH3 domain containing ring finger 2	-0,97	0,0444
ENSG00000162695	solute carrier family 30 (zinc transporter), member 7	-0,97	0,0003
ENSG00000123104	inositol 1,4,5-trisphosphate receptor, type 2	-0,97	0,0001
ENSG00000107798	lipase A, lysosomal acid, cholesterol esterase	-0,97	0,0060
ENSG00000157637	solute carrier family 38, member 10	-0,96	0,0003
ENSG00000132003	zinc finger, SWIM-type containing 4	-0,96	0,0451
ENSG00000094804	cell division cycle 6	-0,96	0,0001
ENSG00000136026	cytoskeleton-associated protein 4	-0,96	0,0000
ENSG00000171992	synaptopodin	-0,96	0,0389
ENSG00000100997	abhydrolase domain containing 12	-0,95	0,0007
ENSG00000113621	thioredoxin domain containing 15	-0,95	0,0000
ENSG00000151914	dystonin	-0,95	0,0000
ENSG00000085276	MDS1 and EVI1 complex locus	-0,95	0,0121
ENSG00000185261	KIAA0825	-0,94	0,0164
ENSG00000013375	phosphoglucomutase 3	-0,94	0,0000
ENSG00000146376	Rho GTPase activating protein 18	-0,93	0,0052
ENSG00000173540	GDP-mannose pyrophosphorylase B	-0,93	0,0002
ENSG00000184205	TSPY-like 2	-0,92	0,0059
ENSG00000166833	neuron navigator 2	-0,92	0,0229
ENSG00000102580	DnaJ (Hsp40) homolog, subfamily C, member 3	-0,92	0,0003
ENSG00000164307	endoplasmic reticulum aminopeptidase 1	-0,92	0,0040
ENSG00000253729	protein kinase, DNA-activated, catalytic polypeptide	-0,92	0,0000
ENSG00000013392	RWD domain containing 2A	-0,91	0,0458
ENSG00000204054	long intergenic non-protein coding RNA 963	-0,91	0,0120
ENSG00000005700	inhibitor of Bruton agammaglobulinemia tyrosine kinase	-0,91	0,0001
ENSG00000074695	lectin, mannose-binding, 1	-0,90	0,0000
ENSG00000175106	trans-golgi network vesicle protein 23 homolog C (S. cerevisiae)	-0,90	0,0354
ENSG00000151151	inositol polyphosphate multikinase	-0,90	0,0041
ENSG00000113615	SEC24 family member A	-0,90	0,0000
ENSG00000108448	tripartite motif containing 16-like	-0,89	0,0031
ENSG00000073712	fermitin family member 2	-0,88	0,0001
ENSG00000153956	calcium channel, voltage-dependent, alpha 2/delta subunit 1	-0,88	0,0035
ENSG00000168282	mannosyl (alpha-1,6-)-glycoprotein beta-1,2-N-acetylglucosaminyltransferase	-0,88	0,0005
ENSG00000169359	solute carrier family 33 (acetyl-CoA transporter), member 1	-0,86	0,0001
ENSG00000163249	cyclin Y-like 1	-0,86	0,0016
ENSG00000228716	dihydrofolate reductase	-0,86	0,0036
ENSG00000267757	chromosome 19 open reading frame 83	-0,85	0,0100
ENSG00000107186	multiple PDZ domain protein	-0,85	0,0035
ENSG00000114850	signal sequence receptor, gamma (translocon-associated protein gamma)	-0,85	0,0007

ENSG00000136152	component of oligomeric golgi complex 3	-0,85	0,0021
ENSG00000129317	pseudouridylate synthase 7 homolog (S. cerevisiae)-like	-0,85	0,0003
ENSG00000099219	endoplasmic reticulum metallopeptidase 1	-0,85	0,0164
ENSG00000058262	Sec61 alpha 1 subunit (S. cerevisiae)	-0,85	0,0001
ENSG00000173706	heart development protein with EGF-like domains 1	-0,84	0,0188
ENSG00000023171	GRAM domain containing 1B	-0,83	0,0071
ENSG00000125459	misato 1, mitochondrial distribution and morphology regulator	-0,83	0,0286
ENSG00000119912	insulin-degrading enzyme	-0,82	0,0001
ENSG00000173230	golgin B1	-0,82	0,0050
ENSG00000182400	trafficking protein particle complex 6B	-0,81	0,0039
ENSG00000075420	fibronectin type III domain containing 3B	-0,80	0,0357
ENSG00000172123	schlafen family member 12	-0,80	0,0163
ENSG00000106991	endoglin	-0,80	0,0292
ENSG00000091136	laminin, beta 1	-0,79	0,0405
ENSG00000077232	DnaJ (Hsp40) homolog, subfamily C, member 10	-0,79	0,0014
ENSG00000132589	flotillin 2	-0,79	0,0109
ENSG00000106080	FK506 binding protein 14, 22 kDa	-0,79	0,0021
ENSG00000109270	late endosomal/lysosomal adaptor, MAPK and MTOR activator 3	-0,78	0,0075
ENSG00000170448	nuclear transcription factor, X-box binding-like 1	-0,78	0,0100
ENSG00000187240	dynein, cytoplasmic 2, heavy chain 1	-0,78	0,0106
ENSG00000169499	pleckstrin homology domain containing, family A (phosphoinositide binding specific) member 2	-0,78	0,0169
ENSG00000163840	deltex 3 like, E3 ubiquitin ligase	-0,78	0,0440
ENSG00000083312	transportin 1	-0,78	0,0018
ENSG00000155660	protein disulfide isomerase family A, member 4	-0,78	0,0034
ENSG00000115355	coiled-coil domain containing 88A	-0,77	0,0006
ENSG00000101310	Sec23 homolog B (S. cerevisiae)	-0,77	0,0018
ENSG00000107290	senataxin	-0,77	0,0014
ENSG00000172071	eukaryotic translation initiation factor 2-alpha kinase 3	-0,76	0,0027
ENSG00000198910	L1 cell adhesion molecule	-0,76	0,0375
ENSG00000214944	Rho guanine nucleotide exchange factor (GEF) 28	-0,76	0,0341
ENSG00000120708	transforming growth factor, beta-induced, 68kDa	-0,76	0,0100
ENSG00000131711	microtubule-associated protein 1B	-0,75	0,0006
ENSG00000145623	oncostatin M receptor	-0,75	0,0466
ENSG00000116285	ERBB receptor feedback inhibitor 1	-0,75	0,0484
ENSG00000184164	cysteine-rich with EGF-like domains 2	-0,75	0,0005
ENSG00000221926	tripartite motif containing 16	-0,74	0,0060
ENSG00000119729	ras homolog family member Q	-0,74	0,0038
ENSG00000149428	hypoxia up-regulated 1	-0,74	0,0042
ENSG00000110330	baculoviral IAP repeat containing 2	-0,74	0,0080
ENSG00000151012	solute carrier family 7 (anionic amino acid transporter light chain, xc-system), member 11	-0,73	0,0089
ENSG00000138709	La ribonucleoprotein domain family, member 1B	-0,73	0,0170
ENSG00000105971	caveolin 2	-0,73	0,0446
ENSG00000204186	zinc finger, DBF-type containing 2	-0,73	0,0044
ENSG00000187792	zinc finger protein 70	-0,73	0,0483
ENSG00000068912	endoplasmic reticulum lectin 1	-0,73	0,0022
ENSG00000144591	GDP-mannose pyrophosphorylase A	-0,73	0,0099
ENSG00000112541	phosphodiesterase 10A	-0,72	0,0254
ENSG00000145817	Yip1 domain family, member 5	-0,72	0,0026
ENSG00000051108	homocysteine-inducible, endoplasmic reticulum stress-inducible, ubiquitin-like domain member 1	-0,72	0,0341
ENSG00000138448	integrin, alpha V	-0,71	0,0207
ENSG00000198589	LPS-responsive vesicle trafficking, beach and anchor containing	-0,71	0,0194
ENSG00000136731	UDP-glucose glycoprotein glucosyltransferase 1	-0,70	0,0016
ENSG00000139618	breast cancer 2, early onset	-0,70	0,0102
ENSG00000168615	ADAM metallopeptidase domain 9	-0,70	0,0194
ENSG00000120742	stress-associated endoplasmic reticulum protein 1	-0,70	0,0045
ENSG00000115902	solute carrier family 1 (glutamate/neutral amino acid transporter), member 4	-0,70	0,0440
ENSG00000128059	phosphoribosyl pyrophosphate amidotransferase	-0,70	0,0157
ENSG00000163479	signal sequence receptor, beta (translocon-associated protein beta)	-0,69	0,0053
ENSG00000147649	metadherin	-0,69	0,0071
ENSG00000113328	cyclin G1	-0,69	0,0400
ENSG00000134049	immediate early response 3 interacting protein 1	-0,68	0,0227
ENSG00000163527	STT3B, subunit of the oligosaccharyltransferase complex (catalytic)	-0,67	0,0018
ENSG00000175224	autophagy related 13	-0,67	0,0030
ENSG00000177683	THAP domain containing 5	-0,67	0,0194
ENSG00000162298	synovial apoptosis inhibitor 1, synoviolin	-0,67	0,0018
ENSG00000110048	oxysterol binding protein	-0,66	0,0018
ENSG00000147535	phosphatidic acid phosphatase type 2 domain containing 1B	-0,66	0,0400
ENSG00000113282	clathrin interactor 1	-0,66	0,0062
ENSG00000067167	translocation associated membrane protein 1	-0,65	0,0082
ENSG00000120686	ubiquitin-fold modifier 1	-0,65	0,0075
ENSG00000164292	Rho-related BTB domain containing 3	-0,65	0,0420
ENSG00000118596	solute carrier family 16 (monocarboxylate transporter), member 7	-0,64	0,0315
ENSG00000115520	coenzyme Q10 homolog B (S. cerevisiae)	-0,64	0,0482
ENSG00000164209	solute carrier family 25, member 46	-0,64	0,0092
ENSG00000106397	procollagen-lysine, 2-oxoglutarate 5-dioxygenase 3	-0,64	0,0089
ENSG00000148248	surfeit 4	-0,64	0,0051
ENSG00000136603	SKI-like proto-oncogene	-0,64	0,0171
ENSG00000204713	tripartite motif containing 27	-0,64	0,0290

ENSG00000102081	fragile X mental retardation 1	-0,64	0,0118
ENSG00000114416	fragile X mental retardation, autosomal homolog 1	-0,63	0,0141
ENSG00000127022	calnexin	-0,63	0,0232
ENSG00000023287	RB1-inducible coiled-coil 1	-0,63	0,0052
ENSG00000071537	sel-1 suppressor of lin-12-like (C. elegans)	-0,63	0,0156
ENSG00000011405	phosphatidylinositol-4-phosphate 3-kinase, catalytic subunit type 2 alpha	-0,63	0,0266
ENSG00000141458	Niemann-Pick disease, type C1	-0,62	0,0118
ENSG00000086758	HECT, UBA and WWE domain containing 1, E3 ubiquitin protein ligase	-0,62	0,0134
ENSG00000068878	proteasome (prosome, macropain) activator subunit 4	-0,62	0,0092
ENSG00000170921	tetratricopeptide repeat, ankyrin repeat and coiled-coil containing 2	-0,62	0,0106
ENSG00000119523	ALG2, alpha-1,3/1,6-mannosyltransferase	-0,61	0,0125
ENSG00000116127	Alstrom syndrome 1	-0,61	0,0193
ENSG00000144224	UBX domain protein 4	-0,61	0,0071
ENSG00000130396	myeloid/lymphoid or mixed-lineage leukemia (trithorax homolog, Drosophila); translocated to, 4	-0,61	0,0367
ENSG00000152332	U2AF homology motif (UHM) kinase 1	-0,61	0,0223
ENSG00000135677	glucosamine (N-acetyl)-6-sulfatase	-0,61	0,0298
ENSG00000115486	gamma-glutamyl carboxylase	-0,61	0,0183
ENSG00000110344	ubiquitination factor E4A	-0,61	0,0109
ENSG00000176142	transmembrane protein 39A	-0,61	0,0147
ENSG00000177888	zinc finger and BTB domain containing 41	-0,60	0,0485
ENSG00000155304	heat shock protein 70kDa family, member 13	-0,60	0,0371
ENSG00000135837	centrosomal protein 350kDa	-0,60	0,0129
ENSG00000116406	ER degradation enhancer, mannosidase alpha-like 3	-0,60	0,0307
ENSG00000145725	diphosphoinositol pentakisphosphate kinase 2	-0,59	0,0237
ENSG00000180398	multiple coagulation factor deficiency 2	-0,58	0,0067
ENSG00000121621	kinesin family member 18A	-0,58	0,0483
ENSG00000157106	SMG1 phosphatidylinositol 3-kinase-related kinase	-0,58	0,0124
ENSG00000177034	metaxin 3	-0,58	0,0354
ENSG00000127914	A kinase (PRKA) anchor protein 9	-0,56	0,0361
ENSG00000086598	transmembrane emp24 domain trafficking protein 2	-0,55	0,0484
ENSG00000154305	melanoma inhibitory activity family, member 3	-0,53	0,0280
ENSG00000047932	golgi-associated PDZ and coiled-coil motif containing	-0,52	0,0386
ENSG00000049860	hexosaminidase B (beta polypeptide)	-0,51	0,0443
ENSG00000112159	MDN1, midasin homolog (yeast)	-0,51	0,0459
ENSG00000140632	glyoxylate reductase 1 homolog (Arabidopsis)	0,51	0,0298
ENSG00000156411	chromosome 14 open reading frame 2	0,55	0,0433
ENSG00000105011	anti-silencing function 1B histone chaperone	0,56	0,0354
ENSG00000183741	chromobox homolog 6	0,56	0,0437
ENSG00000166965	RCC1 domain containing 1	0,58	0,0314
ENSG00000198890	protein arginine methyltransferase 6	0,59	0,0237
ENSG00000147123	NADH dehydrogenase (ubiquinone) 1 beta subcomplex, 11, 17.3kDa	0,60	0,0290
ENSG00000135048	transmembrane protein 2	0,60	0,0393
ENSG00000029993	high mobility group box 3	0,60	0,0113
ENSG00000183943	protein kinase, X-linked	0,61	0,0420
ENSG00000125520	SLC2A4 regulator	0,62	0,0089
ENSG00000163812	zinc finger, DHHC-type containing 3	0,63	0,0259
ENSG00000169410	protein tyrosine phosphatase, non-receptor type 9	0,63	0,0411
ENSG00000108262	G protein-coupled receptor kinase interacting ArfGAP 1	0,65	0,0227
ENSG00000106484	mesoderm specific transcript	0,65	0,0248
ENSG00000099814	centrosomal protein 170B	0,65	0,0305
ENSG00000102221	jade family PHD finger 3	0,66	0,0193
ENSG00000188242	uncharacterized LOC25845	0,67	0,0410
ENSG00000066735	kinesin family member 26A	0,67	0,0089
ENSG00000164318	EGF-like, fibronectin type III and laminin G domains	0,68	0,0400
ENSG00000236081	ELFN1 antisense RNA 1	0,68	0,0441
ENSG00000105552	branched chain amino-acid transaminase 2, mitochondrial	0,69	0,0099
ENSG00000130724	charged multivesicular body protein 2A	0,69	0,0413
ENSG00000171703	transcription elongation factor A (SII), 2	0,69	0,0229
ENSG00000196352	CD55 molecule, decay accelerating factor for complement (Cromer blood group)	0,69	0,0373
ENSG00000243279	PRA1 domain family, member 2	0,70	0,0482
ENSG00000130821	solute carrier family 6 (neurotransmitter transporter), member 8	0,70	0,0089
ENSG00000173156	ras homolog family member D	0,70	0,0482
ENSG00000269190	F-box protein 17	0,71	0,0404
ENSG00000213015	zinc finger protein 580	0,71	0,0180
ENSG00000128989	cAMP-regulated phosphoprotein, 19kDa	0,72	0,0263
ENSG00000174010	kelch-like family member 15	0,72	0,0232
ENSG00000083807	solute carrier family 27 (fatty acid transporter), member 5	0,73	0,0451
ENSG00000169184	meningioma (disrupted in balanced translocation) 1	0,73	0,0170
ENSG00000158186	muscle RAS oncogene homolog	0,74	0,0106
ENSG00000172992	dephospho-CoA kinase domain containing	0,74	0,0378
ENSG00000133243	BTB (POZ) domain containing 2	0,75	0,0143
ENSG00000107816	leucine zipper, putative tumor suppressor 2	0,75	0,0089
ENSG00000269609	RPARP antisense RNA 1	0,75	0,0362
ENSG00000185989	RAS p21 protein activator 3	0,76	0,0236
ENSG00000123358	nuclear receptor subfamily 4, group A, member 1	0,76	0,0180
ENSG00000099875	MAP kinase interacting serine/threonine kinase 2	0,78	0,0237
ENSG00000196547	mannosidase, alpha, class 2A, member 2	0,78	0,0031
ENSG00000205922	one cut homeobox 3	0,78	0,0420
ENSG00000175768	translocase of outer mitochondrial membrane 5 homolog (yeast)	0,79	0,0484

ENSG00000141401	inositol(myo)-1(or 4)-monophosphatase 2	0,79	0,0354
ENSG00000137713	protein phosphatase 2, regulatory subunit A, beta	0,79	0,0036
ENSG00000171105	insulin receptor	0,79	0,0075
ENSG00000196372	ankyrin repeat and SOCS box containing 13	0,79	0,0041
ENSG00000160213	cystatin B (stefin B)	0,80	0,0045
ENSG00000171813	PWWP domain containing 2B	0,81	0,0075
ENSG00000130193	thioesterase superfamily member 6	0,81	0,0402
ENSG00000157240	frizzled class receptor 1	0,82	0,0055
ENSG00000136888	ATPase, H+ transporting, lysosomal 13kDa, V1 subunit G1	0,82	0,0069
ENSG00000168542	collagen, type III, alpha 1	0,83	0,0287
ENSG00000110987	B-cell CLL/lymphoma 7A	0,83	0,0089
ENSG00000169715	metallothionein 1E	0,85	0,0085
ENSG00000090971	N-acetyltransferase 14 (GCN5-related, putative)	0,85	0,0046
ENSG00000126822	pleckstrin homology domain containing, family G (with RhoGef domain) member 3	0,85	0,0013
ENSG00000270885	RAS-like, family 10, member B	0,85	0,0287
ENSG00000059804	solute carrier family 2 (facilitated glucose transporter), member 3	0,86	0,0044
ENSG00000125534	pancreatic progenitor cell differentiation and proliferation factor	0,86	0,0003
ENSG00000111684	lysophosphatidylcholine acyltransferase 3	0,86	0,0075
ENSG00000131459	glutamine-fructose-6-phosphate transaminase 2	0,87	0,0389
ENSG00000090975	phosphatidylinositol transfer protein, membrane-associated 2	0,87	0,0060
ENSG00000108515	enolase 3 (beta, muscle)	0,88	0,0047
ENSG00000155254	MARVEL domain containing 1	0,89	0,0016
ENSG00000124766	SRY (sex determining region Y)-box 4	0,89	0,0192
ENSG00000175130	MARCKS-like 1	0,89	0,0044
ENSG00000038295	tolloid-like 1	0,89	0,0158
ENSG00000077782	fibroblast growth factor receptor 1	0,91	0,0089
ENSG00000115507	orthodenticle homeobox 1	0,91	0,0482
ENSG00000266208	NA	0,91	0,0170
ENSG00000107829	F-box and WD repeat domain containing 4	0,92	0,0106
ENSG00000179085	dolichyl-phosphate mannosyltransferase polypeptide 3	0,93	0,0480
ENSG00000179922	zinc finger protein 784	0,94	0,0222
ENSG00000137103	transmembrane protein 8B	0,94	0,0431
ENSG00000166228	pterin-4 alpha-carbinolamine dehydratase/dimerization cofactor of hepatocyte nuclear factor 1 alpha	0,95	0,0099
ENSG00000156381	ankyrin repeat domain 9	0,96	0,0186
ENSG00000157870	family with sequence similarity 213, member B	0,97	0,0017
ENSG00000116991	signal-induced proliferation-associated 1 like 2	0,97	0,0007
ENSG00000198208	ribosomal protein S6 kinase-like 1	0,97	0,0170
ENSG00000106003	LFNG O-fucosylpeptide 3-beta-N-acetylglucosaminyltransferase	1,00	0,0370
ENSG00000204388	heat shock 70kDa protein 1B	1,01	0,0000
ENSG00000204682	cancer susceptibility candidate 10	1,01	0,0037
ENSG00000130762	Rho guanine nucleotide exchange factor (GEF) 16	1,01	0,0045
ENSG00000239887	chromosome 1 open reading frame 226	1,02	0,0329
ENSG00000174607	UDP glycosyltransferase 8	1,02	0,0180
ENSG00000156026	mitochondrial calcium uniporter	1,03	0,0183
ENSG00000272398	CD24 molecule	1,04	0,0001
ENSG00000005379	benzodiazepine receptor (peripheral) associated protein 1	1,06	0,0239
ENSG00000160094	zinc finger protein 362	1,07	0,0329
ENSG00000186395	keratin 10	1,08	0,0010
ENSG00000125845	bone morphogenetic protein 2	1,08	0,0170
ENSG00000168528	serine incorporator 2	1,09	0,0044
ENSG00000126803	heat shock 70kDa protein 2	1,09	0,0495
ENSG00000174721	fibroblast growth factor binding protein 3	1,11	0,0071
ENSG00000266714	myosin XVB pseudogene	1,11	0,0046
ENSG00000179981	teashirt zinc finger homeobox 1	1,11	0,0002
ENSG00000163053	solute carrier family 16, member 14	1,11	0,0013
ENSG00000136295	tweety family member 3	1,12	0,0097
ENSG00000178172	serine peptidase inhibitor, Kazal type 6	1,14	0,0158
ENSG00000250208	FZD10 antisense RNA 1 (head to head)	1,15	0,0196
ENSG00000204389	heat shock 70kDa protein 1A	1,15	0,0003
ENSG00000166823	mesoderm posterior basic helix-loop-helix transcription factor 1	1,18	0,0229
ENSG00000261150	epiplakin 1	1,19	0,0008
ENSG00000164976	KIAA1161	1,22	0,0010
ENSG00000183092	brain-enriched guanylate kinase-associated	1,22	0,0001
ENSG00000119686	feline leukemia virus subgroup C cellular receptor family, member 2	1,22	0,0011
ENSG00000204291	collagen, type XV, alpha 1	1,28	0,0032
ENSG00000151090	thyroid hormone receptor, beta	1,45	0,0001
ENSG00000092758	collagen, type IX, alpha 3	1,57	0,0019
ENSG00000163331	death associated protein-like 1	1,59	0,0017
ENSG00000207827	microRNA 30a	2,08	0,0000

Table 9: RNA sequencing targets Tet-On PANC-1 cells, untreated

Gene ID	Gene name	Fold change [log2]	Adjusted p-value
ENSG00000100220	RNA 2',3'-cyclic phosphate and 5'-OH ligase	-3,29	0,0000
ENSG00000196611	matrix metallopeptidase 1 (interstitial collagenase)	-2,72	0,0000
ENSG00000102271	kelch-like family member 4	-2,30	0,0032
ENSG00000182836	phosphatidylinositol-specific phospholipase C, X domain containing 3	-1,81	0,0000
ENSG00000104313	EYA transcriptional coactivator and phosphatase 1	4,06	0,0028

Table 10: RNA sequencing targets Tet-On MIA PaCa-2 cells, untreated

Gene ID	Gene name	Fold change [log2]	Adjusted p-value
ENSG00000116833	nuclear receptor subfamily 5, group A, member 2	-2,82	0,0000
ENSG00000100220	RNA 2',3'-cyclic phosphate and 5'-OH ligase	-2,67	0,0000
ENSG00000112981	NME/NM23 family member 5	-2,61	0,0000
ENSG00000123843	complement component 4 binding protein, beta	-2,32	0,0001
ENSG00000113140	secreted protein, acidic, cysteine-rich (osteonectin)	-2,30	0,0000
ENSG00000168477	tenascin XB	-2,29	0,0000
ENSG00000163430	follistatin-like 1	-2,28	0,0000
ENSG00000271980	NA	-2,22	0,0135
ENSG00000105855	integrin, beta 8	-2,19	0,0000
ENSG00000260822	NA	-2,13	0,0003
ENSG00000138640	family with sequence similarity 13, member A	-2,08	0,0000
ENSG00000155324	GRAM domain containing 3	-2,01	0,0002
ENSG00000116741	regulator of G-protein signaling 2	-2,01	0,0028
ENSG00000090376	interleukin-1 receptor-associated kinase 3	-2,00	0,0003
ENSG00000144642	RNA binding motif, single stranded interacting protein 3	-1,97	0,0038
ENSG00000134247	prostaglandin F2 receptor inhibitor	-1,97	0,0000
ENSG00000272398	CD24 molecule	-1,96	0,0000
ENSG00000168542	collagen, type III, alpha 1	-1,88	0,0061
ENSG00000114638	uroplakin 1B	-1,87	0,0000
ENSG00000169891	RALBP1 associated Eps domain containing 2	-1,85	0,0011
ENSG00000185745	interferon-induced protein with tetratricopeptide repeats 1	-1,85	0,0006
ENSG00000171016	pygopus family PHD finger 1	-1,78	0,0001
ENSG00000152402	guanylate cyclase 1, soluble, alpha 2	-1,76	0,0055
ENSG00000110848	CD69 molecule	-1,76	0,0012
ENSG00000123407	homeobox C12	-1,75	0,0000
ENSG00000102554	Kruppel-like factor 5 (intestinal)	-1,73	0,0186
ENSG00000104290	frizzled class receptor 3	-1,72	0,0007
ENSG00000095637	sorbin and SH3 domain containing 1	-1,60	0,0001
ENSG00000109654	tripartite motif containing 2	-1,57	0,0000
ENSG00000052850	ALX homeobox 4	-1,57	0,0346
ENSG00000259330	NA	-1,56	0,0305
ENSG00000169116	prostate androgen-regulated mucin-like protein 1	-1,56	0,0303
ENSG00000067992	pyruvate dehydrogenase kinase, isozyme 3	-1,54	0,0038
ENSG00000047597	X-linked Kx blood group	-1,52	0,0295
ENSG00000135525	microtubule-associated protein 7	-1,52	0,0031
ENSG00000263272	NA	-1,50	0,0172
ENSG00000134531	epithelial membrane protein 1	-1,50	0,0000
ENSG00000138771	shroom family member 3	-1,45	0,0007
ENSG00000109452	inositol polyphosphate-4-phosphatase, type II, 105kDa	-1,42	0,0001
ENSG00000055732	mucolipin 3	-1,42	0,0003
ENSG00000146267	failed axon connections homolog (Drosophila)	-1,41	0,0046
ENSG00000086300	sorting nexin 10	-1,40	0,0001
ENSG00000111700	solute carrier organic anion transporter family, member 1B3	-1,40	0,0220
ENSG00000157214	STEAP family member 2, metalloreductase	-1,36	0,0110
ENSG00000198478	SH3 domain binding glutamate-rich protein like 2	-1,36	0,0460
ENSG00000265972	thioredoxin interacting protein	-1,36	0,0006
ENSG00000161654	LSM12 homolog (S. cerevisiae)	-1,36	0,0485
ENSG00000177189	ribosomal protein S6 kinase, 90kDa, polypeptide 3	-1,34	0,0001
ENSG00000234545	family with sequence similarity 133, member B	-1,32	0,0409
ENSG00000006468	ets variant 1	-1,31	0,0007
ENSG00000165868	heat shock 70kDa protein 12A	-1,30	0,0037
ENSG00000163710	procollagen C-endopeptidase enhancer 2	-1,30	0,0005
ENSG00000135272	MyoD family inhibitor domain containing	-1,25	0,0081
ENSG00000086619	ERO1-like beta (S. cerevisiae)	-1,25	0,0302
ENSG00000171766	glycine amidinotransferase (L-arginine:glycine amidinotransferase)	-1,24	0,0081
ENSG00000235609	NA	-1,24	0,0119
ENSG00000119917	interferon-induced protein with tetratricopeptide repeats 3	-1,22	0,0135
ENSG00000115540	MOB family member 4, phocein	-1,21	0,0344
ENSG00000182287	adaptor-related protein complex 1, sigma 2 subunit	-1,21	0,0066

ENSG00000164647	six transmembrane epithelial antigen of the prostate 1	-1,21	0,0409
ENSG00000165474	gap junction protein, beta 2, 26kDa	-1,20	0,0186
ENSG00000023445	baculoviral IAP repeat containing 3	-1,18	0,0202
ENSG00000107798	lipase A, lysosomal acid, cholesterol esterase	-1,18	0,0003
ENSG00000119922	interferon-induced protein with tetratricopeptide repeats 2	-1,17	0,0087
ENSG00000134970	transmembrane emp24 protein transport domain containing 7	-1,17	0,0463
ENSG00000136928	gamma-aminobutyric acid (GABA) B receptor, 2	-1,16	0,0190
ENSG00000071794	helicase-like transcription factor	-1,15	0,0085
ENSG00000184500	protein S (alpha)	-1,15	0,0055
ENSG00000166402	tubby bipartite transcription factor	-1,15	0,0015
ENSG00000153898	mucolipin 2	-1,14	0,0008
ENSG00000171517	lysophosphatidic acid receptor 3	-1,14	0,0074
ENSG00000165169	dynein, light chain, Tctex-type 3	-1,14	0,0186
ENSG00000248905	formin 1	-1,14	0,0202
ENSG00000171928	trans-golgi network vesicle protein 23 homolog B (S. cerevisiae)	-1,14	0,0138
ENSG00000185442	family with sequence similarity 174, member B	-1,13	0,0498
ENSG00000070214	solute carrier family 44 (choline transporter), member 1	-1,12	0,0025
ENSG00000112237	cyclin C	-1,12	0,0062
ENSG00000136114	thrombospondin, type I, domain containing 1	-1,12	0,0295
ENSG00000133731	inositol(myo)-1(or 4)-monophosphatase 1	-1,11	0,0182
ENSG00000188641	dihydropyrimidine dehydrogenase	-1,11	0,0025
ENSG00000156313	retinitis pigmentosa GTPase regulator	-1,10	0,0222
ENSG00000025039	Ras-related GTP binding D	-1,10	0,0015
ENSG00000141429	polypeptide N-acetylgalactosaminyltransferase 1	-1,10	0,0037
ENSG00000169255	beta-1,3-N-acetylgalactosaminyltransferase 1 (globoside blood group)	-1,07	0,0169
ENSG00000196074	synaptonemal complex protein 2	-1,07	0,0469
ENSG00000105810	cyclin-dependent kinase 6	-1,07	0,0037
ENSG00000231607	deleted in lymphocytic leukemia 2 (non-protein coding)	-1,05	0,0287
ENSG00000146592	cAMP responsive element binding protein 5	-1,05	0,0482
ENSG00000187240	dynein, cytoplasmic 2, heavy chain 1	-1,04	0,0050
ENSG00000114346	epithelial cell transforming 2	-1,04	0,0123
ENSG00000129084	proteasome (prosome, macropain) subunit, alpha type, 1	-1,04	0,0202
ENSG00000120756	plastin 1	-1,04	0,0092
ENSG00000139163	ethanolamine kinase 1	-1,04	0,0142
ENSG00000158186	muscle RAS oncogene homolog	-1,04	0,0216
ENSG00000127995	CAS1 domain containing 1	-1,03	0,0431
ENSG00000176261	zinc finger and BTB domain containing 8 opposite strand	-1,03	0,0033
ENSG00000032742	intraflagellar transport 88	-1,03	0,0216
ENSG00000184937	Wilms tumor 1	-1,02	0,0479
ENSG00000065809	family with sequence similarity 107, member B	-1,02	0,0482
ENSG00000143156	NME/NM23 family member 7	-1,01	0,0247
ENSG00000137414	family with sequence similarity 8, member A1	-0,99	0,0199
ENSG00000120992	lysophospholipase I	-0,99	0,0405
ENSG00000155100	OTU domain containing 6B	-0,99	0,0186
ENSG00000172086	lysine-rich coiled-coil 1	-0,99	0,0094
ENSG00000156256	ubiquitin specific peptidase 16	-0,99	0,0040
ENSG00000069702	transforming growth factor, beta receptor III	-0,98	0,0212
ENSG00000114446	intraflagellar transport 57	-0,98	0,0017
ENSG00000163605	protein phosphatase 4, regulatory subunit 2	-0,98	0,0362
ENSG00000127124	human immunodeficiency virus type I enhancer binding protein 3	-0,98	0,0186
ENSG00000137710	radixin	-0,98	0,0061
ENSG00000101868	polymerase (DNA directed), alpha 1, catalytic subunit	-0,98	0,0031
ENSG00000123552	ubiquitin specific peptidase 45	-0,98	0,0172
ENSG00000122435	tRNA methyltransferase 13 homolog (S. cerevisiae)	-0,98	0,0295
ENSG00000050405	LIM domain and actin binding 1	-0,97	0,0010
ENSG00000108064	transcription factor A, mitochondrial	-0,97	0,0322
ENSG00000152422	X-ray repair complementing defective repair in Chinese hamster cells 4	-0,97	0,0105
ENSG00000110330	baculoviral IAP repeat containing 2	-0,97	0,0216
ENSG00000173674	eukaryotic translation initiation factor 1A, X-linked	-0,97	0,0409
ENSG00000151239	twinfilin actin-binding protein 1	-0,97	0,0318
ENSG00000154727	GA binding protein transcription factor, alpha subunit 60kDa	-0,96	0,0298
ENSG00000146476	chromosome 6 open reading frame 211	-0,96	0,0186
ENSG00000014123	UFM1-specific ligase 1	-0,96	0,0186
ENSG00000174842	glomulin, FKBP associated protein	-0,96	0,0192
ENSG00000143498	TATA box binding protein (TBP)-associated factor, RNA polymerase I, A, 48kDa	-0,96	0,0475
ENSG00000069869	neural precursor cell expressed, developmentally down-regulated 4, E3 ubiquitin protein ligase	-0,96	0,0019
ENSG00000163714	U2 snRNP-associated SURP domain containing	-0,95	0,0222
ENSG00000029363	BCL2-associated transcription factor 1	-0,95	0,0202
ENSG00000118855	major facilitator superfamily domain containing 1	-0,95	0,0202
ENSG00000166266	cullin 5	-0,95	0,0205
ENSG00000123178	SPRY domain containing 7	-0,95	0,0302
ENSG00000174695	transmembrane protein 167A	-0,95	0,0473
ENSG00000047230	CTP synthase 2	-0,95	0,0410
ENSG00000164031	DnaJ (Hsp40) homolog, subfamily B, member 14	-0,94	0,0437
ENSG00000128656	chimerin 1	-0,94	0,0303
ENSG00000115145	signal transducing adaptor molecule (SH3 domain and ITAM motif) 2	-0,94	0,0382
ENSG00000165195	phosphatidylinositol glycan anchor biosynthesis, class A	-0,93	0,0475
ENSG00000173145	nucleolar complex associated 3 homolog (S. cerevisiae)	-0,93	0,0311
ENSG00000174173	tRNA methyltransferase 10 homolog C (S. cerevisiae)	-0,93	0,0247
ENSG00000153130	short coiled-coil protein	-0,93	0,0458

ENSG00000162433	adenylate kinase 4	-0,93	0,0482
ENSG00000165813	coiled-coil domain containing 186	-0,92	0,0409
ENSG00000080345	replication timing regulatory factor 1	-0,92	0,0137
ENSG00000112742	TTK protein kinase	-0,92	0,0480
ENSG00000118515	serum/glucocorticoid regulated kinase 1	-0,92	0,0298
ENSG00000136051	KIAA1033	-0,92	0,0180
ENSG00000092020	protein phosphatase 2, regulatory subunit B'', gamma	-0,92	0,0318
ENSG00000039319	zinc finger, FYVE domain containing 16	-0,92	0,0263
ENSG00000198130	3-hydroxyisobutyryl-CoA hydrolase	-0,92	0,0286
ENSG00000102172	spermine synthase	-0,91	0,0286
ENSG00000139687	retinoblastoma 1	-0,91	0,0437
ENSG00000197045	glia maturation factor, beta	-0,91	0,0479
ENSG00000163728	tetratricopeptide repeat domain 14	-0,91	0,0261
ENSG00000198898	capping protein (actin filament) muscle Z-line, alpha 2	-0,91	0,0247
ENSG00000144228	speckle-type POZ protein-like	-0,90	0,0463
ENSG00000164332	ubiquitin-like domain containing CTD phosphatase 1	-0,90	0,0212
ENSG00000111554	Mdm1 nuclear protein homolog (mouse)	-0,90	0,0202
ENSG00000115419	glutaminase	-0,90	0,0466
ENSG00000159079	chromosome 21 open reading frame 59	-0,90	0,0361
ENSG00000105849	TWIST neighbor	-0,90	0,0302
ENSG00000166200	COP9 signalosome subunit 2	-0,90	0,0204
ENSG00000169251	NMD3 ribosome export adaptor	-0,90	0,0048
ENSG00000152778	interferon-induced protein with tetratricopeptide repeats 5	-0,89	0,0104
ENSG00000111711	golgi transport 1B	-0,89	0,0456
ENSG00000111875	anti-silencing function 1A histone chaperone	-0,89	0,0302
ENSG00000036054	TBC1 domain family, member 23	-0,88	0,0298
ENSG00000091039	oxysterol binding protein-like 8	-0,88	0,0304
ENSG00000102595	UDP-glucose glycoprotein glucosyltransferase 2	-0,88	0,0420
ENSG00000111615	KRR1, small subunit (SSU) processome component, homolog (yeast)	-0,87	0,0055
ENSG00000122417	outer dense fiber of sperm tails 2-like	-0,87	0,0332
ENSG00000156374	polycomb group ring finger 6	-0,87	0,0182
ENSG00000138386	NGFI-A binding protein 1 (EGR1 binding protein 1)	-0,87	0,0238
ENSG00000122545	septin 7	-0,87	0,0210
ENSG00000004961	holocytochrome c synthase	-0,87	0,0275
ENSG00000116750	ubiquitin carboxyl-terminal hydrolase L5	-0,87	0,0496
ENSG00000258289	churchill domain containing 1	-0,87	0,0482
ENSG00000033178	ubiquitin-like modifier activating enzyme 6	-0,87	0,0362
ENSG00000107614	tRNA aspartic acid methyltransferase 1	-0,86	0,0458
ENSG00000196776	CD47 molecule	-0,86	0,0353
ENSG00000117475	basic leucine zipper nuclear factor 1	-0,86	0,0233
ENSG00000169019	COMM domain containing 8	-0,86	0,0409
ENSG00000067533	ribosomal RNA processing 15 homolog (S. cerevisiae)	-0,86	0,0480
ENSG00000127989	mitochondrial transcription termination factor 1	-0,86	0,0314
ENSG00000121879	phosphatidylinositol-4,5-bisphosphate 3-kinase, catalytic subunit alpha	-0,86	0,0475
ENSG00000136143	succinate-CoA ligase, ADP-forming, beta subunit	-0,86	0,0463
ENSG00000118965	WD repeat domain 35	-0,86	0,0326
ENSG00000204262	collagen, type V, alpha 2	-0,86	0,0067
ENSG00000077232	DnaJ (Hsp40) homolog, subfamily C, member 10	-0,86	0,0482
ENSG00000081154	PEST proteolytic signal containing nuclear protein	-0,85	0,0482
ENSG00000163507	KIAA1524	-0,85	0,0197
ENSG00000164305	caspase 3, apoptosis-related cysteine peptidase	-0,85	0,0437
ENSG00000169895	synapse associated protein 1	-0,85	0,0318
ENSG00000151414	NIMA-related kinase 7	-0,85	0,0303
ENSG00000171109	mitofusin 1	-0,85	0,0302
ENSG00000122884	prolyl 4-hydroxylase, alpha polypeptide I	-0,85	0,0469
ENSG00000145725	diphosphoinositol pentakisphosphate kinase 2	-0,85	0,0219
ENSG00000166681	nerve growth factor receptor (TNFRSF16) associated protein 1	-0,85	0,0291
ENSG00000198836	optic atrophy 1 (autosomal dominant)	-0,84	0,0227
ENSG00000185222	WW domain binding protein 5	-0,84	0,0496
ENSG00000093144	enoyl CoA hydratase domain containing 1	-0,84	0,0298
ENSG00000126777	kinectin 1 (kinesin receptor)	-0,84	0,0298
ENSG00000133657	ATPase type 13A3	-0,84	0,0405
ENSG00000005175	RNA polymerase II associated protein 3	-0,84	0,0480
ENSG00000175054	ATR serine/threonine kinase	-0,82	0,0286
ENSG00000153201	RAN binding protein 2	-0,82	0,0169
ENSG00000095002	mutS homolog 2	-0,82	0,0286
ENSG00000139324	transmembrane and tetratricopeptide repeat containing 3	-0,82	0,0482
ENSG00000134758	ring finger protein 138, E3 ubiquitin protein ligase	-0,82	0,0475
ENSG00000184203	protein phosphatase 1, regulatory (inhibitor) subunit 2	-0,82	0,0314
ENSG00000164163	ATP-binding cassette, sub-family E (OABP), member 1	-0,82	0,0298
ENSG00000117155	synovial sarcoma, X breakpoint 2 interacting protein	-0,82	0,0399
ENSG00000188342	general transcription factor IIF, polypeptide 2, 30kDa	-0,80	0,0318
ENSG00000029725	rabaptin, RAB GTPase binding effector protein 1	-0,80	0,0295
ENSG00000198843	selenoprotein T	-0,80	0,0221
ENSG00000130294	kinesin family member 1A	-0,80	0,0439
ENSG00000122376	family with sequence similarity 35, member A	-0,80	0,0480
ENSG00000148634	HECT and RLD domain containing E3 ubiquitin protein ligase 4	-0,79	0,0482
ENSG00000104093	Dmx-like 2	-0,79	0,0489
ENSG00000119912	insulin-degrading enzyme	-0,79	0,0364
ENSG00000168564	CDKN2A interacting protein	-0,78	0,0325
ENSG00000136021	SCY1-like 2 (S. cerevisiae)	-0,77	0,0437
ENSG00000080200	beta-gamma crystallin domain containing 3	-0,75	0,0482

ENSG00000133119	replication factor C (activator 1) 3, 38kDa	-0,74	0,0482
ENSG00000198677	tetratricopeptide repeat domain 37	-0,74	0,0409
ENSG00000119326	catenin (cadherin-associated protein), alpha-like 1	-0,73	0,0410
ENSG00000168615	ADAM metallopeptidase domain 9	-0,72	0,0489
ENSG00000112078	potassium channel tetramerization domain containing 20	-0,71	0,0469
ENSG00000004700	RecQ helicase-like	-0,71	0,0469
ENSG00000101166	slowmo homolog 2 (Drosophila)	-0,70	0,0409
ENSG00000100644	hypoxia inducible factor 1, alpha subunit (basic helix-loop-helix transcription factor)	-0,69	0,0388
ENSG00000184371	colony stimulating factor 1 (macrophage)	0,77	0,0286
ENSG00000102119	emerin	0,82	0,0286
ENSG00000091136	laminin, beta 1	0,82	0,0325
ENSG00000165757	KIAA1462	0,83	0,0298
ENSG00000123146	CD97 molecule	0,83	0,0216
ENSG00000164535	diacylglycerol lipase, beta	0,86	0,0355
ENSG00000166337	TAF10 RNA polymerase II, TATA box binding protein (TBP)-associated factor, 30kDa	0,88	0,0431
ENSG00000108106	ubiquitin-conjugating enzyme E2S	0,90	0,0482
ENSG00000122862	serglycin	0,90	0,0405
ENSG00000166106	ADAM metallopeptidase with thrombospondin type 1 motif, 15	0,91	0,0246
ENSG00000138411	HECT, C2 and WW domain containing E3 ubiquitin protein ligase 2	0,91	0,0475
ENSG00000100311	platelet-derived growth factor beta polypeptide	0,91	0,0286
ENSG00000118777	ATP-binding cassette, sub-family G (WHITE), member 2 (Junior blood group)	0,91	0,0409
ENSG00000106070	growth factor receptor-bound protein 10	0,92	0,0381
ENSG00000134030	CBP80/20-dependent translation initiation factor	0,93	0,0326
ENSG00000103196	cysteine-rich secretory protein LCCL domain containing 2	0,94	0,0454
ENSG00000178057	NADH dehydrogenase (ubiquinone) complex I, assembly factor 3	0,94	0,0306
ENSG00000085185	BCL6 corepressor-like 1	0,94	0,0475
ENSG00000149527	phospholipase C, eta 2	0,95	0,0275
ENSG00000270647	TAF15 RNA polymerase II, TATA box binding protein (TBP)-associated factor, 68kDa	0,95	0,0346
ENSG00000111676	atrophin 1	0,96	0,0310
ENSG00000142227	epithelial membrane protein 3	0,96	0,0302
ENSG00000148143	zinc finger protein 462	0,96	0,0333
ENSG00000163083	inhibin, beta B	0,96	0,0222
ENSG00000242265	paternally expressed 10	0,97	0,0286
ENSG00000130702	laminin, alpha 5	0,98	0,0222
ENSG00000272016	NA	0,99	0,0479
ENSG00000167779	insulin-like growth factor binding protein 6	0,99	0,0482
ENSG00000146072	tumor necrosis factor receptor superfamily, member 21	0,99	0,0197
ENSG00000131759	retinoic acid receptor, alpha	0,99	0,0291
ENSG00000118257	neuropilin 2	1,00	0,0302
ENSG00000214548	maternally expressed 3 (non-protein coding)	1,01	0,0286
ENSG00000186111	phosphatidylinositol-4-phosphate 5-kinase, type I, gamma	1,02	0,0248
ENSG00000187098	microphthalmia-associated transcription factor	1,02	0,0298
ENSG00000168298	histone cluster 1, H1e	1,03	0,0344
ENSG00000211459	NA	1,04	0,0482
ENSG00000118898	periplakin	1,05	0,0032
ENSG00000126705	AT hook, DNA binding motif, containing 1	1,06	0,0352
ENSG00000166025	angiomotin like 1	1,06	0,0104
ENSG00000160211	glucose-6-phosphate dehydrogenase	1,07	0,0004
ENSG00000135749	pecanex-like 2 (Drosophila)	1,07	0,0303
ENSG00000275379	histone cluster 1, H3i	1,10	0,0362
ENSG00000277972	NA	1,11	0,0235
ENSG00000144681	SH3 and cysteine rich domain	1,11	0,0122
ENSG00000141068	kinase suppressor of ras 1	1,11	0,0270
ENSG00000179361	AT rich interactive domain 3B (BRIGHT-like)	1,11	0,0314
ENSG00000198888	NADH dehydrogenase, subunit 1 (complex I)	1,12	0,0403
ENSG00000147394	zinc finger protein 185 (LIM domain)	1,12	0,0295
ENSG00000105699	lipolysis stimulated lipoprotein receptor	1,13	0,0261
ENSG00000163053	solute carrier family 16, member 14	1,13	0,0119
ENSG00000065534	myosin light chain kinase	1,14	0,0068
ENSG00000113739	stanniocalcin 2	1,14	0,0007
ENSG00000273703	histone cluster 1, H2bm	1,15	0,0456
ENSG00000184270	histone cluster 2, H2ab	1,17	0,0409
ENSG00000110628	solute carrier family 22, member 18	1,17	0,0347
ENSG00000125534	pancreatic progenitor cell differentiation and proliferation factor	1,18	0,0202
ENSG00000230629	NA	1,19	0,0179
ENSG00000196787	histone cluster 1, H2ai	1,20	0,0482
ENSG00000099812	mitotic spindle positioning	1,21	0,0186
ENSG00000173267	synuclein, gamma (breast cancer-specific protein 1)	1,22	0,0395
ENSG00000196866	histone cluster 1, H2ad	1,24	0,0482
ENSG00000265763	zinc finger protein 488	1,26	0,0222
ENSG00000184678	histone cluster 2, H2be	1,27	0,0173
ENSG00000074527	netrin 4	1,27	0,0040
ENSG00000103034	NDRG family member 4	1,28	0,0302
ENSG00000203814	histone cluster 2, H2bf	1,29	0,0302
ENSG00000197903	histone cluster 1, H2bk	1,30	0,0359
ENSG00000112139	MAM domain containing glycosylphosphatidylinositol anchor 1	1,32	0,0096
ENSG00000158373	histone cluster 1, H2bd	1,32	0,0219
ENSG00000185215	tumor necrosis factor, alpha-induced protein 2	1,34	0,0006

ENSG00000022267	four and a half LIM domains 1	1,34	0,0009
ENSG00000164690	sonic hedgehog	1,36	0,0008
ENSG00000168874	atonal homolog 8 (Drosophila)	1,38	0,0266
ENSG00000064205	WNT1 inducible signaling pathway protein 2	1,39	0,0102
ENSG00000163661	pentraxin 3, long	1,41	0,0226
ENSG00000148671	adipogenesis regulatory factor	1,42	0,0062
ENSG00000158055	grainyhead-like 3 (Drosophila)	1,43	0,0066
ENSG00000201315	NA	1,43	0,0398
ENSG00000171368	tubulin polymerization promoting protein	1,43	0,0325
ENSG00000141753	insulin-like growth factor binding protein 4	1,44	0,0001
ENSG00000109321	amphiregulin	1,45	0,0098
ENSG00000252835	small Cajal body-specific RNA 21	1,49	0,0202
ENSG00000243562	NA	1,50	0,0489
ENSG00000028137	tumor necrosis factor receptor superfamily, member 1B	1,50	0,0006
ENSG00000167767	keratin 80	1,52	0,0000
ENSG00000260035	NA	1,52	0,0067
ENSG00000112379	KIAA1244	1,55	0,0002
ENSG00000264169	NA	1,57	0,0353
ENSG00000180730	shisa family member 2	1,58	0,0218
ENSG00000163171	CDC42 effector protein (Rho GTPase binding) 3	1,64	0,0000
ENSG00000057294	plakophilin 2	1,65	0,0387
ENSG00000241529	NA	1,66	0,0068
ENSG00000272620	AFAP1 antisense RNA 1	1,66	0,0000
ENSG00000198246	solute carrier family 29 (equilibrative nucleoside transporter), member 3	1,67	0,0011
ENSG00000179046	tripartite motif family-like 2	1,68	0,0031
ENSG00000116991	signal-induced proliferation-associated 1 like 2	1,74	0,0001
ENSG00000148677	ankyrin repeat domain 1 (cardiac muscle)	1,74	0,0475
ENSG00000275803	NA	1,77	0,0302
ENSG00000263968	NA	1,81	0,0097
ENSG00000275961	NA	1,81	0,0037
ENSG00000244230	NA	1,82	0,0026
ENSG00000239607	NA	1,82	0,0164
ENSG00000266794	NA	1,85	0,0409
ENSG00000263841	NA	1,93	0,0311
ENSG00000106123	EPH receptor B6	1,97	0,0002
ENSG00000244294	NA	2,33	0,0055
ENSG00000276213	NA	2,49	0,0019

Table 11: RNA sequencing targets Tet-On EFM-192A cells, untreated

Gene ID	Gene name	Fold change [log2]	Adjusted p-value
ENSG00000135046	annexin A1	-2,44	0,0000
ENSG00000100220	RNA 2',3'-cyclic phosphate and 5'-OH ligase	-1,76	0,0000
ENSG00000177469	polymerase I and transcript release factor	-1,35	0,0000
ENSG00000173706	heart development protein with EGF-like domains 1	-1,02	0,0269
ENSG00000169213	RAB3B, member RAS oncogene family	-0,94	0,0151
ENSG00000167914	gasdermin A	-0,84	0,0269
ENSG00000006062	mitogen-activated protein kinase kinase kinase 14	-0,83	0,0483
ENSG00000067225	pyruvate kinase, muscle	-0,80	0,0003
ENSG00000207827	microRNA 30a	-0,76	0,0003
ENSG00000120708	transforming growth factor, beta-induced, 68kDa	-0,69	0,0252
ENSG00000197043	annexin A6	-0,69	0,0035
ENSG00000160211	glucose-6-phosphate dehydrogenase	-0,65	0,0403
ENSG00000276043	ubiquitin-like with PHD and ring finger domains 1	-0,55	0,0464
ENSG00000196924	filamin A, alpha	-0,55	0,0179
ENSG00000119900	opioid growth factor receptor-like 1	0,63	0,0380
ENSG00000198805	purine nucleoside phosphorylase	0,64	0,0181
ENSG00000128989	cAMP-regulated phosphoprotein, 19kDa	0,65	0,0301
ENSG00000115902	solute carrier family 1 (glutamate/neutral amino acid transporter), member 4	0,66	0,0378
ENSG00000146733	phosphoserine phosphatase	0,67	0,0147
ENSG00000101255	tribbles pseudokinase 3	0,68	0,0230
ENSG00000150593	programmed cell death 4 (neoplastic transformation inhibitor)	0,73	0,0107
ENSG00000064270	ATPase, Ca++ transporting, type 2C, member 2	0,75	0,0483
ENSG00000187735	transcription elongation factor A (SII), 1	0,76	0,0181
ENSG00000154359	LON peptidase N-terminal domain and ring finger 1	0,76	0,0181
ENSG00000155313	ubiquitin specific peptidase 25	0,77	0,0002
ENSG00000245694	colorectal neoplasia differentially expressed (non-protein coding)	0,79	0,0455
ENSG00000144824	pleckstrin homology-like domain, family B, member 2	0,79	0,0212
ENSG00000149212	sestrin 3	0,80	0,0107
ENSG00000168672	family with sequence similarity 84, member B	0,81	0,0091
ENSG00000106799	transforming growth factor, beta receptor 1	0,81	0,0011
ENSG00000121039	retinol dehydrogenase 10 (all-trans)	0,82	0,0403
ENSG00000119866	B-cell CLL/lymphoma 11A (zinc finger protein)	0,82	0,0380

ENSG00000164294	glutathione peroxidase 8 (putative)	0,82	0,0245
ENSG00000095209	transmembrane protein 38B	0,83	0,0111
ENSG00000135373	ets homologous factor	0,83	0,0181
ENSG00000120925	ring finger protein 170	0,83	0,0111
ENSG00000111912	nuclear receptor coactivator 7	0,85	0,0179
ENSG00000065809	family with sequence similarity 107, member B	0,86	0,0178
ENSG00000155158	tetratricopeptide repeat domain 39B	0,87	0,0403
ENSG00000092621	phosphoglycerate dehydrogenase	0,91	0,0486
ENSG00000275896	NA	0,94	0,0115
ENSG00000067208	ecotropic viral integration site 5	0,95	0,0119
ENSG00000112715	vascular endothelial growth factor A	0,95	0,0102
ENSG00000199753	small nucleolar RNA, C/D box 104	0,96	0,0464
ENSG00000234741	growth arrest-specific 5 (non-protein coding)	0,98	0,0181
ENSG00000148943	lin-7 homolog C (C. elegans)	0,99	0,0107
ENSG00000118276	UDP-Gal:betaGlcNAc beta 1,4- galactosyltransferase, polypeptide 6	1,00	0,0011
ENSG00000221963	apolipoprotein L, 6	1,02	0,0000
ENSG00000124333	vesicle-associated membrane protein 7	1,02	0,0011
ENSG00000265972	thioredoxin interacting protein	1,03	0,0331
ENSG00000261326	NA	1,04	0,0003
ENSG00000066735	kinesin family member 26A	1,08	0,0289
ENSG00000125430	heparan sulfate (glucosamine) 3-O-sulfotransferase 3B1	1,13	0,0091
ENSG00000085563	ATP-binding cassette, sub-family B (MDR/TAP), member 1	1,14	0,0001
ENSG00000212588	small nucleolar RNA, H/ACA box 26	1,17	0,0180
ENSG00000212607	small nucleolar RNA, H/ACA box 45B	1,17	0,0048
ENSG00000135842	family with sequence similarity 129, member A	1,18	0,0000
ENSG00000209082	NA	1,18	0,0245
ENSG00000221539	small nucleolar RNA, C/D box 99	1,20	0,0403
ENSG00000206630	small nucleolar RNA, C/D box 60	1,21	0,0105
ENSG00000221241	small nucleolar RNA, C/D box 88A	1,30	0,0173
ENSG00000207181	small nucleolar RNA, H/ACA box 14B	1,32	0,0043
ENSG00000238835	small Cajal body-specific RNA 18	1,33	0,0091
ENSG00000074935	tubulin, epsilon 1	1,33	0,0007
ENSG00000100889	phosphoenolpyruvate carboxykinase 2 (mitochondrial)	1,37	0,0000
ENSG00000116852	kinesin family member 21B	1,53	0,0000
ENSG00000070669	asparagine synthetase (glutamine-hydrolyzing)	1,55	0,0000
ENSG00000145362	ankyrin 2, neuronal	1,63	0,0031
ENSG00000151012	solute carrier family 7 (anionic amino acid transporter light chain, xc-system), member 11	1,67	0,0001
ENSG00000128965	ChaC, cation transport regulator homolog 1 (E. coli)	1,78	0,0007
ENSG00000168209	DNA-damage-inducible transcript 4	1,98	0,0000
ENSG00000196268	zinc finger protein 493	2,12	0,0000
ENSG00000182568	SATB homeobox 1	2,19	0,0000
ENSG00000001626	cystic fibrosis transmembrane conductance regulator (ATP-binding cassette sub-family C, member 7)	2,38	0,0000

Table 12: RNA sequencing targets Tet-On Reh cells, untreated

Gene ID	Gene name	Fold change [log2]	Adjusted p-value
ENSG00000135318	5'-nucleotidase, ecto (CD73)	-2,43	0,0000
ENSG00000197046	sialic acid binding Ig-like lectin 15	-2,35	0,0021
ENSG00000187678	sprouty homolog 4 (Drosophila)	-2,22	0,0013
ENSG00000136859	angiopoietin-like 2	-1,92	0,0000
ENSG00000120278	pleckstrin homology domain containing, family G (with RhoGef domain) member 1	-1,64	0,0000
ENSG00000179344	major histocompatibility complex, class II, DQ beta 1	-1,61	0,0034
ENSG00000244301	NA	-1,33	0,0160
ENSG00000124942	AHNAK nucleoprotein	-1,26	0,0009
ENSG00000138771	shroom family member 3	-1,16	0,0009
ENSG00000223865	major histocompatibility complex, class II, DP beta 1	-1,13	0,0021
ENSG00000116977	lectin, galactoside-binding, soluble, 8	-1,07	0,0000
ENSG00000188725	small integral membrane protein 15	-1,02	0,0021
ENSG00000130635	collagen, type V, alpha 1	-1,01	0,0089
ENSG00000105369	CD79a molecule, immunoglobulin-associated alpha	-0,91	0,0067
ENSG00000173805	huntingtin-associated protein 1	-0,91	0,0068
ENSG00000107819	sideroflexin 3	-0,91	0,0489
ENSG00000086619	ERO1-like beta (S. cerevisiae)	-0,87	0,0462
ENSG00000244405	ets variant 5	-0,85	0,0064
ENSG00000058668	ATPase, Ca++ transporting, plasma membrane 4	-0,84	0,0129
ENSG00000231389	major histocompatibility complex, class II, DP alpha 1	-0,80	0,0044
ENSG00000124126	phosphatidylinositol-3,4,5-trisphosphate-dependent Rac exchange factor 1	-0,77	0,0160

ENSG00000125266	ephrin-B2	0,70	0,0313
ENSG00000198805	purine nucleoside phosphorylase	0,70	0,0092
ENSG00000139289	pleckstrin homology-like domain, family A, member 1	0,72	0,0212
ENSG00000115758	ornithine decarboxylase 1	0,73	0,0131
ENSG00000189184	protocadherin 18	1,07	0,0045
ENSG00000107719	phosphatase domain containing, paladin 1	1,12	0,0009
ENSG00000166073	G protein-coupled receptor 176	1,12	0,0071
ENSG00000165168	cytochrome b-245, beta polypeptide	1,15	0,0000
ENSG00000146376	Rho GTPase activating protein 18	1,30	0,0161
ENSG00000153823	phosphotyrosine interaction domain containing 1	1,36	0,0000
ENSG00000138650	protocadherin 10	1,44	0,0021
ENSG00000130702	laminin, alpha 5	1,48	0,0044
ENSG00000123700	potassium inwardly-rectifying channel, subfamily J, member 2	1,49	0,0035
ENSG00000271615	NA	1,51	0,0000
ENSG00000145147	slit homolog 2 (Drosophila)	1,55	0,0481
ENSG00000075213	sema domain, immunoglobulin domain (Ig), short basic domain, secreted, (semaphorin) 3A	1,61	0,0032
ENSG00000185686	preferentially expressed antigen in melanoma	1,72	0,0000
ENSG00000030419	IKAROS family zinc finger 2 (Helios)	1,94	0,0000
ENSG00000129422	microtubule associated tumor suppressor 1	2,05	0,0000
ENSG00000164920	odd-skipped related transciption factor 2	2,50	0,0000
ENSG00000207264	RNA, U6 small nuclear 15, pseudogene	4,88	0,0192

Supplementary figures

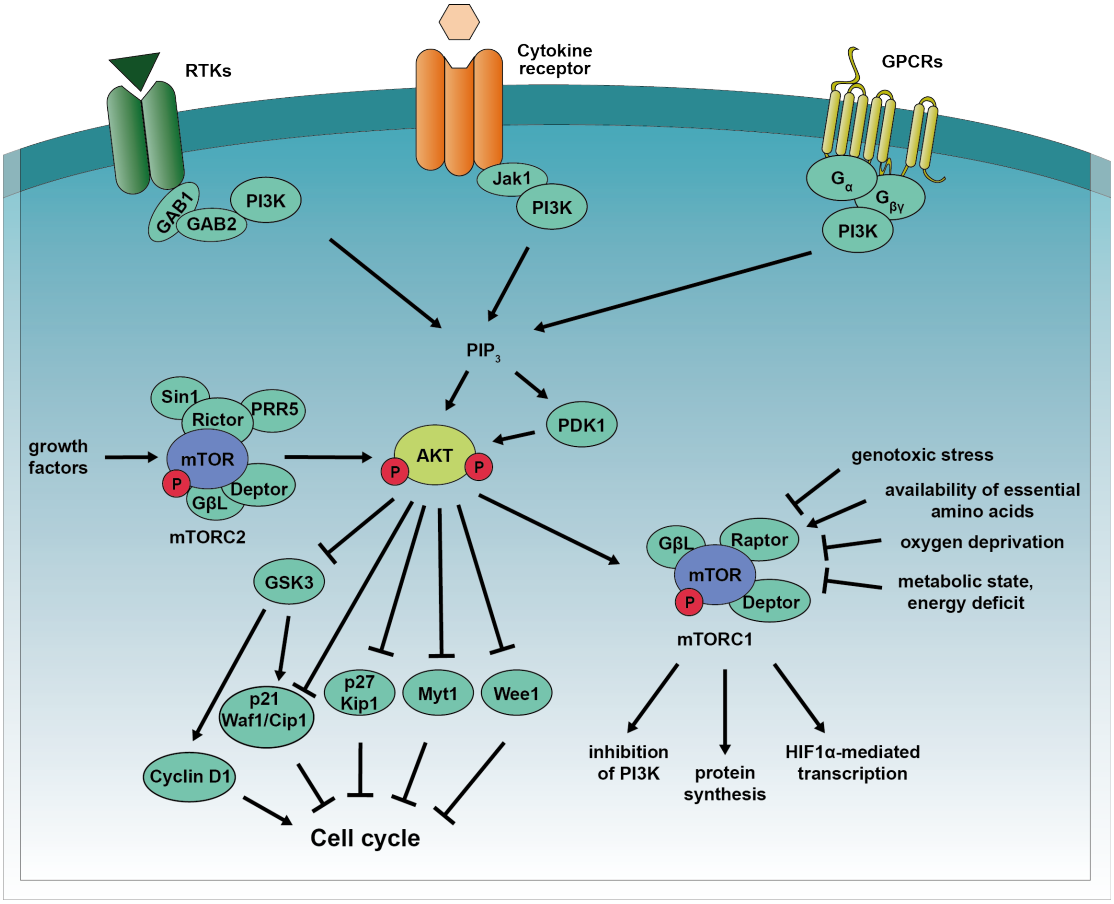

Figure 33: PI3K/AKT signaling

The PI3K/AKT signaling cascade can be activated via receptor tyrosine kinases (RTKs), cytokine receptors, and G-protein-coupled receptors (GPCRs). Stimulation of any of these receptors causes recruitment and activation of the kinase PI3K (phosphoinositide 3-kinase), which catalyzes the formation of PIP_3 (phosphatidylinositol-3,4,5-triphosphate). PIP_3 recruits the kinases PDK1 (pyruvate dehydrogenase lipoamide kinase isozyme 1) and AKT (also known as protein kinase B, PKB) to the plasma membrane and thereby enables PDK1-mediated phosphorylation of AKT on threonine 308. Furthermore, full activation of AKT also requires phosphorylation by activated mTORC2 (mechanistic target of rapamycin complex 2) on serine 473. mTORC2 itself is likewise activated by growth factor signaling. In contrast, mTORC1 (mechanistic target of rapamycin complex 1) lies downstream of AKT signaling and mediates activation of protein synthesis as well as of HIF1α-mediated transcription. This complex is also activated by the availability of essential amino acids, while genotoxic stress, oxygen deprivation and energy deficiency inhibit mTORC1 activity. AKT signaling initiates cell cycle progression by inhibiting cell cycle inhibitors such as p21 and p27 and by increasing the activation of cyclin D1.

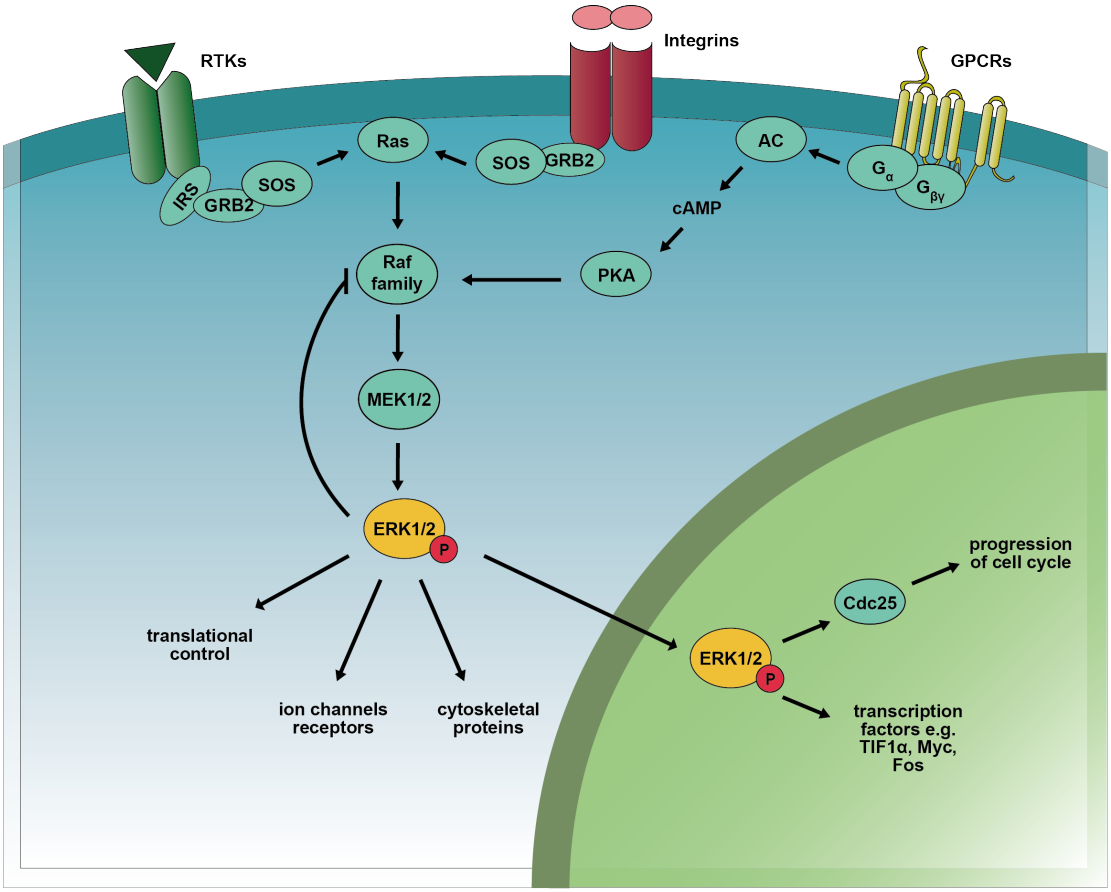

Figure 34: ERK MAPK signaling

Activation of receptor tyrosine kinases (RTKs) or integrins by their respective ligands leads to the recruitment of the adaptor protein GRB2, which in turn recruits SOS. The guanine nucleotide exchange factor SOS subsequently facilitates the release of GDP from the small GTPase Ras, which enables its exchange to GTP and thus Ras activation. Ras-GTP initiates the ERK MAPK signaling cascade by activating members of the Raf family that serve as MAP kinase kinase kinases. Raf phosphorylates and thus activates MEK1/2, which in turn phosphorylates ERK1/2. Phosphorylated ERK1/2 is able to translocate to the nucleus where it stimulates the activity of various downstream targets and mediates cell cycle progression. Besides this Ras-centered route of activation, ERK MAPK signaling can also be initiated by stimulated GPCRs, which promote the activation of trimeric G proteins signaling to the adenylyl cyclase (AC). Formation of cAMP subsequently triggers the activation of PKA and subsequently of Raf.

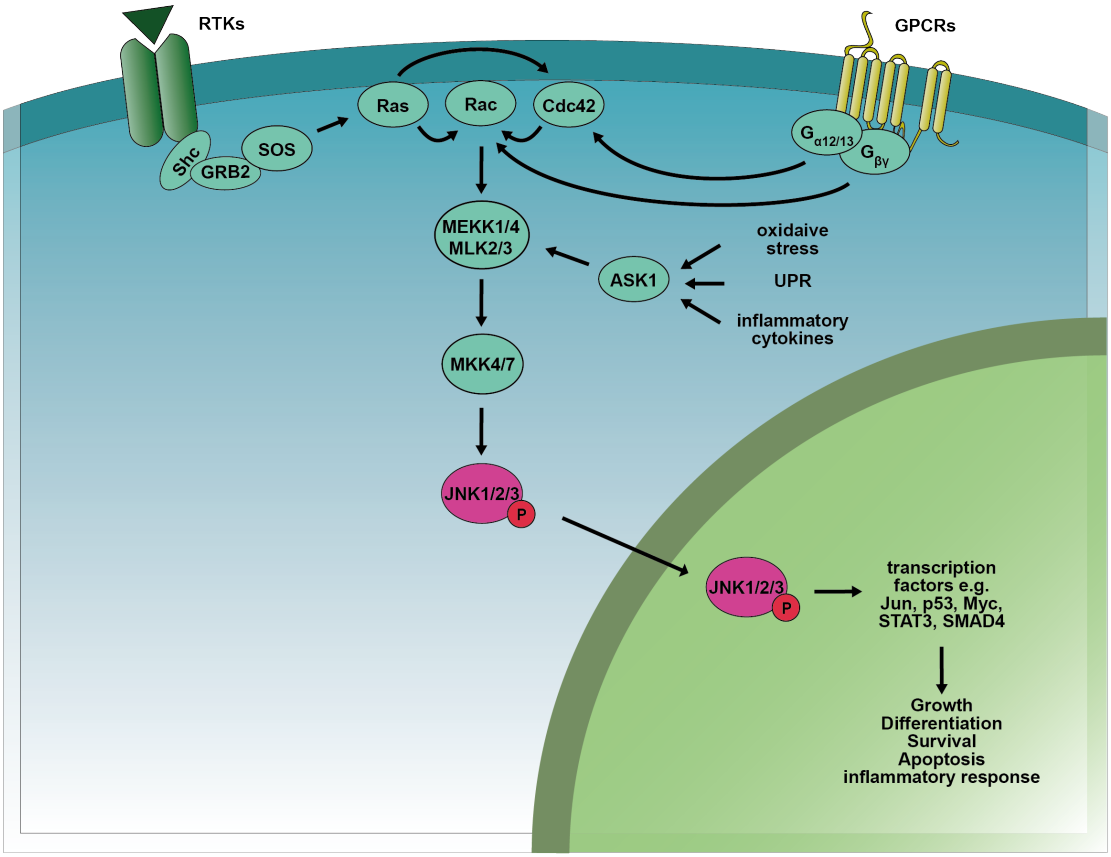

Figure 35: JNK MAPK signaling

The JNK MAPK pathway can be activated by receptor tyrosine kinases (RTKs) signaling via GRB2-SOS, Ras, and Rac or by GPCRs stimulating Rac via the activation of trimeric GTPases and Cdc42. Consequently, Rac activates the MAP kinase kinase kinases MEKK1/4 or MLK2/3 to phosphorylate MKK4/7 serving as MAP kinase kinases. MKK4/7 in turn phosphorylates and thus activates JNK1/2/3. Phosphorylated JNK1/2/3 migrates to the nucleus where it positively or negatively regulates the activity of various transcription factors, which ultimately influences growth, differentiation, survival, apoptosis or the inflammatory response of the cell. Furthermore, the JNK MAPK pathway can also be triggered via activation of ASK1 by oxidative stress, the UPR or inflammatory cytokines.

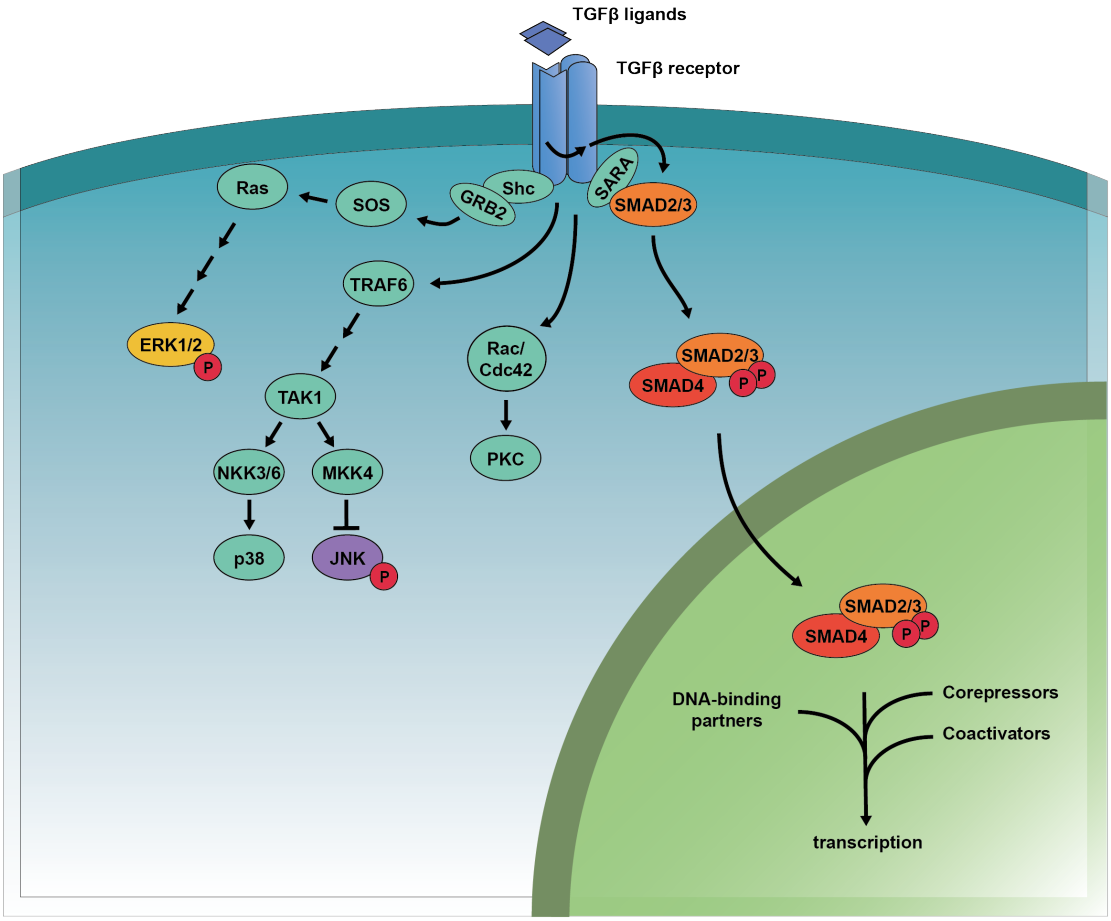

Figure 36: TGFβ signaling

TGFβ signaling is initiated by ligand-induced oligomerization of two type I and two type II receptors, which allows the constitutively active type II receptors to phosphorylate a glycine-serine-rich region in the type I receptors. This phosphorylation provides a docking site for SMAD2 and SMAD3 and enables phosphorylation of these proteins by the type I receptor. Once modified, SMAD2/3 dissociates from the receptor and forms a complex with SMAD4. This complex migrates to the nucleus and associates with DNA-binding partners, coactivators, and corepressors to transcriptionally activate several downstream targets. Furthermore, stimulated TGFβ receptors can also activate ERK1/2 via GRB2, SOS, and Ras as well as JNK via TRAF6 and TAK1.

7.2. Index of figures

7.3. Index of tables

7.4. Abbreviations

%	Percent
% [v/v]	Volume percent
% [w/v}	Weight percent
°C	Degrees Celsius
1NM-PP1	1-Naphthylmethylpyrazolo[3,5-*d*]pyrimidine
3’ UTR	3’-untranslated region
5’ UTR	5’-untranslated region
A	(deoxy)Adenosine nucleotide
AEBSF	4-(2-Aminoethyl) Benzenesulfonyl fluoride hydrochloride
AMP	Adenosine-monophosphate
Arg	Arginine
ATP	Adenosine-triphosphate
ATPase	ATP hydrolase
BCA	Bicinchoninic acid
Blasti	Blasticidin
BrdU	Bromodeoxyuridine
BSA	Bovine serum albumin
bZIP domain	Basic leucine zipper domain
C	(deoxy)Cytosine nucleotide
C. elegans	*Caenorhabditis elegans*
cAMP	Cyclic adenosine monophosphate
CDK	Cyclin-dependent kinase
cDNA	Complementary deoxyribonucleic acid
CKI	Cyclin-dependent kinase inhibitor
CO_2	Carbon dioxide
Cpm	Counts per minute
DAPI	4',6-Diamidino-2-phenylindole
DEAD	Aspartate-Glutamate-Alanine-Aspartate
DMEM	Dulbecco’s modified Eagle's medium
DMSO	Dimethyl sulfoxide
DNA	Deoxyribonucleic acid
DNase	Deoxyribonuclease
Dox	Doxycycline
DSP	Dithiobis(succinimidyl propionate)
DTT	Dithiothreitol
ECL	Enhanced chemiluminescence
EcoR	Ecotropic receptor
EDTA	2,2’,2’’,2’’’-(Ethane-1,2-diyldinitrilo)tetraacetic acid

ER	Endoplasmic reticulum
ERAD	ER-associated protein degradation
FACS	Fluorescence-activated cell sorting
FBS	Fetal bovine serum
FSC	Forward scatter
G	(deoxy)Guanosine nucleotide
g	Gram
$G_{0/1/2}$ phase	Gap phase 0/1/2
G418	Neomycin
GDP	Guanosine diphosphate
GFP	Green fluorescent protein
GO	Gene ontology
GPCR	G protein-coupled receptor
GTP	Guanosine-5'-triphosphate
GTPase	GTP hydrolase
h	Hour
HEPES	4-(2-Hydroxyethyl)-1-piperazineethanesulfonic acid
HIV	Human immunodeficiency virus
I	Inosine nucleotide
Ile	Isoleucine
kDa	Kilodalton
l	Liter
LB medium	Lysogeny broth medium
M	Molar
M phase	Mitosis phase
MAPK	Mitogen-activated protein kinase
MEF	Mouse embryonic fibroblasts
MGUS	Monoclonal gammopathy of undetermined significance
MHC	Major histocompatibility complex
min	Minute
ml	Milliliter
mRNA	Messenger ribonucleic acid
MTT	3-(4,5-dimethylthiazol-2-yl)-2,5-diphenyltetrazolium bromide
N.S.	Not significant
Neo	Neomycin
nM	Nanomolar
nm	Nanometers
OH	Hydroxyl
PAGE	Polyacrylamide gel electrophoresis

PAR-CLIP	Photoactivatable-Ribonucleoside-Enhanced Crosslinking
PBS	Phosphate buffered saline
PBST	PBS-Tween
PCR	Polymerase chain reaction
pH	Pondus Hydrogenii
PH domain	Pleckstrin homology domain
PIP_3	Phosphatidylinositol (3,4,5)-trisphosphate
PMSF	Phenylmethanesulfonyl fluoride
Pre-tRNA	Precursor transfer ribonucleic acid
Puro	Puromycin
RIDD	Regulated IRE1α-dependent decay
RNA	Ribonucleic acid
RNAi	RNA interference
RNase	Ribonuclease
rpm	Revolutions per minute
RPMI medium	Roswell Park Memorial Institute medium
RT	Room temperature
RT-PCR	Real-time polymerase chain reaction
RT-qPCR	Quantitative reverse transcriptase polymerase chain reaction
RTK	Receptor tyrosine kinase
rtTA	Reverse tetracycline transactivator
s	Second
S phase	DNA synthesis phase
S. cerevisiae	*Saccharomyces cerevisiae*
SDS	Sodium dodecyl sulphate
SEM	Standard error of the mean
SH2 domain	Src Homology 2 domain
shRNA	Small hairpin ribonucleic acid
SSC	Sideward scatter
SSC buffer	Saline sodium citrate buffer
T	Deoxythymidine nucleotide
TEMED	N,N,N',N'-Tetramethyl-ethane-1,2-diamine
Tet	Tetracycline
Tet-On	Tetracycline-inducible expression
Tg	Thapsigargin
Tm	Tunicamycin
Tris-HCl	2-Amino-2-hydroxymethyl-propane-1,3-diol hydrochloride
tRNA	Transfer ribonucleic acid
Tyr	Tyrosine

U	Uridine nucleotide
U	Unit
UPR	Unfolded protein response
V	Volt
VSVG	Vesicular Stomatitis Virus Glycoprotein
µg	Microgram
µl	Microliter
µM	Micromolar

7.5. Names and abbreviations of genes

ACTB	Actin, Beta
ADRA1B	Adrenoceptor Alpha 1B
AKT	V-Akt Murine Thymoma Viral Oncogene Homolog 1
ANK3	Ankyrin 3
AR	Androgen Receptor
ASK1	Apoptosis Signal-Regulating Kinase 1
ASNS	Asparagine Synthetase (Glutamine-Hydrolyzing)
ASW	Ashwin
ATF4	Activating Transcription Factor 4
ATF6	Activating Transcription Factor 6
AtRNL	Arabidopsis thaliana RNA ligase
BAD	BCL2-Associated Agonist Of Cell Death
BAX	BCL2-Associated X Protein
BIP	Immunoglobulin Heavy Chain-Binding Protein
BLOS1	Biogenesis Of Lysosomal Organelles Complex-1, Subunit 1
CAK	CDK-Activating Kinase
CGI99	UPF0568 Protein C14orf166
CHOP	CCAAT/Enhancer-Binding Protein Homologous Protein
CIP/WAF1	CDK-Interaction Protein/Wild type p53-Activated Fragment 1
CNP1	2',3'-Cyclic Nucleotide 3' Phosphodiesterase 1
DDR2	Discoidin Domain Receptor Tyrosine Kinase 2
DDX1	ATP-dependent RNA helicase DDX1
DNAJB9	DnaJ (Hsp40) Homolog, Subfamily B, Member 9
DST	Dystonin
EDEM1	ER Degradation Enhancer, Mannosidase Alpha-Like 1
eIF2α	Eukaryotic Translation Initiation Factor 2 Subunit Alpha
ERK	Extracellular Signal-Regulated Kinase

FAM98B	Family With Sequence Similarity 98, Member B
FGF	Fibroblast Growth Factor
GAB2	GRB2-Associated Binding Protein 2
GADD34	Growth Arrest And DNA-Damage-Inducible 34
GRB2	Growth Factor Receptor-Bound Protein 2
GSK3	Glycogen Synthase Kinase 3
HIF1α	Hypoxia Inducible Factor 1, Alpha Subunit
INK	Cyclin-Dependent Kinase Inhibitor
IRE1α	Inositol-Requiring Enzyme 1 Alpha
JNK	C-Jun N-Terminal Kinase
KIP	Kinase-Interacting Protein
MACF1	Microtubule-actin crosslinking factor 1
MEF2C	Myocyte Enhancer Factor 2C
MEK	MAPK/ERK Kinase 1
MEKK	MAPK/ERK Kinase Kinase
MKK	MAP Kinase Kinase
MLK	Mixed Lineage Kinase
mTORC	Mechanistic Target Of Rapamycin Complex
NF- κB	Nuclear factor-κB
PARP	Poly (ADP-Ribose) Polymerase
PDGF	Platelet-Derived Growth Factor
PDGFRB	Platelet-Derived Growth Factor Receptor, Beta Polypeptide
PDK1	3-Phosphoinositide Dependent Protein Kinase
PERK	PRKR-Like Endoplasmic Reticulum Kinase
PGF	Placental Growth Factor
PI3K	Phosphatidylinositol 3-Kinase
PKA	Protein Kinase A
RTCB	tRNA-splicing ligase RtcB homolog
RTCD1	RNA Terminal Phosphate Cyclase Domain-Containing Protein 1
S1P/S2P	Site-1 protease/site-2 protease
SCARA3	Scavenger Receptor Class A, Member 3
Sen	tRNA splicing endonuclease, *S. cerevisiae*
SMAD	Sma- And Mad-Related Protein
SOS	Son Of Sevenless Homolog
SPECC1	Sperm Antigen With Calponin Homology And Coiled-Coil Domains 1
SSTR2	Somatostatin Receptor 2
TAK1	TGF-Beta-Activated Kinase 1
TDP-43	TAR DNA-Binding Protein 43

TGFBR	Transforming Growth Factor, Beta Receptor
TGFβ	Transforming Growth Factor Beta
Tpt1	tRNA 2'-phosphotransferase 1, *S. cerevisiae*
TRAF2	TNF Receptor-Associated Factor 2
TRAF7	TNF Receptor-Associated Factor 7
Trl1	tRNA Ligase, *S. cerevisiae*
TRPT1	tRNA Phosphotransferase 1
TSEN	tRNA Splicing Endonuclease
TTN	Titin
VEGF	Vascular Endothelial Growth Factor
XBP1	X-Box Binding Protein 1
XBP1s	X-Box Binding Protein 1, spliced
XBP1u	X-Box Binding Protein 1, unspliced

7.6. Scientific publication

Published online: November 6, 2014

Article

TRANSPARENT PROCESS OPEN ACCESS

THE EMBO JOURNAL

The mammalian tRNA ligase complex mediates splicing of *XBP1* mRNA and controls antibody secretion in plasma cells

Jennifer Jurkin[1,†], Theresa Henkel[1,†], Anne Færch Nielsen[2], Martina Minnich[3], Johannes Popow[4], Therese Kaufmann[1], Katrin Heindl[5], Thomas Hoffmann[3], Meinrad Busslinger[3] & Javier Martinez[1,*]

Abstract

The unfolded protein response (UPR) is a conserved stress-signaling pathway activated after accumulation of unfolded proteins within the endoplasmic reticulum (ER). Active UPR signaling leads to unconventional, enzymatic splicing of *XBP1* mRNA enabling expression of the transcription factor XBP1s to control ER homeostasis. While IRE1 has been identified as the endoribonuclease required for cleavage of this mRNA, the corresponding ligase in mammalian cells has remained elusive. Here, we report that RTCB, the catalytic subunit of the tRNA ligase complex, and its co-factor archease mediate *XBP1* mRNA splicing both *in vitro* and *in vivo*. Depletion of RTCB in plasma cells of *Rtcb*$^{fl/fl}$ *Cd23*-Cre mice prevents XBP1s expression, which normally is strongly induced during plasma cell development. RTCB-depleted plasma cells show reduced and disorganized ER structures as well as severe defects in antibody secretion. Targeting RTCB and/or archease thus represents a promising strategy for the treatment of a growing number of diseases associated with elevated expression of XBP1s.

Keywords antibody secretion; archease; plasma cells; RTCB; *XBP1* mRNA splicing
Subject Categories Immunology; RNA Biology
DOI 10.15252/embj.201490332 | Received 17 September 2014 | Accepted 17 October 2014

Introduction

In mammalian cells, around 6% of all tRNAs are encoded as intron-containing pre-tRNA sequences that must undergo splicing in order to become active in protein translation (reviewed in Popow *et al*, 2012). tRNA splicing requires the tRNA ligase complex consisting of RTCB as the catalytic subunit, the DEAD-box helicase DDX1 and three subunits of unknown function: FAM98B, ASW and CGI-99 (Popow *et al*, 2011). Full enzymatic activity of RTCB depends on guanylation, which is provided by the co-factor archease working in cooperation with DDX1 (Popow *et al*, 2014).

In *Saccharomyces cerevisiae*, tRNA maturation is likewise catalyzed by the homologous tRNA ligase Trl1 altogether conducting three enzymatic reactions comprising hydrolysis of the 2′, 3′-cyclic phosphate to yield a 3′-hydroxyl (OH), 2′-phosphate terminus (cyclic phosphodiesterase activity), phosphorylation of the terminal 5′-OH group at the tRNA 3′ exon (GTP-dependent, RNA-polynucleotide kinase activity) and ligation of tRNA exon halves (ATP-dependent, RNA ligase activity) (Greer *et al*, 1983; Phizicky *et al*, 1986; Apostol *et al*, 1991; Sawaya *et al*, 2003). The phosphate incorporated into the newly formed phosphodiester bond therefore originates from the nucleotide triphosphate co-factor required for the kinase reaction (Greer *et al*, 1983; Phizicky *et al*, 1986). In contrast, the mammalian tRNA ligase RTCB directly joins 2′, 3′-cyclic phosphate and 5′-OH termini, leading to incorporation of the precursor-derived cyclic phosphate into the splice junction (Filipowicz & Shatkin, 1983; Filipowicz *et al*, 1983; Laski *et al*, 1983). This mechanism is referred to as 3′-5′ ligation. While the mammalian tRNA ligase complex is well characterized *in vitro*, less is known about its functions *in vivo*.

2′, 3′-cyclic phosphates and 5′-OH termini not only do characterize tRNA splicing but also are generated during unconventional splicing of *XBP1* mRNA as part of the unfolded protein response (UPR), a stress-signaling pathway activated upon accumulation of unfolded proteins in the ER lumen (reviewed in Hetz, 2012). Cytoplasmic splicing of *XBP1* mRNA is initiated by the ER transmembrane endonuclease IRE1 and is required for expression of the transcription factor XBP1s. Although in total there are three different UPR signaling branches in mammalian cells, the IRE1-XBP1 axis is the most ancient and conserved pathway and its improper functioning has been associated with many human diseases, such as cancer, autoimmunity and neurodegenerative disorders (reviewed in Hetz *et al*, 2013).

1 Institute of Molecular Biotechnology of the Austrian Academy of Sciences (IMBA), Vienna, Austria
2 European Molecular Biology Organization (EMBO), Heidelberg, Germany
3 Institute of Molecular Pathology (IMP), Vienna, Austria
4 European Molecular Biology Laboratory (EMBL), Heidelberg, Germany
5 Whitehead Institute for Biomedical Research, Cambridge, MA, USA
*Corresponding author. Tel: +43 1 79044 4840; E-mail: javier.martinez@imba.oeaw.ac.at
†These authors contributed equally to this work

Published online: November 6, 2014
The EMBO Journal RTCB regulates antibody secretion in plasma cells *Jennifer Jurkin et al*

Given its high conservation, studies in yeast critically contributed to the mechanistic understanding of unconventional mRNA splicing during the UPR. In *S. cerevisiae*, the endonuclease Ire1p directly senses perturbations in ER homeostasis and gains endoribonuclease activity to remove an intron from *HAC1* mRNA—the homologue of mammalian *XBP1* mRNA—that was retained after nuclear splicing. Cleavage by Ire1p generates mRNA exons displaying 2′, 3′-cyclic phosphate and 5′-OH termini, which are subsequently joined by the tRNA ligase Trl1 (Cox & Walter, 1996; Sidrauski *et al*, 1996; Sidrauski & Walter, 1997).

Similar to *HAC1* mRNA splicing in *S. cerevisiae*, the mRNA encoding for the mammalian transcription factor XBP1 retains a short, 26-nucleotide intron after canonical splicing, which is recognized and removed by activated IRE1 (Yoshida *et al*, 2001). Subsequent ligation of *XBP1* mRNA exon halves causes a frame shift that changes parts of the open reading frame and enables translation of XBP1s. In contrast to XBP1u, the protein product of unspliced *XBP1* mRNA, XBP1s is a potent transcription factor and regulates genes required to restore ER homeostasis such as chaperones or proteins involved in ER-associated protein degradation (ERAD) (Lee *et al*, 2003). Although unconventional splicing of *XBP1* mRNA resembles *HAC1* mRNA splicing in yeast, the mammalian RNA ligase involved in *XBP1* mRNA splicing has remained elusive.

A constitutively active UPR is a feature of specialized secretory cells (reviewed in Moore & Hollien, 2012). Antibody-secreting plasma cells for instance dramatically induce XBP1s expression during plasma cell differentiation from stimulated B cells (Reimold *et al*, 2001; Gass *et al*, 2002; Iwakoshi *et al*, 2003b), which coordinately induces changes in cellular structures to create a professional secretory phenotype enabling high rates of antibody production (Shaffer *et al*, 2004; McGehee *et al*, 2009; Taubenheim *et al*, 2012). Induction of the UPR in antibody-secreting cells differs from conventional UPR activation in that it is an integral part of the plasma cell differentiation program (Reimold *et al*, 2001; Iwakoshi *et al*, 2003b; Shaffer *et al*, 2004; Klein *et al*, 2006; Nera *et al*, 2006; Schmidlin *et al*, 2008). Accordingly, B cells deficient in XBP1 are unable to expand ER structures (Taubenheim *et al*, 2012), and mice lacking XBP1 show reduced serum immunoglobulin levels and impaired immunoglobulin response to immunization (Reimold *et al*, 2001; Iwakoshi *et al*, 2003b; Todd *et al*, 2009; Taubenheim *et al*, 2012). These findings suggest that induction of the UPR and XBP1 is required by plasma cells to achieve high rates of antibody secretion. Yet the role of XBP1 in plasma cells was proposed to extend beyond its function in the UPR. Initial studies of mice with *Xbp1* deletion in the entire lymphoid system revealed that the absence of XBP1 does not only impact on antibody secretion but also severely affect plasma cell development (Reimold *et al*, 2001). However, more recent studies of a B-cell-specific conditional *Xbp1* mutant mouse model revealed either no or mild effects on plasma cell differentiation that were restricted to later stages of plasma cell development (Hu *et al*, 2009; Todd *et al*, 2009; Taubenheim *et al*, 2012). Additional roles for XBP1 have been proposed in the regulation of the plasma cell survival factor IL-6 (Iwakoshi *et al*, 2003b) and in homing of plasma cells to the bone marrow (Hu *et al*, 2009).

To analyze a possible function of the mammalian tRNA ligase complex in *XBP1* mRNA ligation, we depleted RTCB and its co-factor archease in HeLa cell lines and generated a mature B-cell-specific *Rtcb* knockout mouse. Data from these two models demonstrate an essential function of the tRNA ligase in *XBP1* mRNA splicing and the mammalian UPR and reveal a novel role of RTCB in supporting high rates of antibody secretion in plasma cells.

Results

An *in vitro* assay for *XBP1* mRNA splicing in HeLa cells

We established an *in vitro* splicing assay to monitor *XBP1* mRNA ligation using an internally radiolabeled human *XBP1* transcript encompassing the 26-nucleotide intron. This transcript is cleaved with recombinant, constitutively active IRE1 to form RNA fragments mimicking *XBP1* mRNA exon halves (Fig 1A and B). Upon addition of HeLa whole-cell extracts, these fragments were converted into a single, longer species representing the spliced form of *XBP1* mRNA (Fig 1A and B). Ligation activity was proportional to the protein concentration of cell extract added (Supplementary Fig S1A) and confirmed by splicing assays using either 5′ end- or 3′ end-labeled *XBP1* mRNA fragments (Supplementary Fig S1B and C).

Having established this assay, we depleted proteins with a potential role in *XBP1* mRNA splicing by RNAi and monitored the ligation activity in the resulting cell extracts. Since UPR-induced mRNA splicing is mediated by the tRNA ligase Trl1 in yeast (Sidrauski *et al*, 1996), we focused on the components of the human tRNA ligase complex (Popow *et al*, 2011, 2014). Indeed, depletion of its catalytic subunit RTCB largely impaired *in vitro* ligation of *XBP1* mRNA exon halves (Fig 1C). The same effect was seen after depletion of

Figure 1. *In vitro* splicing of *XBP1* mRNA and subcellular localization of RTCB and archease.

A Schematic representation of the *in vitro* assay to monitor *XBP1* mRNA splicing. A radiolabelled human *XBP1* transcript encompassing the intron is pre-cleaved with recombinant, constitutively active IRE1 to form RNA fragments mimicking *XBP1* mRNA exon halves. Subsequent incubation with HeLa whole-cell extracts provides the ligation activity required to convert these fragments into a single, longer species representing the spliced form of *XBP1* mRNA.

B An internally labeled fragment of *XBP1* mRNA including the intron (lane 1) was incubated with HeLa whole-cell extracts (Wce, lanes 4–7) or pre-cleaved with recombinant IRE1 endonuclease and afterward supplemented with buffer (lanes 8–11) or Wce (lanes 12–15) for the indicated time periods. After addition of Wce, cleaved *XBP1* mRNA fragments were efficiently converted into the spliced form *XBP1* mRNA (compare to lane 2). A nucleotide (nt) size marker is shown in lane 3. An unspecific band is marked with an asterisk.

C HeLa cells were transfected with control siRNA (siGFP) or siRNAs against *RTCB*, archease or both and harvested 3 days post-transfection. Whole-cell extracts were incubated with a 3′ end-labeled *XBP1* mRNA pre-cleaved by recombinant IRE1 for 15 min.

D Subcellular localization of RTCB and archease assessed by Western blot analysis of fractions obtained after subcellular fractionation of HeLa cells treated with 300 nM thapsigargin (Tg) for the indicated time periods. HSP90 (cytoplasm), calnexin (membranes) and lamin A/C (nucleus) were used as marker proteins for the individual fractions collected (n = 5).

E Subcellular localization of RTCB and archease visualized by immunofluorescence staining of HeLa cells treated with 300 nM Tg for the indicated time periods. The nucleus is visualized by DAPI staining. Calnexin staining is used to mark the ER membrane (n = 4).

Published online: November 6, 2014

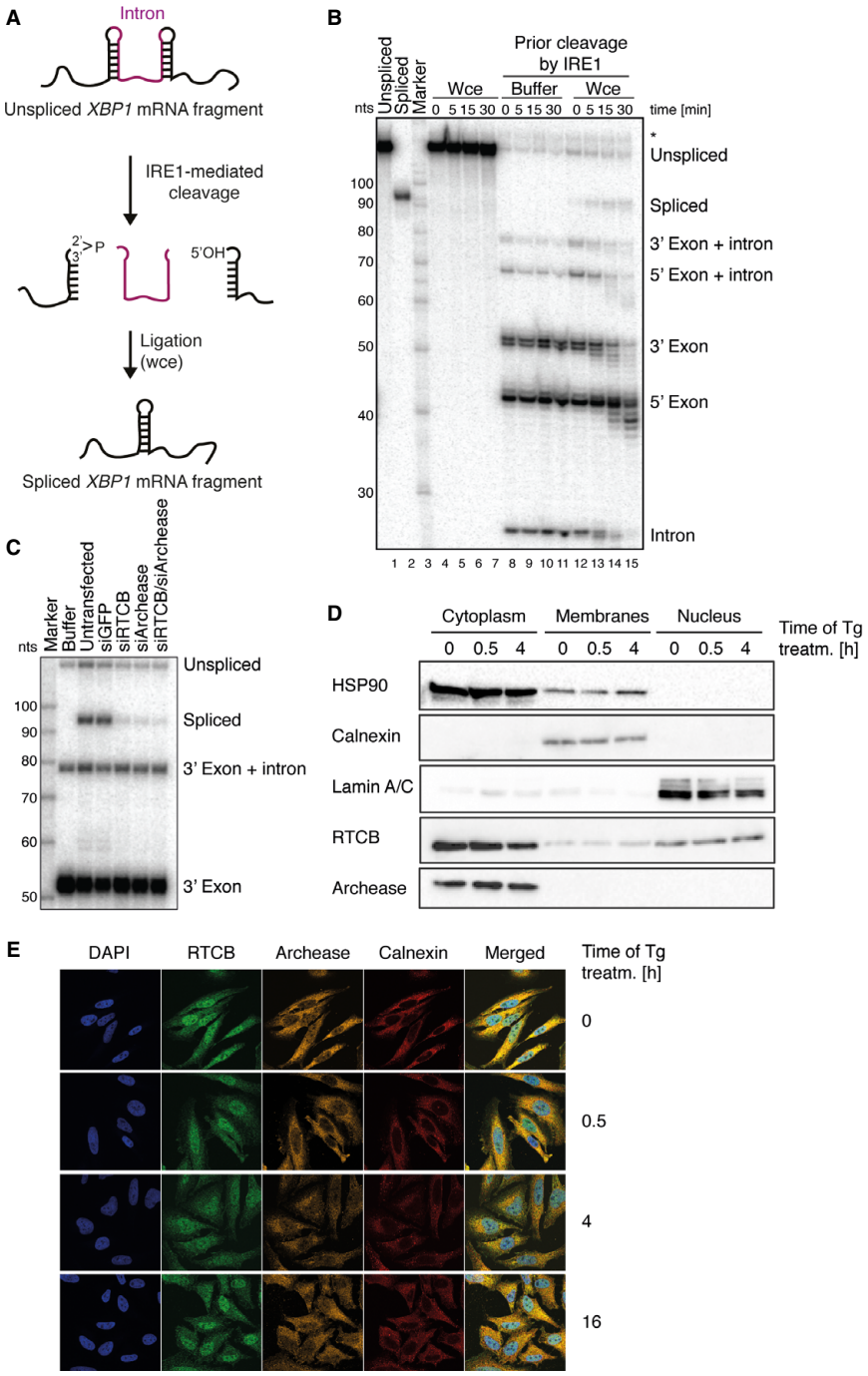

Figure 1.

Published online: November 6, 2014
The EMBO Journal RTCB regulates antibody secretion in plasma cells *Jennifer Jurkin et al*

archease or both proteins (Fig 1C), while addition of recombinant, wild-type archease but not of catalytically inactive archease mutants stimulated the RNA ligation activity in wild-type cell extracts (Popow *et al*, 2014) (Supplementary Fig S1D). Taken together, these results argue that both RTCB and archease are required for ligation of *XBP1* mRNA exon halves *in vitro*.

RTCB and archease localize to the cytoplasm of HeLa cells

Mammalian tRNA splicing is thought to be a predominantly nuclear process (De Robertis *et al*, 1981; Nishikura & De Robertis, 1981; Lund & Dahlberg, 1998), while unconventional splicing of *XBP1* mRNA takes place in the cytoplasm (Cox *et al*, 1993; Sidrauski *et al*, 1996; Sidrauski & Walter, 1997; Yanagitani *et al*, 2009). To address whether the subcellular localization of RTCB and archease is compatible with a role in both processes, we performed subcellular fractionation experiments (Fig 1D) and immunofluorescence staining (Fig 1E) in control cells and upon UPR induction by means of thapsigargin (Tg) treatment, an inhibitor of ER Ca^{2+}-ATPases. We detected RTCB both in the nucleus and in the cytoplasm, which is in agreement with a recent report identifying the tRNA ligase as part of RNA transport complexes shuttling between these two compartments (Perez-Gonzalez *et al*, 2014). In contrast, archease was strongly enriched in the cytoplasm (Fig 1D) and found in perinuclear regions stained by the ER membrane marker calnexin (Fig 1E). This subcellular distribution of both proteins was stable and did not change after Tg treatment (Fig 1D and E). Thus, while no active recruitment to the site of *XBP1* mRNA splicing occurs upon UPR induction, a substantial fraction of RTCB and archease constitutively localizes to the vicinity of the ER membrane and could therefore function in cytoplasmic *XBP1* mRNA ligation in living cells.

Simultaneous depletion of RTCB and archease abolishes *XBP1* mRNA splicing in cell culture

To test whether RTCB or archease facilitates ligation of endogenous *XBP1* mRNA in HeLa cells, we efficiently depleted both proteins by doxycycline (Dox)-inducible expression of small hairpin RNAs (shRNAs) using the miR-E backbone (Fellmann *et al*, 2013) (Fig 2A). As reported before (Popow *et al*, 2011), depletion of RTCB also led to a simultaneous depletion of DDX1 and FAM98B (Supplementary Fig S2A), two subunits of the tRNA ligase complex. Following UPR induction, reduced XBP1s expression was mainly detected in archease-depleted cells (Fig 2A). In contrast to RTCB, archease does not possess any RNA ligation activity and is not constitutively associated with the tRNA ligase complex (Popow *et al*, 2014). Consequently, affinity purifications of FLAG-archease showed no detectable RNA ligation activity in *XBP1* mRNA splicing assays unlike immunoprecipitations of FLAG-RTCB and FLAG-DDX1 (Supplementary Fig S1E). RTCB-depleted HeLa cells, however, supported XBP1s expression almost to wild-type levels (Fig 2A). As revealed by RT–PCR experiments using primers flanking the non-conventional splice sites, also the amount of *XBP1s* mRNA was reduced upon archease knockdown, resulting in a decreased ratio of spliced (*XBP1s*) to unspliced (*XBP1u*) mRNA in comparison with control samples (Fig 2B and Supplementary Fig S2B). While in apparent contrast to our *in vitro* splicing assays, these results are in agreement with earlier studies showing that RNAi-mediated depletion of RTCB alone does not impair *XBP1* mRNA splicing (Iwawaki & Tokuda, 2011). Therefore, archease appears to be crucial for
non-conventional splicing of *XBP1* mRNA as its stimulatory activity (Popow *et al*, 2014) sustains ligation activity in the presence of reduced amounts of RTCB.

Since depletion of neither RTCB nor archease sufficed to fully abrogate XBP1s induction, we simultaneously depleted both proteins in HeLa cells. After Tg treatment, XBP1s was no longer detectable at the protein level (Fig 2C) and greatly reduced at the mRNA level (Fig 2D and Supplementary Fig S2C). This result was supported by RT–qPCR experiments showing a clear reduction in *XBP1s* mRNA expression (Fig 2E). As the transcription factor XBP1s auto-regulates its own promoter (Yoshida *et al*, 2001; Lee *et al*, 2002), the levels of total *XBP1* mRNA (Fig 2F) and *XBP1u* mRNA (Fig 2G) likewise failed to accumulate, especially at later stages of UPR signaling. Thus, sufficient inhibition of tRNA ligase activity can only be achieved by simultaneous targeting of archease.

Accumulation of XBP1s leads to the transcriptional activation of downstream target genes such as the ERAD component *EDEM1* and the co-chaperone *DNAJB9* (Lee *et al*, 2003), which serve to decrease the load of unfolded proteins within the ER. We observed increased expression of *EDEM1* and *DNAJB9* mRNA in control cells after 8–16 h of Tg treatment (Fig 2H and I). This response was abolished in cells simultaneously depleted of both, RTCB and archease. In contrast, we detected a less strong reduction in the expression of the general stress responders HSPA5 (BiP), a member of the HSP70 family, and the pro-apoptotic transcription factor CHOP (Supplementary Fig S2D and E), both of which depend on the activation of other branches of UPR signaling and thus are less susceptible to changes in XBP1s levels (Yoshida *et al*, 2001; Lee *et al*, 2003; Chen *et al*, 2014). More importantly, the moderately affected expression

Figure 2. Simultaneous depletion of RTCB and archease abolishes XBP1s expression in cell culture.

A, B Tetracycline-inducible (Tet-ON) HeLa cells were incubated with 1 μg/ml doxycycline (Dox) for six consecutive days to stimulate expression of shRNAs targeting *RTCB*, archease or non-targeting control followed by treatment with 300 nM Tg for the indicated time periods. Induction of XBP1s (XBP1 spliced) expression was monitored by Western blot (A) and RT–PCR (B) analysis. The relative contribution of *XBP1s* mRNA to total levels of *XBP1* mRNA was analyzed by densitometry ($n = 3$).

C, D Tet-ON HeLa cells expressing shRNAs targeting *RTCB* and archease or a control cell line expressing two copies of the control shRNA were treated and analyzed as in (A, B) ($n = 5$).

E–I Tet-ON HeLa cells expressing shRNAs targeting *RTCB* and archease or a control cell line expressing two copies of the control shRNA were treated with Dox (1 μg/ml, 6 days) and Tg (300 nM, 24-h time course). Relative mRNA levels of *XBP1s* and *XBP1u* as well as total *XBP1* mRNA and induction of *EDEM1* and *DNAJB9* mRNA were analyzed by RT–qPCR ($n = 5$, mean expression levels and SEM are displayed). Expression levels were normalized to *ACTB* mRNA levels and to the untreated control sample. Two-way ANOVA was used to analyze the statistical significance of differences in mRNA levels between control and RTCB/archease-depleted cells (*$P < 0.05$, **$P < 0.01$, ***$P < 0.001$, ****$P < 0.0001$).

Published online: November 6, 2014

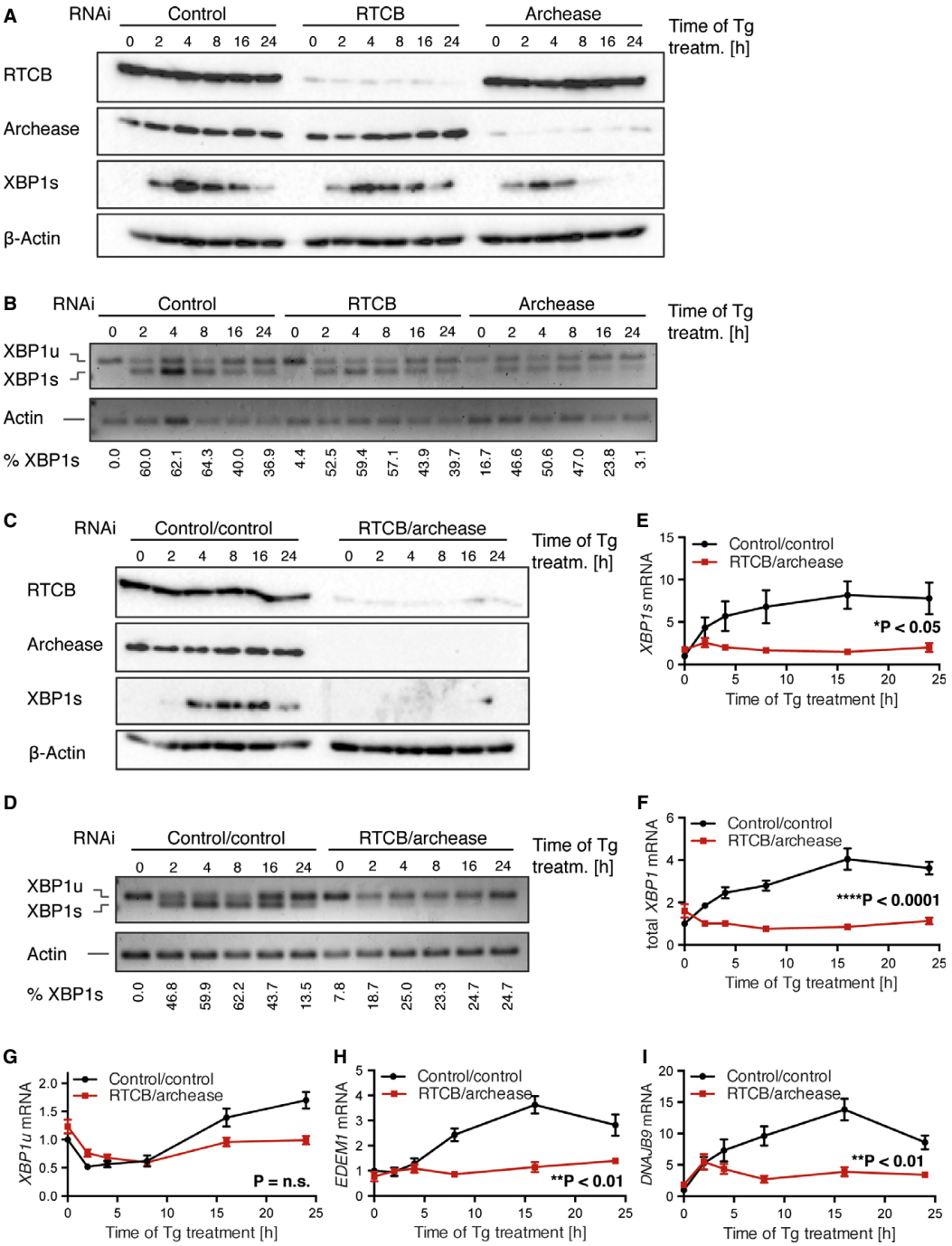

Figure 2.

Published online: November 6, 2014
The EMBO Journal

of CHOP upon depletion of RTCB and archease suggests that inhibition of tRNA ligase activity does not impair the induction of apoptosis under conditions of prolonged ER stress (Hetz, 2012). Likewise, the levels of *BLOS1* and *PDGFRB* mRNAs, known substrates of regulated IRE1-dependent decay (RIDD), an mRNA degradation pathway initiated by IRE1-mediated cleavage (Hollien & Weissman, 2006; Hollien *et al*, 2009), remained unchanged after RTCB and archease depletion and were equally reduced after induction of the UPR (Supplementary Fig S2F and G). This result confirms that depletion of RTCB and archease in the context of UPR activation does not interfere with the endonucleolytic activity of IRE1, but specifically disrupts *XBP1* mRNA splicing and thus the induction of XBP1s-specific downstream target genes.

RTCB and archease have been linked to tRNA splicing and thus to the maturation of intron-containing pre-tRNAs in eukaryotes and in archaebacteria (Popow *et al*, 2011, 2014; Desai *et al*, 2014). Although only a subset of all tRNAs are encoded by intron-containing pre-tRNA sequences, each organism possesses at least one tRNA isoacceptor family of which all or almost all members depend on splicing in order to become functional in translation. In humans, these include Ile-TAT, Arg-TCT, Tyr-ATA and Tyr-GTA. Using probes specifically recognizing only splicing-dependent tRNAs (Ile-tRNAs and Arg-tRNAs), we observed a decrease in the levels of mature transcripts as a consequence of RTCB and archease depletion (Supplementary Fig S3A and B). In contrast, levels of splicing-independent methionine tRNAs remained unchanged (Supplementary Fig S3A and B) as were global protein translation rates measured by metabolic labeling (^{35}S-methionine and ^{35}S-cysteine) (Supplementary Fig S3C and D). These results thus indicate that the reduced levels of splicing-dependent mature tRNAs do not lead to a global defect in protein synthesis in RTCB- and archease-depleted cells.

RTCB is required for the generation of XBP1s during plasma cell differentiation

Apart from being caused by stress agents that perturb ER functions, the UPR can also arise as a part of a developmental program that is initiated during the differentiation of secretory cells. This includes differentiation of activated B cells into antibody-secreting plasma cells. Given the newly identified function of RTCB in *XBP1* mRNA splicing in cell culture, we next studied the *in vivo* function of RTCB during plasma cell differentiation. To this end, we established a B-cell-specific mouse knockout model—*Rtcb*$^{fl/fl}$ *Cd23*-Cre—which initiates Cre-mediated deletion in immature B cells of the spleen and leads to efficient gene deletion in all mature B-cell types (Kwon *et al*, 2008). We determined the efficiency of *Rtcb* deletion in B220-enriched splenocytes by PCR genotyping, which demonstrated an almost complete deletion of *Rtcb* in *Rtcb*$^{fl/fl}$ *Cd23*-Cre B cells (Supplementary Fig S4A). As a result, the RTCB protein was almost absent in *Rtcb*$^{fl/fl}$ *Cd23*-Cre B cells, together with diminished levels of other tRNA ligase complex members, such as DDX1 and FAM98B, but not CGI-99 (Supplementary Fig S4B). Flow cytometric analysis showed that the different B-cell subsets were present in similar numbers in the spleen of *Rtcb*$^{fl/fl}$ *Cd23*-Cre, *Rtcb*$^{fl/+}$ *Cd23*-Cre and control mice (Supplementary Fig S4C and D).

We next investigated the role of RTCB in the splicing of *Xbp1* mRNA and the expression of XBP1s protein during plasma cell differentiation. For this purpose, we isolated splenic B cells from control (*Rtcb*$^{fl/fl}$ or *Rtcb*$^{fl/+}$), heterozygous (*Rtcb*$^{fl/+}$ *Cd23*-Cre) or homozygous (*Rtcb*$^{fl/fl}$ *Cd23*-Cre) mice and stimulated them with lipopolysaccharide (LPS) for 4 days, which induced differentiation via activated B cells and pre-plasmablasts to plasmablasts. By immunoblot analysis, we observed a transient increase in RTCB and DDX1 protein expression in wild-type cells at day 2 of LPS stimulation (compared to β-actin expression), whereas RTCB protein was absent in *Rtcb*$^{fl/fl}$ *Cd23*-Cre cells during the entire culture period (Fig 3A). Again, we noticed a concomitant depletion of other tRNA ligase complex members, such as DDX1, FAM98B or CGI-99 (Fig 3A). Furthermore, we analyzed the induction of XBP1 protein expression during LPS stimulation (d0–d4) (Fig 3B). In wild-type and heterozygous B cells, both the inactive XBP1u and the active XBP1s protein were readily induced by day 2, whereas RTCB-deficient cells up-regulated XBP1u only transiently and failed to produce XBP1s (Fig 3B). At day 4, cells present in the LPS cultures can be subdivided according to the surface expression of CD22 and CD138 into activated B cells (CD138$^-$ CD22$^+$), pre-plasmablasts (CD138$^-$ CD22^{low}) and plasmablasts (CD138$^+$ CD22$^-$), which secrete high amounts of antibodies (M. Minnich and M. Busslinger, unpublished observation). We evaluated XBP1s levels in sorted RTCB-deficient pre-plasmablasts and plasmablasts (Fig 3C). These cell populations showed significantly decreased levels of XBP1s. Interestingly, we observed incomplete depletion of RTCB in the differentiated *Rtcb*$^{fl/fl}$ *Cd23*-Cre plasmablasts (Fig 3C), indicating that the absence of RTCB in plasmablasts is not well tolerated, thus selecting for non-deleted cells. In addition to XBP1s protein, we also studied *Xbp1* mRNA levels and found that, similar to *Rtcb* mRNA, both *Xbp1s* and total *Xbp1* mRNAs were significantly reduced in unfractionated RTCB-deficient cells at day 4 of LPS stimulation (Fig 3D). We also observed decreased mRNA levels of the XBP1 target gene *Edem1* (Yoshida *et al*, 2003). It was previously reported that expression of the secreted (μS) but not the membrane bound form (μM) of the Igμ heavy chain depends on XBP1s (Taubenheim *et al*, 2012; Benhamron *et al*, 2013). We therefore investigated the presence of these transcripts and found that IgμS transcripts were strongly decreased, whereas IgμM mRNA levels were only minimally affected (Fig 3D).

RTCB is required for immunoglobulin secretion by plasmablasts *in vitro*

After *in vitro* stimulation with LPS, *Rtcb*$^{fl/fl}$ *Cd23*-Cre B cells were able to develop into CD138$^+$ CD22$^-$ plasmablasts and CD138$^-$ CD22^{low} pre-plasmablasts, although the percentages of CD138$^+$ CD22$^-$ plasmablasts were slightly reduced as compared to wild-type or heterozygous controls (Supplementary Fig S5A). This reduction was likely caused by a defect in proliferation rather than differentiation (Supplementary Fig S5B). As measured by ELISA, IgM levels were significantly reduced in culture supernatants of RTCB-deficient pre-plasmablasts and plasmablasts (Fig 4A). ELISPOT analysis of sorted plasmablasts revealed similar numbers of IgM-secreting cells for both the control and experimental genotypes (Fig 4B). However, in this assay, *Rtcb*$^{fl/fl}$ *Cd23*-Cre plasmablasts gave rise to significantly smaller sports than control plasmablasts, indicating that these cells secrete lower levels of immunoglobulins in the absence of RTCB (Fig 4B). In summary, these data indicate that the loss of RTCB strongly interferes with the capacity of plasmablasts to secrete

Published online: November 6, 2014

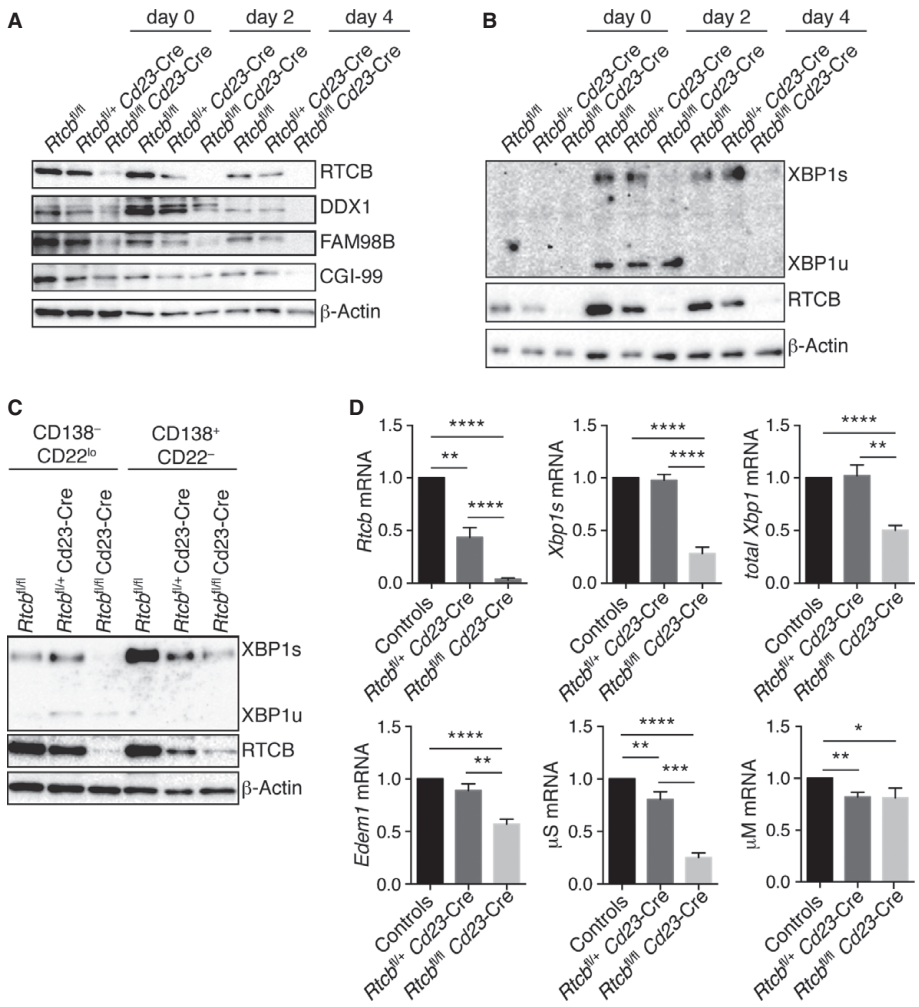

Figure 3. RTCB is required for induction of XBP1s during plasma cell differentiation.

B220$^+$ splenocytes of control (*Rtcb*$^{fl/fl}$ or *Rtcb*$^{fl/+}$), *Rtcb*$^{fl/+}$ *Cd23*-Cre or *Rtcb*$^{fl/fl}$ *Cd23*-Cre mice were stimulated with 20 μg/ml LPS for 4 days.

A, B Protein levels of RTCB, tRNA ligase complex members (DDX1, FAM98B, CGI-99) and XBP1 were monitored by Western blot analysis ($n > 3$).

C FACS-sorted CD138$^+$ CD22$^-$ plasmablasts or CD138$^-$ CD22^{low} pre-plasmablasts were probed for expression of the indicated proteins by Western blot analysis ($n = 2$).

D Relative mRNA levels of *Rtcb*, *Xbp1s*, total *Xbp1*, *Edem1*, μM and μS were analyzed by RT–qPCR in fractionated LPS-stimulated cells at day 4 ($n = 4$, mean expression levels and SEM are displayed). Expression levels were normalized to *Actb* mRNA levels and to B cells from control mice. An unpaired Student's *t*-test was used to analyze the statistical significance of differences in mRNA levels (*$P < 0.05$, **$P < 0.01$, ***$P < 0.001$, ****$P < 0.0001$).

antibodies, although the ability of RTCB-deficient B cells to differentiate into plasmablasts remains largely intact.

Activation of XBP1 during differentiation of plasma cells was shown to increase the capacity of the ER, preparing these cells to cope with the enormous amount of immunoglobulin production and secretion (Taubenheim *et al*, 2012). We analyzed the ER morphology of RTCB-deficient plasmablasts by electron microscopy and found disorganized and less dense ER structures as compared to wild-type plasmablasts, which displayed an extensively layered and organized ER, characteristic of antibody-secreting plasma cells (Fig 4C). To exclude that the reduced antibody-secreting capacity of RTCB-deficient plasmablasts is caused by defects in global protein synthesis, we analyzed mature tRNA levels and protein synthesis rates of *Rtcb*$^{fl/fl}$ *Cd23*-Cre cells after 4 days of LPS stimulation. In

Published online: November 6, 2014
The EMBO Journal

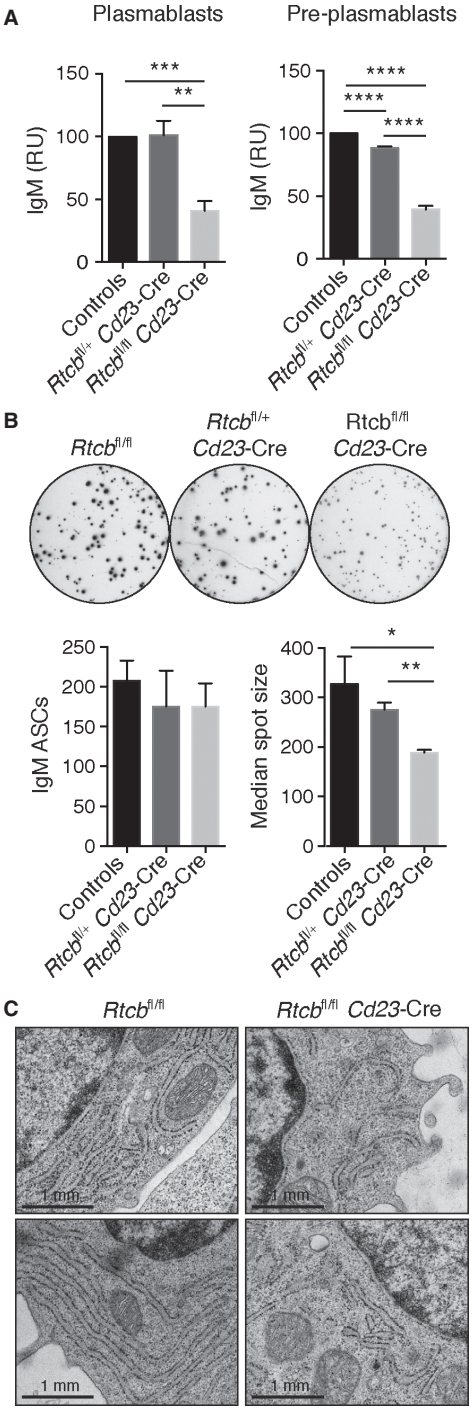

Figure 4. RTCB is required for immunoglobulin secretion by antibody-secreting cells *in vitro*.

B220$^+$ cells were enriched from the spleen of control (*Rtcb*$^{fl/fl}$ or *Rtcb*$^{fl/+}$), *Rtcb*$^{fl/+}$ *Cd23*-Cre or *Rtcb*$^{fl/fl}$ *Cd23*-Cre mice and cultured in the presence of 20 μg/ml LPS for 3 days.

A IgM ELISA. Identical numbers of FACS-sorted CD138$^+$ CD22$^-$ plasmablasts or CD138$^-$ CD22^{low} pre-plasmablasts of the indicated genotypes were plated for 24 h prior to ELISA analysis of their supernatants. The data are presented as relative units (RU) compared to control cells (n = 4, mean and SEM are displayed). An unpaired Student's t-test was used to analyze the statistical significance (**P < 0.01, ***P < 0.001, ****P < 0.0001).

B IgM ELISPOT analysis. FACS-sorted CD138$^+$ CD22$^-$ plasmablasts (500 cells) were plated for 16–18 h. A representative assay is shown in the top panel. Bar diagrams in the low panel show the average number of IgM-secreting cells and their median spot size (measured in pixels), respectively (n = 4 mean and SEM are displayed). An unpaired Student's t-test was used to analyze the statistical significance (*P < 0.05, **P < 0.01).

C Plasmablasts were analyzed by electron microscopy. Representative plasmablasts of the indicated genotypes are shown.

mouse, all genes encoding for the isoacceptor families Tyr-GTA and Leu-CAA contain introns and thus have to be spliced in order to give rise to mature tRNAs. Analyzing these two splicing-dependent tRNA families, we found that mature Tyr- and Leu-tRNAs, but not splicing-independent Met-tRNAs, were reduced but still present in RTCB-depleted plasmablasts (Supplementary Fig S6A). However, despite a decreased level of mature tRNAs, *Rtcb*$^{fl/fl}$ *Cd23*-Cre cells did not display global changes in protein synthesis rates as shown by unchanged levels of ^{35}S-methionine and ^{35}S-cysteine incorporation after metabolic labeling (Supplementary Fig S6B). In LPS-stimulated *Rtcb*$^{fl/fl}$ *Cd23*-Cre cells, we could, however, reproducibly observe a decreased intensity of a single band of ~75 kDa that corresponds to the expected size of the secreted Igμ heavy chain.

RTCB-deficient B cells differentiate into plasma cells with an impaired capacity to secrete immunoglobulins *in vivo*

We finally characterized the role of RTCB in the generation and function of antibody-secreting cells *in vivo*. To this end, we examined plasma cell differentiation during a T-cell-independent immune response by immunizing mice with trinitrophenyl (TNP)-coupled LPS. At day 14 after immunization, we observed equal numbers of plasma cells (CD28$^+$ CD138$^+$ Lin$^-$) in the spleen of immunized control *Rtcb*$^{fl/fl}$ and *Rtcb*$^{fl/fl}$ *Cd23*-Cre mice (Fig 5A). However, the number of TNP-specific antibody-secreting cells was reduced in *Rtcb*$^{fl/fl}$ *Cd23*-Cre mice when assessed by ELISPOT assay (Fig 5B). The size of the spots was also reproducibly smaller, indicating low immunoglobulin production by RTCB-deficient antibody-secreting cells (Fig 5B). Likewise, TNP-specific serum immunoglobulin levels measured by ELISA were significantly reduced in *Rtcb*$^{fl/fl}$ *Cd23*-Cre mice (Fig 5C). Together, these data strengthen our *in vitro* results and confirm that the ability of RTCB-deficient B cells to generate plasma cells remains largely intact while their capacity to secrete immunoglobulins is strongly affected.

Discussion

In this study, we have shown that RTCB, the catalytic subunit of the mammalian tRNA ligase complex, mediates ligation of *XBP1* mRNA

Published online: November 6, 2014

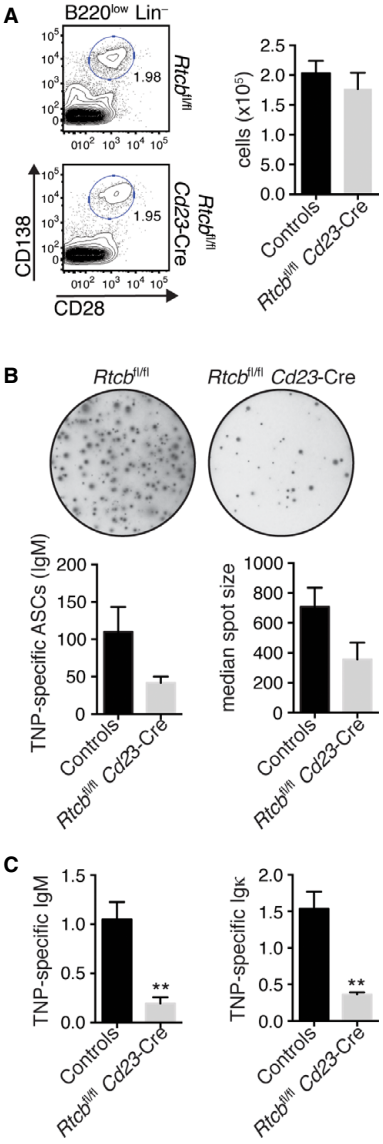

Figure 5. RTCB-deficient B cells show an impaired capacity to secrete immunoglobulins *in vivo*.
Control (*Rtcb*$^{fl/fl}$ or *Rtcb*$^{fl/+}$) and *Rtcb*$^{fl/fl}$ *Cd23*-Cre mice were injected intraperitoneally with 50 μg of TNP-(0.5)-LPS and analyzed 2 weeks after immunization.

A Plasma cell numbers in the spleen were determined by flow cytometry. Representative contour plots are shown. Bar diagrams represent total plasma cell numbers (n = 4, mean and SEM are displayed). Plasma cells were defined as CD28$^+$ CD138$^+$ B220^{low} Lin$^-$ (CD4$^-$ CD8$^-$ CD21$^-$ F4/80$^-$).

B IgM ELISPOT analysis of MACS-enriched CD138$^+$ cells after plating identical numbers for 16–18 h. A representative assay is shown in the upper panel. Bar diagrams show the average number of IgM-secreting cells and their median spot size (measured in pixels), respectively (n = 3 mean and SEM are displayed).

C The serum titers of TNP-specific IgM and Igκ were determined by ELISA (n = 4 mean and SEM are displayed). An unpaired Student's t-test was used to analyze the statistical significance of differences (**$P < 0.01$).

exon halves during the UPR. We extended this finding and revealed the role of RTCB in the differentiation of B cells into plasma cells *in vivo*, a process that is characterized by *XBP1* mRNA splicing and physiological induction of the UPR.

Moreover, we described the critical function of archease, a co-factor of the tRNA ligase complex (Popow *et al*, 2014), in *XBP1* mRNA splicing. Recent work by Lu *et al* has reported similar findings. While full depletion of RTCB alone was enough to block XBP1s expression in genetically engineered plasma cells (this study) as well as in genetically engineered mouse ES cells (Lu *et al*, 2014), only a minor effect was seen after shRNA-mediated RTCB depletion in HeLa cells. This result is in line with a previous report showing no decrease in *XBP1* mRNA splicing efficiency upon knockdown of RTCB by means of siRNAs (Iwawaki & Tokuda, 2011). We therefore propose that a few ligase complexes—probably associated with the ER membrane—may suffice to splice *XBP1* mRNA upon induction of ER stress as long as archease is present to stimulate enzymatic rates (Popow *et al*, 2014). Hence, full impairment of XBP1s induction can only be achieved by RNAi-mediated depletion of both, RTCB and its co-factor archease, as indicated by our data.

The important function of archease during the UPR is further supported by its subcellular distribution. Even though tRNA splicing is thought to be a predominantly nuclear process (De Robertis *et al*, 1981; Nishikura & De Robertis, 1981; Lund & Dahlberg, 1998), we found archease and the majority of RTCB localizing to cytoplasmic compartments. This subcellular distribution of RTCB coincides with a recent report describing the tRNA ligase as part of an RNA transport complex shuttling between nucleus and cytoplasm (Perez-Gonzalez *et al*, 2014). This flexible localization of RTCB and the cytoplasmic distribution of archease suggest that shuttling of the tRNA ligase not only supports RNA transport but also enables guanylation of RTCB by archease. Furthermore, localization of RTCB in the cytoplasm allows interaction with IRE1α at the ER membrane (Lu *et al*, 2014). Given its importance for full enzymatic activity of the tRNA ligase complex, we speculate that also archease might—directly or indirectly—associate with IRE1 and therefore localize to foci of increased *XBP1* mRNA splicing.

We chose the antibody-secreting capacity of plasma cells, normally characterized by chronic activation of the UPR and high levels of XBP1s expression, as a physiological example to confirm the role of RTCB in *XBP1* mRNA splicing *in vivo*. To this end, we generated a conditional RTCB knockout mouse model, *Rtcb*$^{fl/fl}$ *Cd23*-Cre, in which RTCB is specifically deleted in mature B cells. Neither overall B-cell numbers nor plasma cell differentiation were affected in these mice *in vivo*. However, we detected slightly decreased percentages of plasmablasts after *ex vivo* LPS stimulation of RTCB-depleted B cells. According to previous reports, proliferation and plasma cell differentiation are tightly linked, in that the probability of activated B cells to develop into plasma cells increases with the number of cell divisions (Hasbold *et al*, 2004). Using cell trace experiments, we observed that most wild-type cells that

Published online: November 6, 2014
The EMBO Journal RTCB regulates antibody secretion in plasma cells *Jennifer Jurkin et al*

became plasmablasts had undergone multiple rounds of cell divisions, while *Rtcb*$^{fl/fl}$ *Cd23*-Cre plasmablasts had completed a significantly lower number of division cycles, Thus, indirect effects caused by the decreased proliferation rates observed in RTCB-deficient cells, rather than specific defects in plasma cell lineage choices, might contribute to the decrease in plasmablasts detected in RTCB-depleted B-cell cultures *in vitro*. As deficiency in XBP1 itself does not affect B-cell proliferation (Todd *et al*, 2009; Taubenheim *et al*, 2012), the reduced proliferation rates seen in *Rtcb*$^{fl/fl}$ *Cd23*-Cre B cells are most probably due to functions of RTCB that are unrelated to *Xbp1* mRNA splicing. In line with this, a recent report described reduced proliferation rates in RTCB-depleted unstressed ES cells, a condition in which XBP1s is not expressed (Lu *et al*, 2014).

Besides dramatic changes in ER morphology, RTCB-depleted plasma cells showed reduced rates of antibody secretion both *in vitro* and *in vivo* and thus resembled the phenotype previously observed in a B-cell-specific *Xbp1* knockout mouse (Hu *et al*, 2009; Todd *et al*, 2009; Taubenheim *et al*, 2012). Although our data strongly suggest that the defect in antibody secretion seen in RTCB-deficient plasma cells is a result of their inability to generate XBP1s, we cannot exclude that additional defects contribute to this phenotype. Due to its implication in tRNA splicing, deficiencies in global protein synthesis might be expected, leading to decreased production and secretion of proteins, including IgM. However, in contrast to a recent report (Lu *et al*, 2014), we did not observe any defect in global protein synthesis in *ex vivo* stimulated RTCB-deficient plasmablasts. This discrepancy might arise from the different cell systems used, that is, pluripotent ES cells versus differentiated B cells. Since tRNAs have been reported to be extremely stable with half-lives of weeks, it is tempting to speculate that fully differentiated or non-proliferating cells are able to maintain mature tRNA levels constant over longer periods of time and that cell division numbers rather than time after RTCB depletion might crucially influence abundance of mature tRNAs and consequently protein synthesis rates.

Collectively, our data show that RTCB together with its cofactor archease mediates *XBP1* mRNA splicing during the UPR. Upon RTCB depletion, plasma cells fail to induce expression of XBP1s during differentiation. They are also unable to expand ER structures and show reduced rates of antibody secretion both *in vitro* and *in vivo*. These findings constitute the first report of an *in vivo* function of the mammalian tRNA ligase complex. Furthermore, the identification of the long-sought *XBP1* mRNA splicing ligase opens new avenues in the treatment of a growing number of diseases associated with elevated levels of XBP1s expression such as multiple myeloma (Nakamura *et al*, 2006; Carrasco *et al*, 2007; Chapman *et al*, 2011), triple-negative breast cancer (Chen *et al*, 2014), pre-B-cell acute lymphoblastic leukemia (ALL) (Kharabi Masouleh *et al*, 2014) and B-cell chronic lymphocytic leukemia (CLL) (Tang *et al*, 2014).

Materials and Methods

Cell culture and siRNA transfection

HeLa cells were cultured at 37°C, with 5% CO_2 in 1× Dulbecco's modified Eagle's medium (Invitrogen) supplemented with 10% fetal bovine serum (Sigma), 3 mM glutamine (Sigma), 100 U/ml penicillin and 100 μg/ml streptomycin sulfate (Sigma). For lenti- or retroviral packaging, LentiX (Clontech) or PlatE cells (CellBiolabs) were cultured as described above. siRNA transfections were performed using Lipofectamine 2000 reagent (Invitrogen) according to the manufacturer's instructions. For *in vitro* studies, archease and RTCB were depleted using ON-TARGETplus siRNAs (Dharmacon).

Preparation of whole-cell extracts

HeLa cells were grown to confluency and harvested in 1× lysis buffer (30 mM HEPES pH 7.4, 100 mM KCl, 5 mM $MgCl_2$, 10% (v/v) glycerol, 0.2% (v/v) Nonidet P-40, 0.5 mM DTT, 0.1 mM phenylmethylsulfonyl fluoride (PMSF)) supplemented with Phosphatase Inhibitor Cocktail Set II (Merck). Extracts were diluted to 3 μg/μl total protein concentration unless otherwise indicated.

Preparation of *XBP1* mRNA fragment

Human *XBP1* pre-mRNA fragment was transcribed using AmpliScribe T7-Flash (Epicentre) according to the manufacturer's protocol. Templates for the spliced and unspliced form of human *XBP1* mRNA were obtained by PCR on genomic DNA and cDNA, respectively, using the following primers: T7-hXBP118FW, 5′-TAA TAC GAC TCA CTA TAG GGG AAT GAA GTG AGG CCA GT-3′ and hXBP118RV, 5′-AAT CCA TGG GGA GAT GTT CTG GAG-3′. Sequence was confirmed by sequencing. The recovered transcripts were dissolved in 1× RNAi buffer (30 mM HEPES pH 7.4, 100 mM KCl, 5 μM $MgCl_2$, 0.5 μM DTT, 10 (v/v) % glycerol) and annealed to end-matching LNA oligos (1 μM) (to minimize exonucleolytic cleavage upon incubation with cell extracts) by 30 s incubation at 95°C followed by cooling to room temperature. The LNA-modified oligos hXBP-5 (5′-CAT TCC C-3′) and hXBP-3 (5′-AAT CCA G-3′) were obtained from Exiqon. Internally labeled *XBP1* mRNA transcript was synthesized in the presence of ^{32}P-αGTP (Perkin Elmer). For 5′ end labeling, RNA was dephosphorylated using calf intestinal phosphatase (NEB), treated with proteinase K and subsequently labeled using T4 polynucleotide kinase (NEB) and ^{32}P-γATP (Perkin Elmer). All reactions were performed as described by the manufacturer. RNA 3′ end labeling was achieved by direct ligation to ^{32}P-pCp (Perkin Elmer) using RNA ligase I (NEB), according to manufacturer's protocol. All labeled transcripts were purified by preparative PAGE and dissolved in 1× RNAi buffer.

In vitro RNA splicing assay

LNA-stabilized *XBP1* pre-mRNA fragment (0.1 μM) was pre-incubated with recombinant IRE1 (Volkmann *et al*, 2011) for 5 min in 1× tRNA ligation buffer (400 mM KCl, 125 mM spermidine, 20 mM ATP, 20 mM GTP, 10 mM DTT, 25 mM $MgCl_2$) prior to addition of HeLa whole-cell extracts (2 μg/μl) or FLAG-IP eluate. Following incubation, samples were treated with proteinase K extraction buffer (200 mM Tris–HCl pH 7.5, 25 mM EDTA pH 8.0, 300 mM NaCl, 2% SDS, 0.3 μg/μl proteinase K) at 65°C for 20 min; RNA was phenol–chloroform extracted, precipitated and loaded on 10% PAGE. Gels were exposed using phosphorimaging, and the obtained signal was quantified using the evaluation software ImageQuant (GE Life Sciences) and corrected by subtraction of appropriate background values. When relevant, recombinant archease (to a final

Published online: November 6, 2014
Jennifer Jurkin et al RTCB regulates antibody secretion in plasma cells **The EMBO Journal**

concentration of 0.2 μg/μl) or a corresponding volume of buffer (10 mM Tris–HCl pH 8.0, 100 mM NaCl, 1 mM dithiothreitol (DTT), 10% (v/v) glycerol) was added to the reaction. Decade marker (Ambion) was used for size determination for analytical PAGE.

Protein and enzyme preparation for *in vitro* ligation assay

Recombinant IRE1 enzyme was obtained as described before (Volkmann *et al*, 2011). Cloning and preparation of recombinant hexahistidine-tagged human archease as well as generation of stably transfected HEK293 cell lines and affinity purification of FLAG-archease, FLAG-DDX1 and FLAG-RTCB was performed as described (Popow *et al*, 2014).

Immunofluorescence

Wild-type HeLa cells were seeded on coverslips and treated with 300 nM thapsigargin (Tg) for 30 min, 4 or 16 h, respectively. Cells were fixed with 2% (w/v) paraformaldehyde at room temperature for 20 min, permeabilized by incubation in 0.2% (v/v) Triton X-100/PBS for 5 min and incubated in blocking solution (5% (w/v) BSA, 0.1% (v/v) Tween-20 in PBS, sterile-filtered) for 30 min at room temperature. Primary antibodies were dissolved in blocking solution and added to the coverslips for 1 h. The following antibodies and dilutions were used: RTCB (Santa Cruz, 1:500), archease (monoclonal, 1:2) and calnexin (Santa Cruz, 1:100). The archease monoclonal antibody was generated by immunizing mice with wild-type histidine-tagged archease purified as described previously (Popow *et al*, 2014). Cells were washed three times in 0.1% PBST and incubated with fluorescent secondary antibodies diluted in blocking solution for 1 h: Alexa Fluor 488 donkey anti-rabbit IgG (Invitrogen, 1:500), Alexa Fluor 568 donkey anti-mouse IgG (Invitrogen, 1:500), and Alexa Fluor 647 donkey anti-goat IgG (Invitrogen, 1:500). Coverslips were again washed four times with 0.1% PBST and subsequently mounted in ProLong Gold Antifade Mountant with DAPI (Invitrogen). Images were taken at least 24 h after mounting using a laser-scanning confocal microscope (LSM780, Zeiss).

Electron microscopy

$B220^+$ B cells were stimulated for 3 days with LPS and then centrifuged for 3 min at 1,200 *g*. After centrifugation, the supernatant was carefully aspirated and cells were fixed using 2.5% glutaraldehyde in 1× PBS pH 7.4 for 1 h at room temperature. Cells were then rinsed with the same buffer, pelleted and resuspended in 3% low melting point agarose. Samples were post-fixed in 2% osmium tetroxide in ddH_2O, washed, dehydrated in a graded series of ethanol solutions and embedded in Agar 100 resin. Ultrathin sections were cut at a nominal thickness of 70 nm, post-stained with 2% aqueous uranyl acetate followed by Reynold's lead citrate. Sections were examined with an FEI Morgagni 268D (FEI, Eindhoven, The Netherlands) operated at 80 kV. Images were acquired using an 11 megapixel Morada CCD camera (Olympus-SIS).

Subcellular fractionation

Wild-type HeLa cells were seeded at equal cell densities and treated with 300 nM Tg for 30 min or 4 h. Subcellular fractionation analysis was performed using the Subcellular Protein Fractionation kit for Cultured Cells (Thermo Scientific) according to manufacturer's instructions. Equal percentages of the fractions obtained were subsequently used for Western blot analysis as described below.

Western blotting

Tet-ON HeLa shRNA cell lines were treated with Dox for six consecutive days and stressed with 300 nM Tg over a 24-h time course. Cells were harvested after 0, 2, 4, 8, 16 and 24 h and lysed in high salt buffer (20 mM Tris pH 7.5, 400 mM NaCl, 0.5% (v/v) NP-40, 0.3% (v/v) Triton X-100) supplemented with 0.1 mM PMSF (Sigma) and protease inhibitor cocktail (Roche). Protein concentration was determined using Bradford assay (Bio-Rad), and 30 μg of each sample were separated by SDS–PAGE. For B cells, cells were counted, directly lysed in 1× SDS loading buffer at 95°C for 5 min and loaded at $1–2 \times 10^6$ cells per lane. Proteins were transferred to Immobilon-P membranes (Millipore) and probed with the following antibodies using standard protocols: lamin A/C (Sigma, 4C11 1:1,000), HSP90 (Abcam, 3A3 1:2,000), calnexin (Santa Cruz, C-20 1:1,000), RTCB (described previously (Popow *et al*, 2011), 1:5,000), monoclonal antibody against archease was generated by immunization of mice, fusion of splenocytes and generation of hybridoma (Monoclonal Antibody Facility, Max F. Perutz Laboratories, Vienna 1:500), β-actin (Sigma, A2006 1:5,000), XBP1s (BioLegend, 1:500), DDX1 (Bethyl, A300-521A 1:1,000), FAM98B (Sigma, HPA008320 1:500) and CGI-99 (Sigma, HPA039824 1:1,000).

Cloning of shRNAs

For RNAi-mediated depletion of RTCB and/or archease, shRNAs were designed as described earlier (Dow *et al*, 2012). The respective 97-mer oligonucleotides (IDT, see sequences below; guide sequences are marked in bold) were cloned into the optimized miR-E backbone of RT3GEN (Fellmann *et al*, 2013) or into a derived construct expressing a blasticidin resistance cassette instead of Neo (RT3GEB). For cloning, the following primers were used (Fellmann *et al*, 2013): miR-E_fwd: 5′-TAC AAT ACT CGA GAA GGT ATA TTG CTG TTG ACA GTG AGC G-3′ and miR-E_rev: 5′-TTA GAT GAA TTC TAG CCC CTT GAA GTC CGA GGC AGT AGG CA-3′. A detailed description of the cloning procedure and the control shRNA used has been published elsewhere (Zuber *et al*, 2011).

Control shRNA 97mer: TGCTGTTGACAGTGAGCGCAGGAATTATAATGCTTATCTATAGTGAAGCCACAGATGTATAGATAAGCATTATAATTCCTATGCCTACTGCCTCGGA

RTCB shRNA 97mer: TGCTGTTGACAGTGAGCGACAGGTTGAAGGTGTTTTCTATTAGTGAAGCCACAGATGTA**ATAGAAAACACCTTCAACCTGC**TGCCTACTGCCTCGGA

Archease shRNA 97mer: TGCTGTTGACAGTGAGCGAAAGATGTTAGAGATTACAATTTAGTGAAGCCACAGATGTA**AATTGTAATCTCTAACATCTTC**TGCCTACTGCCTCGGA

Generation of Tet-ON HeLa cell lines and Tet-RNAi studies

To generate ecotropically infectable Tet-ON HeLa cells, we constructed a lentivirus coexpressing the ecotropic receptor (EcoR), rtTA3 and Puro by shuttling the according expression cassette from pRIEP (Zuber *et al*, 2011) into the pWPXLd backbone (Addgene

Published online: November 6, 2014
The EMBO Journal RTCB regulates antibody secretion in plasma cells *Jennifer Jurkin et al*

plasmid 12258). HeLa cells transduced with pWPXLd-EF1-EcoR-IRES-rtTA3-PGK-Puro (pWPXLd-RIEP) were selected with 2 μg/ml puromycin (VWR) and subsequently transduced with ecotropically packaged RT3GEN Tet-shRNA expression vectors as described earlier (Zuber *et al*, 2011). For single knockdown conditions, cells were transduced with a single shRNA expression vector and selected with 1 mg/ml G418 (Gibco). Double knockdown cells were obtained by sequentially infecting two shRNA expression vectors and subsequent selection using 1 mg/ml G418 and 10 μg/ml blasticidin (VWR). Tet-regulated shRNA expression was induced by treatment of these cells with 1 μg/ml doxycycline (Dox, Sigma) added to the medium. Cell culture medium supplemented with selection antibiotics and Dox was replaced every second day.

Quantitative reverse-transcriptase PCR

RNA from Tet-ON HeLa shRNA cell lines treated with Dox for six consecutive days and stressed with 300 nM Tg over a 24-h time course (harvesting after 0, 2, 4, 8, 16 and 24 h) was isolated using TRIzol reagent (Invitrogen). Total RNA was DNase-treated and reverse-transcribed using the Maxima First Strand cDNA synthesis kit for RT–qPCR with dsDNase (Thermo Scientific) according to the manufacturer's instructions. cDNA was diluted 1:10 before analysis by quantitative PCR using GoTaq qPCR Master Mix (Promega). The PCR was performed in a 20-μl reaction volume and pipetted using a Bravo LT96 Liquid Handling system (Agilent). The following exon–exon spanning primers were designed using Primer3 software (version 0.4.0): human *ACTB*: 5′-TTG CCG ACA GGA TGC AGA AGG A-3′ (fwd) and 5′-AGG TGG ACA GCG AGG CCA GGA T-3′ (rev); human *XBP1s*: 5′-GAG TCC GCA GCA GGT G-3′ [fwd, primer spanning the non-conventional exon–exon junction, reported previously (Majumder *et al*, 2012)] and 5′-GGA AGG GCA TTT GAA GAA CA-3′ (rev); human total *XBP1*: 5′-GCG CTG AGG AGG AAA CTG AAA AAC-3′ (fwd) and 5′-CCA AGC GCT GTC TTA ACT CC-3′ (rev); human *XBP1u*: 5′-ACT ACG TGC ACC TCT GCA G-3′ (fwd) and 5′-GGA AGG GCA TTT GAA GAA CA-3′ (rev); human *EDEM1*: 5′-GAT TCC ATA TCC TCG GGT GA-3′ (fwd) and 5′-ATC CCA AAT TCC ACC AGG AG-3′ (rev); human *DNAJB9*: 5′-TGC TGA AGC AAA ATT CAG AGA-3′ (fwd) and 5′-CCA CTA GTA AAA GCA CTG TGT CCA-3′ (rev); human *HSPA5*: 5′-GTG GAA TGA CCC GTC TGT G-3′ (fwd) and 5′-GTG GAA TGA CCC GTC TGT G-3′ (rev); human *CHOP*: 5′-CAT TGC CTT TCT CCT TCG GG-3′ (fwd) and 5′-CCA GAG AAG CAG GGT CAA GA-3′ (rev); human *BLOS1*: 5′-GAG GCG AGA GGC TAT CAC TG-3′ (fwd) and 5′-GCC TGG TTG AAG TTC TCC AC-3′ (rev); human *PDGFRB*: 5′-GCT CAC ACT GAC CAA CCT CA-3′ (fwd) and 5′-TCT TCT CGT GCA GTG TCA CC-3′ (rev); mouse *Rtcb:* 5′-GTT TGC CAT AGG GAA CAT GG-3′ (fwd) and 5′-GGT TCT TAG CAA GCG GAC AC-3′ (rev); primers for mouse *Xbp1s* (Rodriguez *et al*, 2012), mouse total *Xbp1* (Iwakoshi *et al*, 2003a), mouse *Edem1* (Lisbona *et al*, 2009), mouse μS (Taubenheim *et al*, 2012), mouse μM (Taubenheim *et al*, 2012) and mouse *Actb* (Lisbona *et al*, 2009) have been described previously. The reaction was performed using the following parameters: 50°C for 10 min, 95°C for 5 min, followed by 60 cycles in total at 95°C for 10 s and 60°C for 30 s. The quality of PCR primers was evaluated by melting curve analysis, DNA gel electrophoresis of the PCR products and determination of amplification efficiency. The obtained data were analyzed according to the $\Delta\Delta C_t$ method normalizing to human *ACTB* or mouse *Actb* mRNA levels. Additionally, expression levels were normalized to the untreated control sample.

RT–PCR

Human *XBP1s* and *XBP1u* mRNA levels were monitored by semi-quantitative real-time PCR using cDNA synthesized from dsDNase-treated RNA as described above, RedTaq ReadyMix™ PCR Reaction Mix (Sigma) and the following primers: 5′- TAA TAC GAC TCA CTA TAG GGG AAT GAA GTG AGG CCA GT-3′ and 5′-AAT CCA TGG GGA GAT GTT CTG GAG-3′. For *ACTB* mRNA levels, the following primers were used: 5′-TTG CCG ACA GGA TGC AGA AGG A-3′ (fwd) and 5′-AGG TGG ACA GCG AGG CCA GGA T-3′ (rev). PCR products were resolved by agarose gel electrophoresis. Densitometric analysis was performed using Fiji software (version 1.47i) and corrected by subtraction of the appropriate background values.

Northern blotting

Northern blot analysis was done as previously described (Karaca *et al*, 2014). Hybridization with 100 pmol of the following [5′-^{32}P]-labeled DNA probes was performed at 50°C overnight: leucine tRNA 5′ exon probe: 5′-CTT GAG TCT GGC GCC TTA GAC-3′; tyrosine tRNA 3′ exon probe 5′-TCG AAC CAG CGA CCT AAG GAT-3′; arginine tRNA 5′ exon probe: 5′-TAG AAG TCC AAT GCG CTA TCC-3′; isoleucine tRNA 5′ exon probe: 5′-TAT AAG TAC CGC GCG CTA ACC-3′; and methionine tRNA 5′ exon probe: 5′-GGG CCC AGC ACG CTT CCG CTG CGC CAC TCT GC-3′. Equal loading was confirmed by hybridization of the blots with a [5′-^{32}P]-labeled DNA probe detecting U6 snRNA (5′-GCA GGG GCC ATG CTA ATC TTC TCT GTA TCG-3′).

Metabolic labeling

Tet-ON HeLa shRNA cell lines were treated with Dox for six consecutive days. B220^{+} B cells were stimulated with LPS for 4 days. Thereafter, cells were starved in DMEM without L-methionine and L-cysteine (Gibco) for 2 h at 37°C and subsequently cultured for 1 h at 37 °C in Met and Cys-free DMEM supplemented with 16 MBq/ml [^{35}S]-labeled methionine and cysteine (Perkin Elmer, EasyTag™ EXPRESS^{35}S Protein Labeling Mix). HeLa cells were lysed in lysis buffer (2% (w/v) SDS, 20 mM HEPES pH 7.4), and proteins were pelleted by acetone precipitation overnight. After spinning, the obtained protein pellet was resuspended in lysis buffer. Protein concentration was determined by BCA assay (Thermo Scientific). Scintillation counts were measured and normalized to the respective protein concentrations (HeLa cells) or cell numbers (B cells). For autoradiography, cells were directly lysed in 1× SDS loading buffer at 95°C for 5 min. Proteins were separated by SDS–PAGE and transferred to Immobilon-P membranes (Millipore). Following autoradiography, membranes were incubated with the indicated antibodies.

Mice

The conditional *Rtcb*$^{tm1a(KOMP)Wtsi}$ ES cells were purchased from the EUCOMM/KOMP-CSD collection (MGI-ID 4362526, clone G09). ES cells were injected into C57BL/6J-*Tyr*$^{c-2J}$ blastocysts to generate *Rtcb*$^{fl\text{-}laczneo/+}$ mice. The *Rtcb*$^{fl/+}$ allele was obtained by crossing these mice to the FLPe (Rodriguez *et al*, 2000). To detect deletion of

Published online: November 6, 2014

the *Rtcb* allele, the following primers were used for PCR genotyping of *Rtcb* mutant mice: 5′-GCC AAG CAT GTC CTG TAG AC-3′, 5′-AGA AAA GGG ATG GCT GAG TC-3′ and 5′-GGT CCC TTT TGC CTT CTG-3′. The wild-type *Rtcb* allele was identified as a 1,320-bp, the $Rtcb^{fl}$ allele as a 1,488-bp, and the deleted allele as a 706-bp PCR fragment. Both $Rtcb^{fl/fl}$ and *Cd23*-Cre (Kwon *et al*, 2008) mice were maintained on the C56/Bl6 background. All animal experiments were done according to valid project licenses, which were approved and regularly controlled by the Austrian Veterinary Authorities.

Immunizations and plasma cell analysis

Mice were injected intraperitoneally with 50 μg TNP-0.5-LPS (Bio-Search Technologies) in PBS. After 14 days, the frequencies of TNP-specific antibody-secreting cells in the spleen were determined using the mouse IgM ELISPOT Kit (Mabtech) according to the manufacturer's protocol. TNP-14-BSA (BioSearch Technologies)-coated plates were used for capturing total anti-TNP-IgM antibodies secreted by individual cells. After extensive washing, the spots were counted with an AID ELISPOT reader system (AID Diagnostika). The measurement of the spots was performed automatically using the Definiens Software Suite. Prior to the analysis, the image data were processed by performing a shading correction. The spots were found using threshold segmentation and subsequent watershed segmentation. The serum titer of TNP-specific IgM or IgM antibodies was determined by ELISA using plates that were coated with 10 μg/ml of TNP-14-BSA in PBS as described previously (Nutman, 2001) with slight modifications: goat anti-mouse IgM (μ-chain specific) peroxidase or biotinylated anti-kappa light chain/streptavidin-HRP (BioLegend) was used as secondary antibodies. SureBlue™ TMB Microwell Peroxidase Substrate (Kirkegaard & Perry Laboratories) was used as substrate. Reactions were stopped with TMB stop solution (Kirkegaard & Perry Laboratories), and absorbance was read at 450 nm on a Tecan Genios Pro Fluorescence, Absorbance Reader (Tecan Trading AG).

Ex vivo B-cell stimulations

B cells were isolated from spleens by positive enrichment of $B220^+$ B cells by MACS sorting (Miltenyi Biotech). The purified B cells were plated at 0.3×10^6 cells/ml in IMDM medium (IMP/IMBA Media Kitchen) supplemented with 20% fetal calf serum (Sigma), 50 μM 2-mercaptoethanol, 3 mM glutamine (Sigma), 100 U/ml penicillin and 100 μg/ml streptomycin sulfate (Sigma), and 20 mM HEPES were subsequently treated for up to 4 days with 20 μg/ml LPS from *Escherichia coli* (Sigma). For cell proliferation analysis, the purified B cells were first stained with 5 μM CellTrace Violet reagent (Invitrogen) before stimulation according to the manufacturer's protocol. IgM present in cell culture supernatants was measured using the Mouse IgM ELISA Ready-SET-Go kit (eBioscience) according to the manufacturer's protocol. The numbers of IgM-specific ASCs in the cultures were determined using the mouse IgM ELISPOT Kit (Mabtech) according to the manufacturer's protocol.

Flow cytometry

Mice at 6–8 weeks of age were used for FACS analysis of mature B-cell subsets. Single cell suspensions from spleen or *in vitro* cultured B cells were incubated with CD16/CD32 Fc block (eBioscience) to inhibit unspecific antibody binding. For flow cytometry, cells were stained with the following antibodies: anti-B220 FITC (RA3-6B2), anti-IgM PE-Cy7 (II-41), anti-IgD FITC (11-26), anti-CD21 PE (8D9), anti-CD1d biot (1B1), CD4 APC (GK1.5), anti-CD8α APC (53-6.7) anti-CD8β APC (H35-17.2), anti-F4/80 APC (BM8), anti-CD28 PE-Cy7 (37.51) from eBioscience; anti-CD19 Pacific Blue (6D5), anti-CD23 Alexa Fluor 647 (B3B4), anti-B220 Brilliant Violet 780™ (RA3-6B2), anti-CD22 APC (Ox-27), streptavidin APC-Cy7 from BioLegend; and anti-CD138 PE (281-2) from BD. Flow cytometric analysis was performed using a LSRII instrument (BD Biosciences) and the FlowJo Software. For FACS sorting, the BD FACSAria or FACSAriaIII flow cytometer (BD Biosciences) was used.

Statistical analysis

Results were statistically compared using a two-way ANOVA or an unpaired Student's *t*-test. A *P*-value of $P < 0.05$ was considered significant.

Supplementary information for this article is available online: http://emboj.embopress.org

Acknowledgements
We are grateful to Jutta Dammann for technical support; Nicole Fellner and Harald Kotisch for electron microscopy; Marietta Weninger, Thomas Lendl and Gabriele Stengl for FACS sorting; Gerald Schmauss for FACS sorting and image analysis of ELISPOT data; Arabella Meixner, Aleksandra Smus and Esther Rauscher for help with ES cell work and mouse husbandry; Hans-Christian Theußl for blastocyst injection and generation of chimeric animals; Kazufumi Mochizuki for providing the HSP90 antibody; Tomas Aragon, Diego Rojas-Rivera, Claudio Hetz and Stefan Weitzer for advice; and all members of our laboratory for discussions and support. This work has been funded by the Fonds zur Förderung der wissenschaftlichen Forschung (FWF-P24687), the Institute of Molecular Biotechnology Austria (IMBA), a Hertha Firnberg PostDoctoral Fellowship (JJ), a Boehringer Ingelheim Fonds PhD Fellowship and the Doctoral Program for RNA Biology (TH) and the Young Investigator Program (YIP-EMBO) (JM).

Author contributions
JJ and TH designed and carried out experiments and wrote the manuscript; AFN designed and carried out experiments; TK performed experiments; MM designed experiments; MB supervised the B cell part of the project; JP and KH contributed to experiments; TH designed the shRNA cloning strategy; JM supervised the project and contributed to writing the manuscript.

Conflict of interest
AFN is employed at *The EMBO Journal* as a scientific editor. AFN was not involved in any way in the review process or the editorial evaluation of this manuscript and is not privy to the referee identities. The remaining authors declare that they have no conflict of interest.

References

Apostol BL, Westaway SK, Abelson J, Greer CL (1991) Deletion analysis of a multifunctional yeast tRNA ligase polypeptide. Identification of essential and dispensable functional domains. *J Biol Chem* 266: 7445–7455

Published online: November 6, 2014
The EMBO Journal RTCB regulates antibody secretion in plasma cells *Jennifer Jurkin et al*

Benhamron S, Hadar R, Iwawaky T, So JS, Lee AH, Tirosh B (2013) Regulated IRE1-dependent decay participates in curtailing immunoglobulin secretion from plasma cells. *Eur J Immunol* 44: 867 – 876

Carrasco DR, Sukhdeo K, Protopopova M, Sinha R, Enos M, Carrasco DE, Zheng M, Mani M, Henderson J, Pinkus GS, Munshi N, Horner J, Ivanova EV, Protopopov A, Anderson KC, Tonon G, DePinho RA (2007) The differentiation and stress response factor XBP-1 drives multiple myeloma pathogenesis. *Cancer Cell* 11: 349 – 360

Chapman MA, Lawrence MS, Keats JJ, Cibulskis K, Sougnez C, Schinzel AC, Harview CL, Brunet JP, Ahmann GJ, Adli M, Anderson KC, Ardlie KG, Auclair D, Baker A, Bergsagel PL, Bernstein BE, Drier Y, Fonseca R, Gabriel SB, Hofmeister CC *et al* (2011) Initial genome sequencing and analysis of multiple myeloma. *Nature* 471: 467 – 472

Chen X, Iliopoulos D, Zhang Q, Tang Q, Greenblatt MB, Hatziapostolou M, Lim E, Tam WL, Ni M, Chen Y, Mai J, Shen H, Hu DZ, Adoro S, Hu B, Song M, Tan C, Landis MD, Ferrari M, Shin SJ *et al* (2014) XBP1 promotes triple-negative breast cancer by controlling the HIF1alpha pathway. *Nature* 508: 103 – 107

Cox JS, Shamu CE, Walter P (1993) Transcriptional induction of genes encoding endoplasmic reticulum resident proteins requires a transmembrane protein kinase. *Cell* 73: 1197 – 1206

Cox JS, Walter P (1996) A novel mechanism for regulating activity of a transcription factor that controls the unfolded protein response. *Cell* 87: 391 – 404

De Robertis EM, Black P, Nishikura K (1981) Intranuclear location of the tRNA splicing enzymes. *Cell* 23: 89 – 93

Desai KK, Cheng CL, Bingman CA, Phillips Jr GN, Raines RT (2014) A tRNA splicing operon: archease endows RtcB with dual GTP/ATP cofactor specificity and accelerates RNA ligation. *Nucleic Acids Res* 42: 3931 – 3942

Dow LE, Premsrirut PK, Zuber J, Fellmann C, McJunkin K, Miething C, Park Y, Dickins RA, Hannon GJ, Lowe SW (2012) A pipeline for the generation of shRNA transgenic mice. *Nat Protoc* 7: 374 – 393

Fellmann C, Hoffmann T, Sridhar V, Hopfgartner B, Muhar M, Roth M, Lai DY, Barbosa IA, Kwon JS, Guan Y, Sinha N, Zuber J (2013) An optimized microRNA backbone for effective single-copy RNAi. *Cell Rep* 5: 1704 – 1713

Filipowicz W, Konarska M, Gross HJ, Shatkin AJ (1983) RNA 3′-terminal phosphate cyclase activity and RNA ligation in HeLa cell extract. *Nucleic Acids Res* 11: 1405 – 1418

Filipowicz W, Shatkin AJ (1983) Origin of splice junction phosphate in tRNAs processed by HeLa cell extract. *Cell* 32: 547 – 557

Gass JN, Gifford NM, Brewer JW (2002) Activation of an unfolded protein response during differentiation of antibody-secreting B cells. *J Biol Chem* 277: 49047 – 49054

Greer CL, Peebles CL, Gegenheimer P, Abelson J (1983) Mechanism of action of a yeast RNA ligase in tRNA splicing. *Cell* 32: 537 – 546

Hasbold J, Corcoran LM, Tarlinton DM, Tangye SG, Hodgkin PD (2004) Evidence from the generation of immunoglobulin G-secreting cells that stochastic mechanisms regulate lymphocyte differentiation. *Nat Immunol* 5: 55 – 63

Hetz C (2012) The unfolded protein response: controlling cell fate decisions under ER stress and beyond. *Nat Rev Mol Cell Biol* 13: 89 – 102

Hetz C, Chevet E, Harding HP (2013) Targeting the unfolded protein response in disease. *Nat Rev Drug Discov* 12: 703 – 719

Hollien J, Weissman JS (2006) Decay of endoplasmic reticulum-localized mRNAs during the unfolded protein response. *Science* 313: 104 – 107

Hollien J, Lin JH, Li H, Stevens N, Walter P, Weissman JS (2009) Regulated Ire1-dependent decay of messenger RNAs in mammalian cells. *J Cell Biol* 186: 323 – 331

Hu CC, Dougan SK, McGehee AM, Love JC, Ploegh HL (2009) XBP-1 regulates signal transduction, transcription factors and bone marrow colonization in B cells. *EMBO J* 28: 1624 – 1636

Iwakoshi NN, Lee AH, Glimcher LH (2003a) The X-box binding protein-1 transcription factor is required for plasma cell differentiation and the unfolded protein response. *Immunol Rev* 194: 29 – 38

Iwakoshi NN, Lee AH, Vallabhajosyula P, Otipoby KL, Rajewsky K, Glimcher LH (2003b) Plasma cell differentiation and the unfolded protein response intersect at the transcription factor XBP-1. *Nat Immunol* 4: 321 – 329

Iwawaki T, Tokuda M (2011) Function of yeast and amphioxus tRNA ligase in IRE1alpha-dependent XBP1 mRNA splicing. *Biochem Biophys Res Commun* 413: 527 – 531

Karaca E, Weitzer S, Pehlivan D, Shiraishi H, Gogakos T, Hanada T, Jhangiani SN, Wiszniewski W, Withers M, Campbell IM, Erdin S, Isikay S, Franco LM, Gonzaga-Jauregui C, Gambin T, Gelowani V, Hunter JV, Yesil G, Koparir E, Yilmaz S *et al* (2014) Human CLP1 mutations alter tRNA biogenesis, affecting both peripheral and central nervous system function. *Cell* 157: 636 – 650

Kharabi Masouleh B, Geng H, Hurtz C, Chan LN, Logan AC, Chang MS, Huang C, Swaminathan S, Sun H, Paietta E, Melnick AM, Koeffler P, Muschen M (2014) Mechanistic rationale for targeting the unfolded protein response in pre-B acute lymphoblastic leukemia. *Proc Natl Acad Sci USA* 111: E2219 – E2228

Klein U, Casola S, Cattoretti G, Shen Q, Lia M, Mo T, Ludwig T, Rajewsky K, Dalla-Favera R (2006) Transcription factor IRF4 controls plasma cell differentiation and class-switch recombination. *Nat Immunol* 7: 773 – 782

Kwon K, Hutter C, Sun Q, Bilic I, Cobaleda C, Malin S, Busslinger M (2008) Instructive role of the transcription factor E2A in early B lymphopoiesis and germinal center B cell development. *Immunity* 28: 751 – 762

Laski FA, Fire AZ, RajBhandary UL, Sharp PA (1983) Characterization of tRNA precursor splicing in mammalian extracts. *J Biol Chem* 258: 11974 – 11980

Lee K, Tirasophon W, Shen X, Michalak M, Prywes R, Okada T, Yoshida H, Mori K, Kaufman RJ (2002) IRE1-mediated unconventional mRNA splicing and S2P-mediated ATF6 cleavage merge to regulate XBP1 in signaling the unfolded protein response. *Genes Dev* 16: 452 – 466

Lee AH, Iwakoshi NN, Glimcher LH (2003) XBP-1 regulates a subset of endoplasmic reticulum resident chaperone genes in the unfolded protein response. *Mol Cell Biol* 23: 7448 – 7459

Lisbona F, Rojas-Rivera D, Thielen P, Zamorano S, Todd D, Martinon F, Glavic A, Kress C, Lin JH, Walter P, Reed JC, Glimcher LH, Hetz C (2009) BAX inhibitor-1 is a negative regulator of the ER stress sensor IRE1alpha. *Mol Cell* 33: 679 – 691

Lu Y, Liang FX, Wang X (2014) A synthetic biology approach identifies the mammalian UPR RNA ligase RtcB. *Mol Cell* 55: 758 – 770

Lund E, Dahlberg JE (1998) Proofreading and aminoacylation of tRNAs before export from the nucleus. *Science* 282: 2082 – 2085

Majumder M, Huang C, Snider MD, Komar AA, Tanaka J, Kaufman RJ, Krokowski D, Hatzoglou M (2012) A novel feedback loop regulates the response to endoplasmic reticulum stress via the cooperation of cytoplasmic splicing and mRNA translation. *Mol Cell Biol* 32: 992 – 1003

McGehee AM, Dougan SK, Klemm EJ, Shui G, Park B, Kim YM, Watson N, Wenk MR, Ploegh HL, Hu CC (2009) XBP-1-deficient plasmablasts show normal protein folding but altered glycosylation and lipid synthesis. *J Immunol* 183: 3690 – 3699

Moore KA, Hollien J (2012) The unfolded protein response in secretory cell function. *Annu Rev Genet* 46: 165 – 183

Nakamura M, Gotoh T, Okuno Y, Tatetsu H, Sonoki T, Uneda S, Mori M, Mitsuya H, Hata H (2006) Activation of the endoplasmic reticulum stress

Published online: November 6, 2014

pathway is associated with survival of myeloma cells. *Leuk Lymphoma* 47: 531 – 539

Nera KP, Kohonen P, Narvi E, Peippo A, Mustonen L, Terho P, Koskela K, Buerstedde JM, Lassila O (2006) Loss of Pax5 promotes plasma cell differentiation. *Immunity* 24: 283 – 293

Nishikura K, De Robertis EM (1981) RNA processing in microinjected Xenopus oocytes. Sequential addition of base modifications in the spliced transfer RNA. *J Mol Biol* 145: 405 – 420

Nutman TB (2001) Measurement of polyclonal immunoglobulin synthesis using ELISA. *Curr Protoc Immunol* Chapter 7: Unit 7 12

Perez-Gonzalez A, Pazo A, Navajas R, Ciordia S, Rodriguez-Frandsen A, Nieto A (2014) hCLE/C14orf166 associates with DDX1-HSPC117-FAM98B in a novel transcription-dependent shuttling RNA-transporting complex. *PLoS ONE* 9: e90957

Phizicky EM, Schwartz RC, Abelson J (1986) *Saccharomyces cerevisiae* tRNA ligase. Purification of the protein and isolation of the structural gene. *J Biol Chem* 261: 2978 – 2986

Popow J, Englert M, Weitzer S, Schleiffer A, Mierzwa B, Mechtler K, Trowitzsch S, Will CL, Luhrmann R, Soll D, Martinez J (2011) HSPC117 is the essential subunit of a human tRNA splicing ligase complex. *Science* 331: 760 – 764

Popow J, Schleiffer A, Martinez J (2012) Diversity and roles of (t)RNA ligases. *Cell Mol Life Sci* 69: 2657 – 2670

Popow J, Jurkin J, Schleiffer A, Martinez J (2014) Analysis of orthologous groups reveals archease and DDX1 as tRNA splicing factors. *Nature* 511: 104 – 107

Reimold AM, Iwakoshi NN, Manis J, Vallabhajosyula P, Szomolanyi-Tsuda E, Gravallese EM, Friend D, Grusby MJ, Alt F, Glimcher LH (2001) Plasma cell differentiation requires the transcription factor XBP-1. *Nature* 412: 300 – 307

Rodriguez CI, Buchholz F, Galloway J, Sequerra R, Kasper J, Ayala R, Stewart AF, Dymecki SM (2000) High-efficiency deleter mice show that FLPe is an alternative to Cre-loxP. *Nat Genet* 25: 139 – 140

Rodriguez DA, Zamorano S, Lisbona F, Rojas-Rivera D, Urra H, Cubillos-Ruiz JR, Armisen R, Henriquez DR, Cheng EH, Letek M, Vaisar T, Irrazabal T, Gonzalez-Billault C, Letai A, Pimentel-Muinos FX, Kroemer G, Hetz C (2012) BH3-only proteins are part of a regulatory network that control the sustained signalling of the unfolded protein response sensor IRE1alpha. *EMBO J* 31: 2322 – 2335

Sawaya R, Schwer B, Shuman S (2003) Genetic and biochemical analysis of the functional domains of yeast tRNA ligase. *J Biol Chem* 278: 43928 – 43938

Schmidlin H, Diehl SA, Nagasawa M, Scheeren FA, Schotte R, Uittenbogaart CH, Spits H, Blom B (2008) Spi-B inhibits human plasma cell differentiation by repressing BLIMP1 and XBP-1 expression. *Blood* 112: 1804 – 1812

Shaffer AL, Shapiro-Shelef M, Iwakoshi NN, Lee AH, Qian SB, Zhao H, Yu X, Yang L, Tan BK, Rosenwald A, Hurt EM, Petroulakis E, Sonenberg N, Yewdell JW, Calame K, Glimcher LH, Staudt LM (2004) XBP1, downstream of Blimp-1, expands the secretory apparatus and other organelles, and increases protein synthesis in plasma cell differentiation. *Immunity* 21: 81 – 93

Sidrauski C, Cox JS, Walter P (1996) tRNA ligase is required for regulated mRNA splicing in the unfolded protein response. *Cell* 87: 405 – 413

Sidrauski C, Walter P (1997) The transmembrane kinase Ire1p is a site-specific endonuclease that initiates mRNA splicing in the unfolded protein response. *Cell* 90: 1031 – 1039

Tang CH, Ranatunga S, Kriss CL, Cubitt CL, Tao J, Pinilla-Ibarz JA, Del Valle JR, Hu CC (2014) Inhibition of ER stress-associated IRE-1/XBP-1 pathway reduces leukemic cell survival. *J Clin Invest* 124: 2585 – 2598

Taubenheim N, Tarlinton DM, Crawford S, Corcoran LM, Hodgkin PD, Nutt SL (2012) High rate of antibody secretion is not integral to plasma cell differentiation as revealed by XBP-1 deficiency. *J Immunol* 189: 3328 – 3338

Todd DJ, McHeyzer-Williams LJ, Kowal C, Lee AH, Volpe BT, Diamond B, McHeyzer-Williams MG, Glimcher LH (2009) XBP1 governs late events in plasma cell differentiation and is not required for antigen-specific memory B cell development. *J Exp Med* 206: 2151 – 2159

Volkmann K, Lucas JL, Vuga D, Wang X, Brumm D, Stiles C, Kriebel D, Der-Sarkissian A, Krishnan K, Schweitzer C, Liu Z, Malyankar UM, Chiovitti D, Canny M, Durocher D, Sicheri F, Patterson JB (2011) Potent and selective inhibitors of the inositol-requiring enzyme 1 endoribonuclease. *J Biol Chem* 286: 12743 – 12755

Yanagitani K, Imagawa Y, Iwawaki T, Hosoda A, Saito M, Kimata Y, Kohno K (2009) Cotranslational targeting of XBP1 protein to the membrane promotes cytoplasmic splicing of its own mRNA. *Mol Cell* 34: 191 – 200

Yoshida H, Matsui T, Yamamoto A, Okada T, Mori K (2001) XBP1 mRNA is induced by ATF6 and spliced by IRE1 in response to ER stress to produce a highly active transcription factor. *Cell* 107: 881 – 891

Yoshida H, Matsui T, Hosokawa N, Kaufman RJ, Nagata K, Mori K (2003) A time-dependent phase shift in the mammalian unfolded protein response. *Dev Cell* 4: 265 – 271

Zuber J, McJunkin K, Fellmann C, Dow LE, Taylor MJ, Hannon GJ, Lowe SW (2011) Toolkit for evaluating genes required for proliferation and survival using tetracycline-regulated RNAi. *Nat Biotechnol* 29: 79 – 83

7.7. Curriculum vitae

Personal data

NAME:	Dipl. Biochem. Theresa Henkel
DATE AND PLACE OF BIRTH:	12th of October 1987, Waiblingen (Germany)
NATIONALITY:	German

Education and career

since 05/2012 **PHD STUDENT AT THE INSTITUTE FOR MOLECULAR BIOTECHNOLOGY (IMBA)**
Laboratory of Javier Martinez, PhD
Title of thesis: „Cytoplasmic functions of the tRNA ligase complex in health and disease“

10/2006 –12/2011 **UNIVERSITY STUDIES, MAJOR IN BIOCHEMISTRY AT "GOETHE UNIVERSITÄT", FRANKFURT**
Degree: diploma
Diploma thesis in the laboratory of Prof. Ivan Dikic: „The role of proteasomal ubiquitin receptor Rpn13 in growth and development“

Practical experience

DIPLOMA THESIS AT INSTITUTE OF BIOCHEMISTRY II, GOETHE UNIVERSITY, FRANKFURT; APRIL –DECEMBER 2011
Laboratory head: Prof. Dr. Ivan Dikic
Focus of research:
Characterization of the interaction of proteasomal uniquitin receptor Rpn13 with autophagy receptors

HARVARD STEM CELL INSTITUTE, BOSTON (USA); APRIL –SEPTEMBER 2010
Laboratory head: MD David T. Scadden
Focus of research:
Function of the proteasome in maintaining of pluripotency or supporting differentiation of stem cells
Changes in gene expression after inhibition of the proteasome

MAX PLANCK INSTITUTE OF BIOPHYSICS, FRANKFURT; FEBRUARY 2010
Laboratory heads: Prof. Dr. Ernst Bamberg, Prof. Dr. Werner Kühlbrandt
Focus of activity:
Variable electrophysicochemical methods including patch and voltage clamp
Protein crystallization

GOETHE UNIVERSITY, FRANKFURT; AUGUST –SEPTEMBER 2009
Laboratory head: Prof. Dr. Robert Tampé
Focus of research:
Reduction of antigen presentation after Epstein-Barr virus infections
Possible mechanisms of membrane insertion of BNLF2a (early protein of the lytic cycle of the Epstein-Barr virus)

GEORG-SPEYER-HAUS, FRANKFURT; JANUARY –FEBRUARY 2009
Laboratory head: Dr. Martin Zörnig
Focus of research:
Identification of antiapoptotic proteins
Segregation of soluble antiapoptotic proteins within exosomes

PAUL-EHRLICH-INSTITUT, LANGEN; NOVEMBER - DECEMBER 2008
Multiple laboratories
Focuses of activity:
Variable immunological and biomolecular techniques

Scientific publications

Jurkin, J.* and Henkel, T.*, Nielsen AF, Minnich M, Popow J, Kaufmann T, Heindl K, Hoffmann T, Busslinger M, Martinez J.; The mammalian tRNA ligase complex mediates splicing of XBP1 mRNA and controls antibody secretion in plasma cells.
EMBO J 33, 2922-36 (2014). *** these authors contributed equally**

Catic A, Suh CY, Hill CT, Daheron L, **Henkel T**, Orford KW, Dombkowski DM, Liu T, Liu XS, Scadden DT.; Genome-wide map of nuclear protein degradation shows NCoR1 turnover as a key to mitochondrial gene regulation. Cell 155(6):1380-95 (2013)

7.8. Acknowledgements

I would like to first of all thank Javier Martinez, not only for giving me the opportunity to work on this exciting project but also for his constant support, endless optimism, his belief in my skills and his continuous advice, especially concerning soft skills.

Furthermore, I would like to thank all past and present members of the Martinez' lab for creating a great working atmosphere and for making the time of my PhD so pleasant. I really enjoy our coffee breaks full of stories and laughter and value the constant support you were giving! I am deeply grateful to Jennifer Jurkin for always listening and being ready to help, not only concerning technical problems but also offering advice related to day-to-day issues. To Stefan Weitzer for willing to share his sheer endless knowledge and for critical advice whenever it was needed. To Therese Kaufmann for her sunny nature, many laughs and her big talent in bringing together everyone for coffee breaks and social activities. To Jutta Dammann for her helping hand, psychological support and for taking care of so many day-to-day problems. To Anne Faerch Nielsen for starting off with the UPR project and for help during manuscript preparations as well as to Silvia Panizza for support especially with tRNA-unrelated questions. To Johannes Popow for many insights into the biology of tRNAs. To Paola Pinto for sharing coffee breaks and Brazilian culinary delights as well as to Dhaarsi Koneswarakantha and Igor Asanovic for their creativity and positive spirit. Many thanks also go to my internship student Olga Boryczka, Marissa Stebegg and Alice Wenger for their interest in my project and for their willingness to contribute as much as possible.

I am grateful for having had the opportunity to work at IMBA with all of its excellent core facilities. The constant training and support offered on campus really made and asset to my project. I am thankful to all members of the core facilities for always making me feel like I could approach anyone with every problem, question or wish that came to my mind. Special thanks go to Gerald Schmauss, Thomas Lendl, Marietta Weninger and Gabriele Petri for help with FACS analysis and the many hours they spent sorting my cells. Furthermore, I thank Alexander Schleiffer, Maria Novatchkova and Ido Tamir for doing all the bioinformatic analysis and for their patience in explaining their work to me as well as the CSF NGS team for sample preparation and RNA sequencing.

I would also like to take this opportunity to thank the members of my PhD committee, Josef Penninger, Renée Schroeder and Johannes Zuber, for knowledgeable advice and support. Many thanks go to members of the Zuber lab, in particular Thomas Hoffmann, Barbara Hopfgartner, Martina Weißenböck, Matthias Muhar, Sumit Deswai and Julian Jude, for advice with the shRNA system and for sharing cell lines, reagents and vectors. I am also thankful to members of the Hetz laboratory in Chile,

especially to Diego Rojas Rivera, for providing insights into UPR biology. Furthermore, I thank Laurie Glimcher for sharing the GFP-RV-XBP1s plasmid.

Special thanks go to the Boehringer Ingelheim Fonds for financial support of my PhD but also for soft skill training and for making me part of this big family. I really enjoyed being a BIF fellowship holder.

Finally, I would like to deeply thank my parents, Heidi and Friedhelm, my sister Luisa, my grandmother Anneliese as well as Werner, Claudia and Peter for their never ending support during all of my life. Without your love, encouragement and believe in me I would not have reached what I am today. Last but not least I would like to thank Jerry for his love, kindness, support and patience but also for his intelligence and the great time we are spending together. You make my life a lot brighter.

8. References

Abelson, J., Trotta, C.R., and Li, H. (1998). tRNA splicing. The Journal of biological chemistry *273*, 12685-12688.

Acosta-Alvear, D., Zhou, Y., Blais, A., Tsikitis, M., Lents, N.H., Arias, C., Lennon, C.J., Kluger, Y., and Dynlacht, B.D. (2007). XBP1 controls diverse cell type- and condition-specific transcriptional regulatory networks. Molecular cell *27*, 53-66.

Adachi, Y., Yamamoto, K., Okada, T., Yoshida, H., Harada, A., and Mori, K. (2008). ATF6 is a transcription factor specializing in the regulation of quality control proteins in the endoplasmic reticulum. Cell structure and function *33*, 75-89.

Akiyama, T., Ohuchi, T., Sumida, S., Matsumoto, K., and Toyoshima, K. (1992). Phosphorylation of the retinoblastoma protein by cdk2. Proceedings of the National Academy of Sciences of the United States of America *89*, 7900-7904.

Amitsur, M., Levitz, R., and Kaufmann, G. (1987). Bacteriophage T4 anticodon nuclease, polynucleotide kinase and RNA ligase reprocess the host lysine tRNA. The EMBO journal *6*, 2499-2503.

Anders, S., Reyes, A., and Huber, W. (2012). Detecting differential usage of exons from RNA-seq data. Genome research *22*, 2008-2017.

Apostol, B.L., Westaway, S.K., Abelson, J., and Greer, C.L. (1991). Deletion analysis of a multifunctional yeast tRNA ligase polypeptide. Identification of essential and dispensable functional domains. The Journal of biological chemistry *266*, 7445-7455.

Aragon, T., van Anken, E., Pincus, D., Serafimova, I.M., Korennykh, A.V., Rubio, C.A., and Walter, P. (2009). Messenger RNA targeting to endoplasmic reticulum stress signalling sites. Nature *457*, 736-740.

Araki, K., and Nagata, K. (2011). Protein folding and quality control in the ER. Cold Spring Harbor perspectives in biology *3*, a007526.

Arts, G.J., Kuersten, S., Romby, P., Ehresmann, B., and Mattaj, I.W. (1998). The role of exportin-t in selective nuclear export of mature tRNAs. The EMBO journal *17*, 7430-7441.

Baldi, M.I., Mattoccia, E., Bufardeci, E., Fabbri, S., and Tocchini-Valentini, G.P. (1992). Participation of the intron in the reaction catalyzed by the Xenopus tRNA splicing endonuclease. Science *255*, 1404-1408.

Baltz, A.G., Munschauer, M., Schwanhausser, B., Vasile, A., Murakawa, Y., Schueler, M., Youngs, N., Penfold-Brown, D., Drew, K., Milek, M.*, et al.* (2012). The mRNA-bound proteome and its global occupancy profile on protein-coding transcripts. Molecular cell *46*, 674-690.

Barbosa-Tessmann, I.P., Chen, C., Zhong, C., Schuster, S.M., Nick, H.S., and Kilberg, M.S. (1999a). Activation of the unfolded protein response pathway induces human asparagine synthetase gene expression. The Journal of biological chemistry *274*, 31139-31144.

Barbosa-Tessmann, I.P., Chen, C., Zhong, C., Siu, F., Schuster, S.M., Nick, H.S., and Kilberg, M.S. (2000). Activation of the human asparagine synthetase gene by the amino acid response and the endoplasmic reticulum stress response pathways occurs by common genomic elements. The Journal of biological chemistry *275*, 26976-26985.

Barbosa-Tessmann, I.P., Pineda, V.L., Nick, H.S., Schuster, S.M., and Kilberg, M.S. (1999b). Transcriptional regulation of the human asparagine synthetase gene by carbohydrate availability. The Biochemical journal *339 (Pt 1)*, 151-158.

Bettigole, S.E., Lis, R., Adoro, S., Lee, A.H., Spencer, L.A., Weller, P.F., and Glimcher, L.H. (2015). The transcription factor XBP1 is selectively required for eosinophil differentiation. Nature immunology *16*, 829-837.

Bleoo, S., Sun, X., Hendzel, M.J., Rowe, J.M., Packer, M., and Godbout, R. (2001). Association of human DEAD box protein DDX1 with a cleavage stimulation factor involved in 3'-end processing of pre-MRNA. Molecular biology of the cell *12*, 3046-3059.

Bobrovnikova-Marjon, E., Grigoriadou, C., Pytel, D., Zhang, F., Ye, J., Koumenis, C., Cavener, D., and Diehl, J.A. (2010). PERK promotes cancer cell proliferation and tumor growth by limiting oxidative DNA damage. Oncogene *29*, 3881-3895.

Bommiasamy, H., Back, S.H., Fagone, P., Lee, K., Meshinchi, S., Vink, E., Sriburi, R., Frank, M., Jackowski, S., Kaufman, R.J.*, et al.* (2009). ATF6alpha induces XBP1-independent expansion of the endoplasmic reticulum. Journal of cell science *122*, 1626-1636.

Burset, M., Seledtsov, I.A., and Solovyev, V.V. (2000). Analysis of canonical and non-canonical splice sites in mammalian genomes. Nucleic acids research *28*, 4364-4375.

Calfon, M., Zeng, H., Urano, F., Till, J.H., Hubbard, S.R., Harding, H.P., Clark, S.G., and Ron, D. (2002). IRE1 couples endoplasmic reticulum load to secretory capacity by processing the XBP-1 mRNA. Nature *415*, 92-96.

Carrasco, D.R., Sukhdeo, K., Protopopova, M., Sinha, R., Enos, M., Carrasco, D.E., Zheng, M., Mani, M., Henderson, J., Pinkus, G.S.*, et al.* (2007). The differentiation and stress response factor XBP-1 drives multiple myeloma pathogenesis. Cancer cell *11*, 349-360.

Castanotto, D., Sakurai, K., Lingeman, R., Li, H., Shively, L., Aagaard, L., Soifer, H., Gatignol, A., Riggs, A., and Rossi, J.J. (2007). Combinatorial delivery of small interfering RNAs reduces RNAi efficacy by selective incorporation into RISC. Nucleic acids research *35*, 5154-5164.

Chakravarty, A.K., and Shuman, S. (2012). The sequential 2',3'-cyclic phosphodiesterase and 3'-phosphate/5'-OH ligation steps of the RtcB RNA splicing pathway are GTP-dependent. Nucleic acids research *40*, 8558-8567.

Chan, P.P., and Lowe, T.M. (2009). GtRNAdb: a database of transfer RNA genes detected in genomic sequence. Nucleic acids research *37*, D93-97.

Chawla, A., Chakrabarti, S., Ghosh, G., and Niwa, M. (2011). Attenuation of yeast UPR is essential for survival and is mediated by IRE1 kinase. The Journal of cell biology *193*, 41-50.

Chen, H., and Qi, L. (2010). SUMO modification regulates the transcriptional activity of XBP1. The Biochemical journal *429*, 95-102.

Chen, H.C., Lin, W.C., Tsay, Y.G., Lee, S.C., and Chang, C.J. (2002). An RNA helicase, DDX1, interacting with poly(A) RNA and heterogeneous nuclear ribonucleoprotein K. The Journal of biological chemistry *277*, 40403-40409.

Chen, X., Iliopoulos, D., Zhang, Q., Tang, Q., Greenblatt, M.B., Hatziapostolou, M., Lim, E., Tam, W.L., Ni, M., Chen, Y.*, et al.* (2014). XBP1 promotes triple-negative breast cancer by controlling the HIF1alpha pathway. Nature *508*, 103-107.

Choffat, Y., Suter, B., Behra, R., and Kubli, E. (1988). Pseudouridine modification in the tRNA(Tyr) anticodon is dependent on the presence, but independent of the size and sequence, of the intron in eucaryotic tRNA(Tyr) genes. Molecular and cellular biology *8*, 3332-3337.

Coudreuse, D., and Nurse, P. (2010). Driving the cell cycle with a minimal CDK control network. Nature *468*, 1074-1079.

Cox, J.S., Chapman, R.E., and Walter, P. (1997). The unfolded protein response coordinates the production of endoplasmic reticulum protein and endoplasmic reticulum membrane. Molecular biology of the cell *8*, 1805-1814.

Cox, J.S., and Walter, P. (1996). A novel mechanism for regulating activity of a transcription factor that controls the unfolded protein response. Cell *87*, 391-404.

Credle, J.J., Finer-Moore, J.S., Papa, F.R., Stroud, R.M., and Walter, P. (2005). On the mechanism of sensing unfolded protein in the endoplasmic reticulum. Proceedings of the National Academy of Sciences of the United States of America *102*, 18773-18784.

Cross, B.C., Bond, P.J., Sadowski, P.G., Jha, B.K., Zak, J., Goodman, J.M., Silverman, R.H., Neubert, T.A., Baxendale, I.R., Ron, D.*, et al.* (2012). The molecular basis for selective inhibition of unconventional mRNA splicing by an IRE1-binding small molecule. Proceedings of the National Academy of Sciences of the United States of America *109*, E869-878.

Cubillos-Ruiz, J.R., Silberman, P.C., Rutkowski, M.R., Chopra, S., Perales-Puchalt, A., Song, M., Zhang, S., Bettigole, S.E., Gupta, D., Holcomb, K.*, et al.* (2015). ER Stress Sensor XBP1 Controls Anti-tumor Immunity by Disrupting Dendritic Cell Homeostasis. Cell *161*, 1527-1538.

Culver, G.M., McCraith, S.M., Consaul, S.A., Stanford, D.R., and Phizicky, E.M. (1997). A 2'-phosphotransferase implicated in tRNA splicing is essential in Saccharomyces cerevisiae. The Journal of biological chemistry *272*, 13203-13210.

Culver, G.M., McCraith, S.M., Zillmann, M., Kierzek, R., Michaud, N., LaReau, R.D., Turner, D.H., and Phizicky, E.M. (1993). An NAD derivative produced during transfer RNA splicing: ADP-ribose 1"-2" cyclic phosphate. Science *261*, 206-208.

De Robertis, E.M., Black, P., and Nishikura, K. (1981). Intranuclear location of the tRNA splicing enzymes. Cell *23*, 89-93.

DeBoever, C., Ghia, E.M., Shepard, P.J., Rassenti, L., Barrett, C.L., Jepsen, K., Jamieson, C.H., Carson, D., Kipps, T.J., and Frazer, K.A. (2015). Transcriptome sequencing reveals potential mechanism of cryptic 3' splice site selection in SF3B1-mutated cancers. PLoS computational biology *11*, e1004105.

Dejeans, N., Pluquet, O., Lhomond, S., Grise, F., Bouchecareilh, M., Juin, A., Meynard-Cadars, M., Bidaud-Meynard, A., Gentil, C., Moreau, V.*, et al.* (2012). Autocrine control of glioma cells adhesion and migration through IRE1alpha-mediated cleavage of SPARC mRNA. Journal of cell science *125*, 4278-4287.

Dow, L.E., Premsrirut, P.K., Zuber, J., Fellmann, C., McJunkin, K., Miething, C., Park, Y., Dickins, R.A., Hannon, G.J., and Lowe, S.W. (2012). A pipeline for the generation of shRNA transgenic mice. Nature protocols *7*, 374-393.

Drogat, B., Auguste, P., Nguyen, D.T., Bouchecareilh, M., Pineau, R., Nalbantoglu, J., Kaufman, R.J., Chevet, E., Bikfalvi, A., and Moenner, M. (2007). IRE1 signaling is essential for ischemia-induced vascular endothelial growth factor-A expression and contributes to angiogenesis and tumor growth in vivo. Cancer research *67*, 6700-6707.

Duronio, R.J., and Xiong, Y. (2013). Signaling pathways that control cell proliferation. Cold Spring Harbor perspectives in biology *5*, a008904.

Dyson, N. (1998). The regulation of E2F by pRB-family proteins. Genes & development *12*, 2245-2262.

Emmott, E., Munday, D., Bickerton, E., Britton, P., Rodgers, M.A., Whitehouse, A., Zhou, E.M., and Hiscox, J.A. (2013). The cellular interactome of the coronavirus infectious bronchitis virus nucleocapsid protein and functional implications for virus biology. Journal of virology *87*, 9486-9500.

Englert, M., and Beier, H. (2005). Plant tRNA ligases are multifunctional enzymes that have diverged in sequence and substrate specificity from RNA ligases of other phylogenetic origins. Nucleic acids research *33*, 388-399.

Englert, M., Sheppard, K., Aslanian, A., Yates, J.R., 3rd, and Soll, D. (2011). Archaeal 3'-phosphate RNA splicing ligase characterization identifies the missing component in tRNA maturation. Proceedings of the National Academy of Sciences of the United States of America *108*, 1290-1295.

Engstrom, P.G., Steijger, T., Sipos, B., Grant, G.R., Kahles, A., Ratsch, G., Goldman, N., Hubbard, T.J., Harrow, J., Guigo, R.*, et al.* (2013). Systematic evaluation of spliced alignment programs for RNA-seq data. Nature methods *10*, 1185-1191.

Fellmann, C., Hoffmann, T., Sridhar, V., Hopfgartner, B., Muhar, M., Roth, M., Lai, D.Y., Barbosa, I.A., Kwon, J.S., Guan, Y.*, et al.* (2013). An optimized microRNA backbone for effective single-copy RNAi. Cell reports *5*, 1704-1713.

Fellmann, C., Zuber, J., McJunkin, K., Chang, K., Malone, C.D., Dickins, R.A., Xu, Q., Hengartner, M.O., Elledge, S.J., Hannon, G.J.*, et al.* (2011). Functional identification of optimized RNAi triggers using a massively parallel sensor assay. Molecular cell *41*, 733-746.

Filipowicz, W., Konarska, M., Gross, H.J., and Shatkin, A.J. (1983). RNA 3'-terminal phosphate cyclase activity and RNA ligation in HeLa cell extract. Nucleic acids research *11*, 1405-1418.

Filipowicz, W., and Shatkin, A.J. (1983). Origin of splice junction phosphate in tRNAs processed by HeLa cell extract. Cell *32*, 547-557.

Filipowicz, W., Strugala, K., Konarska, M., and Shatkin, A.J. (1985). Cyclization of RNA 3'-terminal phosphate by cyclase from HeLa cells proceeds via formation of N(3')pp(5')A activated intermediate. Proceedings of the National Academy of Sciences of the United States of America *82*, 1316-1320.

Flores, R., Grubb, D., Elleuch, A., Nohales, M.A., Delgado, S., and Gago, S. (2011). Rolling-circle replication of viroids, viroid-like satellite RNAs and hepatitis delta virus: variations on a theme. RNA biology *8*, 200-206.

Freibaum, B.D., Chitta, R.K., High, A.A., and Taylor, J.P. (2010). Global analysis of TDP-43 interacting proteins reveals strong association with RNA splicing and translation machinery. Journal of proteome research *9*, 1104-1120.

Friend, S.H., Bernards, R., Rogelj, S., Weinberg, R.A., Rapaport, J.M., Albert, D.M., and Dryja, T.P. (1986). A human DNA segment with properties of the gene that predisposes to retinoblastoma and osteosarcoma. Nature *323*, 643-646.

Fujimoto, T., Onda, M., Nagai, H., Nagahata, T., Ogawa, K., and Emi, M. (2003). Upregulation and overexpression of human X-box binding protein 1 (hXBP-1) gene in primary breast cancers. Breast cancer *10*, 301-306.

Gardner, B.M., Pincus, D., Gotthardt, K., Gallagher, C.M., and Walter, P. (2013). Endoplasmic reticulum stress sensing in the unfolded protein response. Cold Spring Harbor perspectives in biology *5*, a013169.

Gardner, B.M., and Walter, P. (2011). Unfolded proteins are Ire1-activating ligands that directly induce the unfolded protein response. Science *333*, 1891-1894.

Garg, T.K., and Chang, J.Y. (2003). Oxidative stress causes ERK phosphorylation and cell death in cultured retinal pigment epithelium: prevention of cell death by AG126 and 15-deoxy-delta 12, 14-PGJ2. BMC ophthalmology *3*, 5.

Geng, Y., Whoriskey, W., Park, M.Y., Bronson, R.T., Medema, R.H., Li, T., Weinberg, R.A., and Sicinski, P. (1999). Rescue of cyclin D1 deficiency by knockin cyclin E. Cell *97*, 767-777.

Geng, Y., Yu, Q., Sicinska, E., Das, M., Schneider, J.E., Bhattacharya, S., Rideout, W.M., Bronson, R.T., Gardner, H., and Sicinski, P. (2003). Cyclin E ablation in the mouse. Cell *114*, 431-443.

Genschik, P., Billy, E., Swianiewicz, M., and Filipowicz, W. (1997). The human RNA 3'-terminal phosphate cyclase is a member of a new family of proteins conserved in Eucarya, Bacteria and Archaea. The EMBO journal *16*, 2955-2967.

Gething, M.J., and Sambrook, J. (1992). Protein folding in the cell. Nature *355*, 33-45.

Gomez, B.P., Riggins, R.B., Shajahan, A.N., Klimach, U., Wang, A., Crawford, A.C., Zhu, Y., Zwart, A., Wang, M., and Clarke, R. (2007). Human X-box binding protein-1 confers both estrogen independence and antiestrogen resistance in breast cancer cell lines. FASEB journal : official publication of the Federation of American Societies for Experimental Biology *21*, 4013-4027.

Gonzalez, T.N., Sidrauski, C., Dorfler, S., and Walter, P. (1999). Mechanism of non-spliceosomal mRNA splicing in the unfolded protein response pathway. The EMBO journal *18*, 3119-3132.

Goodman, H.M., Olson, M.V., and Hall, B.D. (1977). Nucleotide sequence of a mutant eukaryotic gene: the yeast tyrosine-inserting ochre suppressor SUP4-o. Proceedings of the National Academy of Sciences of the United States of America *74*, 5453-5457.

Greer, C.L., Peebles, C.L., Gegenheimer, P., and Abelson, J. (1983). Mechanism of action of a yeast RNA ligase in tRNA splicing. Cell *32*, 537-546.

Harding, H.P., Lackey, J.G., Hsu, H.C., Zhang, Y., Deng, J., Xu, R.M., Damha, M.J., and Ron, D. (2008). An intact unfolded protein response in Trpt1 knockout mice reveals phylogenic divergence in pathways for RNA ligation. Rna *14*, 225-232.

Harding, H.P., Novoa, I., Zhang, Y., Zeng, H., Wek, R., Schapira, M., and Ron, D. (2000). Regulated translation initiation controls stress-induced gene expression in mammalian cells. Molecular cell *6*, 1099-1108.

Harding, H.P., Zeng, H., Zhang, Y., Jungries, R., Chung, P., Plesken, H., Sabatini, D.D., and Ron, D. (2001). Diabetes mellitus and exocrine pancreatic dysfunction in perk-/- mice reveals a role for translational control in secretory cell survival. Molecular cell *7*, 1153-1163.

Harding, H.P., Zhang, Y., and Ron, D. (1999). Protein translation and folding are coupled by an endoplasmic-reticulum-resident kinase. Nature *397*, 271-274.

Hasegawa, D., Calvo, V., Avivar-Valderas, A., Lade, A., Chou, H.I., Lee, Y.A., Farias, E.F., Aguirre-Ghiso, J.A., and Friedman, S.L. (2015). Epithelial Xbp1 is required for cellular proliferation and differentiation during mammary gland development. Molecular and cellular biology *35*, 1543-1556.

Hendershot, L.M. (2004). The ER function BiP is a master regulator of ER function. The Mount Sinai journal of medicine, New York *71*, 289-297.

Herrera, R.E., Sah, V.P., Williams, B.O., Makela, T.P., Weinberg, R.A., and Jacks, T. (1996). Altered cell cycle kinetics, gene expression, and G1 restriction point regulation in Rb-deficient fibroblasts. Molecular and cellular biology *16*, 2402-2407.

Hetz, C. (2012). The unfolded protein response: controlling cell fate decisions under ER stress and beyond. Nature reviews Molecular cell biology *13*, 89-102.

Hetz, C., Bernasconi, P., Fisher, J., Lee, A.H., Bassik, M.C., Antonsson, B., Brandt, G.S., Iwakoshi, N.N., Schinzel, A., Glimcher, L.H.*, et al.* (2006). Proapoptotic BAX and BAK modulate the unfolded protein response by a direct interaction with IRE1alpha. Science *312*, 572-576.

Hetz, C., and Glimcher, L.H. (2009). Fine-tuning of the unfolded protein response: Assembling the IRE1alpha interactome. Molecular cell *35*, 551-561.

Hetz, C., and Mollereau, B. (2014). Disturbance of endoplasmic reticulum proteostasis in neurodegenerative diseases. Nature reviews Neuroscience *15*, 233-249.

Hetz, C., Thielen, P., Matus, S., Nassif, M., Court, F., Kiffin, R., Martinez, G., Cuervo, A.M., Brown, R.H., and Glimcher, L.H. (2009). XBP-1 deficiency in the nervous system protects against amyotrophic lateral sclerosis by increasing autophagy. Genes & development *23*, 2294-2306.

Hollien, J., Lin, J.H., Li, H., Stevens, N., Walter, P., and Weissman, J.S. (2009). Regulated Ire1-dependent decay of messenger RNAs in mammalian cells. The Journal of cell biology *186*, 323-331.

Hollien, J., and Weissman, J.S. (2006). Decay of endoplasmic reticulum-localized mRNAs during the unfolded protein response. Science *313*, 104-107.

Hong, S.Y., and Hagen, T. (2013). Multiple myeloma Leu167Ile (c.499C>A) mutation prevents XBP1 mRNA splicing. British journal of haematology *161*, 898-901.

Hu, P., Han, Z., Couvillon, A.D., Kaufman, R.J., and Exton, J.H. (2006). Autocrine tumor necrosis factor alpha links endoplasmic reticulum stress to the membrane death receptor pathway through IRE1alpha-mediated NF-kappaB activation and down-regulation of TRAF2 expression. Molecular and cellular biology *26*, 3071-3084.

Huarte, M., Sanz-Ezquerro, J.J., Roncal, F., Ortin, J., and Nieto, A. (2001). PA subunit from influenza virus polymerase complex interacts with a cellular protein with homology to a family of transcriptional activators. Journal of virology *75*, 8597-8604.

Huh, W.K., Falvo, J.V., Gerke, L.C., Carroll, A.S., Howson, R.W., Weissman, J.S., and O'Shea, E.K. (2003). Global analysis of protein localization in budding yeast. Nature *425*, 686-691.

Ingolia, N.T., Ghaemmaghami, S., Newman, J.R., and Weissman, J.S. (2009). Genome-wide analysis in vivo of translation with nucleotide resolution using ribosome profiling. Science *324*, 218-223.

Iwakoshi, N.N., Lee, A.H., Vallabhajosyula, P., Otipoby, K.L., Rajewsky, K., and Glimcher, L.H. (2003). Plasma cell differentiation and the unfolded protein response intersect at the transcription factor XBP-1. Nature immunology *4*, 321-329.

Iwawaki, T., and Tokuda, M. (2011). Function of yeast and amphioxus tRNA ligase in IRE1alpha-dependent XBP1 mRNA splicing. Biochemical and biophysical research communications *413*, 527-531.

Jackson, R.J., Hellen, C.U., and Pestova, T.V. (2010). The mechanism of eukaryotic translation initiation and principles of its regulation. Nature reviews Molecular cell biology *11*, 113-127.

Jeronimo, C., Forget, D., Bouchard, A., Li, Q., Chua, G., Poitras, C., Therien, C., Bergeron, D., Bourassa, S., Greenblatt, J.*, et al.* (2007). Systematic analysis of the protein interaction network for the human transcription machinery reveals the identity of the 7SK capping enzyme. Molecular cell *27*, 262-274.

Johnson, J.D., Ogden, R., Johnson, P., Abelson, J., Dembeck, P., and Itakura, K. (1980). Transcription and processing of a yeast tRNA gene containing a modified intervening sequence. Proceedings of the National Academy of Sciences of the United States of America *77*, 2564-2568.

Johnson, P.F., and Abelson, J. (1983). The yeast tRNATyr gene intron is essential for correct modification of its tRNA product. Nature *302*, 681-687.

Jorgensen, P., and Tyers, M. (2004). How cells coordinate growth and division. Current biology : CB *14*, R1014-1027.

Jurkin, J., Henkel, T., Nielsen, A.F., Minnich, M., Popow, J., Kaufmann, T., Heindl, K., Hoffmann, T., Busslinger, M., and Martinez, J. (2014). The mammalian tRNA ligase complex mediates splicing of XBP1 mRNA and controls antibody secretion in plasma cells. The EMBO journal *33*, 2922-2936.

Kanai, Y., Dohmae, N., and Hirokawa, N. (2004). Kinesin transports RNA: isolation and characterization of an RNA-transporting granule. Neuron *43*, 513-525.

Kanda, H., and Miura, M. (2004). Regulatory roles of JNK in programmed cell death. Journal of biochemistry *136*, 1-6.

Karaca, E., Weitzer, S., Pehlivan, D., Shiraishi, H., Gogakos, T., Hanada, T., Jhangiani, S.N., Wiszniewski, W., Withers, M., Campbell, I.M., *et al.* (2014). Human CLP1 mutations alter tRNA biogenesis, affecting both peripheral and central nervous system function. Cell *157*, 636-650.

Karali, E., Bellou, S., Stellas, D., Klinakis, A., Murphy, C., and Fotsis, T. (2014). VEGF Signals through ATF6 and PERK to promote endothelial cell survival and angiogenesis in the absence of ER stress. Molecular cell *54*, 559-572.

Kharabi Masouleh, B., Geng, H., Hurtz, C., Chan, L.N., Logan, A.C., Chang, M.S., Huang, C., Swaminathan, S., Sun, H., Paietta, E., *et al.* (2014). Mechanistic rationale for targeting the unfolded protein response in pre-B acute lymphoblastic leukemia. Proceedings of the National Academy of Sciences of the United States of America.

Kimata, Y., Ishiwata-Kimata, Y., Ito, T., Hirata, A., Suzuki, T., Oikawa, D., Takeuchi, M., and Kohno, K. (2007). Two regulatory steps of ER-stress sensor Ire1 involving its cluster formation and interaction with unfolded proteins. The Journal of cell biology *179*, 75-86.

Kitagawa, M., Higashi, H., Jung, H.K., Suzuki-Takahashi, I., Ikeda, M., Tamai, K., Kato, J., Segawa, K., Yoshida, E., Nishimura, S., *et al.* (1996). The consensus motif for phosphorylation by cyclin D1-Cdk4 is different from that for phosphorylation by cyclin A/E-Cdk2. The EMBO journal *15*, 7060-7069.

Konarska, M., Filipowicz, W., Domdey, H., and Gross, H.J. (1981). Formation of a 2'-phosphomonoester, 3',5'-phosphodiester linkage by a novel RNA ligase in wheat germ. Nature *293*, 112-116.

Korennykh, A.V., Egea, P.F., Korostelev, A.A., Finer-Moore, J., Zhang, C., Shokat, K.M., Stroud, R.M., and Walter, P. (2009). The unfolded protein response signals through high-order assembly of Ire1. Nature *457*, 687-693.

Kosmaczewski, S.G., Edwards, T.J., Han, S.M., Eckwahl, M.J., Meyer, B.I., Peach, S., Hesselberth, J.R., Wolin, S.L., and Hammarlund, M. (2014). The RtcB RNA ligase is an essential component of the metazoan unfolded protein response. EMBO reports *15*, 1278-1285.

Kosmaczewski, S.G., Han, S.M., Han, B., Irving Meyer, B., Baig, H.S., Athar, W., Lin-Moore, A.T., Koelle, M.R., and Hammarlund, M. (2015). RNA ligation in neurons by RtcB inhibits axon regeneration. Proceedings of the National Academy of Sciences of the United States of America *112*, 8451-8456.

Kozar, K., Ciemerych, M.A., Rebel, V.I., Shigematsu, H., Zagozdzon, A., Sicinska, E., Geng, Y., Yu, Q., Bhattacharya, S., Bronson, R.T., *et al.* (2004). Mouse development and cell proliferation in the absence of D-cyclins. Cell *118*, 477-491.

Kozutsumi, Y., Segal, M., Normington, K., Gething, M.J., and Sambrook, J. (1988). The presence of malfolded proteins in the endoplasmic reticulum signals the induction of glucose-regulated proteins. Nature *332*, 462-464.

Kroemer, G., Marino, G., and Levine, B. (2010). Autophagy and the integrated stress response. Molecular cell *40*, 280-293.

Kula, A., Guerra, J., Knezevich, A., Kleva, D., Myers, M.P., and Marcello, A. (2011). Characterization of the HIV-1 RNA associated proteome identifies Matrin 3 as a nuclear cofactor of Rev function. Retrovirology *8*, 60.

Langmead, B., Trapnell, C., Pop, M., and Salzberg, S.L. (2009). Ultrafast and memory-efficient alignment of short DNA sequences to the human genome. Genome biology *10*, R25.

Lappe-Siefke, C., Goebbels, S., Gravel, M., Nicksch, E., Lee, J., Braun, P.E., Griffiths, I.R., and Nave, K.A. (2003). Disruption of Cnp1 uncouples oligodendroglial functions in axonal support and myelination. Nature genetics *33*, 366-374.

Laski, F.A., Fire, A.Z., RajBhandary, U.L., and Sharp, P.A. (1983). Characterization of tRNA precursor splicing in mammalian extracts. The Journal of biological chemistry *258*, 11974-11980.

Lee, A.H., Heidtman, K., Hotamisligil, G.S., and Glimcher, L.H. (2011a). Dual and opposing roles of the unfolded protein response regulated by IRE1alpha and XBP1 in proinsulin processing and insulin secretion. Proceedings of the National Academy of Sciences of the United States of America *108*, 8885-8890.

Lee, A.H., Iwakoshi, N.N., and Glimcher, L.H. (2003). XBP-1 regulates a subset of endoplasmic reticulum resident chaperone genes in the unfolded protein response. Molecular and cellular biology *23*, 7448-7459.

Lee, A.S. (1987). Coordinated Regulation of a Set of Genes by Glucose and Calcium Ionophores in Mammalian-Cells. Trends Biochem Sci *12*, 20-23.

Lee, J., Sun, C., Zhou, Y., Lee, J., Gokalp, D., Herrema, H., Park, S.W., Davis, R.J., and Ozcan, U. (2011b). p38 MAPK-mediated regulation of Xbp1s is crucial for glucose homeostasis. Nature medicine *17*, 1251-1260.

Lee, J.W., Liao, P.C., Young, K.C., Chang, C.L., Chen, S.S., Chang, T.T., Lai, M.D., and Wang, S.W. (2011c). Identification of hnRNPH1, NF45, and C14orf166 as novel host interacting partners of the mature hepatitis C virus core protein. Journal of proteome research *10*, 4522-4534.

Lee, K., Tirasophon, W., Shen, X., Michalak, M., Prywes, R., Okada, T., Yoshida, H., Mori, K., and Kaufman, R.J. (2002). IRE1-mediated unconventional mRNA splicing and S2P-mediated ATF6 cleavage merge to regulate XBP1 in signaling the unfolded protein response. Genes & development *16*, 452-466.

Leung-Hagesteijn, C., Erdmann, N., Cheung, G., Keats, J.J., Stewart, A.K., Reece, D.E., Chung, K.C., and Tiedemann, R.E. (2013). Xbp1s-negative tumor B cells and pre-plasmablasts mediate therapeutic proteasome inhibitor resistance in multiple myeloma. Cancer cell *24*, 289-304.

Li, L., Monckton, E.A., and Godbout, R. (2008). A role for DEAD box 1 at DNA double-strand breaks. Molecular and cellular biology *28*, 6413-6425.

Lipson, K.L., Ghosh, R., and Urano, F. (2008). The role of IRE1alpha in the degradation of insulin mRNA in pancreatic beta-cells. PloS one *3*, e1648.

Lu, Y., Liang, F.X., and Wang, X. (2014). A synthetic biology approach identifies the mammalian UPR RNA ligase RtcB. Molecular cell *55*, 758-770.

Lund, E., and Dahlberg, J.E. (1998). Proofreading and aminoacylation of tRNAs before export from the nucleus. Science *282*, 2082-2085.

Majumder, M., Huang, C., Snider, M.D., Komar, A.A., Tanaka, J., Kaufman, R.J., Krokowski, D., and Hatzoglou, M. (2012). A novel feedback loop regulates the response to endoplasmic

reticulum stress via the cooperation of cytoplasmic splicing and mRNA translation. Molecular and cellular biology *32*, 992-1003.

Malumbres, M., Sotillo, R., Santamaria, D., Galan, J., Cerezo, A., Ortega, S., Dubus, P., and Barbacid, M. (2004). Mammalian cells cycle without the D-type cyclin-dependent kinases Cdk4 and Cdk6. Cell *118*, 493-504.

Martinez, J., Patkaniowska, A., Urlaub, H., Luhrmann, R., and Tuschl, T. (2002). Single-stranded antisense siRNAs guide target RNA cleavage in RNAi. Cell *110*, 563-574.

Matus, S., Glimcher, L.H., and Hetz, C. (2011). Protein folding stress in neurodegenerative diseases: a glimpse into the ER. Current opinion in cell biology *23*, 239-252.

Mauro, C., Crescenzi, E., De Mattia, R., Pacifico, F., Mellone, S., Salzano, S., de Luca, C., D'Adamio, L., Palumbo, G., Formisano, S.*, et al.* (2006). Central role of the scaffold protein tumor necrosis factor receptor-associated factor 2 in regulating endoplasmic reticulum stress-induced apoptosis. The Journal of biological chemistry *281*, 2631-2638.

McBride, J.L., Boudreau, R.L., Harper, S.Q., Staber, P.D., Monteys, A.M., Martins, I., Gilmore, B.L., Burstein, H., Peluso, R.W., Polisky, B.*, et al.* (2008). Artificial miRNAs mitigate shRNA-mediated toxicity in the brain: implications for the therapeutic development of RNAi. Proceedings of the National Academy of Sciences of the United States of America *105*, 5868-5873.

McCraith, S.M., and Phizicky, E.M. (1990). A highly specific phosphatase from Saccharomyces cerevisiae implicated in tRNA splicing. Molecular and cellular biology *10*, 1049-1055.

Meyer, C.A., Jacobs, H.W., Datar, S.A., Du, W., Edgar, B.A., and Lehner, C.F. (2000). Drosophila Cdk4 is required for normal growth and is dispensable for cell cycle progression. The EMBO journal *19*, 4533-4542.

Michallet, A.S., Mondiere, P., Taillardet, M., Leverrier, Y., Genestier, L., and Defrance, T. (2011). Compromising the unfolded protein response induces autophagy-mediated cell death in multiple myeloma cells. PloS one *6*, e25820.

Mimura, N., Fulciniti, M., Gorgun, G., Tai, Y.T., Cirstea, D., Santo, L., Hu, Y., Fabre, C., Minami, J., Ohguchi, H.*, et al.* (2012). Blockade of XBP1 splicing by inhibition of IRE1alpha is a promising therapeutic option in multiple myeloma. Blood *119*, 5772-5781.

Mori, S., Kajita, T., Endo, T., and Yoshihisa, T. (2011). The intron of tRNA-TrpCCA is dispensable for growth and translation of Saccharomyces cerevisiae. Rna *17*, 1760-1769.

Mori, T., Ogasawara, C., Inada, T., Englert, M., Beier, H., Takezawa, M., Endo, T., and Yoshihisa, T. (2010). Dual functions of yeast tRNA ligase in the unfolded protein response: unconventional cytoplasmic splicing of HAC1 pre-mRNA is not sufficient to release translational attenuation. Molecular biology of the cell *21*, 3722-3734.

Morrison, D.K. (2012). MAP kinase pathways. Cold Spring Harbor perspectives in biology *4*.

Nandakumar, J., Schwer, B., Schaffrath, R., and Shuman, S. (2008). RNA repair: an antidote to cytotoxic eukaryal RNA damage. Molecular cell *31*, 278-286.

Nguyen, D.T., Kebache, S., Fazel, A., Wong, H.N., Jenna, S., Emadali, A., Lee, E.H., Bergeron, J.J., Kaufman, R.J., Larose, L.*, et al.* (2004). Nck-dependent activation of extracellular signal-regulated kinase-1 and regulation of cell survival during endoplasmic reticulum stress. Molecular biology of the cell *15*, 4248-4260.

Nikawa, J., Akiyoshi, M., Hirata, S., and Fukuda, T. (1996). Saccharomyces cerevisiae IRE2/HAC1 is involved in IRE1-mediated KAR2 expression. Nucleic acids research *24*, 4222-4226.

Nishikura, K., and De Robertis, E.M. (1981). RNA processing in microinjected Xenopus oocytes. Sequential addition of base modifications in the spliced transfer RNA. Journal of molecular biology *145*, 405-420.

Nishitoh, H., Matsuzawa, A., Tobiume, K., Saegusa, K., Takeda, K., Inoue, K., Hori, S., Kakizuka, A., and Ichijo, H. (2002). ASK1 is essential for endoplasmic reticulum stress-induced neuronal cell death triggered by expanded polyglutamine repeats. Genes & development *16*, 1345-1355.

Novoa, I., Zeng, H., Harding, H.P., and Ron, D. (2001). Feedback inhibition of the unfolded protein response by GADD34-mediated dephosphorylation of eIF2alpha. The Journal of cell biology *153*, 1011-1022.

Ormerod, M.G., Payne, A.W., and Watson, J.V. (1987). Improved program for the analysis of DNA histograms. Cytometry *8*, 637-641.

Otero, J.H., Lizak, B., and Hendershot, L.M. (2010). Life and death of a BiP substrate. Seminars in cell & developmental biology *21*, 472-478.

Papa, F.R., Zhang, C., Shokat, K., and Walter, P. (2003). Bypassing a kinase activity with an ATP-competitive drug. Science *302*, 1533-1537.

Papandreou, I., Denko, N.C., Olson, M., Van Melckebeke, H., Lust, S., Tam, A., Solow-Cordero, D.E., Bouley, D.M., Offner, F., Niwa, M.*, et al.* (2011). Identification of an Ire1alpha endonuclease specific inhibitor with cytotoxic activity against human multiple myeloma. Blood *117*, 1311-1314.

Parada, G.E., Munita, R., Cerda, C.A., and Gysling, K. (2014). A comprehensive survey of non-canonical splice sites in the human transcriptome. Nucleic acids research *42*, 10564-10578.

Park, S.W., Zhou, Y., Lee, J., Lu, A., Sun, C., Chung, J., Ueki, K., and Ozcan, U. (2010). The regulatory subunits of PI3K, p85alpha and p85beta, interact with XBP-1 and increase its nuclear translocation. Nature medicine *16*, 429-437.

Patil, S.S., Alexander, T.B., Uzman, J.A., Lou, C.H., Gohil, H., and Sater, A.K. (2006). Novel gene ashwin functions in Xenopus cell survival and anteroposterior patterning. Developmental dynamics : an official publication of the American Association of Anatomists *235*, 1895-1907.

Paushkin, S.V., Patel, M., Furia, B.S., Peltz, S.W., and Trotta, C.R. (2004). Identification of a human endonuclease complex reveals a link between tRNA splicing and pre-mRNA 3' end formation. Cell *117*, 311-321.

Perez-Gonzalez, A., Pazo, A., Navajas, R., Ciordia, S., Rodriguez-Frandsen, A., and Nieto, A. (2014). hCLE/C14orf166 associates with DDX1-HSPC117-FAM98B in a novel transcription-dependent shuttling RNA-transporting complex. PloS one *9*, e90957.

Perez-Gonzalez, A., Rodriguez, A., Huarte, M., Salanueva, I.J., and Nieto, A. (2006). hCLE/CGI-99, a human protein that interacts with the influenza virus polymerase, is a mRNA transcription modulator. Journal of molecular biology *362*, 887-900.

Phizicky, E.M., Consaul, S.A., Nehrke, K.W., and Abelson, J. (1992). Yeast tRNA ligase mutants are nonviable and accumulate tRNA splicing intermediates. The Journal of biological chemistry *267*, 4577-4582.

Phizicky, E.M., and Hopper, A.K. (2010). tRNA biology charges to the front. Genes & development *24*, 1832-1860.

Phizicky, E.M., Schwartz, R.C., and Abelson, J. (1986). Saccharomyces cerevisiae tRNA ligase. Purification of the protein and isolation of the structural gene. The Journal of biological chemistry *261*, 2978-2986.

Pincus, D., Chevalier, M.W., Aragon, T., van Anken, E., Vidal, S.E., El-Samad, H., and Walter, P. (2010). BiP binding to the ER-stress sensor Ire1 tunes the homeostatic behavior of the unfolded protein response. PLoS biology *8*, e1000415.

Popow, J., Englert, M., Weitzer, S., Schleiffer, A., Mierzwa, B., Mechtler, K., Trowitzsch, S., Will, C.L., Luhrmann, R., Soll, D.*, et al.* (2011). HSPC117 is the essential subunit of a human tRNA splicing ligase complex. Science *331*, 760-764.

Popow, J., Jurkin, J., Schleiffer, A., and Martinez, J. (2014). Analysis of orthologous groups reveals archease and DDX1 as tRNA splicing factors. Nature.

Popow, J., Schleiffer, A., and Martinez, J. (2012). Diversity and roles of (t)RNA ligases. Cellular and molecular life sciences : CMLS *69*, 2657-2670.

Raab, M.S., Podar, K., Breitkreutz, I., Richardson, P.G., and Anderson, K.C. (2009). Multiple myeloma. Lancet *374*, 324-339.

Rappsilber, J., Ryder, U., Lamond, A.I., and Mann, M. (2002). Large-scale proteomic analysis of the human spliceosome. Genome research *12*, 1231-1245.

Re, A., Joshi, T., Kulberkyte, E., Morris, Q., and Workman, C.T. (2014). RNA-protein interactions: an overview. Methods in molecular biology *1097*, 491-521.

Reid, C.E., and Lazinski, D.W. (2000). A host-specific function is required for ligation of a wide variety of ribozyme-processed RNAs. Proceedings of the National Academy of Sciences of the United States of America *97*, 424-429.

Reimold, A.M., Etkin, A., Clauss, I., Perkins, A., Friend, D.S., Zhang, J., Horton, H.F., Scott, A., Orkin, S.H., Byrne, M.C.*, et al.* (2000). An essential role in liver development for transcription factor XBP-1. Genes & development *14*, 152-157.

Reyes, V.M., and Abelson, J. (1988). Substrate recognition and splice site determination in yeast tRNA splicing. Cell *55*, 719-730.

Rhind, N., and Russell, P. (2012). Signaling pathways that regulate cell division. Cold Spring Harbor perspectives in biology *4*.

Ri, M., Tashiro, E., Oikawa, D., Shinjo, S., Tokuda, M., Yokouchi, Y., Narita, T., Masaki, A., Ito, A., Ding, J.*, et al.* (2012). Identification of Toyocamycin, an agent cytotoxic for multiple myeloma cells, as a potent inhibitor of ER stress-induced XBP1 mRNA splicing. Blood cancer journal *2*, e79.

Robertson-Anderson, R.M., Wang, J., Edgcomb, S.P., Carmel, A.B., Williamson, J.R., and Millar, D.P. (2011). Single-molecule studies reveal that DEAD box protein DDX1 promotes oligomerization of HIV-1 Rev on the Rev response element. Journal of molecular biology *410*, 959-971.

Romero-Ramirez, L., Cao, H., Nelson, D., Hammond, E., Lee, A.H., Yoshida, H., Mori, K., Glimcher, L.H., Denko, N.C., Giaccia, A.J.*, et al.* (2004). XBP1 is essential for survival under hypoxic conditions and is required for tumor growth. Cancer research *64*, 5943-5947.

Rubio, C., Pincus, D., Korennykh, A., Schuck, S., El-Samad, H., and Walter, P. (2011). Homeostatic adaptation to endoplasmic reticulum stress depends on Ire1 kinase activity. The Journal of cell biology *193*, 171-184.

Ruegsegger, U., Leber, J.H., and Walter, P. (2001). Block of HAC1 mRNA translation by long-range base pairing is released by cytoplasmic splicing upon induction of the unfolded protein response. Cell *107*, 103-114.

Sadoshima, J., Qiu, Z., Morgan, J.P., and Izumo, S. (1996). Tyrosine kinase activation is an immediate and essential step in hypotonic cell swelling-induced ERK activation and c-fos gene expression in cardiac myocytes. The EMBO journal *15*, 5535-5546.

Sawaya, R., Schwer, B., and Shuman, S. (2003). Genetic and biochemical analysis of the functional domains of yeast tRNA ligase. The Journal of biological chemistry *278*, 43928-43938.

Scheuner, D., Song, B., McEwen, E., Liu, C., Laybutt, R., Gillespie, P., Saunders, T., Bonner-Weir, S., and Kaufman, R.J. (2001). Translational control is required for the unfolded protein response and in vivo glucose homeostasis. Molecular cell *7*, 1165-1176.

Schliess, F., Sinning, R., Fischer, R., Schmalenbach, C., and Haussinger, D. (1996). Calcium-dependent activation of Erk-1 and Erk-2 after hypo-osmotic astrocyte swelling. The Biochemical journal *320 (Pt 1)*, 167-171.

Schwer, B., Sawaya, R., Ho, C.K., and Shuman, S. (2004). Portability and fidelity of RNA-repair systems. Proceedings of the National Academy of Sciences of the United States of America *101*, 2788-2793.

Shaffer, A.L., Shapiro-Shelef, M., Iwakoshi, N.N., Lee, A.H., Qian, S.B., Zhao, H., Yu, X., Yang, L., Tan, B.K., Rosenwald, A.*, et al.* (2004). XBP1, downstream of Blimp-1, expands the secretory apparatus and other organelles, and increases protein synthesis in plasma cell differentiation. Immunity *21*, 81-93.

Shen, J., Chen, X., Hendershot, L., and Prywes, R. (2002). ER stress regulation of ATF6 localization by dissociation of BiP/GRP78 binding and unmasking of Golgi localization signals. Developmental cell *3*, 99-111.

Shen, X., Ellis, R.E., Sakaki, K., and Kaufman, R.J. (2005). Genetic interactions due to constitutive and inducible gene regulation mediated by the unfolded protein response in C. elegans. PLoS genetics *1*, e37.

Sherr, C.J., and Roberts, J.M. (2004). Living with or without cyclins and cyclin-dependent kinases. Genes & development *18*, 2699-2711.

Shinya, S., Kadokura, H., Imagawa, Y., Inoue, M., Yanagitani, K., and Kohno, K. (2011). Reconstitution and characterization of the unconventional splicing of XBP1u mRNA in vitro. Nucleic acids research *39*, 5245-5254.

Sidrauski, C., Cox, J.S., and Walter, P. (1996). tRNA ligase is required for regulated mRNA splicing in the unfolded protein response. Cell *87*, 405-413.

Sidrauski, C., and Walter, P. (1997). The transmembrane kinase Ire1p is a site-specific endonuclease that initiates mRNA splicing in the unfolded protein response. Cell *90*, 1031-1039.

Sinning, R., Schliess, F., Kubitz, R., and Haussinger, D. (1997). Osmosignalling in C6 glioma cells. FEBS letters *400*, 163-167.

Song, Y., Sretavan, D., Salegio, E.A., Berg, J., Huang, X., Cheng, T., Xiong, X., Meltzer, S., Han, C., Nguyen, T.T.*, et al.* (2015). Regulation of axon regeneration by the RNA repair and splicing pathway. Nature neuroscience *18*, 817-825.

Spinelli, S.L., Malik, H.S., Consaul, S.A., and Phizicky, E.M. (1998). A functional homolog of a yeast tRNA splicing enzyme is conserved in higher eukaryotes and in Escherichia coli. Proceedings of the National Academy of Sciences of the United States of America *95*, 14136-14141.

Sriburi, R., Bommiasamy, H., Buldak, G.L., Robbins, G.R., Frank, M., Jackowski, S., and Brewer, J.W. (2007). Coordinate regulation of phospholipid biosynthesis and secretory pathway gene expression in XBP-1(S)-induced endoplasmic reticulum biogenesis. The Journal of biological chemistry *282*, 7024-7034.

Sriburi, R., Jackowski, S., Mori, K., and Brewer, J.W. (2004). XBP1: a link between the unfolded protein response, lipid biosynthesis, and biogenesis of the endoplasmic reticulum. The Journal of cell biology *167*, 35-41.

Stern, B., and Nurse, P. (1996). A quantitative model for the cdc2 control of S phase and mitosis in fission yeast. Trends in genetics : TIG *12*, 345-350.

Strobel, M.C., and Abelson, J. (1986). Effect of intron mutations on processing and function of Saccharomyces cerevisiae SUP53 tRNA in vitro and in vivo. Molecular and cellular biology *6*, 2663-2673.

Suh, D.H., Kim, M.K., Kim, H.S., Chung, H.H., and Song, Y.S. (2012). Unfolded protein response to autophagy as a promising druggable target for anticancer therapy. Annals of the New York Academy of Sciences *1271*, 20-32.

Szweykowska-Kulinska, Z., Senger, B., Keith, G., Fasiolo, F., and Grosjean, H. (1994). Intron-dependent formation of pseudouridines in the anticodon of Saccharomyces cerevisiae minor tRNA(Ile). The EMBO journal *13*, 4636-4644.

Tabas, I., and Ron, D. (2011). Integrating the mechanisms of apoptosis induced by endoplasmic reticulum stress. Nature cell biology *13*, 184-190.

Tanaka, N., Chakravarty, A.K., Maughan, B., and Shuman, S. (2011a). Novel mechanism of RNA repair by RtcB via sequential 2',3'-cyclic phosphodiesterase and 3'-Phosphate/5'-hydroxyl ligation reactions. The Journal of biological chemistry *286*, 43134-43143.

Tanaka, N., Meineke, B., and Shuman, S. (2011b). RtcB, a novel RNA ligase, can catalyze tRNA splicing and HAC1 mRNA splicing in vivo. The Journal of biological chemistry *286*, 30253-30257.

Tanaka, N., and Shuman, S. (2011). RtcB is the RNA ligase component of an Escherichia coli RNA repair operon. The Journal of biological chemistry *286*, 7727-7731.

Tang, C.H., Ranatunga, S., Kriss, C.L., Cubitt, C.L., Tao, J., Pinilla-Ibarz, J.A., Del Valle, J.R., and Hu, C.C. (2014). Inhibition of ER stress-associated IRE-1/XBP-1 pathway reduces leukemic cell survival. The Journal of clinical investigation *124*, 2585-2598.

Tohmonda, T., Miyauchi, Y., Ghosh, R., Yoda, M., Uchikawa, S., Takito, J., Morioka, H., Nakamura, M., Iwawaki, T., Chiba, K.*, et al.* (2011). The IRE1alpha-XBP1 pathway is essential for osteoblast differentiation through promoting transcription of Osterix. EMBO reports *12*, 451-457.

Travers, K.J., Patil, C.K., Wodicka, L., Lockhart, D.J., Weissman, J.S., and Walter, P. (2000). Functional and genomic analyses reveal an essential coordination between the unfolded protein response and ER-associated degradation. Cell *101*, 249-258.

Trotta, C.R., Miao, F., Arn, E.A., Stevens, S.W., Ho, C.K., Rauhut, R., and Abelson, J.N. (1997). The yeast tRNA splicing endonuclease: a tetrameric enzyme with two active site subunits homologous to the archaeal tRNA endonucleases. Cell *89*, 849-858.

Uemura, A., Oku, M., Mori, K., and Yoshida, H. (2009). Unconventional splicing of XBP1 mRNA occurs in the cytoplasm during the mammalian unfolded protein response. Journal of cell science *122*, 2877-2886.

Upton, J.P., Wang, L., Han, D., Wang, E.S., Huskey, N.E., Lim, L., Truitt, M., McManus, M.T., Ruggero, D., Goga, A.*, et al.* (2012). IRE1alpha cleaves select microRNAs during ER stress to derepress translation of proapoptotic Caspase-2. Science *338*, 818-822.

Urano, F., Wang, X., Bertolotti, A., Zhang, Y., Chung, P., Harding, H.P., and Ron, D. (2000). Coupling of stress in the ER to activation of JNK protein kinases by transmembrane protein kinase IRE1. Science *287*, 664-666.

Valenzuela, P., Venegas, A., Weinberg, F., Bishop, R., and Rutter, W.J. (1978). Structure of yeast phenylalanine-tRNA genes: an intervening DNA segment within the region coding for the tRNA. Proceedings of the National Academy of Sciences of the United States of America *75*, 190-194.

van der Wijk, T., Dorrestijn, J., Narumiya, S., Maassen, J.A., de Jonge, H.R., and Tilly, B.C. (1998). Osmotic swelling-induced activation of the extracellular-signal-regulated protein kinases Erk-1 and Erk-2 in intestine 407 cells involves the Ras/Raf-signalling pathway. The Biochemical journal *331 (Pt 3)*, 863-869.

Vidal, R.L., Figueroa, A., Court, F.A., Thielen, P., Molina, C., Wirth, C., Caballero, B., Kiffin, R., Segura-Aguilar, J., Cuervo, A.M.*, et al.* (2012). Targeting the UPR transcription factor XBP1 protects against Huntington's disease through the regulation of FoxO1 and autophagy. Human molecular genetics *21*, 2245-2262.

Volkmann, K., Lucas, J.L., Vuga, D., Wang, X., Brumm, D., Stiles, C., Kriebel, D., Der-Sarkissian, A., Krishnan, K., Schweitzer, C.*, et al.* (2011). Potent and selective inhibitors of the inositol-requiring enzyme 1 endoribonuclease. The Journal of biological chemistry *286*, 12743-12755.

Walter, P., and Ron, D. (2011). The unfolded protein response: from stress pathway to homeostatic regulation. Science *334*, 1081-1086.

Wang, F.M., Chen, Y.J., and Ouyang, H.J. (2011). Regulation of unfolded protein response modulator XBP1s by acetylation and deacetylation. The Biochemical journal *433*, 245-252.

Wang, L., Perera, B.G., Hari, S.B., Bhhatarai, B., Backes, B.J., Seeliger, M.A., Schurer, S.C., Oakes, S.A., Papa, F.R., and Maly, D.J. (2012). Divergent allosteric control of the IRE1alpha endoribonuclease using kinase inhibitors. Nature chemical biology *8*, 982-989.

Wang, X., Martindale, J.L., Liu, Y., and Holbrook, N.J. (1998). The cellular response to oxidative stress: influences of mitogen-activated protein kinase signalling pathways on cell survival. The Biochemical journal *333 (Pt 2)*, 291-300.

Wang, Y., Xing, P., Cui, W., Wang, W., Cui, Y., Ying, G., Wang, X., and Li, B. (2015). Acute Endoplasmic Reticulum Stress-Independent Unconventional Splicing of XBP1 mRNA in the Nucleus of Mammalian Cells. International journal of molecular sciences *16*, 13302-13321.

Ward, P.S., and Thompson, C.B. (2012). Signaling in control of cell growth and metabolism. Cold Spring Harbor perspectives in biology *4*, a006783.

Watson, J.V., Chambers, S.H., and Smith, P.J. (1987). A pragmatic approach to the analysis of DNA histograms with a definable G1 peak. Cytometry *8*, 1-8.

Wrana, J.L. (2013). Signaling by the TGFbeta superfamily. Cold Spring Harbor perspectives in biology *5*, a011197.

Yamamoto, K., Sato, T., Matsui, T., Sato, M., Okada, T., Yoshida, H., Harada, A., and Mori, K. (2007). Transcriptional induction of mammalian ER quality control proteins is mediated by single or combined action of ATF6alpha and XBP1. Developmental cell *13*, 365-376.

Yamamoto, K., Yoshida, H., Kokame, K., Kaufman, R.J., and Mori, K. (2004). Differential contributions of ATF6 and XBP1 to the activation of endoplasmic reticulum stress-responsive cis-acting elements ERSE, UPRE and ERSE-II. Journal of biochemistry *136*, 343-350.

Yanagitani, K., Imagawa, Y., Iwawaki, T., Hosoda, A., Saito, M., Kimata, Y., and Kohno, K. (2009). Cotranslational targeting of XBP1 protein to the membrane promotes cytoplasmic splicing of its own mRNA. Molecular cell *34*, 191-200.

Yanagitani, K., Kimata, Y., Kadokura, H., and Kohno, K. (2011). Translational pausing ensures membrane targeting and cytoplasmic splicing of XBP1u mRNA. Science *331*, 586-589.

Yoshida, H., Matsui, T., Yamamoto, A., Okada, T., and Mori, K. (2001). XBP1 mRNA is induced by ATF6 and spliced by IRE1 in response to ER stress to produce a highly active transcription factor. Cell *107*, 881-891.

Yoshida, H., Oku, M., Suzuki, M., and Mori, K. (2006). pXBP1(U) encoded in XBP1 pre-mRNA negatively regulates unfolded protein response activator pXBP1(S) in mammalian ER stress response. The Journal of cell biology *172*, 565-575.

Yoshida, H., Uemura, A., and Mori, K. (2009). pXBP1(U), a negative regulator of the unfolded protein response activator pXBP1(S), targets ATF6 but not ATF4 in proteasome-mediated degradation. Cell structure and function *34*, 1-10.

Zeng, L., Xiao, Q., Chen, M., Margariti, A., Martin, D., Ivetic, A., Xu, H., Mason, J., Wang, W., Cockerill, G.*, et al.* (2013). Vascular endothelial cell growth-activated XBP1 splicing in endothelial cells is crucial for angiogenesis. Circulation *127*, 1712-1722.

Zhou, J., Liu, C.Y., Back, S.H., Clark, R.L., Peisach, D., Xu, Z., and Kaufman, R.J. (2006). The crystal structure of human IRE1 luminal domain reveals a conserved dimerization interface required for activation of the unfolded protein response. Proceedings of the National Academy of Sciences of the United States of America *103*, 14343-14348.

Zhou, Y., Lee, J., Reno, C.M., Sun, C., Park, S.W., Chung, J., Lee, J., Fisher, S.J., White, M.F., Biddinger, S.B.*, et al.* (2011). Regulation of glucose homeostasis through a XBP-1-FoxO1 interaction. Nature medicine *17*, 356-365.

Zillmann, M., Gorovsky, M.A., and Phizicky, E.M. (1991). Conserved mechanism of tRNA splicing in eukaryotes. Molecular and cellular biology *11*, 5410-5416.

Zuber, J., McJunkin, K., Fellmann, C., Dow, L.E., Taylor, M.J., Hannon, G.J., and Lowe, S.W. (2011). Toolkit for evaluating genes required for proliferation and survival using tetracycline-regulated RNAi. Nature biotechnology *29*, 79-83.